Design and Application of Compact Combustors in Small-Scale JetCat Engines

THESIS

Nathan A. Clark

AFIT-ENY-MS-22-M-284

DEPARTMENT OF THE AIR FORCE
AIR UNIVERSITY

AIR FORCE INSTITUTE OF TECHNOLOGY

Wright-Patterson Air Force Base, Ohio

AFIT-ENY-MS-22-M-284

DESIGN AND APPLICATION OF COMPACT COMBUSTORS IN SMALL-SCALE JETCAT ENGINES

THESIS

Presented to the Faculty

Department of Aeronautics and Astronautics

Graduate School of Engineering and Management

Air Force Institute of Technology

Air University

Air Education and Training Command

in Partial Fulfillment of the Requirements for the

Degree of Master of Science and Engineering

Nathan A. Clark, B.S.

March 2022

AFIT-ENY-MS-22-M-284

DESIGN AND APPLICATION OF COMPACT COMBUSTORS IN SMALL-SCALE JETCAT ENGINES

Nathan A. Clark, B.S.

Committee Membership:

Marc D. Polanka, PhD
Chairman

Lt Col Brian T. Bohan, PhD
Member

Lt Col James L. Rutledge, PhD
Member

Abstract

Ultra-compact combustors (UCC) are an innovative approach to improving overall engine efficiency and thrust-to-weight ratio by reducing the axial length and weight of the engine. Traditionally, ultra-compact combustors achieved these efficiency gains by burning circumferentially rather than axially, however, previous studies looked at integrating a UCC featuring bluff-body flame holders into a small-scale JetCat P90 RXi gas turbine engine utilizing gaseous propane fuel, while maintaining a length savings of 33%. This engine equipped with the novel compact combustor spooled up to idle conditions before flame-out occurred while attempting higher engine speeds. The current investigation aimed to utilize the previous compact combustor design and switch fuels to liquid kerosene for operation in a similarly sized JetCat P160-RXi-B engine. Through this effort, the JetCat P160 equipped with the compact combustor was only able to spool up to a half-idle condition of 15,800 RPM before the engine shut-off due to a lack of stable flame-holding. Afterwards, computational simulations were performed in ANSYS Fluent, which showed the bluff-body flame-holding mechanism designed for propane was not sufficient for liquid kerosene fuel.

A new combustor was designed and equipped with a different flame stabilization technique at a slightly larger scale to ensure sufficient residence time while maintaining an axial length savings of 20%. Manufacturing of the novel combustor featuring an outboard cavity-stabilized flame-holding mechanism was performed at the P400 scale and was integrated within a newly designed non-rotating test facility within the Air Force Research Laboratory to facilitate proving the combustor's operability within a gas turbine engine within rotating turbomachinery.

Acknowledgements

The work presented here would not have been possible without the help and guidance from a number of people. Firstly, I'd like to thank my advisor Dr. Marc Polanka and committee members Lt Col Brian Bohan, and Lt Col James Rutledge. I would not have been able to accomplish this work without the expertise, knowledge, and/or mentorship you have given me whether in the classroom or during weekly meetings.

The manufacturing of both the P160 and P400 compact combustors and supporting hardware would not have been possible without the team at the AFIT model shop. Thank you Mr. Brian Crabtree, Mr. Chris Harkless, Mr. Dean Harshman, Mr. Joe Owings, and Mr. Dan Ryan for all the hard work and laborious hours you all put in to make this project possible. Additionally, I'd like to thank the team at the AFRL model shop since the new P400 test rig would not have been possible without your help and expertise.

I'd also like to thank the group of guys I've come to know and work with throughout my experience designing and building a new test rig within AFRL. Thank you Mr. Brendan Paxton, Mr. Tyler Owens, Mr. Stephen Britton, and Mr. Matthew Darby for the amount of support and help you've given me throughout my time with this project. It's truly been a pleasure working with all of you.

Lastly, I'd like to thank my fiance and my family for all of their love and support they have given me throughout my time at AFIT. Thank you for never giving up on me.

Nathan A. Clark

Table of Contents

Page

Page

List of Figures

List of Tables

List of Abbreviations

Abbreviation		Page
UCC	Ultra Compact Combustor	iv
RPM	Revolutions Per Minute	1
SERL	Small Engine Research Lab	5
CFD	Computational Fluid Dynamics	6
TVC	Trapped-Vortex Combustor	7
HGC	High-g Combustor	7
AFIT	Air Force Institute of Technology	8
OD	Outer Diameter	10
HGV	Hybrid Guide Vane	10
RVC	Radial Vane Cavity	10
PIV	Particle Imaging Velocimetry	11
CFD	Computational Fluid Dynamics	11
COAL	Combustion Optimization Analysis Laboratory	16
AFRL	Air Force Research Laboratory	16
PLIF	Planer Laser-Induced Fluorescence	23
CAD	Computer-Aided Design	39
SST	Shear Stress Transport	39
LBO	Lean Blowout	40
RANS	Reynolds-Averaged Navier Stokes	40
TCFS	Temperature-Range Clipped Flame Section	40
DPM	Discrete Phase Model	41
ID	Inner Diameter	44

Abbreviation		Page
NGV	Nozzle Guide Vane	45
ECU	Engine Control Unit	58
EGT	Exhaust Gas Temperature	59
GSU	Ground Support Unit	61
PID	Proportional Integral Derivative	63
PLC	Programmable Logic Control	63
IGES	Initial Graphics Exchange Specification	71
YSZ	Yttria-Stabilized Zirconia	97
MAF	Mass Air Flow	116
FAR	Fuel-Air Ratio	128
AMF	Air Mass Flow	142

List of Symbols

Symbol		Page
t	Droplet Lifetime	29
ρ	Air Density	29
ρ_l	Fluid Droplet Density	29
D_{AB}	Binary Diffusivity	29
B_Y	Spalding Number	29
S'	Swirl Number	31
α_{sw}	Swirler Vane Angle	31
r_h	Swirler Inner Radius	31
r_t	Swirler Outer Radius	31
PF	Pattern Factor	37
P_f	Profile Factor	37
T_{tmax}	Maximum Combustor Exit Total Temperature	37
T_{tav}	Average Combustor Exit Total Temperature	37
T_{tin}	Combustor Inlet Total Temperature	37
T_{t4}	Combustor Exit Total Temperature	37
Δs	Node Spacing	71
y^+	Dimensionless Wall Distance	74
T_3	Combustor Inlet Temperature	99
P_3	Combustor Inlet Pressure	99
ϕ	Equivalence Ratio	116
TPL	Total Pressure Loss	124
η	Combustion Efficiency	124
$A_{critical}$	Critical Liner Area Factor	125
$T_{4,ideal}$	Adiabatic Flame Temperature	125

DESIGN AND APPLICATION OF COMPACT COMBUSTORS IN SMALL-SCALE JETCAT ENGINES

I. Introduction

1.1 Ultra-Compact Combustors

Millions of dollars are spent annually by commercial airline companies to strive for innovations within gas turbine engines and the aircraft. Improvements in efficiency on the order of 1% can have a large effect on the economic aspect of the airline industry, enabling the aircraft to be more profitable as a result of a slight improvement in efficiency. Additionally, these improvements enable an aircraft to have an increased thrust-to-weight ratio, allowing an aircraft to carry a heavier payload. An ultra-compact combustor (UCC) aims to provide an axial length savings of 33% to a gas turbine engine while ensuring ample residence time to meet combustion efficiency and emissions standards. To prove the UCC's capability within a gas turbine engine, Bohan et al. [1] integrated a UCC equipped with a high-g circumferential cavity into a small-scale JetCat P90-RXi hobbyist engine. As a result, the engine achieved self-sustained operation at a half-idle condition of 14,000 RPM before flame-out occurred at higher mass flow conditions. This flame-out was a result of increased tangential velocities within the circumferential cavity, caused by a constriction within the compact combustor, extinguishing the flame holders present. To improve upon the efforts of Bohan et al. [1], Holobeny et al. [2] designed a compact combustor equipped with bluff-body flame stabilization techniques to enable an increase in combustor fluidic volume, thereby reducing the velocities within the combustor section. As a result,

the new compact combustor, integrated into the same JetCat P90-RXi engine, was able to spool up to an idle condition of 36,000 RPM on gaseous propane fuel before flame-out occurred at increased mass flow rates. To carry on this investigation, it was recommended that the fuel be changed from gaseous propane to liquid kerosene. The present research looked to modify the compact combustor designed by Holobeny et al. [2] to be integrated into the dimensionally similar JetCat P160 RXi-B engine to operate on liquid kerosene fuel, and to scale the P160 compact combustor up to the larger P400 engine scale to investigate improved combustor performance.

1.2 Small Gas Turbine Engine Integration

The small-scale gas turbine engines used in the past and current compact combustor research feature single-stage compressor and turbine sections, as shown in Figure 1. At this scale, a radial compressor more efficiently supplies the engine with an appropriate pressure ratio compared to a multi-stage axial compressor. Additionally, the radial compressor only needs to be powered by a single-stage turbine, which reduces the complexity of the design and reduces the mechanical losses of the system compared to a large-scale gas turbine engine. While the rotating turbomachinery can be scaled down linearly to accommodate the smaller form factor of these hobbyist engines, combustor length is governed by flame length and residence time requirements, which do not scale linearly. As a result, the combustor within the JetCat P90 RXi, for example, needs to occupy roughly 60% of the total length of the engine to meet this requirements. If a novel combustor were designed that could reduce the length of the combustor, this would have significant improvements on the engine's thrust-to-weight ratio.

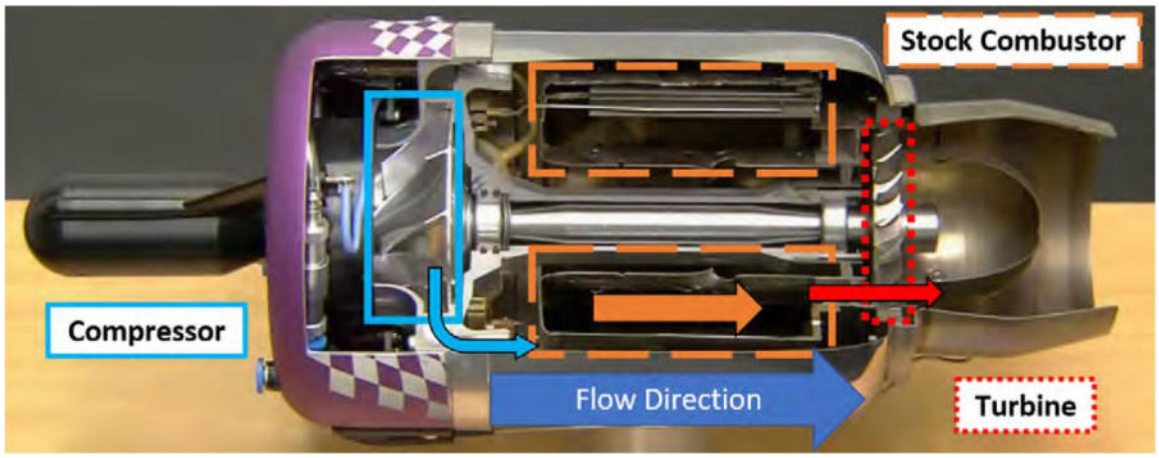

Figure 1. Cut-away of a JetCat P90-RXi Engine [3]

1.3 Objectives

The primary goal of this research was based on previous research performed by Bohan et al. [1] and Holobeny et al. [2], who demonstrated the viability of implementing a UCC into a small-scale gas turbine engine. As Section 2.2.1 discusses, Holobeny et al. [2] were able to integrate a compact combustor equipped with a bluff-body flame-holding mechanism into a JetCat P90 RXi and spool it up to an idle condition of 32,000 RPM using gaseous propane fuel. At higher mass flow rates, the engine flamed-out. A likely culprit was the choice of fueling used, as gaseous propane could be susceptible to pressure fluctuations during the combustion process. Rather than a constant flow rate of propane being injected into the combustor, locally rich and/or lean pockets could develop which could cause an instability and lead to blow-out.

This set the foundation of the current research which sought to operate the compact combustor designed by Holobeny et al. [2] on liquid kerosene rather than gaseous propane. Rather than using the JetCat P90 RXi engine that Holobeny et al. [2] used, a similarly sized JetCat P160-RXi-B engine was used. Thus, the primary goal of this research was to incorporate a compact combustor into a small-scale JetCat engine to operate at full power using liquid kerosene fuel. To achieve this, there were several

sub-objectives to accomplish.

1. Modify the compact combustor designed by Holobeny et al. [2] to be integrated into the JetCat P160-RXi-B engine.

2. Test the compact combustor designed by Holobeny et al. [2] in the JetCat P160-RXi engine with rotating turbomachinery and liquid kerosene fuel to achieve self-sustained operation at the maximum sustainable speed.

3. Design a compact combustor for the larger JetCat P400 scale engine in an effort to resolve the residence time issues associated with the smaller scale engines.

4. Analyze the novel compact combustor at the P400 scale through the use of computational fluid dynamics software at idle, mid-power, and design conditions.

5. Manufacture and test the P400-scale compact combustor in a non-rotating configuration at the three conditions to determine the combustor's viability an a rotating engine configuration.

1.4 Novelty of Research

The research presented here built off the previous work of Holobeny et al. [2]. They incorporated a compact combustor into a small-scale gas turbine engine and achieved self-sustained operation at an idle condition, which was an improvement over the work of Bohan [4], who was the first to achieve any self-sustained operation with a UCC. This work looked to achieve self-sustained operation at higher mass-flow conditions utilizing a more desirable fuel source, all while utilizing a novel combustor design.

This was achieved by modifying the compact combustor designed by Holobeny et al. [2] to integrate into the similarly sized JetCat P160 engine to operate on

liquid kerosene fuel. The previous combustor operated on gaseous propane, which was not an incompressible fluid and was susceptible to pressure fluctuations during operation, which likely caused combustion unsteadiness and led to blowout. Switching fuels to liquid kerosene would solve this issue since kerosene can be considered an incompressible fluid within the operating regime of the engine. To test the current compact combustor in the P160 engine, Air Force Research Laboratory's Small Engine Research Lab (SERL) Test Stand 5 was utilized where the engine followed the same instrumentation setup as Holobeny's [3] P90 configuration.

To make use of the increase in fluidic volume and residence time in larger scale engines, it was desirable to scale the P160 compact combustor up to the P400 scale engine to observe improvements in the combustor's operability. The design of the P400 compact combustor was aided and optimized through the use of computational fluid dynamics, and analyzed at off-design and design conditions to ensure optimal performance across the engine's operating range. With an optimized computational design, a novel non-rotating test rig was designed to test the combustor prior to testing in a rotating configuration.

II. Background

The objective of this research was to design a compact combustor to operate within JetCat P160 and P400 hobbyist engines on liquid kerosene. To meet this objective, several fields were studied. Section 2.1 discusses the theory behind ultra-compact combustor research and how it can reduce required combustor length and thus the overall length of an engine. This prior research led to the development of the bluff-body combustor, which utilizes a principle known as bluff-body flame stabilization, disccused in Section 2.3, as it's primary mechanism to ensure stable combustion while having a reduced combustor length required. Coupled with bluff-body flame stabilization is turbulent premixed combustion, discussed in Section 2.4, where important premixed combustion concepts such as the Damköhler number and liquid-fuel evaporation are discussed. To incorporate a novel combustor design into a small engine, an understanding of the engine and all of its integral components is required, which is discussed in Section 2.5. Additionally, the section discusses parameters such as pattern and profile factors, which need to be addressed in order to ensure proper integration with the rotating turbomachinery. To validate the scaling of the compact combustor from the smaller P160 size to the larger P400 scale, CFD was used. Section 2.6 discusses the relevant models and grid structures that are used for combustor analysis.

2.1 Ultra-Compact Combustor

Axial combustors intake air from the compressor where a portion of the air is introduced into the primary zone to be mixed with fuel and burned, while the rest of the air is directed around the chamber to be introduced into the secondary and dilution zones. To achieve complete combustion prior to the combustor exit plane,

the flame must be contained within the combustor. This means the length of the combustor is governed by the flame length leading to long combustors in order to ensure ample residence time for the fuel to achieve complete combustion. This creates a practical limit in combustor size. To achieve a shorter, more compact combustor, a different mentality in how to have a combustor that achieves a similar residence time is required.

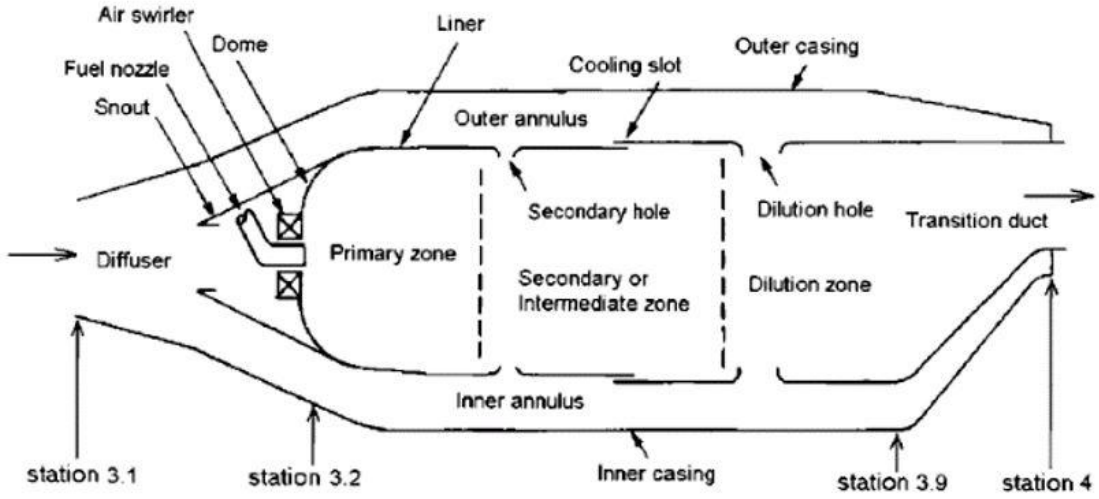

Figure 2. Traditional, axial combustor layout [5]

Two recent combustor designs have been investigated in the literature and aim to reduce the axial length required for a burner section in an engine. These include the trapped vortex combustor (TVC)[6] and high-g combustor (HGC)[7]. While both combustors strive for reduced axial length, both differ from the flow principles they use to achieve this length reduction.

Starting with the trapped vortex combustor, illustrated in Figure 3, a TVC consists of three main components, a forebody, cavity, and an afterbody. Bulk flow travels past the forebody creating a shear layer at the edge of the cavity. Air driver jets from the afterbody inject air into the cavity opposing the direction of the bulk flow. The

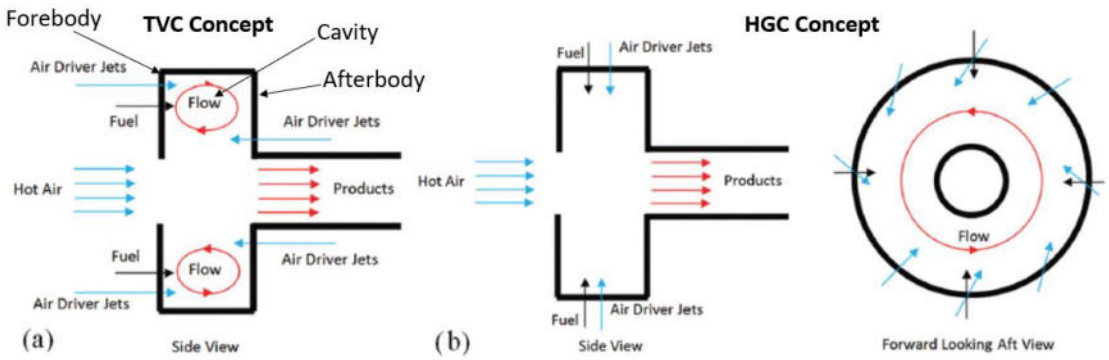

Figure 3. TVC and HGC designs from Brionnes et al. [8]

air driver injection coupled with the shear layer establishes a trapped vortex which aids as a flame holder to promote stable combustion. This vortex allows for a rapid mixing and exchange of products between the cavity and bulk flow [6].

The high-g combustor, also shown in Figure 3, utilizes high-g centrifugal loading as its mechanism to shorten its length while ensuring sufficient residence time. To introduce g-loading into the cavity, air is introduced circumferentially. This g-loading forces the heavier unburned gases to the outer diameter of the cavity while the lighter products migrate toward the bulk flow to be entrained and exhausted. This radial migration significantly increases the residence time since the unburned reactants are held within the cavity until they are burned. Additionally, the g-loading had been shown to enhance the combustion process [5].

2.1.1 Previous UCC Research.

At the Air Force Institute of Technology (AFIT), a majority of research has been aimed towards optimizing high-g combustor performance for use in a gas turbine engine. Figure 4 shows a UCC experimental rig used by Damele et al. [9]. In this UCC configuration, flow entered through a diffuser where a portion was directed towards the core flow or cavity flow. The cavity flow passed through an air driver

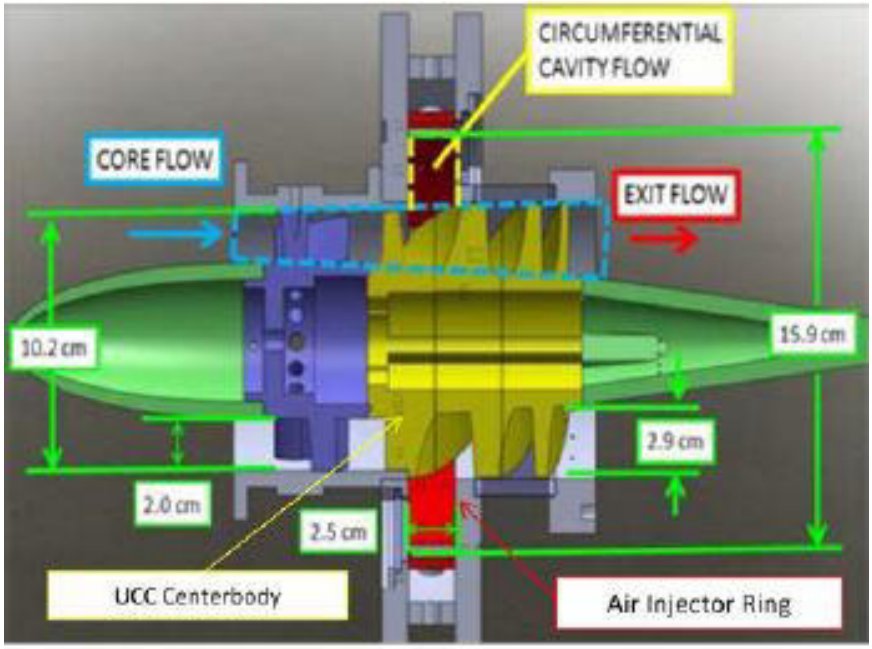

Figure 4. UCC Experimental Rig Used by Damele et al. [9]

plate where it was circumferentially swirled before entering the circumferential cavity. Fuel was sprayed either radially or circumferentially into the cavity and burned. The products from the cavity flow met up with the core flow via a hybrid guide vane, which served as a tool to help migrate the products towards the core flow to be exhausted [9].

One of the challenges of high-g ultra-compact combustors has been controlling product migration from the circumferential cavity to the core flow and the first turbine stage. Due to the high-g loading environment, a majority of the combustion products were entrained towards the outer diameter of the cavity, causing peak temperature locations on the first turbine stage to occur towards the tip of the blades, which significantly reduced turbine life. Damele et al. investigated which experimental parameters largely affected UCC combustor performance and exit temperature and pattern factor profiles [9]. These experimental parameters included variations in cavity equivalence ratio, g-loading, swirl direction, and mass flow ratio. The results

of this investigation found temperature and pattern factor profiles that exhibited a natural skew towards the outer diameter (OD), and further investigation found that these profiles were most sensitive to mass flow ratio. Variation in core-to-cavity flow splits greatly affected the amount of heat released at the exit plane, causing the magnitudes of the peaks in the temperature distributions to change [9].

In efforts to reduce the skew in the temperature distribution towards the OD, Cottle et al. aimed to redesign the hybrid guide vane (HGV) centerbody equipped with a radial vane cavity (RVC) [10]. This RVC, shown in Figure 5, featured a forward and backward facing step placed on the pressure and suction sides of the HGV respectively directly underneath the circumferential cavity. The implementation of these radial cavities were used to pull in combustion products from the circumferential cavity into the center of the vane passages to create a more desirable temperature distribution at the vane exit where peak temperatures occur towards the mid-span [10]. With the RVC implemented in the experimental rig, circumferential flow migration was improved, however it also had the effect of prematurely quenching some of the reactions passing through the guide vane passages leading to reduces exit temperatures.

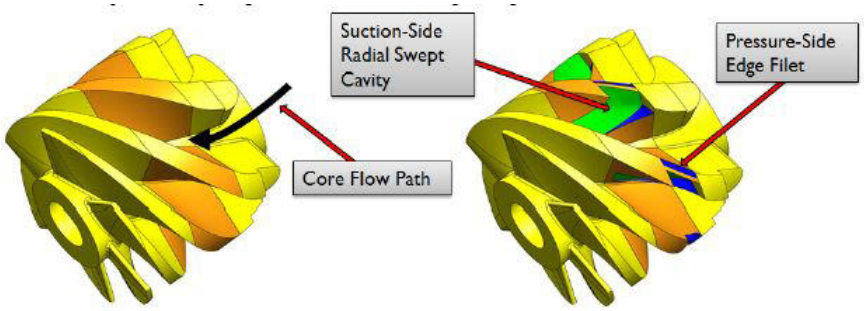

Figure 5. Comparison Between HGV used by Damele et al. (left) and Cottle et al. (right) [10]

To improve product formation within the vane passages, cavity air drivers were implemented to force more air upwards into the circumferential cavity. Both of these modifications led to smoother radial temperature distributions at the exit plane and

reduced radial location of peak temperatures. While product migration was improved, combustion instabilities in the circumferential cavity occurred well within the operating range of the UCC. Due to the radial injection of fuel into the circumferential cavity, less time was allotted for fuel-air mixing which created rich fuel pockets along the OD of cavity. Over time, these fuel pockets would accumulate in size until reactions could no longer be sustained within the cavity and were pushed out of the cavity entirely.

To resolve the fuel accumulation issues discovered by Cottle et al., DeMarco et al. designed a new circumferential cavity [11]. Rather than introducing fuel into the circumferential cavity radially, fuel was introduced tangentially along the surface of the outer ring. This enabled fuel-air mixing throughout the entirety of the circumferential cavity, which dropped the local equivalence ratio, promoted reactions within the full cavity height, and increased tangential velocities and g-loading within the cavity [11].

These changes were implemented with a 6-step ring and a hole-area reduction in the front air driver plate. Looking at the 6-step ring, shown in Figure 6, six backward facing steps were created as primary fuel and air drivers into the circumferential cavity. Additionally, these backward facing steps created recirculation regions which enabled a pilot flame to be anchored at several locations within the cavity, promoting stable combustion across the operating range [11].

When tested, the 6-step ring was unable to sustain continuous combustion at the designed flow split and mass flow conditions. Further investigation through particle imaging velocimetry (PIV) coupled with computational fluid dynamics (CFD) results found that the centrifugal loading within the cavity at design conditions was insufficient at creating strong recirculation regions at the backward facing steps, leading to a lack of flameholders present within the cavity [11]. To resolve this issue, an

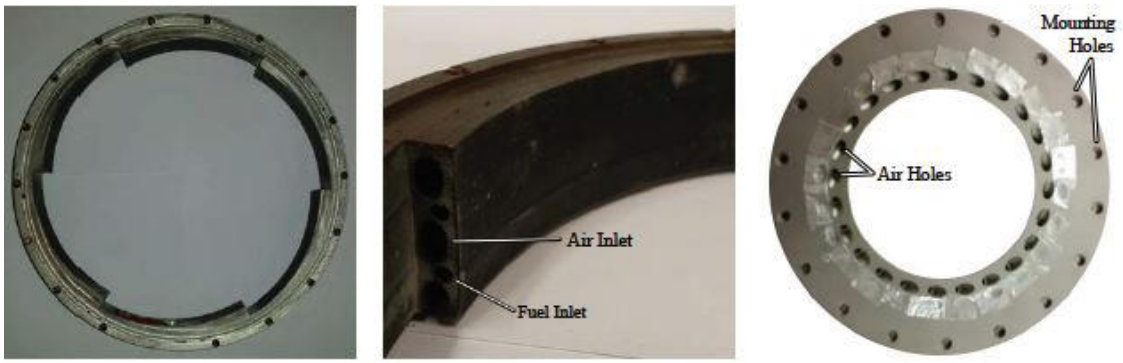

Figure 6. 6-Step UCC Cavity Designed by DeMarco et al. [11]

additional UCC cavity outer ring was manufactured, now featuring twelve steps. The additional steps created additional recirculation regions where flames could be anchored [11]. Additionally, every other step was used for fuel injection only, while the others injected both fuel and air circumferentially into the cavity. These fuel-only steps promoted flame holding while the fuel-air steps helped to control the equivalence ratio within the cavity. With the changes made to the new UCC cavity outer ring, the 12-step ring was able to maintain high combustion stability over a large range of cavity equivalence ratios compared to the stock design used by Cottle et al. [11]. While exit temperatures were found to be lower than the stock design, pattern factor profiles were found to be desirable. Further research by DeMarco et al. found that bulk cavity velocities in the 12-step outer ring lead to very low cavity g-loading, suggesting that combustor performance was a result of residence time [12].

2.1.2 UCC Gas Turbine Engine Integration.

In efforts to progress towards a UCC-gas turbine engine integration, Bohan and Polanka designed a UCC based off of their existing 12-step circumferential cavity research to fit within a JetCat P90 RXi hobbyist engine [1]. To ensure integration with the small gas turbine engine, there were several design challenges to overcome. First,

traditional UCC designs have recessed combustion cavities that lay on the outside of the engine housing [1]. To appeal to modern-day gas turbine engines, the UCC cavity needed to exist inside the engine casing in some manner. Second, a reoccurring challenge with UCC's has been combustion product migration. Traditional UCC's burn circumferentially around the outer diameter of the engine and rely on the core flow to push this circumferential flow axially downstream towards the turbine and exhaust nozzle. This product migration, traditionally, produces uneven temperature distributions, which leads to undesirable pattern factors [1]. Additionally, the hot combustion products remained tied to the OD of the engine housing, which placed an undesirable thermal load on the tips of the turbine rotors [1].

To overcome these design challenges, Bohan and Polanka designed the UCC seen in Figure 7. Air entered through the primary zone inlet ramps and be turned for circumferential injection through an array of backward facing steps. Every other step was responsible for air injection, while the others were responsible for fuel injection similar to the scheme used by Demarco et al. [1]. The backward facing steps acted as flame holders to secure a pilot flame in the recirculation regions behind the steps. The primary zone was separated from the secondary zone through a constriction, which allowed for a transition from circumferential to axial flow.

During experimental testing, self-sustained operation was achieved at a half-idle condition of 14,100 RPM until flameout occurred at higher mass flow rates, which was a result of reactions being pushed out of the primary zone [1]. These reactions were pushed out of the primary zone as a result of the hardware constriction within the UCC, increasing the tangential velocities beyond the stability limit. However, at the half-idle condition, engine exit temperature profiles were comparable to the stock JetCat P90 RXi baseline data, suggesting that the UCC was matching similar performance to the stock combustor with a length savings of 33%.

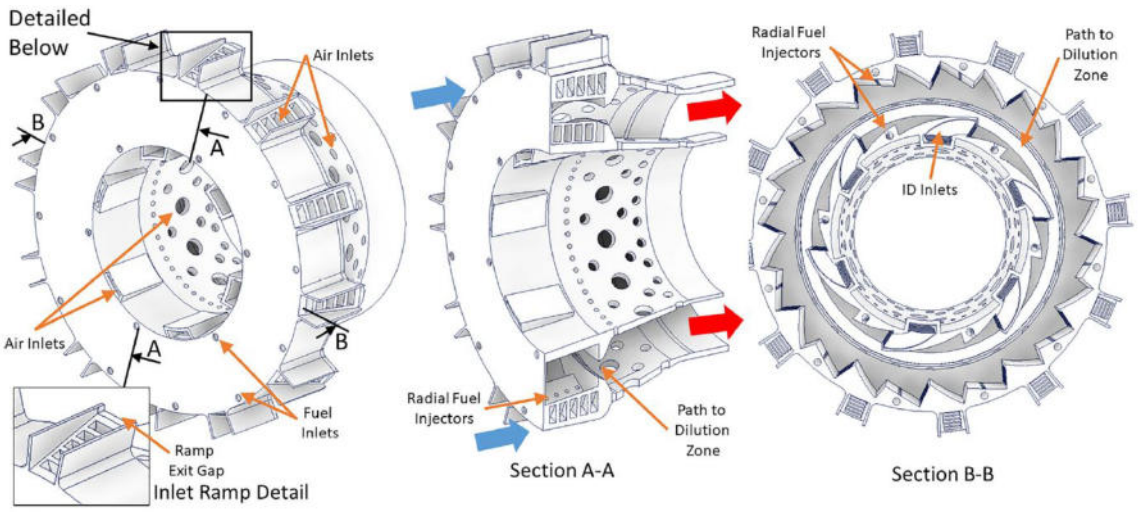

Figure 7. UCC designed by Bohan and Polanka for integration with a JetCat P90 RXi engine [1]

To improve upon Bohan and Polanka's UCC design for the JetCat P90 RXi engine, Holobeny et al. redesigned the UCC to possess a larger chamber volume to reduce the tangential velocities causing blowout at the higher mass flow conditions [3]. Additionally, the redesigned UCC was equipped with better flame holding mechanisms to promote improved flame and combustion stability across an operating range [3]. Figure 8 shows the compact combustor redesigned by Holobeny et al. [3]. Flow left the compressor and pass through the holes on the forward dome along with the dilution holes on the outer diameter of the casing. The compressor-fed air passing through the forward dome struck a plate creating a recirculation region on the backside of the impingement plate. This allowed the fuel to be injected into this region. This enabled the fuel and air to mix and a stable flame holding region to form [**?**]. This novel combustor design achieved a 33% length savings compared to the UCC designed by Bohan and Polanka [3]. A comparison can be seen in Figure 9 where a 32% increase in chamber fluidic volume can be observed.

During non-rotating testing, the UCC repeatedly ignited at low fuel and air flow rates. These tests showed the viability of the bluff-body flameholder's ability to act

as a flameholder and promote stable combustion [3]. An equivalence ratio test was performed where the combustor exhibited a maximum equivalence ratio of 0.235 at an idle condition. This corresponded to an average exit temperature of 1086 K, which was similar to CFD results. Pattern factor profiles were generated both experimentally via a thermocouple rake, and through CFD. Experimentally, the pattern factor was found to be 0.35. During rotating testing, the engine was able to reach an idle condition of 36,000 RPM, however at higher mass flows the engine flamed-out.

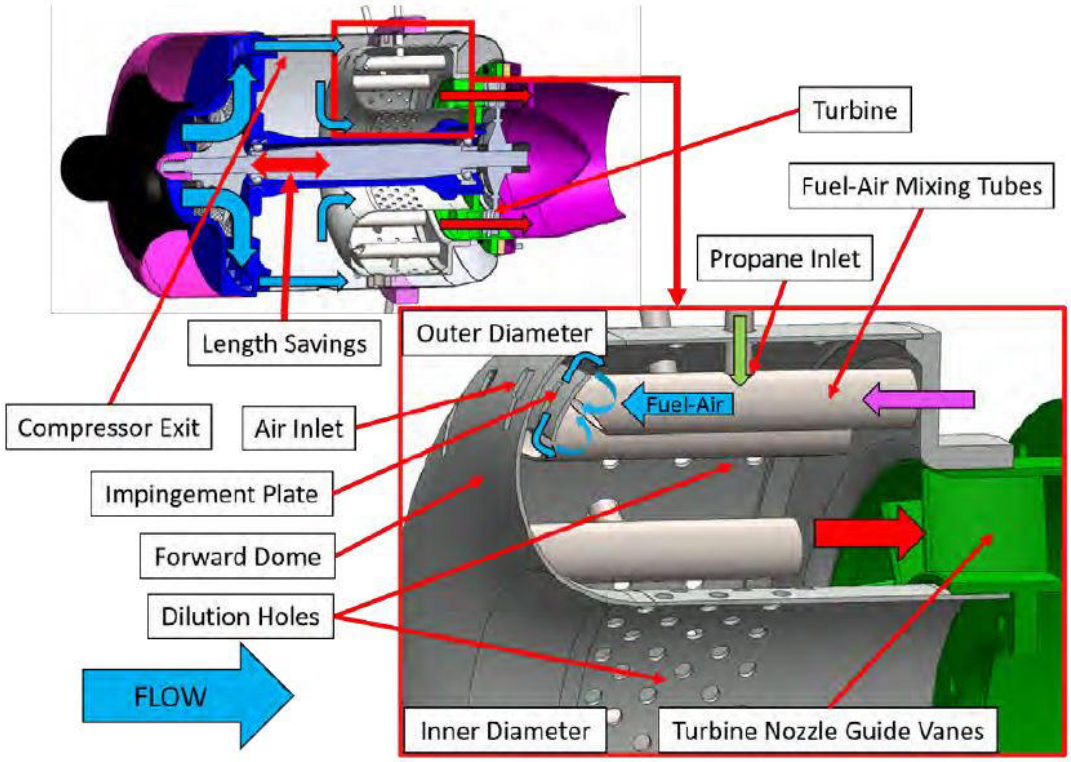

Figure 8. UCC designed by Holobeny et al. for integration with a JetCat P90 RXi engine [3]

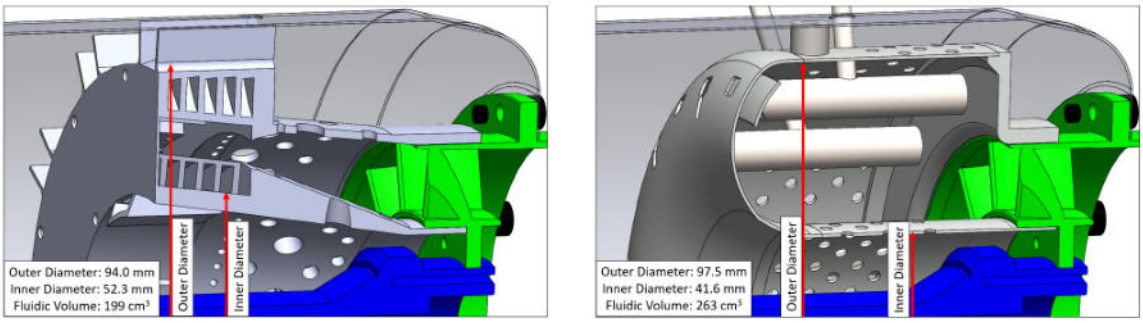

Figure 9. UCC comparison between Bohan and Polanka [1] (left) and Holobeny et al. (right) [13]

2.1.3 Previous JetCat P90 RXi Combustor Testing.

Holobeny et al. tested the JetCat P90 RXi engine equipped with a novel compact combustor in two different stages; a non-rotating and rotating configuration [3]. Tests for the non-rotating configuration were performed in the Combustion Optimization Analysis Laboratory (COAL) within AFIT whereas tests for the rotating configuration were performed within Air Force Research Laboratory's (AFRL) SERL Test Stand 5.

The non-rotating testing enabled the engine, or compact combustor, to be further instrumented and analyzed to determine pattern and profile factors prior to the compressor and turbine being installed. Figure 10 shows the non-rotating test setup used be Holobeny et al. where air was supplied to the engine through a supply line [3]. Additionally, gaseous propane was supplied to the fuel holder ring for fuel injection through propane tanks. On the backside of the JetCat mounts laid a thermocouple rake, shown in Figure 11, which was capable of gathering temperature data at the combustor exit plane over a 60-degree span. This enabled pattern and profile factor distributions to be determined prior to turbine installation to ensure the new compact combustor produced desirable pattern and profile factors [3]. Thermocouple rake data for the non-rotating testing configuration was gathered for three test

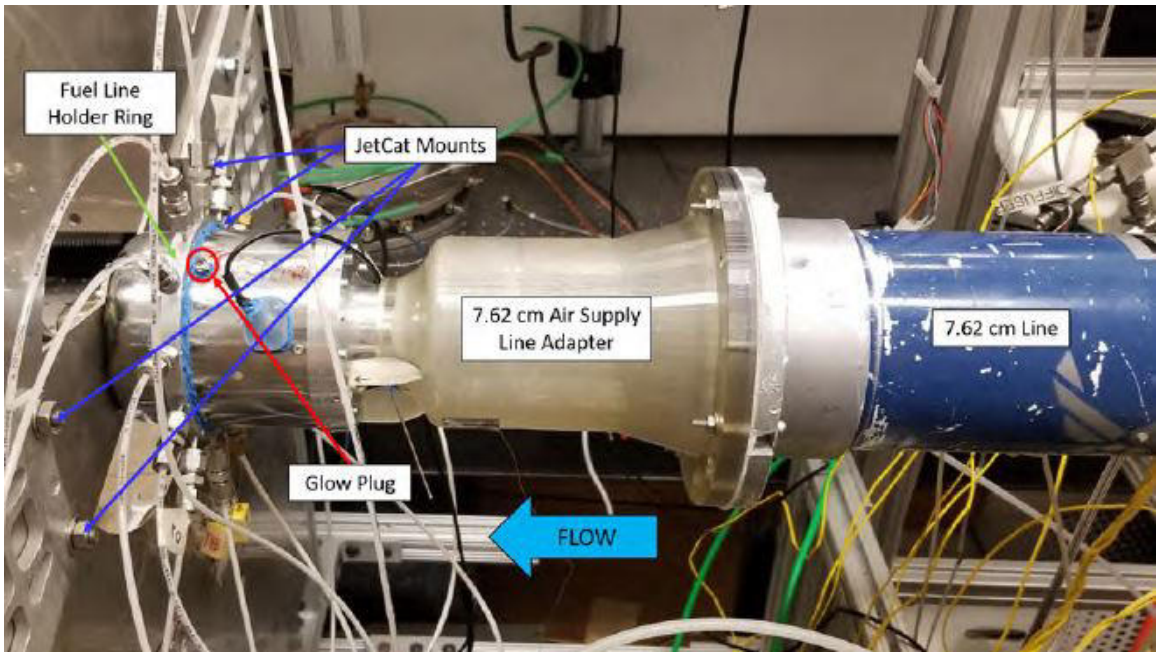

Figure 10. Non-rotating hardware setup used by Holobeny et al. [3]

conditions. These conditions included a light condition, which was the lowest point the engine ignited to begin a consistent burn, a middle condition, which bridged the gap between the lowest point and the idle condition, and an idle condition, which matched the idle air and fuel flow rates from JetCat [3]. The pattern factors for the light and middle conditions were found to be 0.18 and 0.24 respectively, while the idle conditions produced a considerably higher pattern factor of 0.38, which falls within the desirable bounds mentioned in Section 2.5.1 [3].

Additionally, exit temperature measurements were recorded and compared against air mass flow and equivalence ratio, shown in Figure 13. At light and middle conditions, equivalence ratios highest for these cases which led to high average exit temperatures. As air and fuel flow ramped up towards the idle condition, however, the average exit temperature lowered resulting in more desirable exit temperature magnitudes [3].

Rotating testing was performed within AFRL's test stand 5 where Holobeny et

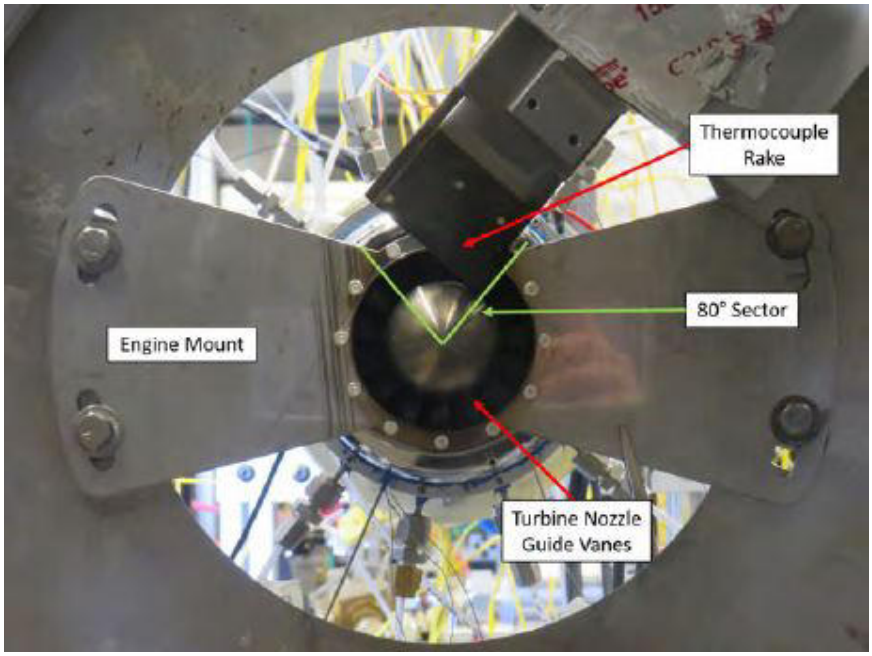

Figure 11. Thermocouple rake used by Holobeny et al. during non-rotating testing [3]

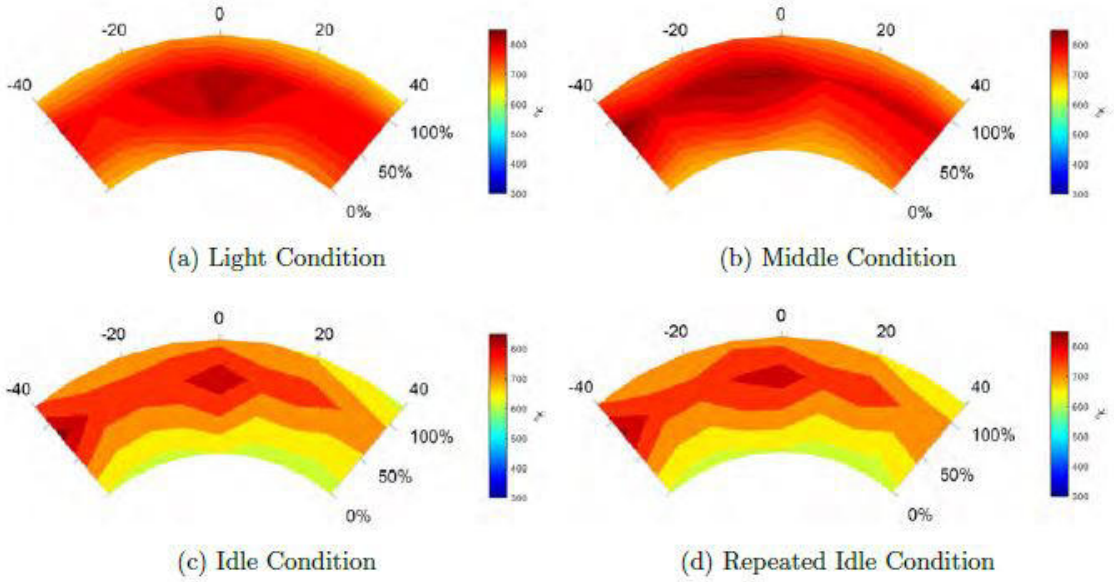

Figure 12. Temperature (K) contours from the thermocouple rake data [3]

al. were able to successfully bring the engine up to an idle condition of 36,000 RPM before flame-out occurred at higher mass flow conditions [2]. Upon disassembly of the

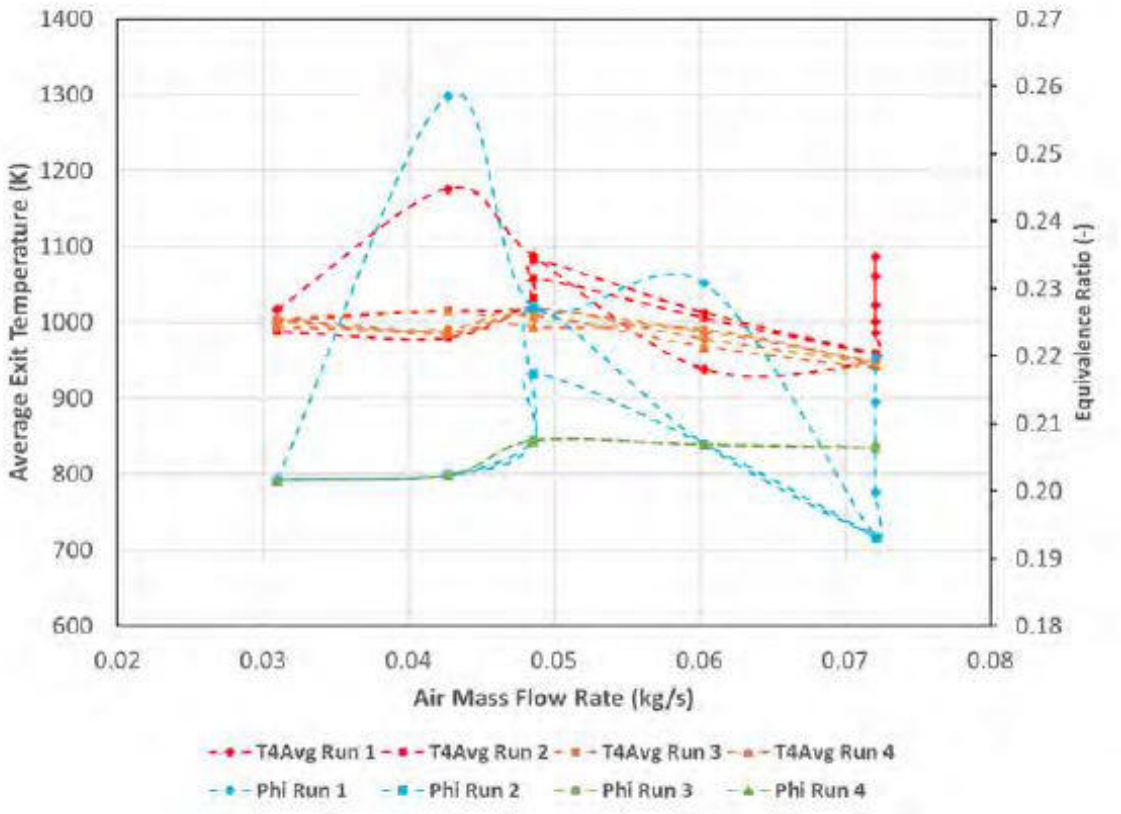

Figure 13. Exit temperature measurements plotted against air mass flow and equivalence ratio [3]

JetCat P90 RXi engine, uneven scalloping patterns were noticed along the backside surfaces of the combustor, shown in Figure 14. These uneven patterns suggest the likelihood of uneven fuel distribution during the 36,000 RPM test run of Holobeny et al. [2]. As Holobeny et al. [2] attempted to spool the engine higher by introducing more fuel, there was too much fuel in these localized areas and not enough in the others to hold a stabilized flame, leading to blowout. This uneven fuel distribution was most likely a result of the fuel nozzles not being choked, causing the injection to be influenced by pressure fluctuations during the combustion process. Transitioning towards liquid fuel injection through the use small 0.020" tubes will mitigate the effects of pressure perturbations, since liquid kerosene is nearly incompressible within

the operating range of the engine, and possibly resolve this fuel distribution issue.

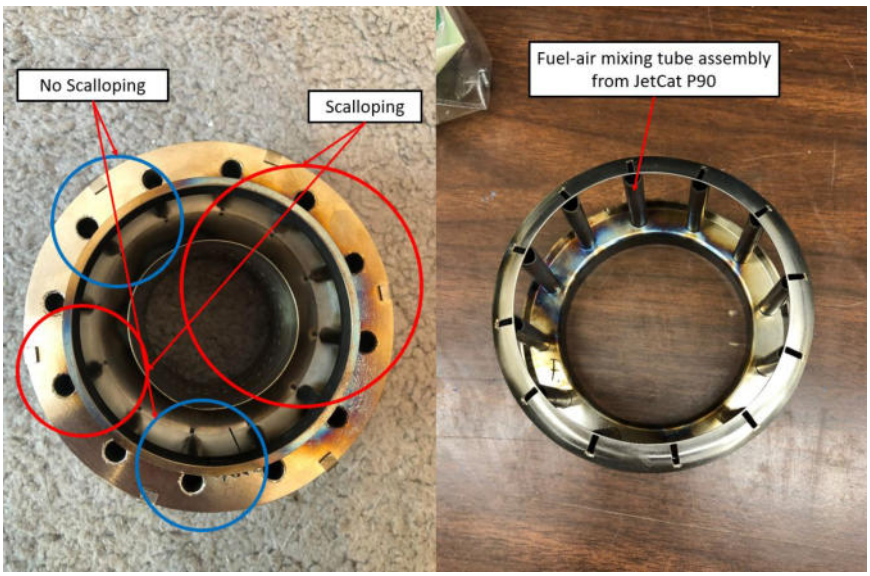

Figure 14. Burn patterns seen on the compact combustor used by Holobeny et al. [2] after testing

2.2 Trapped-Vortex Combustors

A TVC consists of three main components, a forebody, a circumferential cavity, and an afterbody. The forebody is the upstream face of the circumferential cavity, while the afterbody is the downstream face of the cavity. Bulk flow travels past the forebody creating a shear layer at the edge of the cavity. Air driver jets from the afterbody inject air into the cavity opposing the direction of the bulk flow. The air driver injection coupled with the shear layer establishes a trapped vortex which aids as a flame holder to promote stable combustion. This vortex allows for a rapid mixing and exchange of products between the cavity and bulk flow [14].

There are a couple important parameters surrounding TVC design and characterization such as cavity aspect ratio and air loading parameter (AL). Equations 1 and 2 show how the cavity aspect ratio, where L represents the length of the cavity and D_o

represents the diameter of the forebody, and AL are defined, where V_{cavity} represents the volume of the cavity, respectively [4].

$$L/D_o = (-1.62)D_1/Do + 1.79 \tag{1}$$

$$AL = \frac{\dot{m_{air}}}{V_{cavity}\frac{P_{inlet}}{101.325}^{1.75}e^{T_{inlet}/300}} \tag{2}$$

Mair [15] and Little and Whipkey [16] found that a stable vortex is trapped inside a cavity sized for minimum drag. At the minimum drag configuration, which corresponds to a L/D_o=0.60, very little fluid is entrained into the cavity. Colcord and Sirignano [17] found that a long shallow cavity achieved better mixing than a square cavity. Square cavities couldn't maintain a flame beyond Re=5,000, while cavities with an L/D_o=2 could maintain a flame up to a Re=10,000. Additionally, they found that parallel injection, which involves fuel and air being injected on the same plane, showed the highest burning efficiency. Contrasting, reinforcement injection showed the lowest burning efficiency.

Roquemore et al. [18] highlighted the benefits of the TVC showing that the TVC achieved greater than 99% efficiency and had a significantly better (up to 50%) improvement in ignition, and altitude relight compared to a traditional swirl-stabilized combustor. The TVC also achieved a 40-60% reduction in NOx emissions. All of these benefits were gained while achieving a 40% wider operating range over a traditional combustor.

2.3 Bluff-Body Flame Stabilization

Given the turbulent flow regime combustors typically operate within, the flame front is inherently complex which presents several challenges for holding and propagating a flame. To achieve a stable turbulent flame, a resistance to liftoff, flashback,

and blowout is required. Liftoff occurs when the flame is no longer attached to the primary fuel port, flashback occurs when the flame propagates through a region without quenching, and blowout occurs when all reactions are quenched and a flame can no longer propagate and is extinguished [19]. Resisting blowout for an anchored flame in a turbulent regime is often more applicable than flashback or liftoff for gas turbine combustors. To be sufficiently far from blowout occurring, flow techniques in which the local turbulent flame speed are matched with the local mean flow velocity, and ignition techniques are often utilized. Some of these methods include bypass ports, burner tiles, bluff bodies, and swirl or jet-induced recirculating flows [19].

Bypass ports are often utilized in Bunsen burners and propane torches in which low-velocity openings are used as a method to relight the main flame in the event the flame is blown out [19]. Refractory burner tiles are used to create passageways aft of an industrial burner, for example, to stabilize a flame. These burner tiles conduct the combustion temperatures creating a nearly adiabatic wall boundary condition [19]. This causes heat to radiate back towards the flame maintaining higher burning velocities and flame temperatures. Additionally, burner tiles often exhibit large divergence angles which causes separation along the wall leading to the formation of recirculation regions. These recirculation regions entrain hot combustion products and introduces them back upstream with the unburned reactants to cause ignition and a stable flame-holding region [19]. Bluff bodies enable turbulent flames to be stabilized in the wake region further upstream in the flow-field. A general outline of a bluff body stabilized flame can be seen in Figure 15. Within the wake of the bluff body exists a recirculation region which entrains combustion reactants and products to promote flame anchoring and fuel atomization and ignition respectively [19].

Several bluff body shapes have been researched in efforts to reduce the likelihood of blowout occurring. Blowout for bluff body stabilized flames is largely dependent

upon the processes occurring within the recirculation region, which is also dependent upon the upstream flow velocity. To determine roughly at what velocity blowout may occur, the following equation for blowoff velocity, $v_{blowout}$, can be used

$$v_{blowout} = 2\rho_0 L(\frac{S_L^2}{\rho\alpha_T}) \tag{3}$$

where ρ_0 and ρ are the unburned and burned gas densities, L is the characteristic length of the recirculation zone, S_L is the laminar flame speed, and α_T represents the turbulent thermal diffusivity.

Swirl or jet-induced recirculating flows utilizes a recirculation region to anchor a flame. This recirculation zone is created by introducing a swirling component to the incoming fuel-air mixture. This swirling, or creation of recirculation regions, can be created by controlling jet direction in an appropriate manner into the environment. Figure 16 shows several flow patterns in conventional can combustors [19]. The presence of dilution holes enables core flow to enter the combustion cavity. The high velocity jet passing through the dilution hole causes recirculation regions to form along the backsides of the holes which aid in fuel-air mixing and flame anchoring.

To analyze the structure and dynamics of a turbulent bluff-body stabilized flame, Fugger et al. investigated the structure and dynamics of a turbulent bluff-body stabilized premixed propane-air flame [20]. The experimental setup, shown in Figure 17, featured an inlet-chocked orifice plate where a preheated, unvitiated propane-air mixture were introduced. Further downstream was the bluff body, which was a 38.1 mm equilateral triangle where the fuel-air mixture was ignited via an ethylene-air ignitor torch [20]. To visualize the stabilized flame within the wake of the bluff body, several laser diagnostic techniques were used, including planar laser-induced fluorescence (PLIF) and PIV. A CH_2O-PLIF was used to visualize the reactants side of the, while a OH-PLIF was used to visualize the products side, or the flame front. Figure

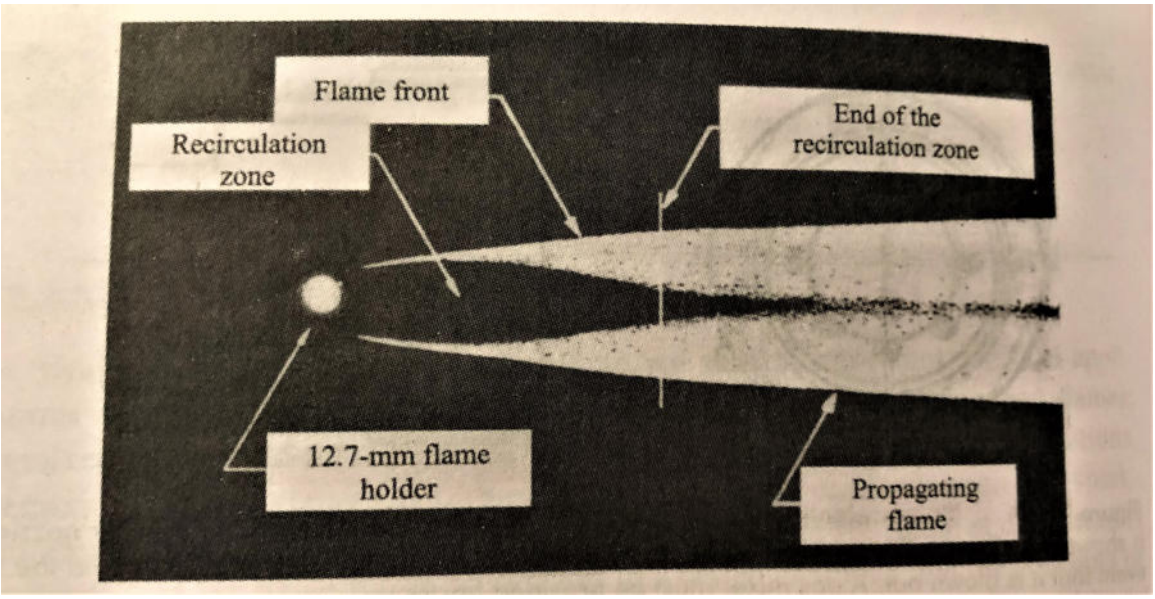

Figure 15. Turbulent flame stabilized by a bluff body [19]

18 shows simultaneous images of CH_2O-PLIF, OH-PLIF, along with the overlap between the two images coupled with PIV data to gain velocity vector data [20]. The CH_2O-PLIF, highlighted green, showed the preheat zone of the flame while the OH-PLIF, highlighted red, showed the flame front. The overlap between the two images, highlighted yellow, illustrated the thin reaction zone that lied between the preheat and flame-front regions respectively. These results agreed with the understanding that turbulent combustion lies within the preheat and reaction zones. Additionally, the highest levels of vorticity present in the flow-field were concentrated to narrow regions in the upper and lower shear layers [20].

Monfort et al. investigated quantifying the entrainment and decay behavior of the recirculation zone directly behind the bluff-body flameholder [21]. To visualize the recirculation region, sodium injection was utilized. Figure 19 showed PIV measurements behind the flameholder for an array of of equivalence ratios. The colorbar shows velocity magnitudes which help visualize the recirculation region behind the bluff-body. The differences between the sizes of the recirculation regions suggested

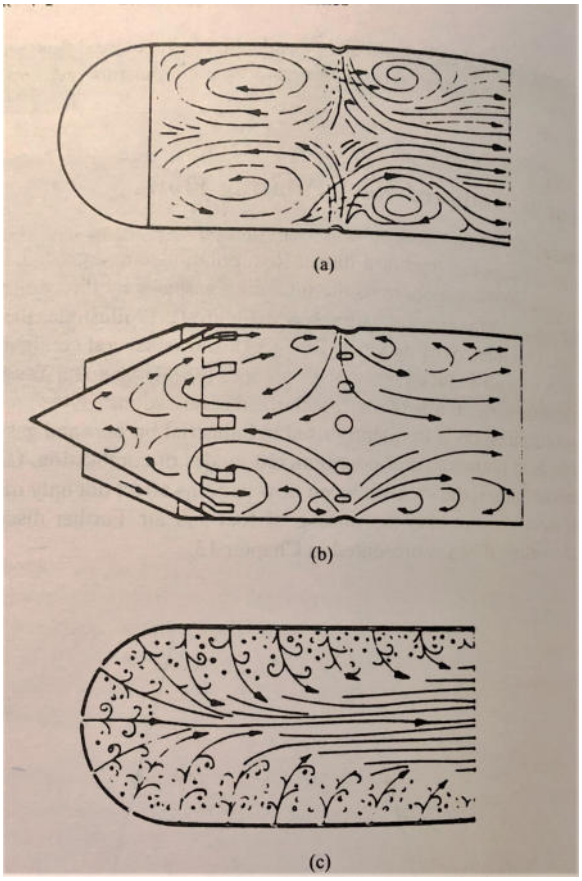

Figure 16. Flow patterns for can combustors with (a) single row of holes, (b) shrouded cone, and (c) multiple rows of holes [19]

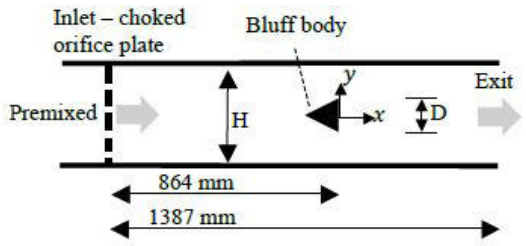

Figure 17. Bluff-body combustor experimental setup [20]

that the decay and entrainment behavior are highly dependent on operating conditions [21].

Allison et al. investigated flame structure of bluff-body stabilized flames and its influence on fuel distribution. The fuel injection was nonpremixed, jet in-cross-flow.

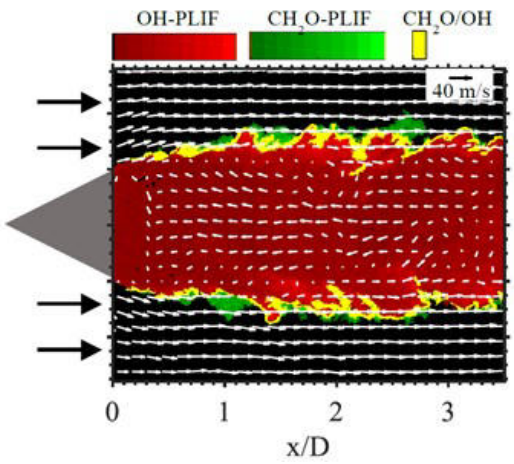

Figure 18. Overlapping PLIF images coupled with velocity vectors for the wake behind the bluff-body [20]

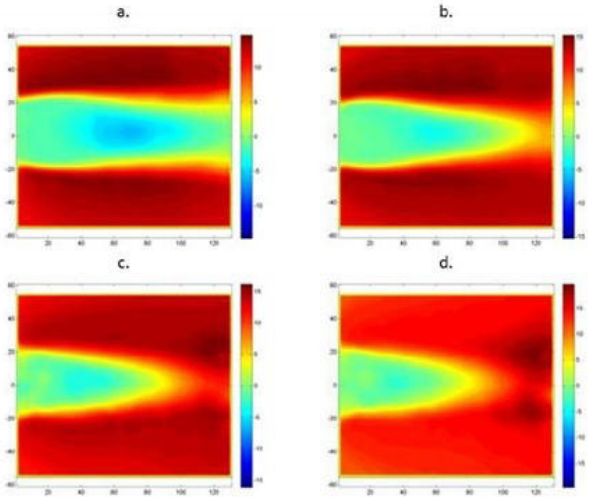

Figure 19. Axial velocity fields from PIV measurements for a bluff-body wake [21]

Chemiluminescence and planar fluoresence imaging of OH radicals were used to visualize the reaction regions behind the flameholders. It was found that combustion occurred in separated zones, which included preheat and reaction zones as expected [22].

2.4 Turbulent Premixed Combustion

Three flame regimes characterize turbulent premixed flames. This regimes are wrinkled laminar flames, flamelets in eddies, and distributed reaction as seen in Figure 20 [19], which illustrates these flame regimes and their relation to the Damköhler number and the turbulent Reynolds number. To differentiate these regimes from one another, various length scales are introduced. These length scales include the Kolmogorov microscale, l_K, and the integral length scale, l_0. The structure of a turbulent flame is governed by the relationship between these length scales and the laminar flame thickness, δ_L [19]. The wrinkled laminar flame regime lies within the kolmogorov length scale, the flamelets in eddies regime lies between the kolmogorov and integral length scales, and the distributed reaction regime lies beyond the integral length scale. In the context of flame structure, when the flame thickness is thinner than the Kolmogorov length scale, the flame can only wrinkle and distort [19]. On the other end of the spectrum, if the length scales are smaller than the flame thickness, the flame is no longer primarily driven by chemistry, but instead by momentum or turbulence [19].

2.4.1 Damköhler Number.

To understand and characterize turbulent premixed flames, the Damköhler number, Da, is often used, which can be described by the equation below

$$Da = \frac{\tau_{flow}}{\tau_{chem}} \tag{4}$$

where τ_{flow} represents the characteristic flow time and τ_{chem} represents the characteristic chemical time [19]. In the context of a burner, the flow time represents the time reactants spend in the burner before they are burned and exhausted, and the

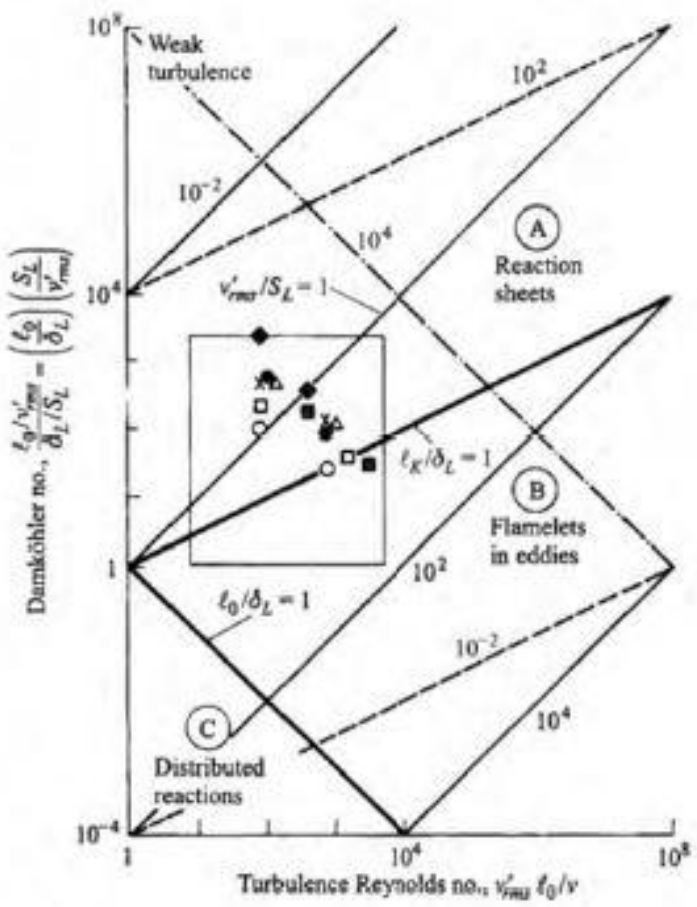

Figure 20. Characterization of turbulent premixed combustion [19]

chemical time represents the time needed for the reactants to under-go the necessary reactions to complete combustion. The Damköhler number can also be expressed in the following way

$$Da = (\frac{l_o}{\delta_L})(\frac{S_L}{v'_{rms}}) \tag{5}$$

where the characteristic flow time, τ_{flow}, is rewritten in terms of the integral length scale, l_o, and the relative turbulence intensity, v'_{rms}, and τ_{chem} is rewritten in terms of the laminar flame thickness, δ_L, and the laminar flame speed, S_L [19]. This formulation puts the Damköhler number into terms that can be interpreted from a given

flow-field. If $Da >> 1$, this corresponds to a fast-chemistry regime where the chemical reaction time is significantly greater than the residence time. The inverse is true if $Da << 1$, where reaction rates are slow compared to the mixing rates [19].

2.4.2 Liquid-Fuel Evaporation.

To transition from gaseous to liquid fuels, fuel atomization needs to be guaranteed to have proper fuel-air mixing and stable combustion. With gaseous fuels, droplet evaporation doesn't apply given the fuel is already atomized to readily mix with the incoming air and combust. For liquid fuels, the D^2 law can be used to estimate the time required for a fuel particle to fully atomize [19]. The D^2 law can be seen below

$$D^2(t) = D_o^2 - Kt \tag{6}$$

where the droplet diameter, $D(t)$, can be determined by knowing the initial droplet diameter, D_o, the evaporation constant, K, and the droplet lifetime, t. The evaporation constant can be described below

$$K = \frac{8\rho D_{AB}}{\rho_l} ln(1 + B_Y) \tag{7}$$

where ρ is the density of the air, ρ_l is the density of the fluid droplet, D_{AB} is binary diffusivity, and B_Y is the Spalding number, or transfer number. Given the fuel is liquid kerosene, or $C_{12}H_{26}$, the Spalding number can be determined, the binary diffusivity from the fuel droplet to the air can be estimated, and thus the evaporation rate can be found [19]. This enables the droplet lifetime to be determined.

To ensure fuel atomization when using a liquid fuel, traditional combustors in large-scale gas turbine engines commonly rely on swirlers, as shown in Figure 21. In this typical engine configuration, air exiting the compressor enters a dump diffuser to

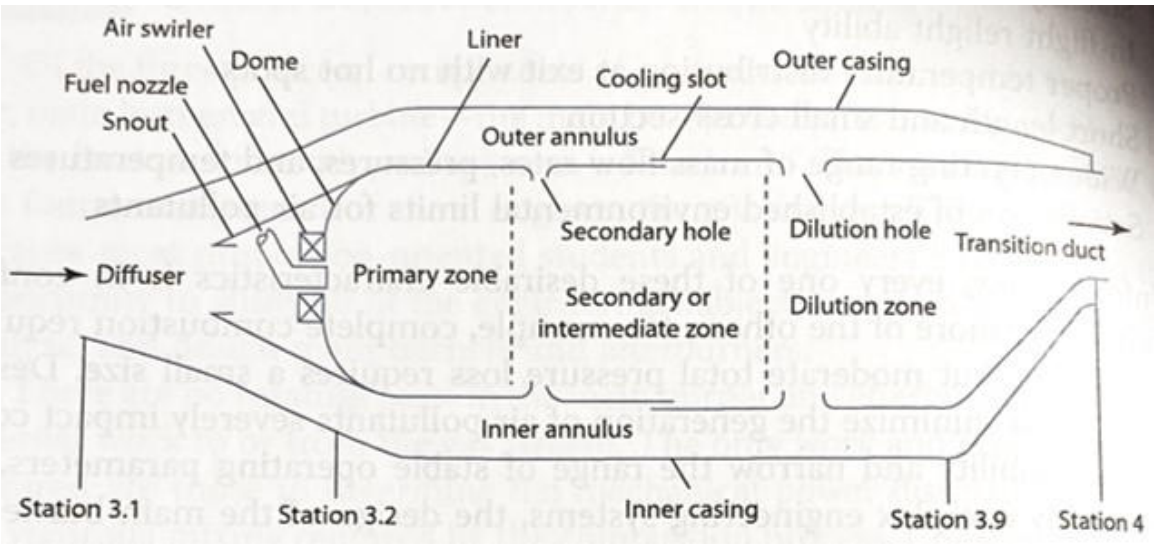

Figure 21. Traditional large-scale gas turbine engine combustor layout [19]

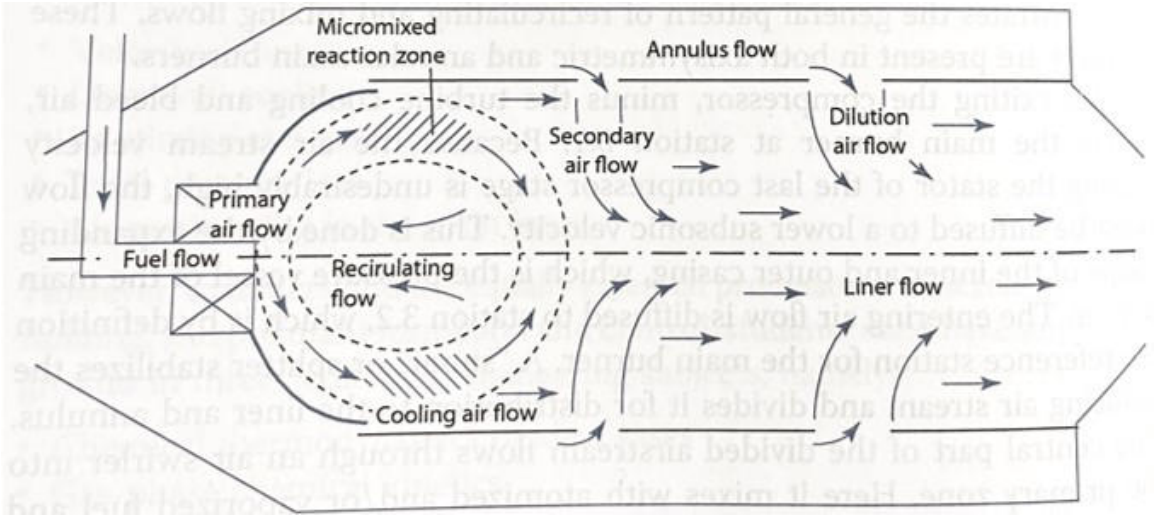

Figure 22. Traditional large-scale gas turbine engine combustor flow patterns [19]

lower the velocity of the air flow prior to burning [23]. A portion of the air flows around the combustor liner's inner and outer annulus, which is fed back inside the combustor to either cool the liner surfaces, quench reactions, or dilute the combustion products prior to turbine inlet. The primary air flow passes through the swirler located on the dome of the combustor liner. Liquid fuel passes through the center of the air swirler where all of the fuel is entrained, vaporized, and mixed with the core flow in the

recirculation region created downstream by the swirler, as shown in greater detail in Figure 22 [23].

The amount of swirl imparted on the flow is defined by the swirl number, $S^{'}$, defined in Equation 8.

$$S^{'} = \frac{2}{3} tan\alpha_{sw} [\frac{1 - (r_h/r_t)^3}{1 - (r_h/r_t)^2}] \tag{8}$$

In Equation 8, α_{sw} represents the angle of the swirler vanes, r_h represents the inner radius of the swirler, and r_t represents the outer radius of the swirler. A swirl number between 0.6 and 1.0 has been shown experimentally to be optimal which correlates to vane angles ranging from 35 to 50 degrees [23]. While this type of fuel injection device is commonly used in modern-day large-scale gas turbine engines, the fuel pressure required to supply the swirlers requires a fuel pump that may be exceedingly large and heavy relative to the size of the engine [24]. This is why small-scale engines rely on vaporization tubes as a means to vaporize the liquid fuel prior to injection within the primary zone of the combustor.

Vaporization tubes, as shown in Figure 23, are a type of fuel injection scheme commonly used in small-scale gas turbine engines which use "hook-like" fuel lines placed within a injection/vaporization tube so that fuel is injected opposing the direction of air flow through the engine [24]. This enables some of the heat released from combustion occurring in the primary zone of the burner to be transferred to the fuel-air mixture traveling down the fuel vaporization tubes, causing the fuel to vaporize and be premixed with air prior to injection towards the end of the tube.

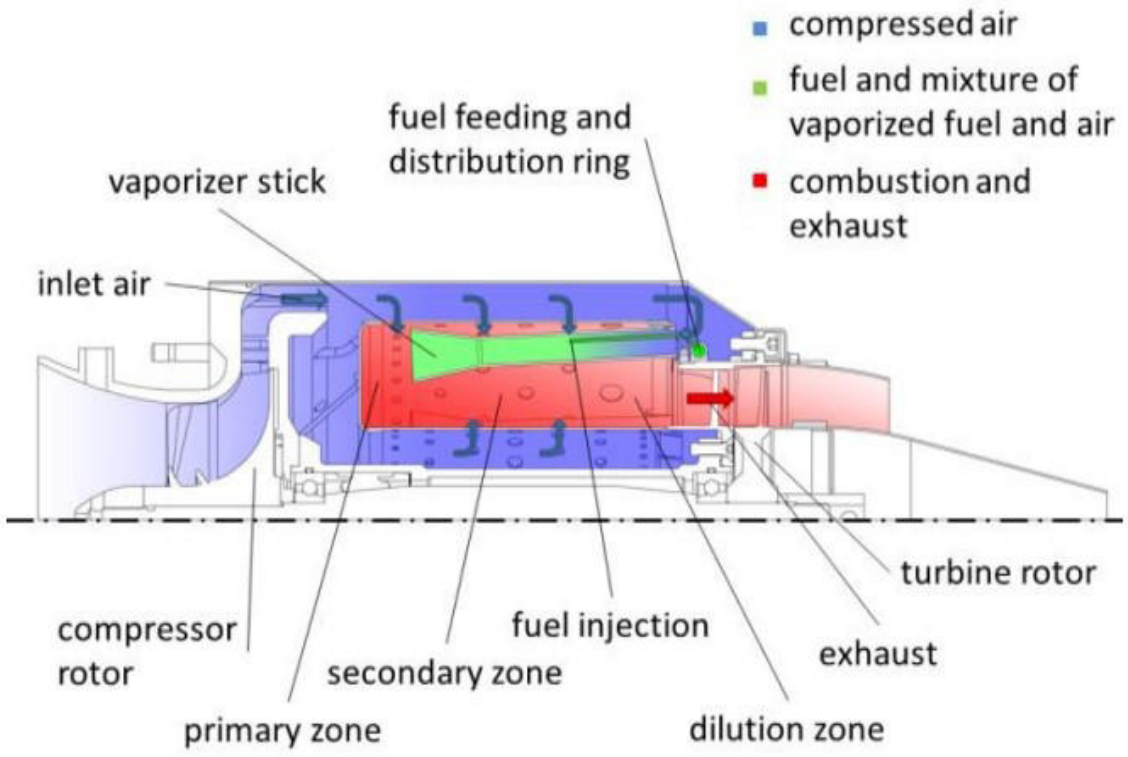

Figure 23. Fuel-injection scheme shown through the cross-section of a small-scale gas turbine engine [24]

2.5 Small Gas Turbine Engines

To investigate the operability of ultra-compact combustors integrated into gas turbine engines, small-scale gas turbine engines such as the the JetCat P90 RXi have been used in prior research due to cost, availability, and design simplicity. Figure 24 shows a cross-section of a JetCat P90 RXi hobbyist engine where the layout closely resembles the JetCat P160 and P400 being used for the current investigation. In this engine configuration, flow passes through a centrifugal compressor into a diffuser/deswirler prior to entering the burner. From the burner, hot combustion products migrate through a single-stage turbine and nozzle guide vane, and exits through a converging nozzle.

Linear scaling of turbomachinery generally applies to compressor and turbine design, however burner design is governed by flame length and residence time requirements, which do not scale linearly. As a result, a large portion of the overall axial length of the small-scale engine is occupied by the burner to satisfy these requirements. This creates motivation towards designing a novel combustor that aims to significantly reduce the total length of the engine. While the combustor has its own design considerations, temperatures downstream of the combustor need to be analyzed to ensure proper integration between the burner and other turbomachinery, especially the turbine. Section 2.2.1 discusses parameters that can be measured to ensure proper integration of a novel combustor design into a gas turbine engine.

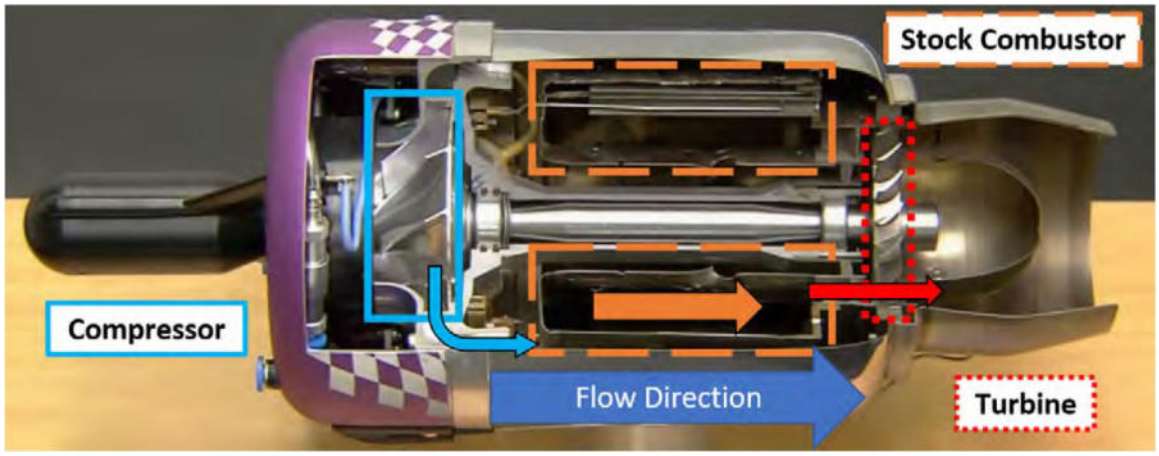

Figure 24. Cutaway of a JetCat P90 RXi gas-turbine engine [3]

DePaola [25] looked at testing four small-scale gas turbine engines and comparing their performance against one another. The four small-scale engines tested were denoted as Engines A, B, C, and D and had published thrust outputs of 210 N, 186 N, 300 N, and 235 N, respectively, at design conditions. Figure 25a shows a comparison of the the measured thrust outputs of each engine, while Figure 25b shows the measured mass air flow rates through each engine. Experimentally, the thrust output measured for Engines A-D were found to be 200 N, 172 N, 293 N, and

220 N, respectively, which corresponds to deviations of -4.8%, -7.5%, -2.3%, and -6.3% from the published values. Regarding fuel consumption, Engines A-D reported fuel consumption rates of 525 gpm, 392 gpm, 804 gpm, and 515 gpm, respectively, from the manufacturer at design condtions. Figure 26 shows the measured fuel consumption rate during testing for each engine yielding values for Engines A-D of 579 gpm, 568 gpm, 866 gpm, and 559 gpm, respectively, representing deviations of 10%, 45%, 7.7%, and 8.5%.

To compare the combustor's performance across all engines, thermocouples were placed upstream of the turbine inlet to measure combustor exit temperatures. Figure 27 shows results from testing for two different engines where lines of constant combustion efficiency are plotted alongside the measured exit temperature data. Figure 27a and 27b correspond to Engine B and C, respectively. In Engine B, only one thermocouple was used to measure turbine inlet conditions across several power sweeps. The results show combustion efficiencies on the order of 95% at the design condition. Regarding Engine C, two thermocouples were used to measure turbine inlet temperature which were clocked 180 degrees from one another. These results differed significantly from each other suggesting a portion of the combustor was burning considerably better than the other. This may be due to a fuel distribution issue where the fuel channel isn't behaving as a plenum and is distributing more fuel to a portion of the combustor than another [25].

Cican et al. [26] analyzed the performance of a JetCat P80 engine on different types of fuels which included kerosene, diesel, kerosene with 5% gasoline, and kerosene with 10% gasoline. To monitor the performance of the small-scale gas turbine engine operating on the various fuels, the turbine inlet temperature, denoted as T_3, and thrust output was monitored. Figure 28 shows plots of the turbine inlet temperature versus run time for the various fuels used where the engine was operated from a

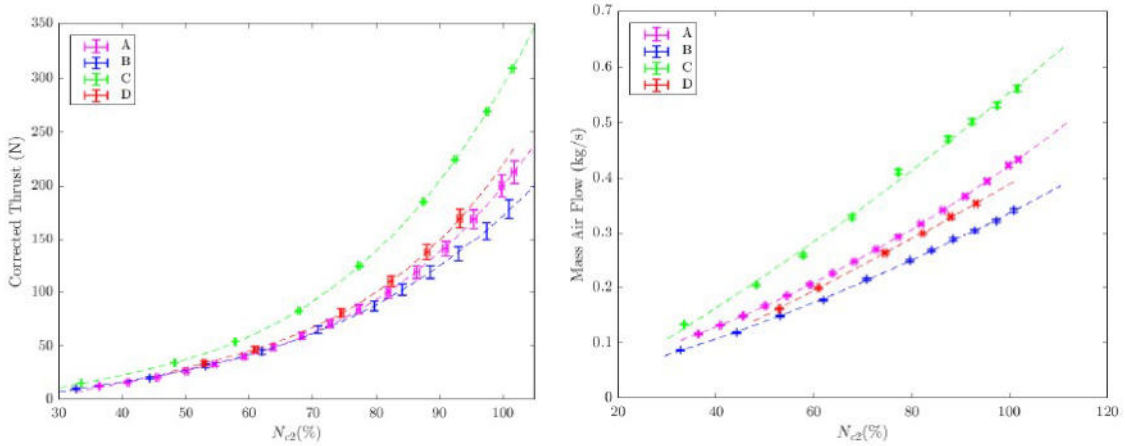

(a) (b)

Figure 25. Corrected thrust and mass air flow versus engine speed for 4 small-scale gas turbine engines [25]

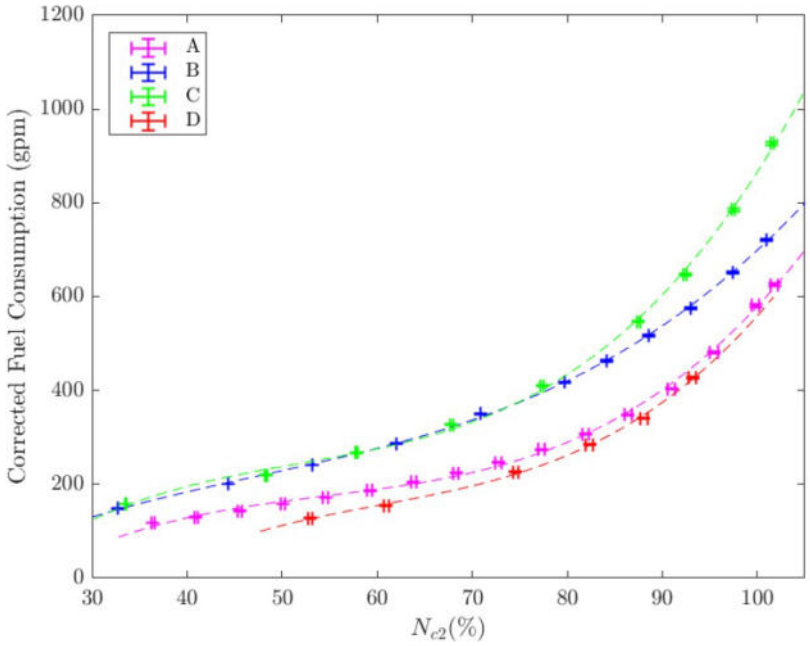

Figure 26. Corrected fuel consumption versus engine speed for 4 small-scale gas turbine engines [25]

stand-still to an idle speed during the elapsed time. Regarding ignition between fuels, Figure 28a shows that diesel fuel was the quickest to ignite during start-up, followed by kerosene, kerosene with 5% gasoline, and kerosene with 10% gasoline. On the 0^{o}C

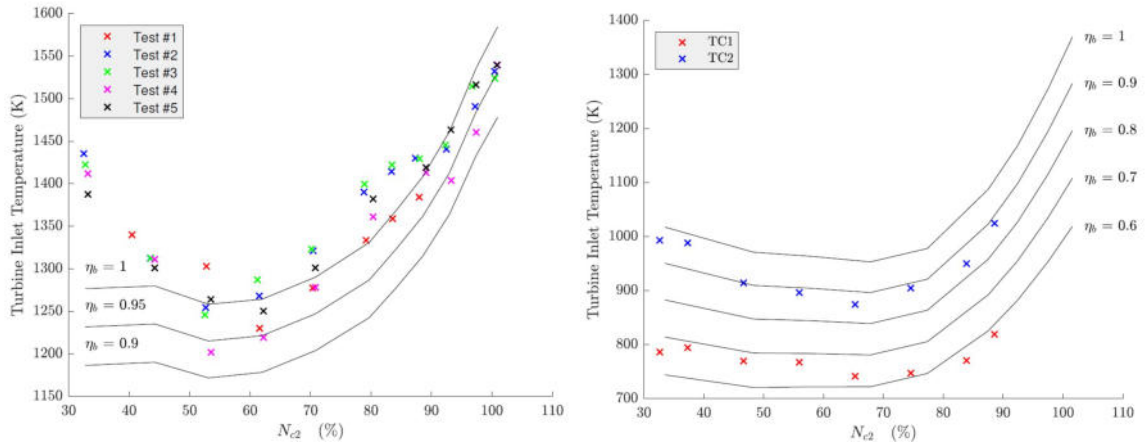

(a) (b)

Figure 27. Turbine inlet temperatures measured for Engines B (left) and C (right) [25]

day, shown in Figure 28b, all of the fuels exhibited similar ignition characteristics and ignited at similar times.

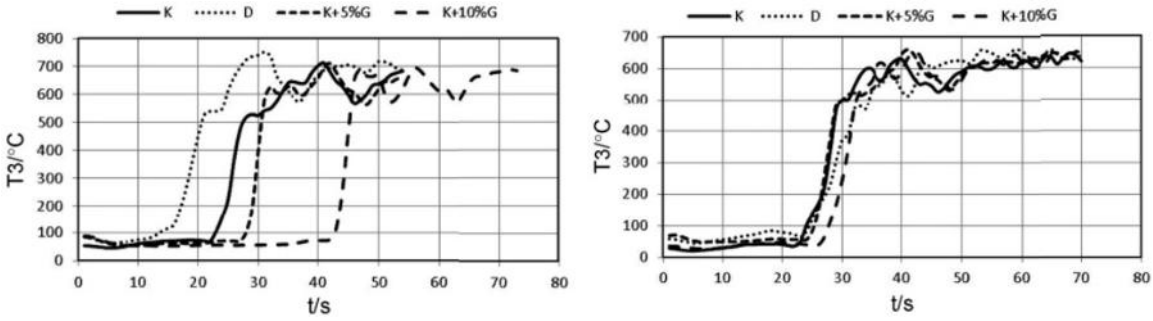

(a) (b)

Figure 28. T_3 versus run time for various fuel types on (a) a 19^{o}C day and (b) a 0^{o}C day [26]

Figure 29 shows thrust versus engine speed where the engine was accelerated from an idle condition of 35,000 RPM to a design condition of 90,000 RPM for all fuel types. Figure 29a shows data collected on a 19 ^{o}C day where the fuels followed a similar trend-line until full power where there was a disparity between the kerosene-gasoline fuels and the pure kerosene and diesel fuels. The kerosene-gasoline fuels produced more thrust compared to the other fuels on this particular test day. Figure 29b shows

data collected on a 0 ^{o}C day, where the engine behaved similarly on all fuel types. The engine produced roughly 50 N of thrust, which was more compared to any of the fuels on the 19 ^{o}C day.

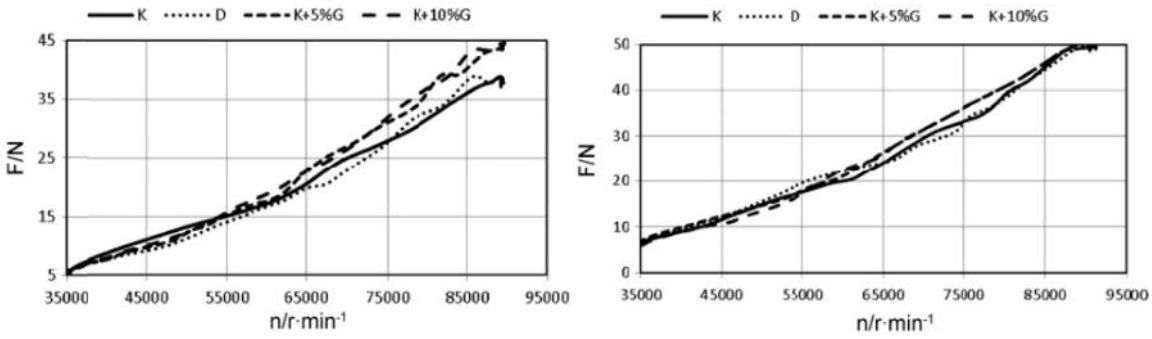

Figure 29. Thrust versus engine speed for various fuel types on (a) a 19^{o}C day and (b) a 0^{o}C day [26]

2.5.1 Pattern and Profile Factors.

Two performance parameters are often utilized to determine temperature uniformity coming from the burner going into the first turbine stage. These parameters include pattern (PF) and profile factor (P_f). Pattern factor can be defined accordingly

$$PF = \frac{T_{tmax} - T_{tav}}{T_{tav} - T_{tin}} \tag{9}$$

where T_{tmax} is the maximum measured temperature at the exit of the burner, T_{tav} is the average of all temperatures at the exit plane of the burner, and T_{tin} is the average of all temperatures at the inlet plane of the burner [27]. Modern-day gas turbine engine burners typically exhibit pattern factors ranging from 0.25 to 0.45, however improvements in combustor performance allowing for rises in T_{t4} have lowered pattern factor requirements down to the range of 0.15 to 0.25 [27].

Where the pattern factor describes the thermal plane entering the first turbine

stage coming from the combustor exit, the profile factor describes the burner average exit temperature distribution and can be defined accordingly

$$P_f = \frac{T_{tmaxav} - T_{tin}}{T_{tav} - T_{tin}} \tag{10}$$

where T_{tmaxav} is the maximum circumferential average temperature at the combustor exit [27]. Typical profile factors range from 1.04 to 1.08 with 1.06 being the design goal [27]. A profile factor of 1 would translate to a uniform temperature distribution going into the first turbine stage. To promote the lifespan of turbine blades, having a temperature distribution slightly skewed towards the tip is recommended in order to extract as much work from the flow while also ensuring turbine life [27].

2.6 Computational Modeling

To aid and validate mechanical designs for use in complex flow-fields, computational fluid dynamics is often a useful tool for providing insight towards possible solutions. ANSYS Fluent is a common commercially available software package with several capabilities involving numerous models for solving turbulence, species transfer, combustion reactions, and heat transfer problems [28]. These areas outlined are crucial for analyzing and validating a novel compact-combustor design. Since several models exist within each category, the works of Bohan [4] and Holobeny [3] served as an outline to aid in grid generation and turbulence modeling selection, discussed in Section 2.6.1 and 2.6.2 respectively, combustion modeling selection, discussed in Section 2.6.3, and conjugate heat transfer selection, discussed in Section 2.6.4. Additionally, since the current compact combustor was going to operate using a liquid fuel source, an understanding of the application of liquid fuel injection was required, and is discussed in Section 2.6.5.

2.6.1 Grid Generation.

When generating a mesh for a computer-aided design (CAD) model, there are fundamentally two grid types to chose from; structured and unstructured. For a structured grid, the cell types must be quadrilaterals for a two-dimensional case or hexahedra for a three-dimensional case. Structured grids are good for boundary layers as the high aspect ratio of the cells help to capture large gradients, however structured grids are typically difficult to generate around complex geometries. For an unstructured grid, the cell types are typically quadrilaterals or triangles for a two-dimensional case or hexahedra, tetrahedra, pyramids, or prisms for a three-dimensional case. Unstructured grids are more easily suited towards complex geometries, however it's likely that there will be highly skewed cells near boundaries. To get the benefits of both of these grid types, a hybrid grid is often used, which allows for transition between structured and unstructured grid types if cell refinement along the wall is required. This type of grid was used by Bohan et al. [29][1] and Holobeny et al. [2] during their computational analysis of ultra compact combustors.

2.6.2 Turbulence Modeling.

Some of the turbulence models that exist within ANSYS Fluent include Spalart-Allmaras, $\kappa - \epsilon$, $\kappa - \omega$, and Reynolds Stress [28]. The $\kappa - \omega$ Shear Stress Transport (SST) model is a Reynolds-Averaged Navier-Stokes(RANS) model that utilizes two equations to solve for the turbulent kinetic energy, κ, and dissipation rate, ω. When the $\kappa - \omega$ SST model is selected, the computational fluid domain is divided into two regions, a near-wall and far-wall region respectively [28]. For the near wall region, the $\kappa - \omega$ turbulence model is used, however for the far-wall region, the $\kappa - \epsilon$ turbulence model is used. Similar to the $\kappa - \omega$ model, the $\kappa - \epsilon$ model is a two equation model, however the turbulent shear stress, ϵ, is solved for rather than the dissipation rate.

This turbulence model is better suited for far-field regions due to the models ability to provide better solutions in this regime [28]. Due to the ability of the $\kappa-\omega$ model to accurately model inner regions of the boundary layer, this model, equipped with an additional shear-stress-transport (SST) model, was used by Bohan [4] and Holobeny [3] when designing their compact combustors for use in JetCat engines.

2.6.3 Combustion Modeling.

To match the methods used by Holobeny [3] and Bohan [4], the partially premixed combustion model equipped with flamelet generated manifold and diffusion flamelets was used in ANSYS Fluent [3][4]. This particular combustion model is ideal for combustors that operate globally lean with a premixed fuel-air mixture. Additionally, the model is able to take into account dilution/cooling holes, which enables the model to predict lean blowout due to quenching [28].

The work of Lin et al. [30] documented a method to better predicting lean blow off (LBO) limits using a RANS based CFD solver for use with propane-air combustion in a swirler. Using the stock input parameters within the partially premixed combustion model in ANSYS Fluent has led to LBO limits being of by as much as 20-30% compared to experimental data [30]. Lin et al. [30] looked at toggling some of the parameters within the combustion model to arrive at a better model that could more accurately predict the LBO limit. The setting that was studied involved the simple indicator, λ, which measures the rate of change in the Damköhler number or temperature. Using a Da-based LBO indicator, compared to temperature based indicators, calculated on the temperature-range clipped flame section (TCFS) was more accurate at predicting the LBO limits within an error of 8.6% [30].

2.6.4 Conjugate Heat Transfer.

A conjugate heat transfer model is required to measure the heat transfer passing through the fluid and solid boundaries. This is applicable to combustors due to hot gases interacting with the metal combustor liner, and cooling flow passing through the secondary zone and dilution holes. Obtaining an accurate combustor wall temperature measurements is ideal to ensure the structural integrity of the combustor itself. Assuming adiabatic boundary conditions may cause the model to over-predict the fluid temperature interacting with the combustor walls, leading to hotter temperatures throughout the entire domain. This was the case with Bohan where downstream temperatures saw as much as a 500 K drop in temperature between the conjugate and adiabatic models [4].

2.6.5 Discrete Phase Modeling.

To simulate liquid kerosene fuel injection within a computational model, the discrete phase model (DPM) solver in ANSYS Fluent is commonly used. The DPM solver uses the Euler-Lagrange approach by considering two phases; the fluid phase and the dispersed phase. The fluid phase is treated as a continuum, while the dispersed phase is solved by tracking several particles, similar to droplets, through the flowfield. These "particles" which are tracked are able to exchange momentum, mass, and energy with the fluid phase, which makes this model appropriate for liquid spray combustion systems because the state of the liquid fuel is constantly changing once it is injected into the combustor [2].

This methodology was used by Briones et al. [31][8] in the case of simulating and investigating the effect of centrifugal forces on turbulent premixed flames where both gaseous (propane-air) and liquid (kerosene-air) fuels were used. Additionally, Brionnes et al. [31] used this methodology when simulating a liquid kerosene spray in-

jection scheme within a outboard cavity-stabilized combustor in tandem with ANSYS Workbench to reach an optimized combustor design by varying dimensional parameters around the combustor and using figures of merit, such as pattern factor, total pressure loss, and combustion efficiency, to reach an optimized design.

III. Methodology

The current investigation looked to take the UCC designed by Holobeny [3] for the JetCat P90 RXi-B engine and modify the combustor to be integrated into the similarly sized JetCat P160 to operate on liquid kerosene fuel rather than gaseous propane. Gaseous propane was previously used due to its ease of control and availability, however, it was more desirable and practical to transition towards liquid fuel operation. The previous compact combustor used by Holobeny et al. [2] for the JetCat P90 RXi equipped with gaseous fuel injection was designed with the intention of transitioning towards liquid fuel injection, which enabled the previous combustor to be integrated into the new engine with only minor modifications. Section 3.1 discusses the previous compact combustor designed for the JetCat P90 engine, while the hardware and necessary changes that needed to be made to be integrated with the JetCat P160 engine are discussed further in Section 3.2. Once the necessary modifications were made, the P160 engine equipped with the revised bluff-body compact combustor was tested using liquid kerosene fuel, as discussed in Section 3.3. Computational simulations were performed afterwards to supplement experimental testing, which is discussed in Sections 3.4 and 3.5.

The second objective of this present study was to design a compact combustor for the larger JetCat P400 engine. Given the experimental and computational results following the JetCat P160 testing with the bluff-body compact combustor the bluff-body flame-holding mechanism present was insufficient at holding a pilot flame within the primary zone of the combustor. This led to the design a new compact combustor utilizing a new flame stabilization scheme; trapped-vortex combustion. To design this alternative combustor, numerous CFD simulations were run to reach a sufficient design based on parameters such as pattern factor, exit temperature profile, pressure drop, and combustion efficiency. The hardware of the TVC used in the P400 engine

is discussed in Section 3.6. The methodology behind the CFD simulations performed for the TVC combustor is discussed in Section 3.7. Finally, Section 3.8 discusses the design and assembly process of the new hardware used for the new P400 test rig.

3.1 Previous JetCat P90 RXi Combustor

The foundation of the present research builds off of the efforts of Holobeny et al. [2], who sought to design, integrate, and test a compact combustor in a JetCat P90 RXi engine to operate on gaseous propane fuel. The stock JetCat P90 engine used by Holobeny et al. [2] can be seen in Figure 30, which features a radial compressor and axial turbine. Several design constraints needed to be accounted for to design a new compact combustor within this framework. A 5.0 mm gap between the OD of the combustor and the ID of the engine casing needed to be maintained to ensure air traveled downstream of the combustor [2]. This constrained the OD of the combustor to 98 mm. Additionally, the compact combustor needed to interface with the turbine NGV housing which had an inner and outer diameter of 42.64 mm and 68.70 mm, respectively [2]. The final constraint involved ensuring clearance for the shaft housing, which gave the compact combustor a minimum ID of 34 mm [2].

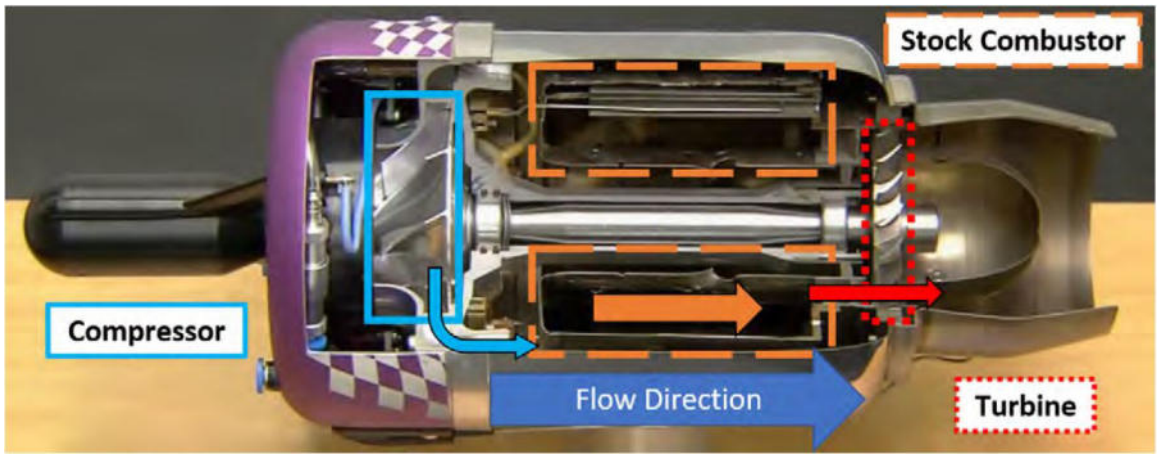

Figure 30. Cross-sectional view of the stock JetCat P90-RXI-B engine [3]

To meet these design constraints, Holobeny et al. [2] designed a compact combustor utilizing bluff-body flame stabilization and fuel-air mixing tubes. Bluff-body flame stabilization was used so that more fluidic volume was present within the combustor per Bohan's [4] recommendation as a result of his findings. This would lower the velocities within the primary zone, thus increasing the residence time and ensuring stable combustion across the operating range of the engine. Additionally, fuel-air mixing tubes mimicking the ones used in the stock engine were used as a method to premix, preheat, and inject the fuel-air mixture into the primary zone of the combustor. Twelve fuel-air mixing tubes were implemented rather than the six originally used in the stock burner to ensure more even fuel distribution and burning. Additionally, this method of fuel injection was chosen due to the easy integration with the stock fueling system of the JetCat P90 engine. Finally, the inner and outer combustor liners matched the dimension of the stock combustor's liners so that they mated accordingly to the nozzle guide vane (NGV) housing and the gap between the outer liner and engine casing was maintained.

Figure 31 shows the compact combustor designed by Holobeny et al. [2] that was integrated into the JetCat P90 engine. While the outer and inner liners closely resemble the stock combustor's design at a shortened length, all of the other components were tailored to the propane fuel delivery system or the bluff-body flame holding mechanism. Starting with the propane fuel delivery components, shown in greater detail towards the left in Figure 31, the propane tube, propane holder ring, and fuel-air mixing tube were responsible for delivering gaseous propane into the primary zone of the combustor. The propane tubes stuck outside of the engine casing where the propane holder ring, which also laid outside of the engine casing, held the tubes in place. The tubes went through the engine casing and the outer liner and rested within the fuel-air mixing tubes so that gaseous propane could flow directly

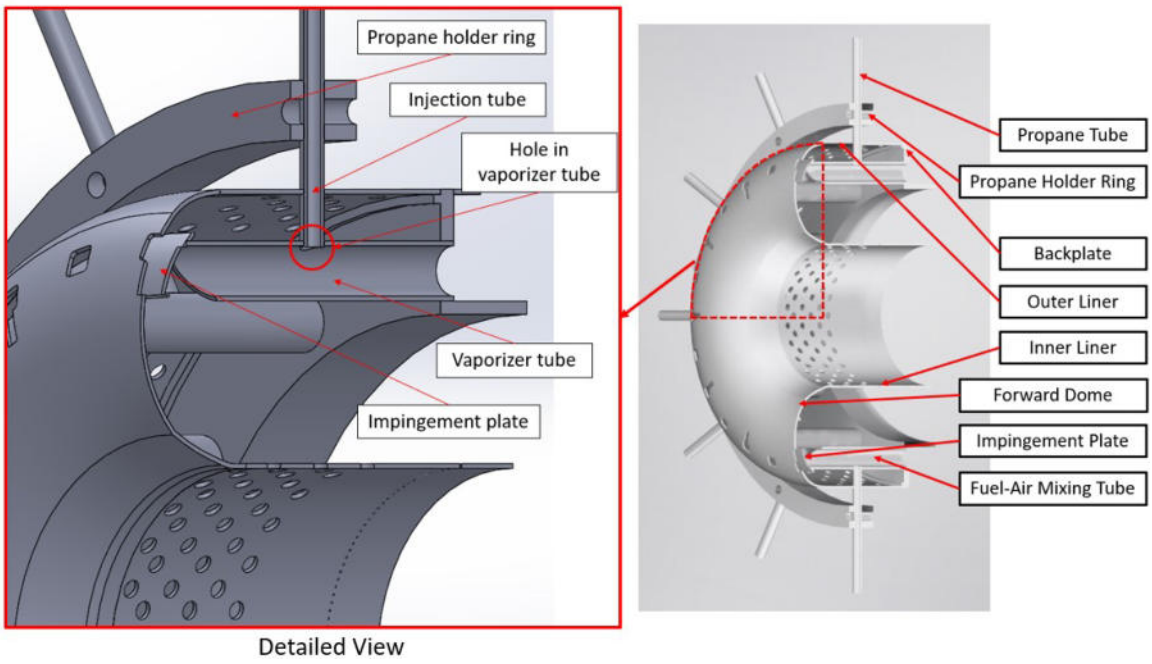

Figure 31. Cross-sectional view of the compact combustor used for the JetCat P90 engine

into them. This meant that the fuel-air mixing tubes were manufactured with a hole along the upper surface intended for this propane injection scheme.

Figure 32 highlights the bluff-body flame holding mechanism present in the P90 compact combustor design. In this combustor configuration, fuel traveled down the fuel-air mixing tubes opposing the direction of flow coming from the compressor. This design allowed heat from the primary zone of the combustor to raise the temperature of the fuel-air mixing tubes and preheat the fuel prior to being injected on the backside of the impingement plate. This impingement plate acted as a bluff-body where air traveled through the air inlet holes on the forward dome to impinge on the upstream face of the impingement plate. As this happens, a fuel-air mixture traveling upstream within the fuel-vaporizer tubes impinges on the backside of the impingement plate. This impinging of fuel and air along the bluff-body causes a recirculation region to form along the backside which promotes a stable pilot flame for combustion.

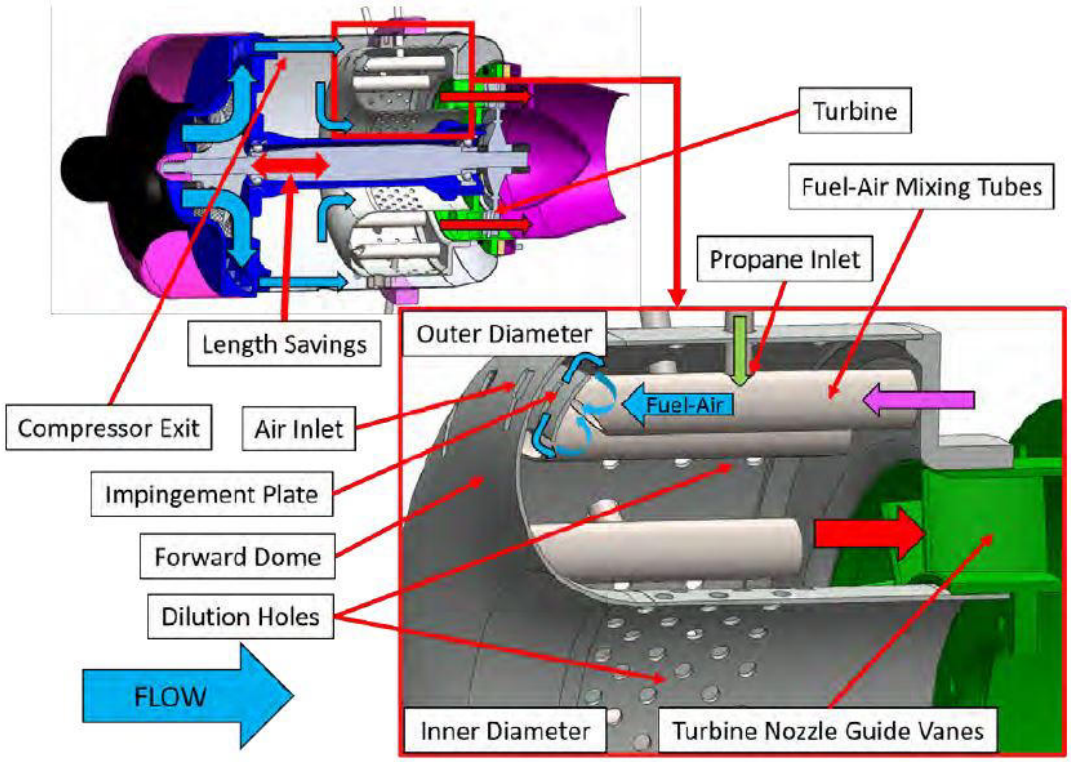

Figure 32. Detailed diagram of the flow-path through Holobeny's [3] bluff-body compact combustor in a JetCat P90 engine

While Holobeny's [?] compact combustor design featured fuel-air mixing tubes intended for gaseous propane fuel, they were also designed with the intention of switching fuels to liquid kerosene for future testing. While modifications needed to be made to the combustor to operate on liquid kerosene fuel, which is discussed in Section 3.2, the same tube length could be used between the P90 and P160 compact combustor designs.

3.2 JetCat P160 Combustor Design

To continue and improve upon the efforts of Holobeny et al. [2] with the JetCat P90 RXi compact combustor design, the JetCat P160 engine was used where the previous compact combustor could be utilized with minor modifications and run on a

more desirable fuel source, liquid kerosene. While the JetCat P90 RXi and P160 RXi engines are in different thrust classes, they are dimensionally similar engines, which enabled compact combustor designed by Holobeny et al. [?] to be used in the P160 engine. Table 1 shows a comparison in both performance and overall dimensions between the JetCat P90 and P160 engines. A few key differences between these engines are that the JetCat P160 utilizes a larger compressor and turbine within the same engine casing. As a result of the larger turbine, a larger NGV housing was used in the JetCat P160 configuration. Additionally, the larger compressor and turbine sections enabled the engine to have a higher pressure ratio and thrust output.

Table 1. JetCat P90 and P160 Engine Comparison Chart [4][32]

	JetCat P90 RXi	**JetCat P160 RXi-B**
Pressure ratio	2.5	3.8
Max air mass flow [kg/s]	0.26	0.38
Max fuel consumption [ml/min]	509	510
Weight [g]	1715	1670
Engine casing diameter [mm]	112	112
Length [mm]	300	297
Idle speed [1/min]	36000	32000
Max speed [1/min]	130000	122000
Thrust at idle [N]	3	7
Max thrust [N]	102	158

To integrate the compact combustor from the JetCat P90 RXi with the JetCat P160, a couple of modifications needed to be made to the compact combustor designed by Holobeny et al. [2]. From Figure 33, there are six key components that make up the compact combustor intended for use in the JetCat P160 engine. These are the forward dome, the outer and inner liners, the fuel-air mixing tubes, the back plate, and the impingement plate. The outer and inner liners, and the impingement plate remained the same between both engine configurations, leaving the forward dome, fuel-air mixing tubes, and back plate to be altered in order to integrate into the JetCat P160 engine.

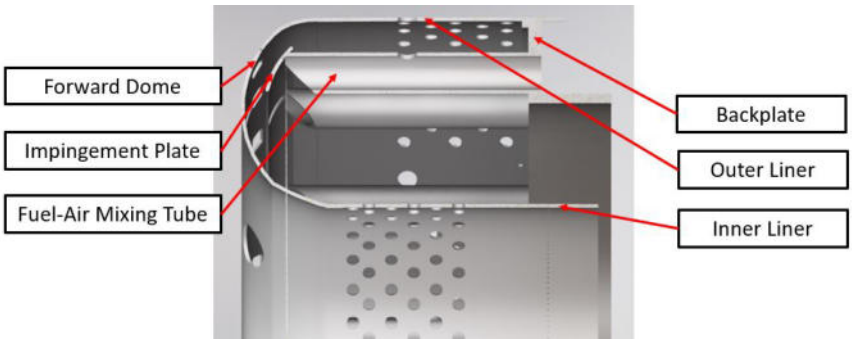

Figure 33. JetCat P160-RXi-B Compact Combustor Diagram

Starting with the forward dome, the stock P160 combustor featured a hole on the front of the combustor aft of the compressor exit to allow access for the glow plug to auto-ignite the vaporized fuel-air mixture within the primary zone. As a result of the 33% axial length reduction of the compact combustor caused by the bluff-body flame stabilization scheme, the glow plug needed to be extended 23.1 mm from its original position and a hole needed to be drilled in the forward dome, shown in Figure 34, of the compact combustor to allow access for the glow plug. Figure 35 shows the JetCat P160 diffuser/deswirler coupled with the shaft housing, fuel manifold, fuel lines, and glow plug equipped with spacers to account for the 33% axial length reduction. Additionally, the fuel line that runs from the fuel manifold into the glow plug to create a kerosene-vapor jet for ignition was extended.

As a result of the P160 engine having a larger turbine compared to the P90 engine, a new combustor backplate was designed to fit over the larger NGV housing, as shown in Figure 36. This new backplate was manufactured out of Inconel-718 which featured an ID that was 4.46 mm larger than the backplate used by Holobeny et al. [**?**] for use in the JetCat P90 RXi engine.

Additionally, new fuel-air mixing tubes needed to be manufactured such that the hole from Holobeny's [3] vaporizer tubes designed for propane injection was omitted. The new tubes, which were manufactured from 316-stainless steel, maintained the

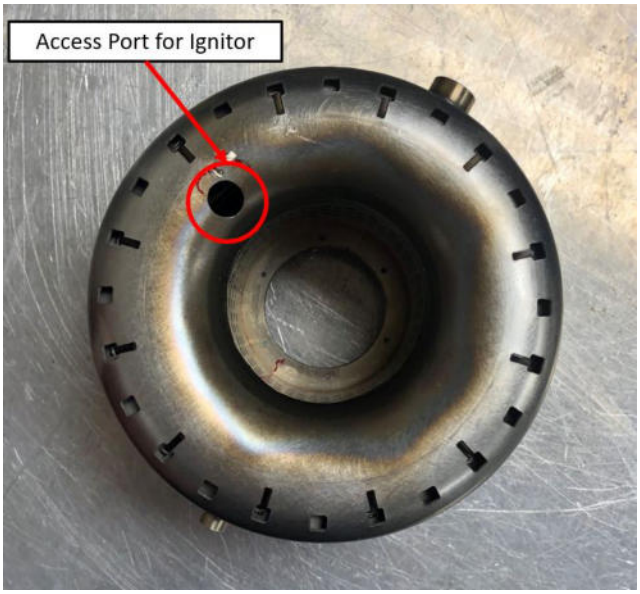

Figure 34. Forward dome of P160 compact combustor modified to allow access for stock glow plug

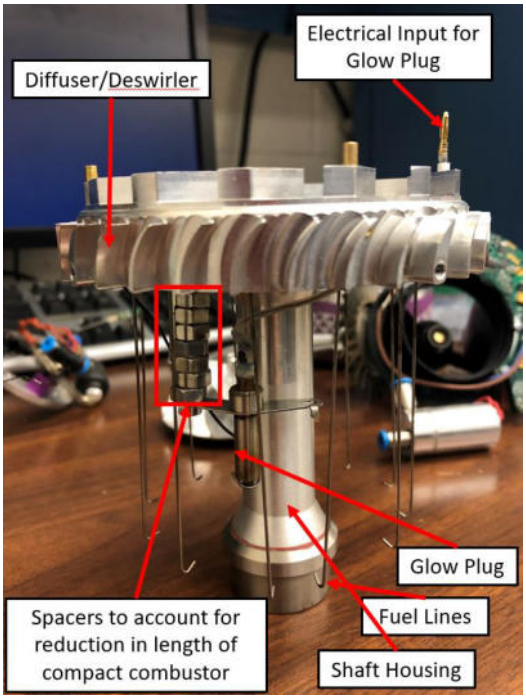

Figure 35. Modifications made to the P160 diffuser/deswirler for compact combustor integration

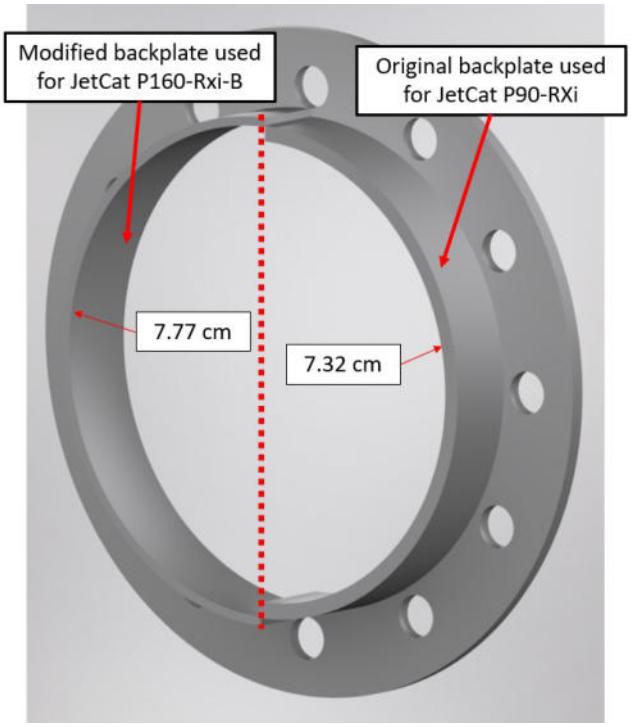

Figure 36. P160 combustor backplate modified for engine integration

same length used by Holobeny et al. [3] for an axial length savings of 33% without the addition of the hole intended for propane fuel injection, as shown in Figure 37b, where Figure 37a shows the original design of Holobeny et al. [2]. These twelve fuel-air mixing tubes were 40 mm long and featured a wall thickness of 0.508 mm. Contrasting, the stock JetCat P90 combustor contained six fuel-air mixing tubes, rather than the twelve used in the present research. Six additional fuel-air mixing tubes were added in the design of Holobeny et al. [3] to improve upon fuel distribution unevenness present in the stock configuration caused by a lack of a pressure differential in the fuel manifold to evenly distribute fuel across the entire circumference of the engine. The stock P160 combustor came equipped with twelve fuel air mixing tubes, which enabled the combustor design of Holobeny et al. [3] to be used without requiring any changes to the stock fuel manifold.

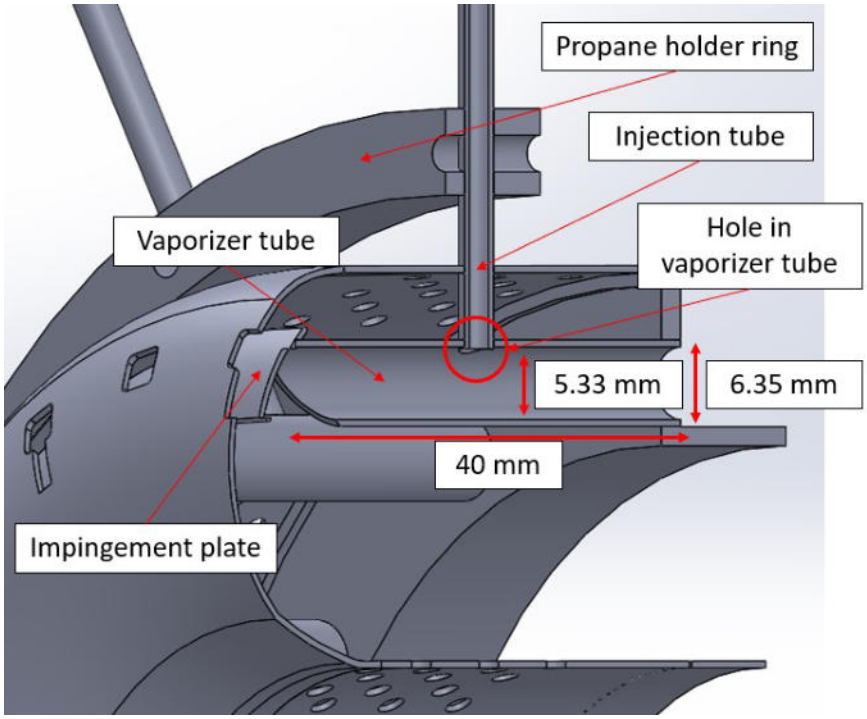

(a)

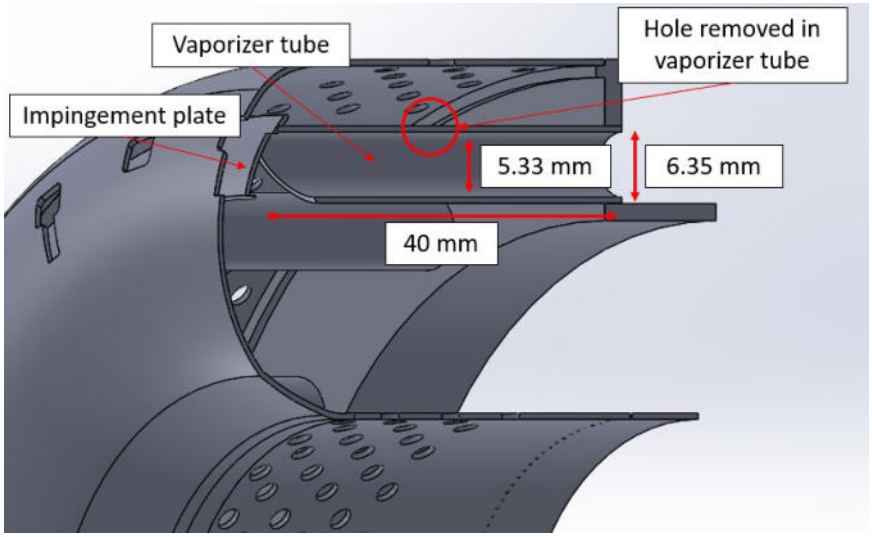

(b)

Figure 37. Comparison between (a) Holobeny et. al's [2] fuel vaporizer tube subassembly versus (b) the current fuel vaporizer tube setup

3.2.1 JetCat P160 Instrumentation.

The locations of the instrumentation on the JetCat P160 RXi-B engine can be seen in Figure 38 where the measurement locations resemble the same instrumentation locations used by Holobeny et al. [?] for a rotating test configuration. From Figure 38a, Omega Type-K 0.05 cm (SCAIN-020G-12) thermocouples with an Inconel-600 sheath were used to record temperatures spanning from the compressor inlet to the combustor exit. To record the temperatures downstream of the turbine, larger Omega Type-K 0.1 cm (SCAIN-040G-12) Inconel-600 sheathed thermocouples were used to withstand the higher temperatures and flow velocities. Six additional OMEGA Type-K 0.020" (SCAIN-020G-12) thermocouples, shown in Figure 38b, were placed within every other fuel-air mixing tube to record the circumferential heating of the fuel tubes during the ignition stage of the start-up sequence. Additionally, to measure total and static pressures at similar points within the engine, 1/16" 316 stainless steel tubes were used to connect about location of the engine to a pressure transducer.

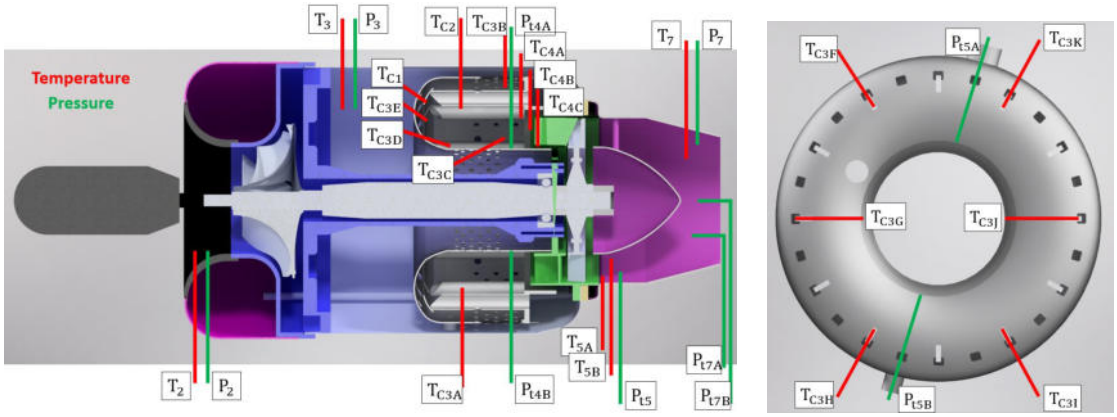

(a) (b)

Figure 38. Temperature and pressure measurement locations used during P160 testing with rotating turbomachinery with both (a) axial and (b) circumferential clocking locations

The back-end of these pressure lines fed to three different OMEGA high performance pressure transducers, shown in Figure 39, which included a Model PX409-

005G5V with a 0-5 psig range, a Model PX409-015G5V with a 0-15 psig range, and a Model PX409-030G5V with a 0-30 psig range, all of which had an accuracy of ±0.08% full scale (FS).

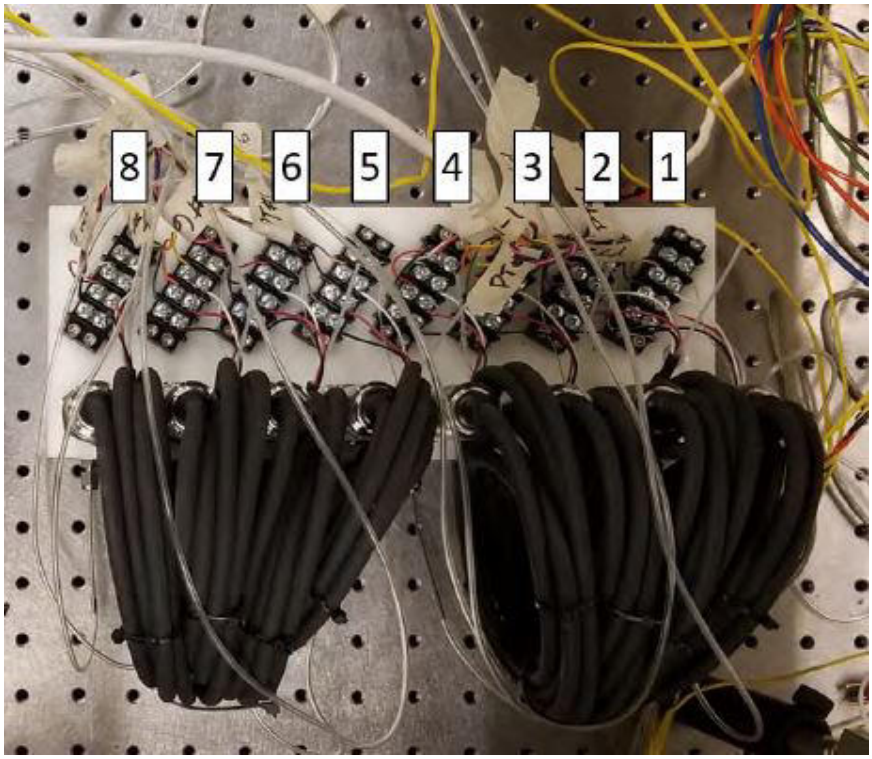

Figure 39. The pressure transducers used for the P160 testing

Four additional temperature measurement locations were added to further analyze combustion regions within the burner. These four additional thermocouples were added to the combustor to help quantify the dilution hole's affect on the combustion flow and compare against Holobeny's [3] CFD results for the P90 as shown in Figure 40. These four additional temperature locations correspond to T_{C3B}, T_{C3C}, T_{C3D}, and T_{C3E} in Figure 38a. From Figure 40, the contours in temperature show the effect the dilution holes had on the inner and outer diameters of the combustor flow, as well as the exit temperature profile [**?**]. Additionally, the dilution air jets served its purpose in pushing the hot combustion products away from the liners, keeping them cool [**?**].

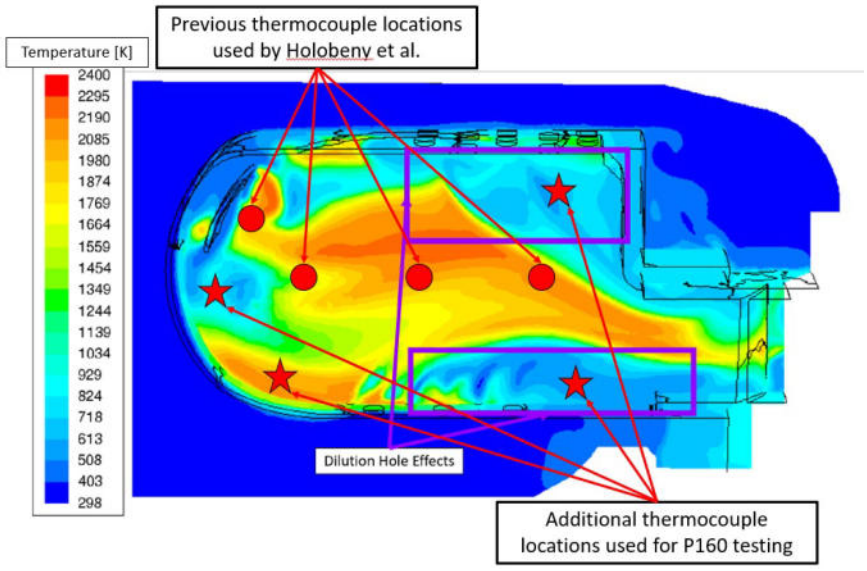

Figure 40. Thermocouple locations used previously by Holobeny et al. [?] and additional locations for JetCat P160 testing compared to CFD results from Holobeny et al. [?]. Adapted from [3].

3.2.2 JetCat P160 Hardware and Assembly.

To properly integrate the JetCat P160-RXi-B engine with a novel compact combustor, all of the components, outlined in Figure 41, within the gas turbine needed to be removed to gain access to and remove the stock burner.

To remove the stock combustor in the JetCat engine, the exhaust nozzle was first removed. This exposed the nozzle guide vane housing along with the single-stage axial turbine. Second, the compressor housing coupled with the starter motor sub-assembly was removed which exposed the single-stage radial compressor. The engine casing was then removed exposing the diffuser/deswirler and fuel manifold sub-assembly, shaft and shaft housing, and burner. To remove the combustor from this point in the disassembly process, either the compressor or turbine could be removed since these two components lock the combustor into place. Once this was done, the stock combustor was successfully removed from the JetCat P160-RXi-B engine.

With the stock combustor from the JetCat P160 engine removed, the current com-

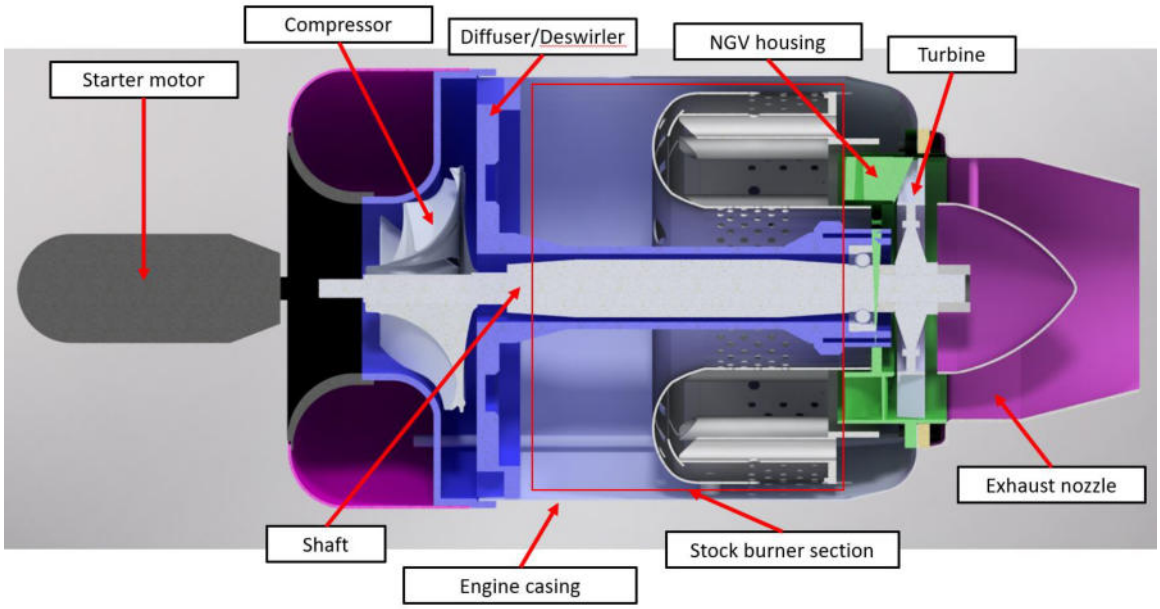

Figure 41. JetCat P160-RXi-B diagram

pact combustor could be assembled and integrated into the engine. The modifications made to the previous compact combustor were discussed in Section 3.2. These design elements included new fuel-air mixing tubes, a new backplate, a new impingement plate, and a new forward dome. All of the components were machined by the AFIT Model Shop out of Inconel-600 0.020" sheet metal, aside for the fuel-air mixing tubes and back plate, which were machined from 316 stainless steel and Inconel-600 plate. Once these components were machined and received from the AFIT Model Shop, all of the components were shipped to Wicked Welding so that the forward dome could be welded to the inner and outer liners, the twelve fuel-air mixing tubes could be welded into the backplate, and the impingement plate could be welded to the vaporizer tubes. Figure 42 shows the manufactured forward dome, and outer and inner liners welded together. The tabs on the outer liner were used to hold the back plate coupled with the vaporizer tubes and impingement plate in place once installed. Figures 43 and 44 show side and top views, respectively, of both the combustor liner and backplate equipped with the vaporizer tubes and impingement plate.

Figure 42. P160 compact combustor outer and inner liner mated to the forward dome after machining and laser-welding

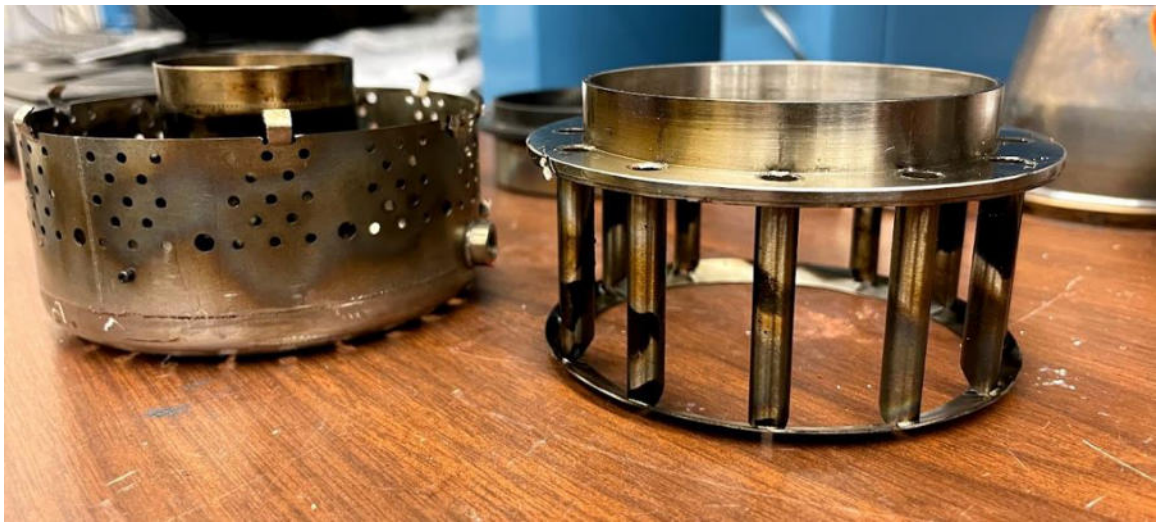

Figure 43. P160 compact combustor liners and fuel vaporizer tube assembly post-machining and laser-welding

To reassemble the engine and fit the current compact combustor into the JetCat P160 engine, the inverse of the disassembly process was performed. First, the fuel lines, shown in Figure 45, were fed through the slots on the forward dome of the

Figure 44. Top-view of the P160 compact combustor components post-machining and laser-welding

combustor. Second, the shaft was fed through the core of the engine where the radial compressor and axial turbine were fitted to either end. Finally, the engine casing was fitted over all of the internal components.

The starter motor coupled with the engine's Engine Control Unit (ECU), compressor housing, NGV housing, and exhaust nozzle weren't initially reinstalled since the engine's rotating turbomachinery needed to be re-balanced as a consequence of the disassembly process, and access to the rotating turbomachinery during the balancing process was required. The engine was sent to Matt Boehle, a research engineer at AFRL, to be balanced. The balancing process entailed spooling the engine up to its maximum operability limit of 122,000 RPM through the use of compressed air. The engine was mounted to a machine that was able to measure lateral and radial forces on the engine's center. To balance the engine, material was removed from the compressor and/or turbine, as shown in Figure 45, until these lateral and radial forces were equal to one another.

With the engine back from balancing, the engine casing and compressor housing

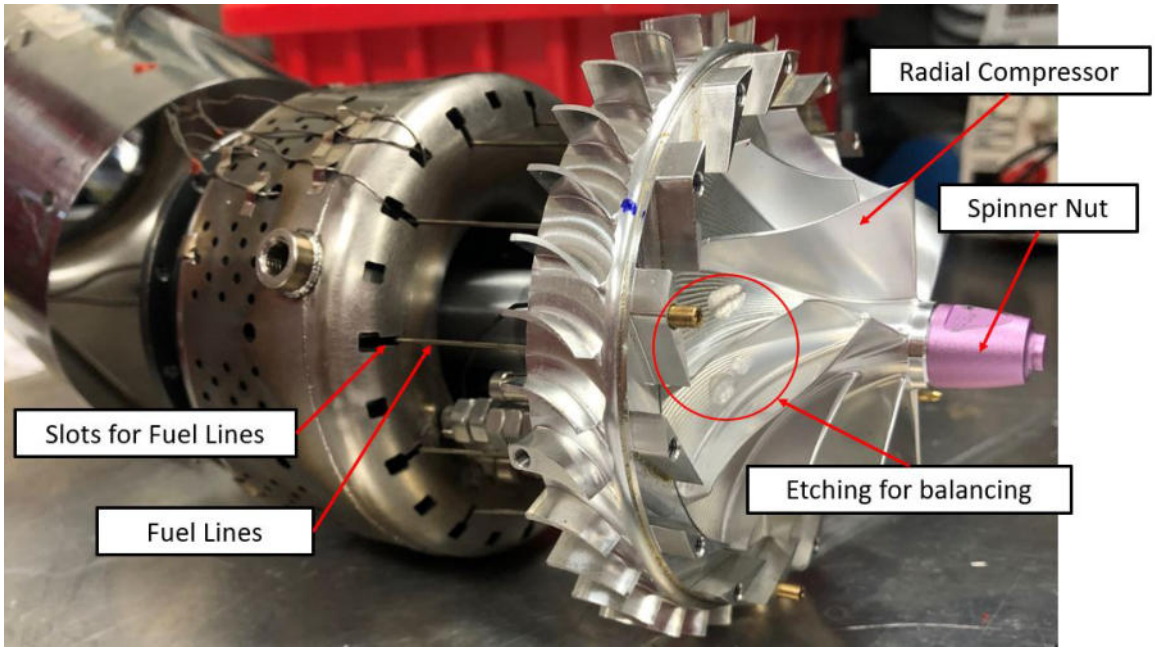

Figure 45. JetCat P160-RXi-B reassembly with instrumented compact combustor

were removed to regain access to the compact combustor so that it could be instrumented. The types of thermocouples and their locations were mentioned in Section 3.2.1. To hold these thermocouples in place, Nichrome strips were placed over the thermocouples where a tack welder was used to bond the Nichrome to the combustor outer liner. These thermocouple wires were fed through various holes machined in the engine casing, which can be seen in Figure 46. With the combustor fully instrumented, the exhaust nozzle, engine casing, compressor housing, fuel solenoids, fuel pump, ECU, exhaust gas temperature (EGT) probe, and starter motor were reinstalled. Then the pressure lines were installed in their corresponding locations. Figure 47 shows the fully instrumented, reassembled engine equipped with a compact combustor. To seal the hole on the engine casing used to feed the thermocouples to their corresponding locations, red Permatex RTV sealant was used.

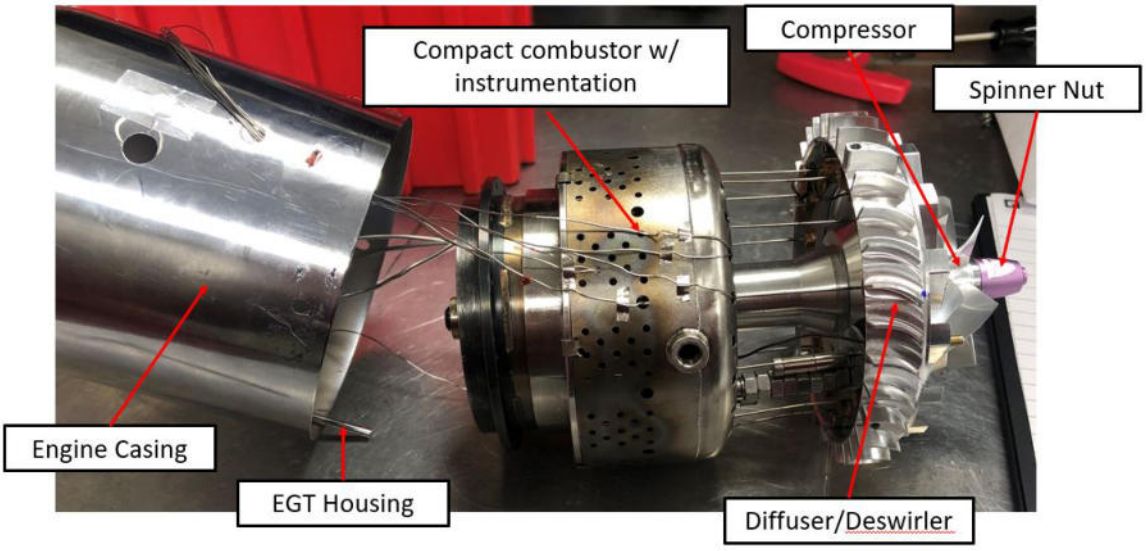

Figure 46. JetCat P160 compact combustor fully instrumented with K-type thermocouples

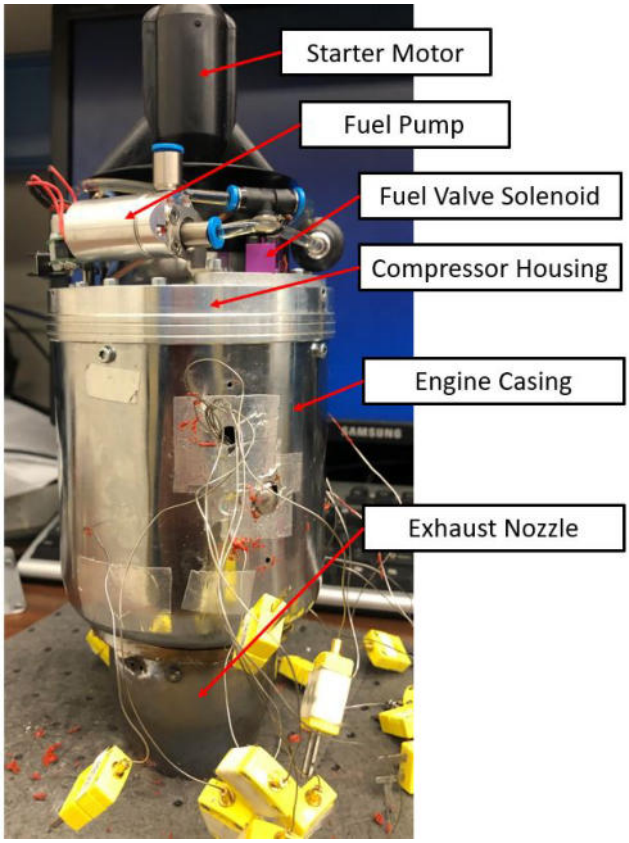

Figure 47. JetCat P160-RXi-B engine fully reassembled with instrumentation

3.2.3 JetCat P160 Test Facility.

To test the operability of the bluff-body compact combustor on liquid kerosene fuel in a JetCat P160 engine, experimental research was conducted within the Air Force Research Laboratory's (AFRL) Small Engines Research Lab (SERL) Test Stand 5. Figure 48 shows the JetCat P160-RXi-B engine on the engine stand within the research facility, which was equipped with compressed air, fuel delivery and storage systems, a thrust stand, and exhaust ducts. Since liquid kerosene was being tested with the JetCat P160 engine, fuel pumps transferred Jet A-1 fuel from the fuel cabinets to the fuel pump inlet located on the outer cowling of the JetCat engine. Also connected to the engine was the power cable for the ECU, which was connected to a 9.9V battery and a ground support unit (GSU). This GSU was capable of starting and stopping the engine, and cycling through several test functions. The engine was mounted to a thrust stand equipped with a thrust-force sensor capable of measuring force up to 445 N with an uncertainty of ±0.03% full scale [25].

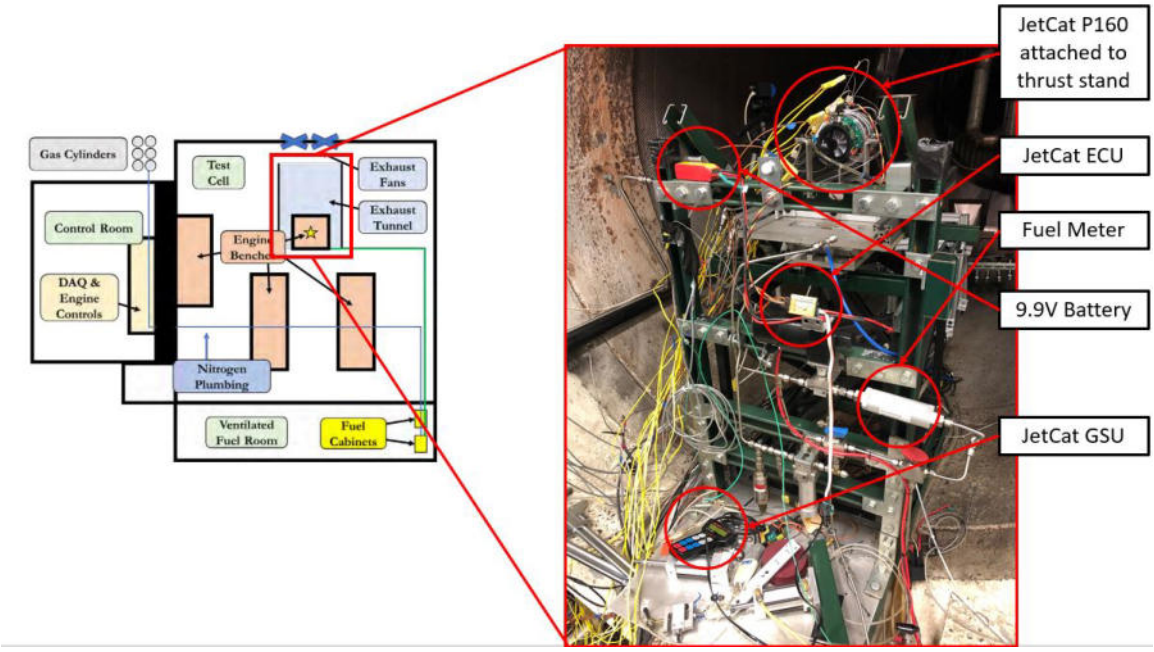

Figure 48. SERL test stand

Both thermocouple and pressure lines were fed to National Instruments data acquisition modules. These pressure and temperature instruments were able to be monitored during testing through a Labview program, as shown in Figure 49. This

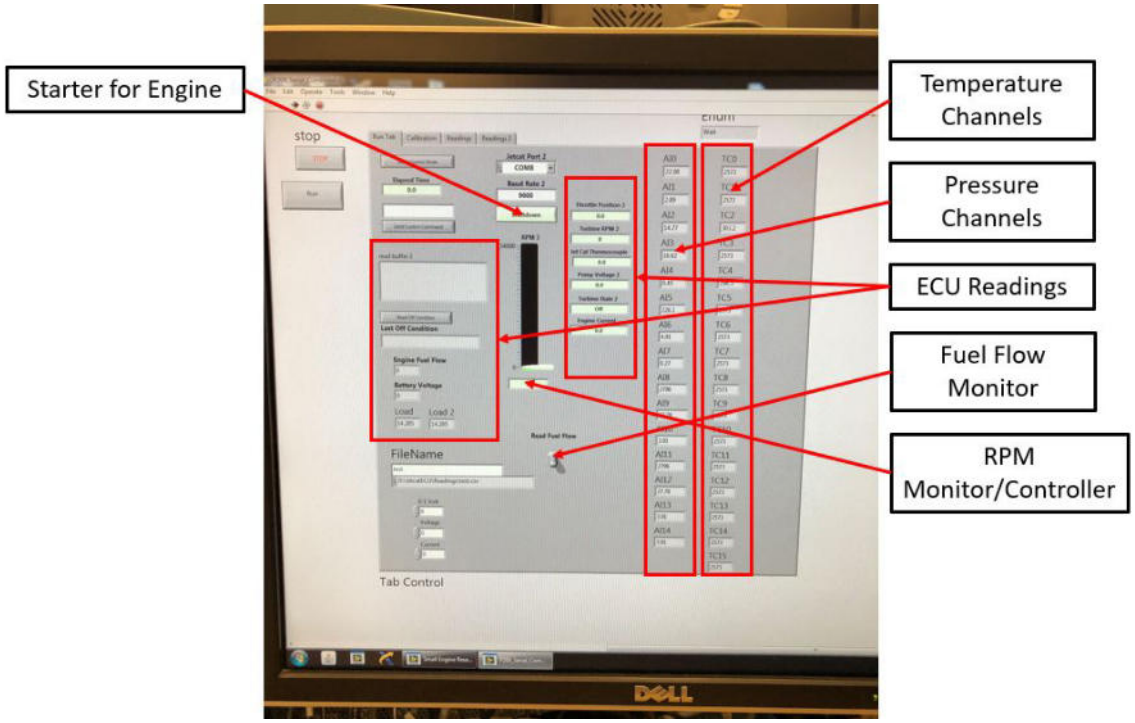

Figure 49. SERL Labview setup

Labview program was created by Nick Grannon, a research engineer within AFRL, which was designed purposely for testing and monitoring small-scale gas turbine engines. This Labview program was able to monitor readings coming from the stock JetCat engine control unit (ECU) through the use of a controller area network (CAN) bus board. This allowed the Labview program to monitor fuel flow rate, exhaust gas temperature, glow plug voltage, fuel pump voltage, battery voltage, and engine speed, along with pressure and temperature measurements coming from the data acquisition modules. The stock JetCat ECU was capable of measuring engine speed through the use of a hall effect sensor and a magnet that was placed within the spinner nut located on the shaft upstream of the compressor. The sensor was capable of measuring

the frequency between the changes in magnetic polarity as the compressor rotated leading to an engine speed reading.

To operate the Labview program, pressing the "Start" button initiated the stock JetCat start-up procedure. First, the glow plug would heat up for six seconds and the starter motor spooled the engine up to 3000 RPM. The engine then cycled through preheat conditions leaving the glow plug on for an additional thirteen seconds, and pumping fuel through a single fuel line terminating in the glow plug. If the JetCat EGT measured a rise in temperature above ambient conditions, it moved on to the ignition stage. At this stage in the start sequence, the starter motor increased the engine speed to 4500 RPM, fuel flow to the glow plug was reduced, the glow plug was heated for an additional two seconds, and the main fuel valve solenoid opened to begin flowing fuel through the fuel-air mixing tubes in the combustor. The ECU looked for a change in EGT greater than five degrees Celsius before the starter motor ramped up to full power, spooling the engine to 6000 RPM and increasing the main fuel flow. After this point, the starter motor disengages from the spinner nut, and the main fuel flow is increased until the the engine is roughly at 90% idle. Once this occurs, a PID controller takes over the fuel pump and the engine reaches its idle condition of 32,000 RPM. Once the engine achieves a self-sustained idle operation, it can be throttled manually to any desired engine speed past the idle condition within the Labview program. To operate and power all of the data acquisition systems and solenoids for fuel delivery, a control panel and programmable logic control (PLC) panel were used, as shown in Figure 50.

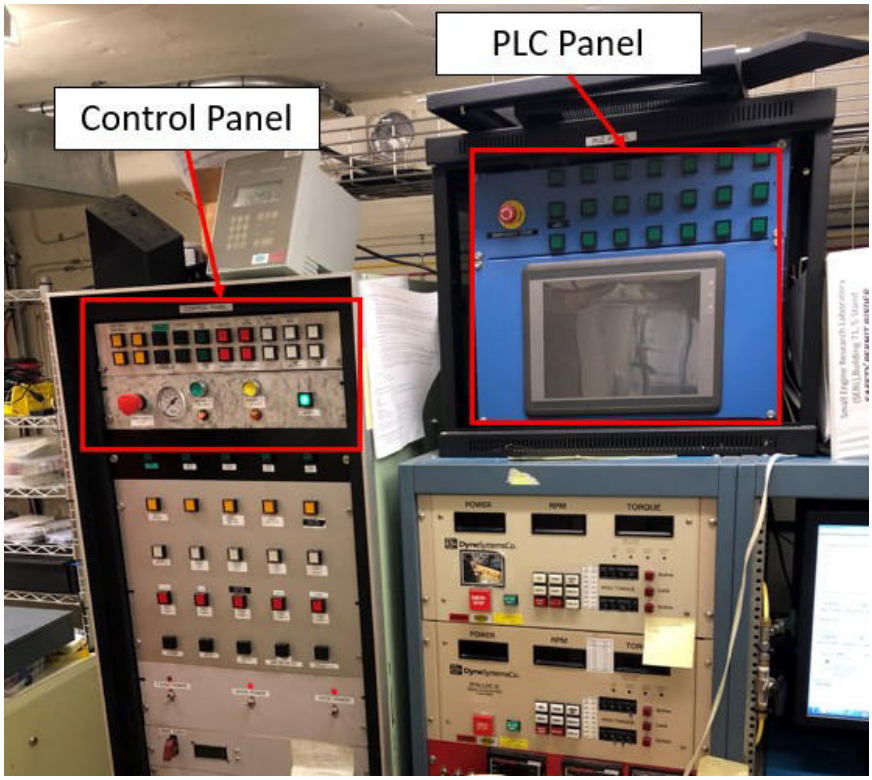

Figure 50. SERL control and PLC panels

3.3 JetCat P160 Experimental Testing

Figure 51 shows the P160 engine equipped with the bluff-body compact combustor mounted on the SERL thrust stand prepared for experimental testing. The P160 combustor struggled to burn around all fuel-tubes equally during its start-up sequence, as supported by the fuel-tube temperature plot shown in Figure 52. The engine start sequence was initiated after 20 seconds. At 25 seconds, the glow plug was powered on, and at roughly 30 seconds, ignition occurred. Tubes TC3F, G, and K, which correspond to the green, dark blue, and light blue lines respectively, warmed up first while there was roughly a 15 second ignition delay for the flame to work its way around the remainder of the combustor. The previously listed tubes were closest to the ignitor and warmed up in a clockwise direction matching the direction of any

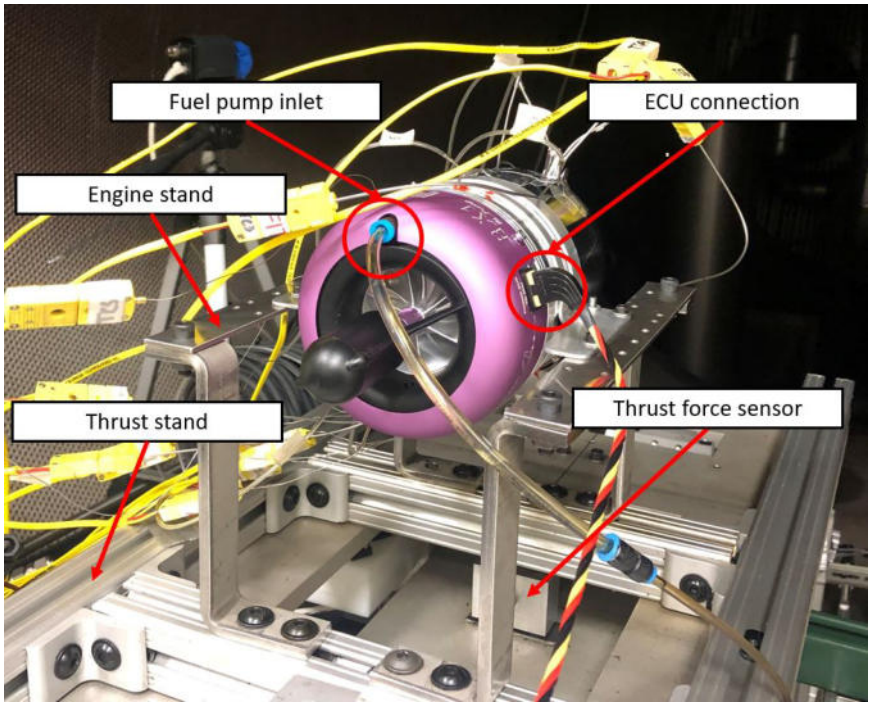

Figure 51. JetCat P160 engine equipped with the bluff-body compact combustor installed on the SERL thrust stand for testing

residual compressor swirl. However, the initial heat release from the first half of the combustor was not strong enough to heat the remainder of the combustor and reach stable combustion. This is shown by TC3H and I, which correspond to the orange and grey lines respectively, being considerably lower in temperature compared to the other fuel air mixing tubes. This led to the engine maxing out at 14,200 RPM and failing to stabilize and reach an idle condition of 32,000 RPM.

To attempt to remedy this issue, the air inlet holes on the forward dome of the combustor were blocked using exhaust ducting tape, as shown in Figure 53. These air inlet holes were crucial for establishing recirculating flame holders on the backside of the impingement plate, however, during start-up the air passing through these holes was making it difficult for the initial pilot flame to work its way around the combustor. Blocking all of the air inlet holes allowed the fuel tubes to preheat more quickly since all of the air entering the compressor could only come from the outer

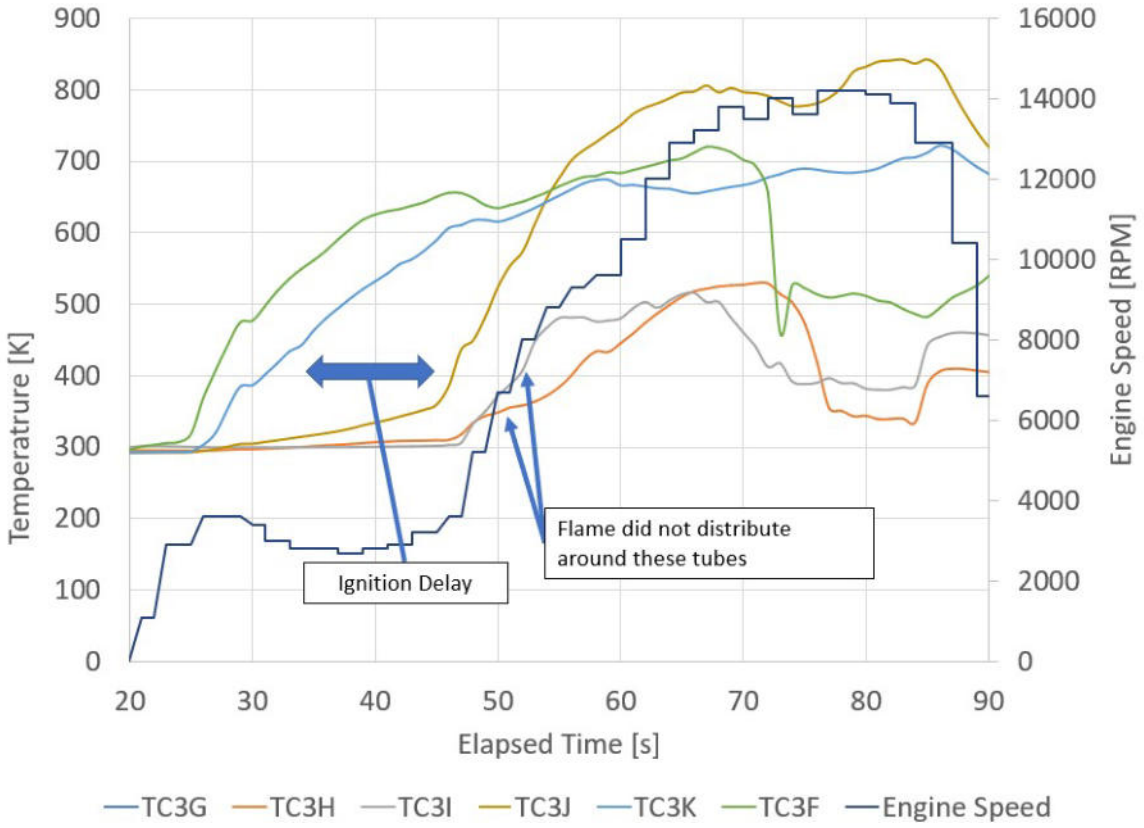

Figure 52. Circumferential fuel-tube temperatures at an engine speed of 14,200 RPM

and inner liners.

To test the application of this idea, experiments were performed where 100%, 58%, and 17% of the air inlet holes were blocked. At the 100% blocked configuration, the engine was able to reach a sustained operation at an idle condition of 32,000 RPM before the ECU shut down the engine due to an over temperature condition one second later. With the air inlet holes fully blocked, the compact combustor was behaving similarly to the stock combustor at a reduced length meaning the combustion wasn't complete at the combustor exit plane, which led to additional combustion occurring in the exhaust. The 17% blocked configuration behaved similarly to the unblocked configuration reaching a maximum engine speed of 14,200 RPM, while the 58% blocked configuration achieved a higher speed of 23,300 RPM as a result of increased flame distribution around the fuel-air mixing tubes.

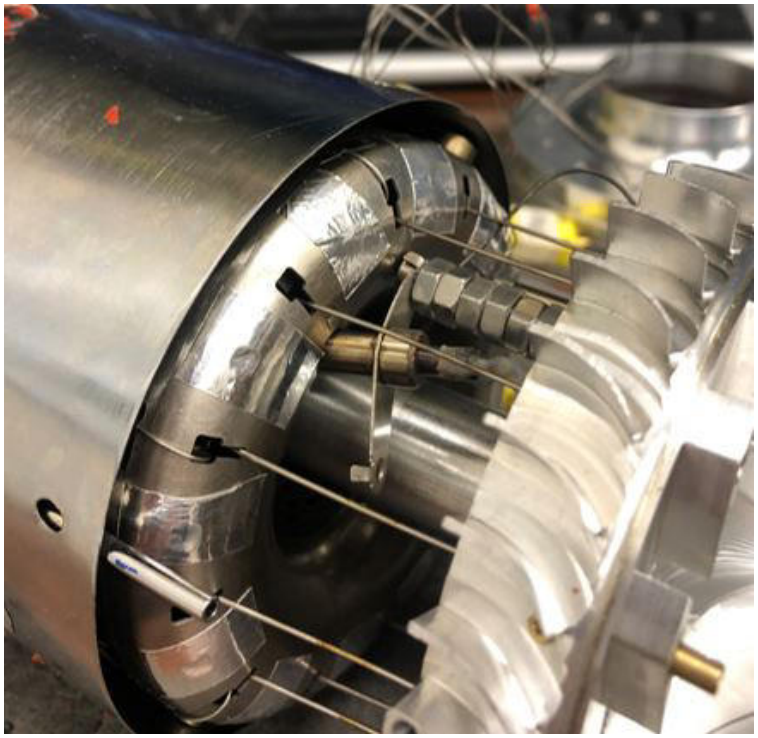

Figure 53. Air inlet holes on forward dome blocked with exhaust ducting tape

To preheat the engine effectively, which entails distributing a flame across the entire circumference of the combustor, it would be preferred to have all of the air inlet holes blocked at initial start-up, and then as an idle condition was approached, open all of the air inlet holes on the forward dome so that the bluff-body flame holding mechanism within the compact combustor was utilized to improve residence time and ensure burning was contained within the combustor.

A restrictor plate was designed, as shown in Figure 54, so that it could be rotated about the shaft housing and allowed the air inlet holes to transition from fully closed to fully open, while not interfering with the fuel lines. Figure 54a shows the CAD model of the blockage assembly which includes the traversing blockage plate placed in front of the forward dome of the combustor, a pivoting arm which passed through both the blockage plate and the engine casing and was coupled to the servo motor. Figure 54b shows the final manufactured blockage plate assembly installed over the forward

dome of the current combustor. The manufactured blockage plate was machined from 316 stainless steel and relied on the OD of the combustor liner to align circumferential rotation rather than the OD of the shaft housing as previously designed. This can be seen in Figure 54b which shows the mounting points used on the OD liner of the combustor to lock the blockage plate axially and allow the plate to only rotate 7.5 degrees to achieve fully open or fully closed conditions, which are shown in Figure 55. During the start-up sequence of engine testing, the blockage plate would be rotated such that the air inlet holes are blocked/closed, as shown in Figure 55a. Once the engine was approaching idle conditions, the blockage plate would be rotated counter-clockwise to open the air inlet holes, as shown in Figure 55b.

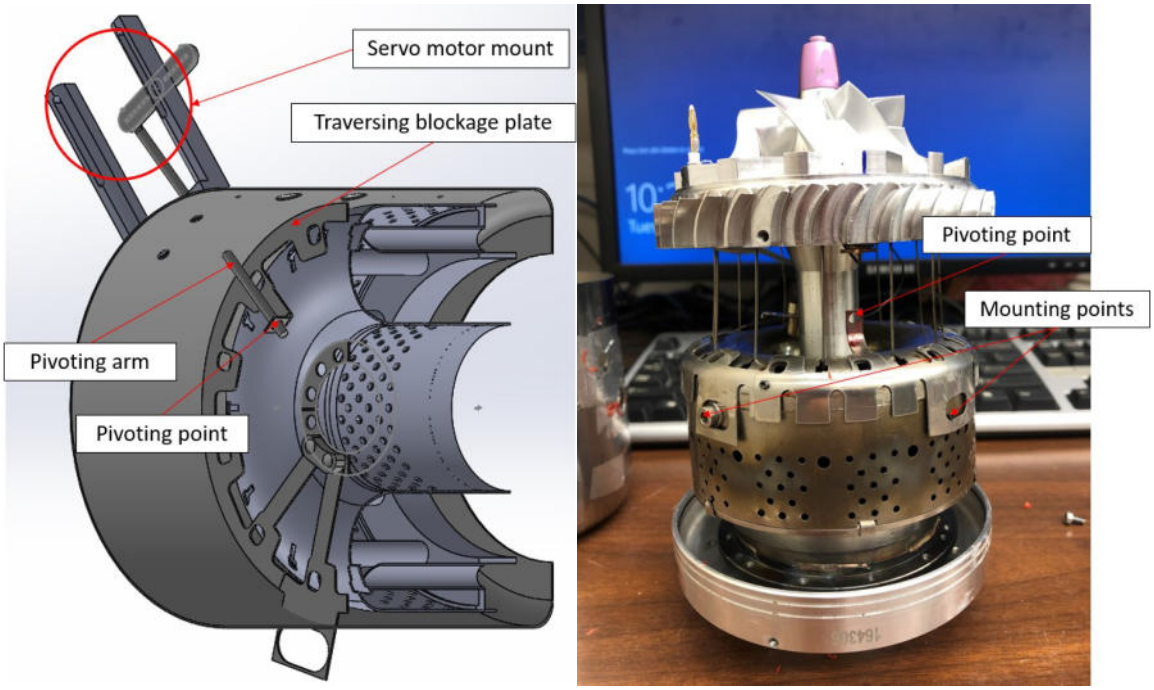

(a) (b)

Figure 54. (a) CAD model of the blockage plate assembly versus (b) the manufactured blockage plate assembly fitted to the combustor liner

Figure 56 shows the servo motor, servo motor mount, and pivoting arm being used during an experimental test of the JetCat P160 engine equipped with the current

combustor. To rotate the plate, the servo motor was connected to an Arduino, which could be controlled by a Labview program. Rotating the servo motor's arm would cause the pivoting arm to rotate about the pivot point located on the outside of the engine casing. This would cause the pivoting arm to translate its movement to rotation of the blockage plate to open and close the forward dome air inlet holes.

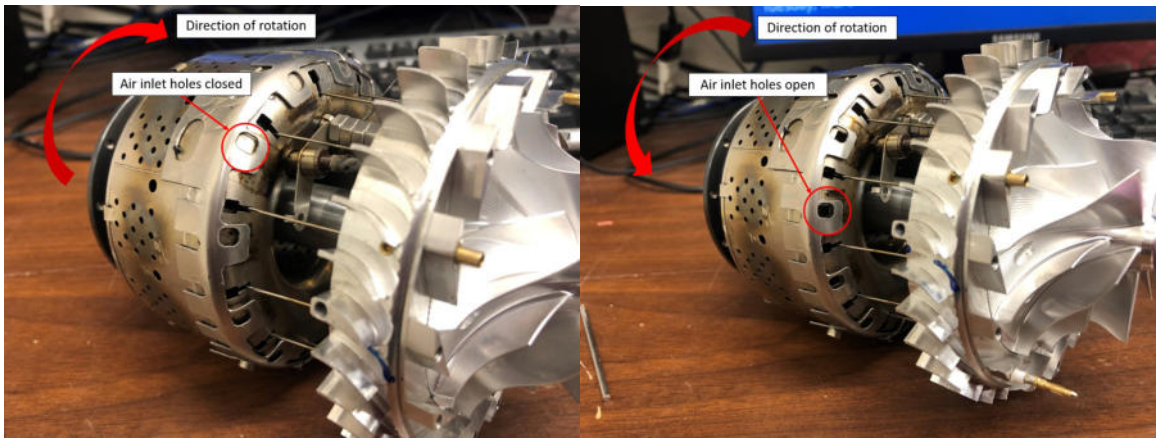

(a) (b)

Figure 55. Assembled blockage plate assembly showing the forward dome air inlet holes (a) closed and (b) open when rotated

With the JetCat P160 RXi-B engine equipped with this articulating blockage assembly, the flame was able to distribute across the entire circumference of the combustor during the start-up sequence with the air inlet holes blocked. Once the fuel tube temperatures were above 500 K, suggesting a flame had distributed around the circumference of the combustor, the air inlet holes were opened at varying engine speeds. This involved opening the air inlet holes by increments of 25% starting at engine speeds ranging from 10,000 to 30,000 RPM. Additionally, the air inlet holes were opened instantly (from 0 to 100%) in the same range of engine speeds. However, when the air inlet holes were opened, regardless of engine speed, the engine wasn't able to reach a sustained operation or an idle condition. Instead, combustion continued to occur in the exhaust preventing the engine speed from increasing.

This outcome suggested that the bluff-body flame stabilization mechanism within the compact combustor was not sufficient for the liquid kerosene fuel and didn't provide sufficient residence time to allow the reactants to achieve complete combustion before reaching the turbine inlet plane.

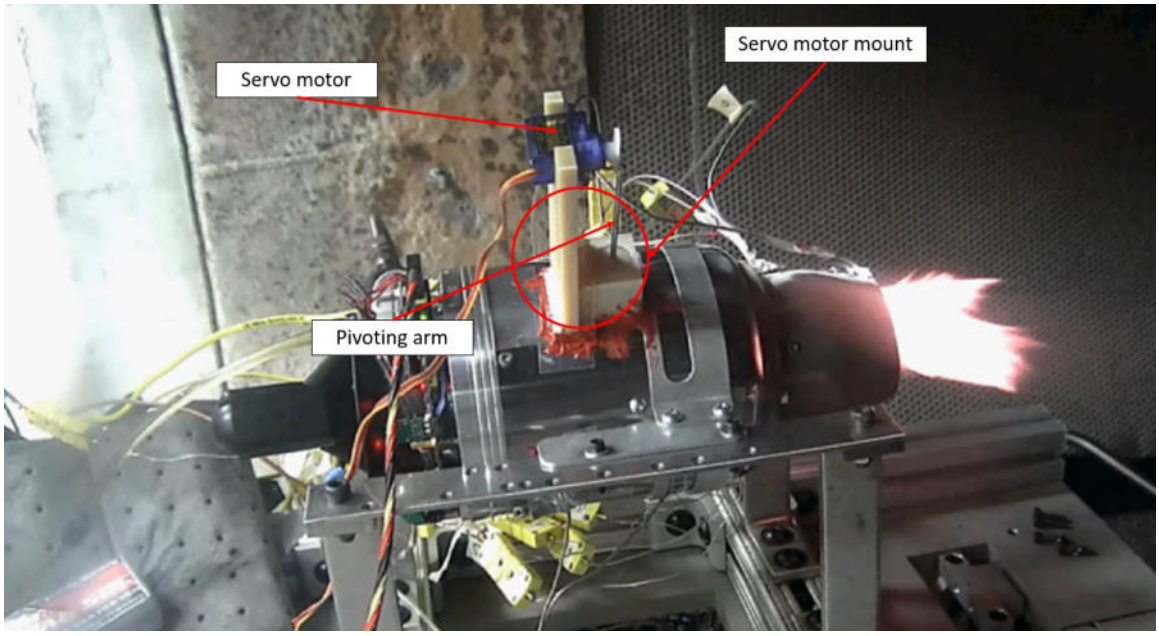

Figure 56. The blockage plate assembly coupled with the servo motor installed and fitted to the engine casing undergoing experimental testing

3.4 JetCat P160 Computational Setup

To understand why a flame was not stabilizing within the P160 combustor, CFD simulations were performed in ANSYS Fluent for half-idle, idle, and design conditions using liquid kerosene fuel. Section 3.4.1 discusses the methodology behind the grid generation used for analyzing the P160 compact combustor. Section 3.4.2 discusses the CFD simulation parameters used in ANSYS Fluent to solve each design point. Finally, Section 3.4.3 discusses the grid independence study performed after the CFD simulation to validate the computational results.

3.4.1 JetCat P160 Compact Combustor Grid Generation.

To generate a grid of the burner section of the P160 engine equipped with the compact combustor, a negative CAD model of a 30^o sector of the burner section was designed in SolidWorks, as shown in Figure 57, and exported as an IGES (Initial Graphics Exchange Specification) file to be read by Pointwise. A 30^o sector was considered since there were twelve vaporizer tubes within the 360^o model. Given that the model was periodic, a 30^o sector could be used in which only one of the vaporizer tubes was simulated. This negative CAD model featured an inlet condition that represented the compressor exit of the engine and an exit condition that represented the turbine inlet of the engine, which included the turbine stators. Once imported into Pointwise, the periodic domains were first created to establish a periodic boundary condition. This boundary condition, once recognized by ANSYS Fluent, enabled the flowfield coming out of one periodic face to enter the other. This boundary condition enabled only a 30^o sector of the combustor to be analyzed, saving computational time.

In Pointwise, the connectors for the entire combustor domain were placed with a uniform node spacing of $\Delta s = 0.015$ mm. Additionally, all of the domains and blocks that were generated had boundary layer decays of 0.80, enabling volume near and around the walls to be refined and the volume far from the walls more coarse. The domains created off of these connectors were all unstructured grids with the exception of those around areas of curvature. These areas did not generate grids that matched the original geometry so structured grids were used in these locations.

Once all of the domains were generated, they were organized into three categories/layers based on whether a particular domain represented a fluid, solid, or fluid-solid interface. This enabled the creation of two blocks: one representing the solid metal of the combustor itself and another representing the fluid flowing through the combustor. With these two blocks generated, boundary conditions were applied

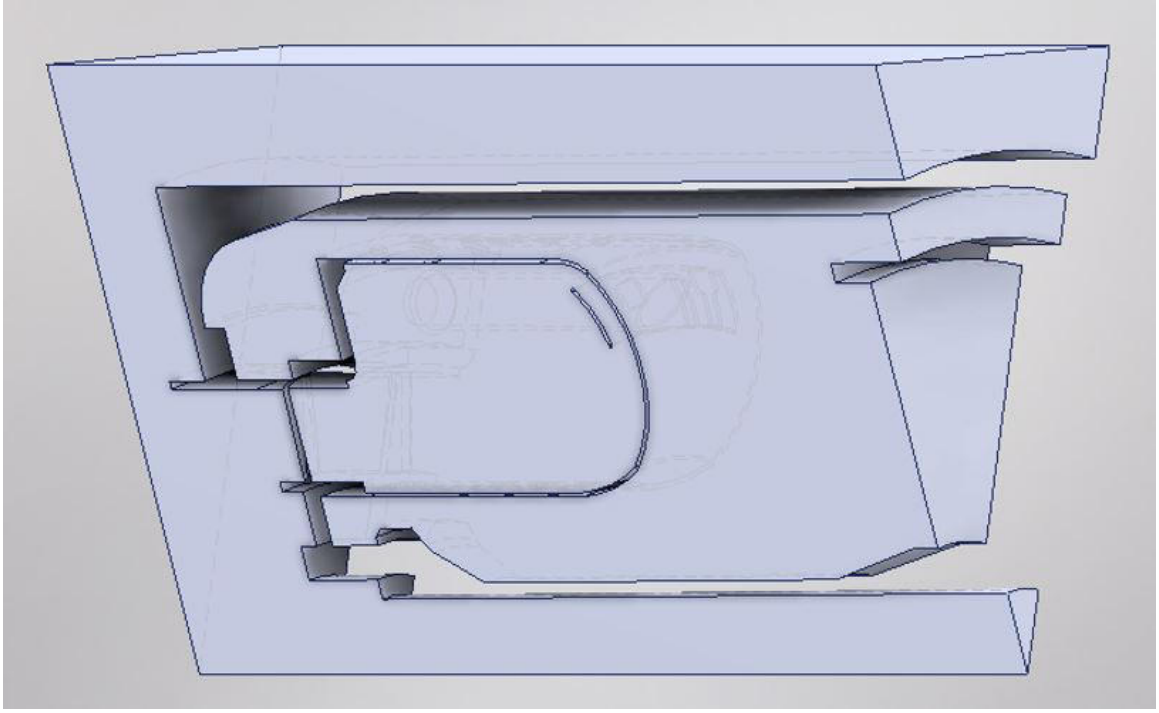

Figure 57. Negative CAD model of a 30-degree sector of the JetCat P160 engine

to the outer shell of the block, as shown in Figure 58, which included a mass-flow inlet, a pressure outlet, an adiabatic wall, a constant surface temperature, and periodic faces.

The last step before generating the Fluent case file for computational analysis was to set the volume conditions. This enables Fluent to recognize and differentiate between the solid and fluid volumes and enable a conjugate heat transfer analysis. With the solid and fluid blocks assigned accordingly, the case file was exported into Fluent with approximately 20 million cells.

3.4.2 JetCat P160 Compact Combustor CFD Simulation.

ANSYS Fluent was used to simulate the performance of the P160 compact combustor under the use of liquid kerosene for half-idle, idle, and design conditions to aid in explaining why the current P160 combustor failed to stabilize at any condition.

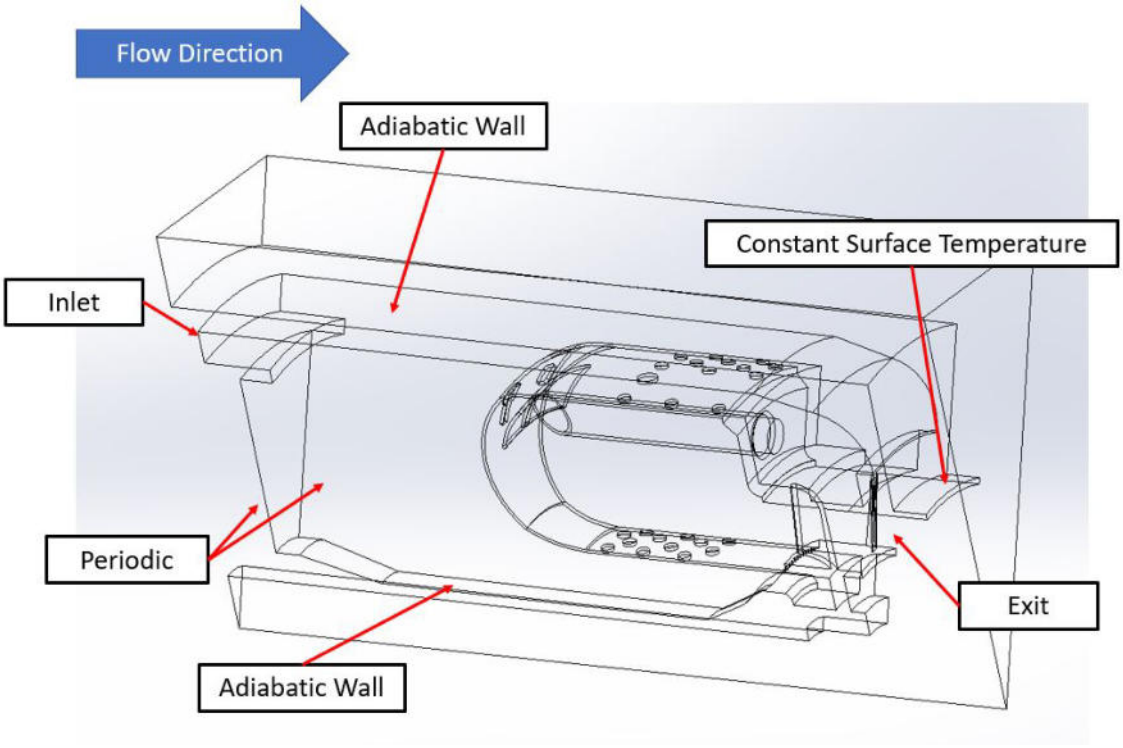

Figure 58. Boundary conditions applied to the 30-degree P160 block in Pointwise

To accurately simulate the flow-field within the combustor, several models were used within ANSYS Fluent. Simulations for all three cases utilized pressure-based, steady-state solvers equipped with a $\kappa - \epsilon$ realizable turbulence model with enhanced wall treatment. Additionally, the combustor was modeled utilizing a partially premixed kerosene-air mixture with flamelet generated manifold and diffusion flamelets. This model could predict quenching due to interactions between the flamelets and wall surfaces, which supplemented the conjugate heat transfer solver. The combustor walls were modeled as Inconel-600 matching the compact combustor physical hardware.

3.4.3 JetCat P160 Compact Combustor Grid Independence Study.

The computational grid used for the solution contained 20 million cells. To verify grid independence, the original grid was globally uniformly refined and coarsened by

20%, which pertained to 15 and 25 million cells, respectively. The average y^+ along the wall between the coarsened, base, and refined grids was 6.85, 6.45, and 6.43, respectively, showing that the wall had sufficient resolution for the $\kappa - \epsilon$ turbulence solver where a y^+ below 300 was recommended [28]. To verify grid independence across all three grids, the inlet to the forward dome and combustor exit plane were the two locations used, as shown in Figure 59, where velocity and temperature data were compared.

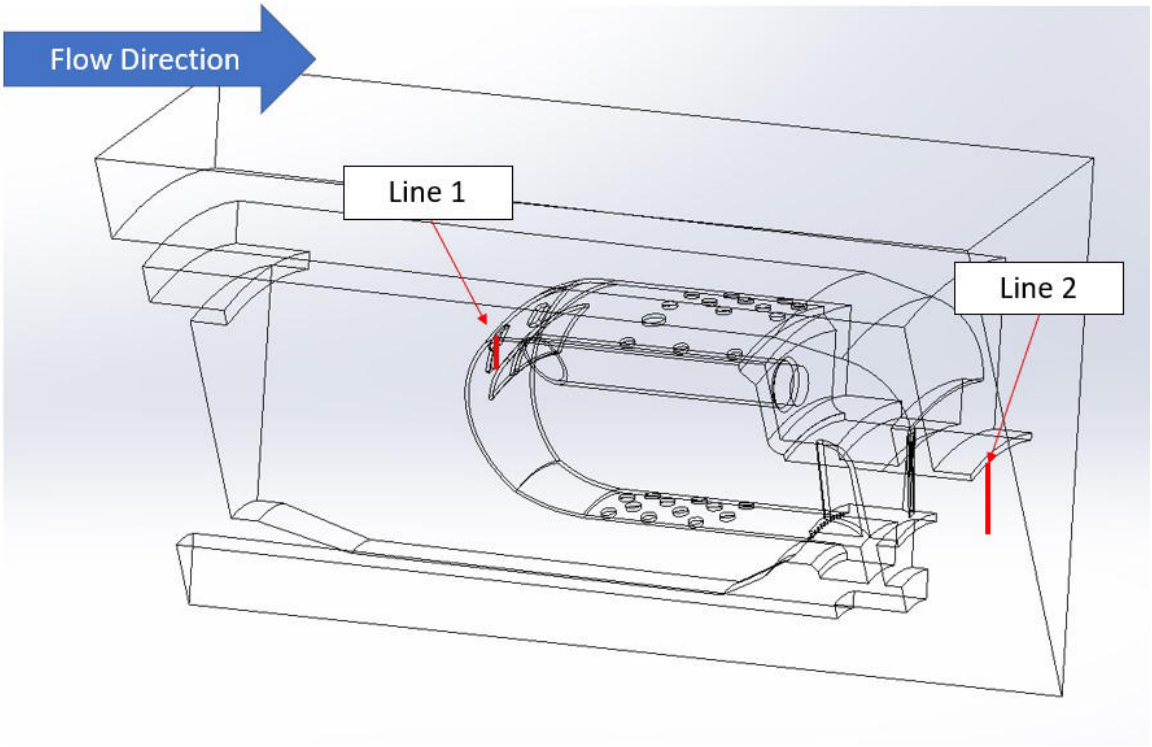

Figure 59. The two lines used to determine grid independence

The velocity profiles for Lines 1 and 2 are shown in Figures 60 and 61, while a circumferentially averaged temperature profile for Line 2 is shown in Figure 62. Starting with the circumferentially averaged velocity profiles for Line 1, there was a maximum variation of roughly 3% between all grid resolutions. Circumferentially averaged temperature and velocity profiles were reported for Line 2 where there was a maximum variation of roughly 2% in temperature, and a maximum variation of

roughly 2% in velocity between all grid resolutions. This small variation between the coarsened and refined grids used in this study suggested the computational results were independent of grid resolution therefore allowing the base grid of 20 million cells to be used for all computational simulations.

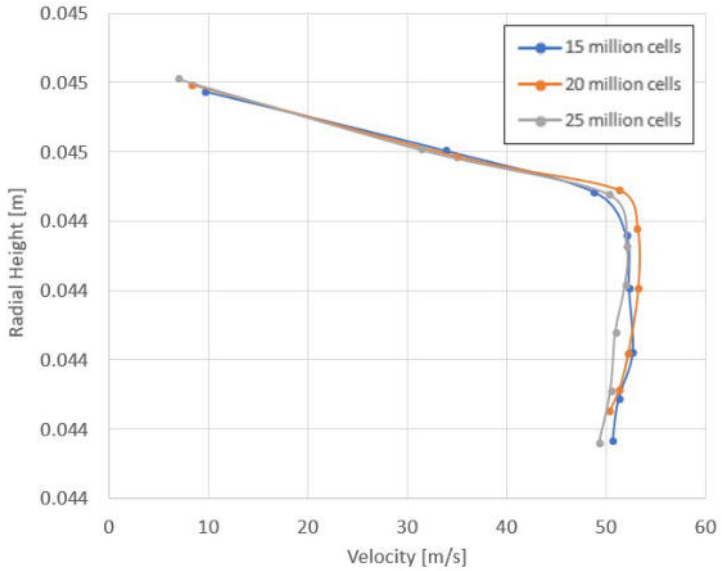

Figure 60. Velocity profile at Line 1

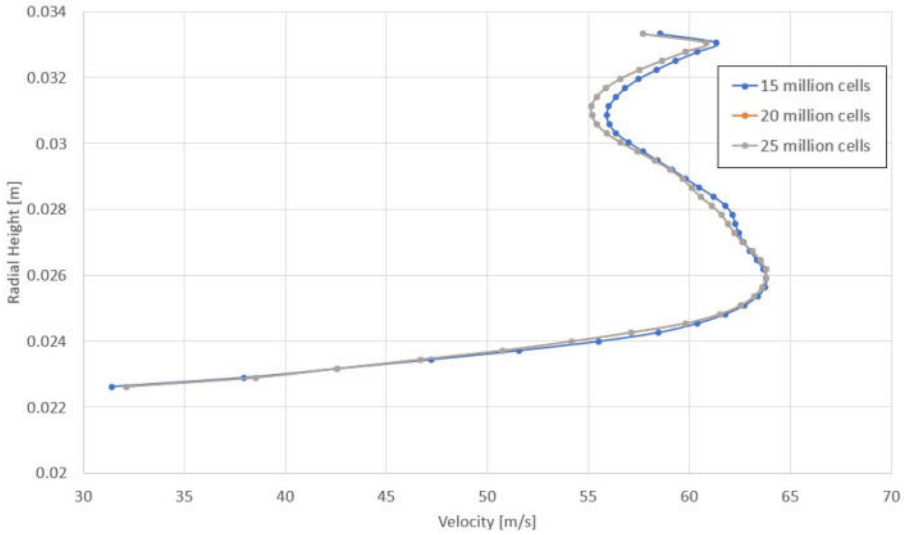

Figure 61. Velocity profile at Line 2

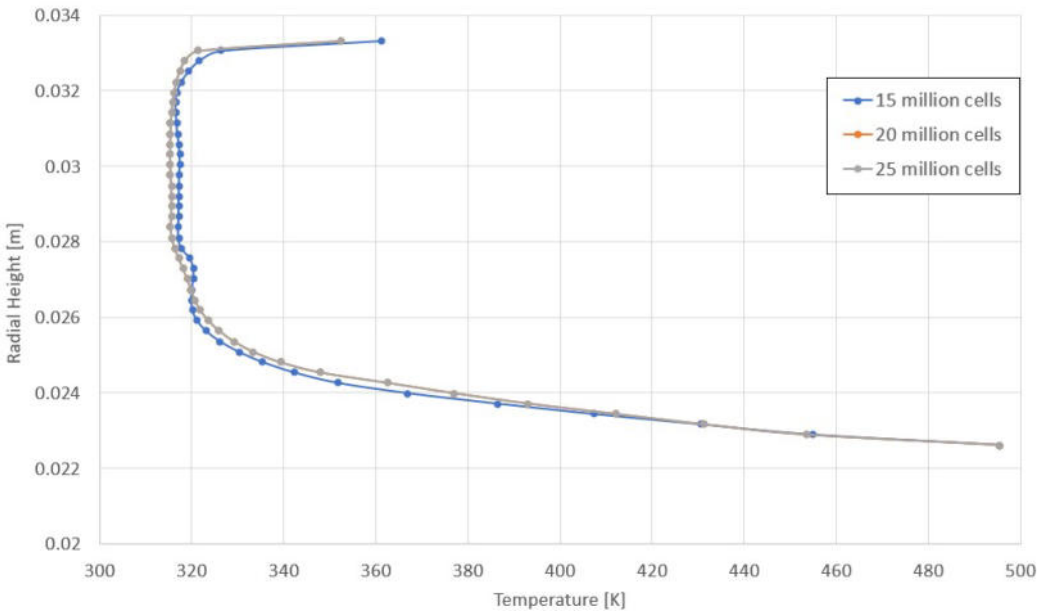

Figure 62. Temperature profile at Line 2

3.5 JetCat P160 compact combustor CFD Results

To supplement the experimental results and determine why a flame was not stabilizing in the combustor, a 30-degree sector of the compact combustor integrated into the JetCat P160 RXi-B engine was analyzed in ANSYS Fluent at half-idle and idle conditions of 15,800 and 32,000 RPM, respectively. For the half-idle case, a pressure-inlet boundary condition was used rather than a mass-flow inlet boundary condition since this quantity could be gathered from experimental data. This condition corresponded to an inlet absolute pressure of 98.62 kPa. For the idle case, a mass-flow inlet boundary condition was used, which corresponded to a flow rate of 5.85 g/s. This case yielded an inlet absolute pressure of 114.35 kPa which matched the experimental data within 12.5%.

Starting with the half-idle condition, Figure 63 shows static temperature contours at a cut-plane half-way through one of the fuel-air mixing tubes in the combustor. This temperature contour plot shows all of the burning occurring near the combustor

exit plane along with a lack of a pilot flame present directly behind the impingement plate. This lack of a pilot flame caused two primary issues: 1) there was no stable flame-holding region in the combustor, which caused the combustion reactions within the combustor to be unanchored, potentially leading to blow-out, and 2) there was not sufficient residence time to burn the fuel-air mixture completely when the intended flame-stabilization technique was not being used, causing burning to continue well past the combustor exit plane.

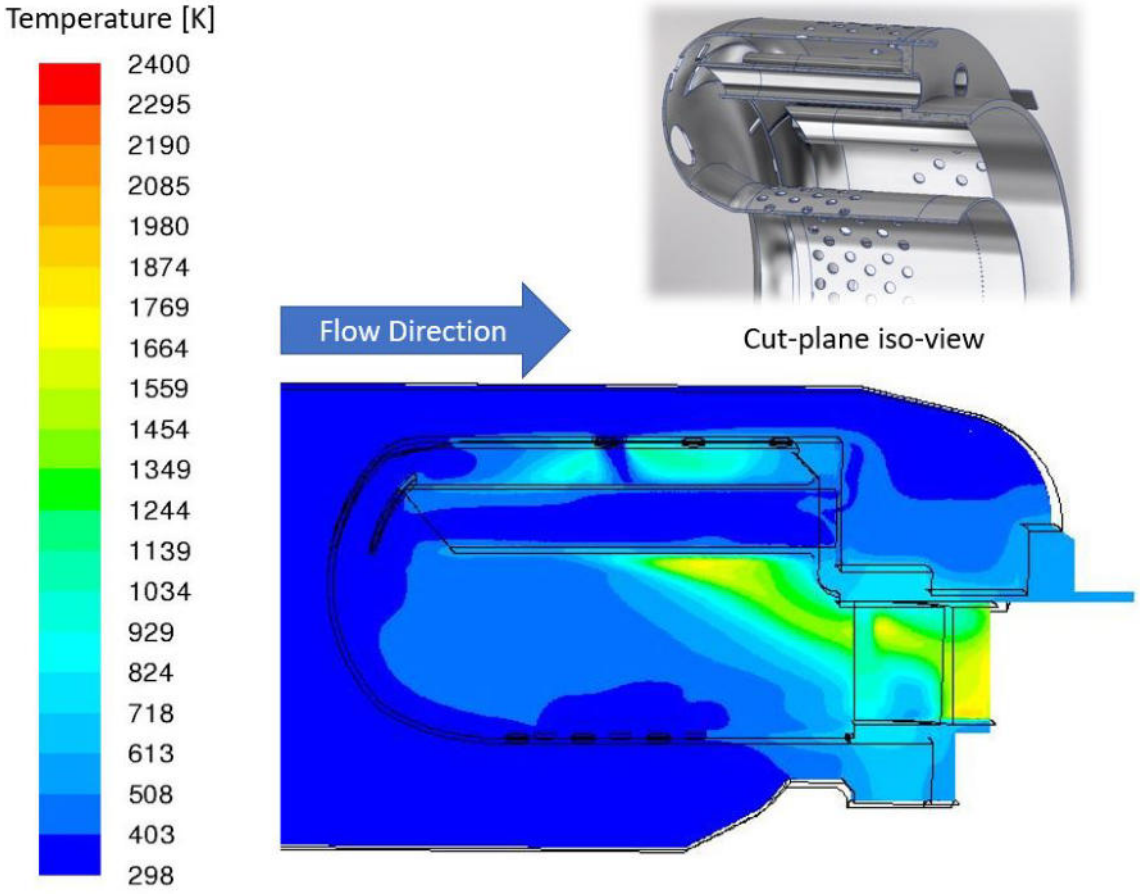

Figure 63. Static temperature contours for a half-idle condition

One of the reasons a pilot flame was not being held directly behind the impingement plate can be seen in Figure 64, which compares the CFD results from Holobeny et al. [2][3] for the P90 design condition against the current combustor at the half-

idle condition. This figure shows velocity vectors along with pathlines colored by velocity magnitude at the center-cut plane in between each of the fuel-air mixing tubes. Holobeny et al. [2][3] found two small recirculation regions directly behind the impingement plate that were sufficient to computationally show stable burning for gaseous propane at idle, mid-power, and design conditions. However, the velocity vectors and pathlines for the current combustor did not match the results from Holobeny et al. [2][3] and instead showed a recirculation region directly above the impingement plate and an additional recirculation region coming off the exit of the fuel-air mixing tube. The lack of recirculation regions directly behind the bluff-body led to insufficient residence time, causing burning to occur much further downstream. Since burning occurred further downstream without the use of stable flame-holders, as the engine speed increased, the reactions were pushed out of the combustor entirely.

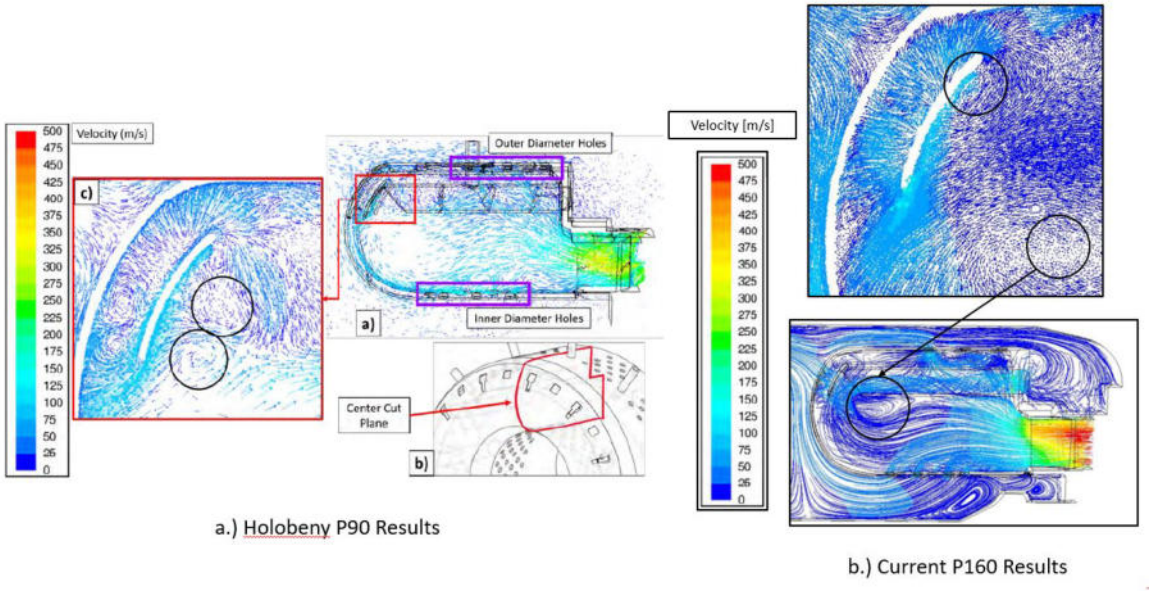

Figure 64. Comparison between a.) Holobeny et. al's [3] design point results versus b.) the current effort

Another reason a pilot flame was not being held directly behind the impingement plate was due to how rich the fuel-air mixture was coming from the exit of the

vaporization tubes, as shown in Figure 65. For the half-idle case, the equivalence ratio of the mixture hitting the backside of the bluff-body was significantly above stoichiometric, which prevented any burning from occurring in that region. Instead, burning occurred along the contours where the equivalence ratios were closer to or below stoichiometric, which happened to lie closer to the exit plane of the combustor.

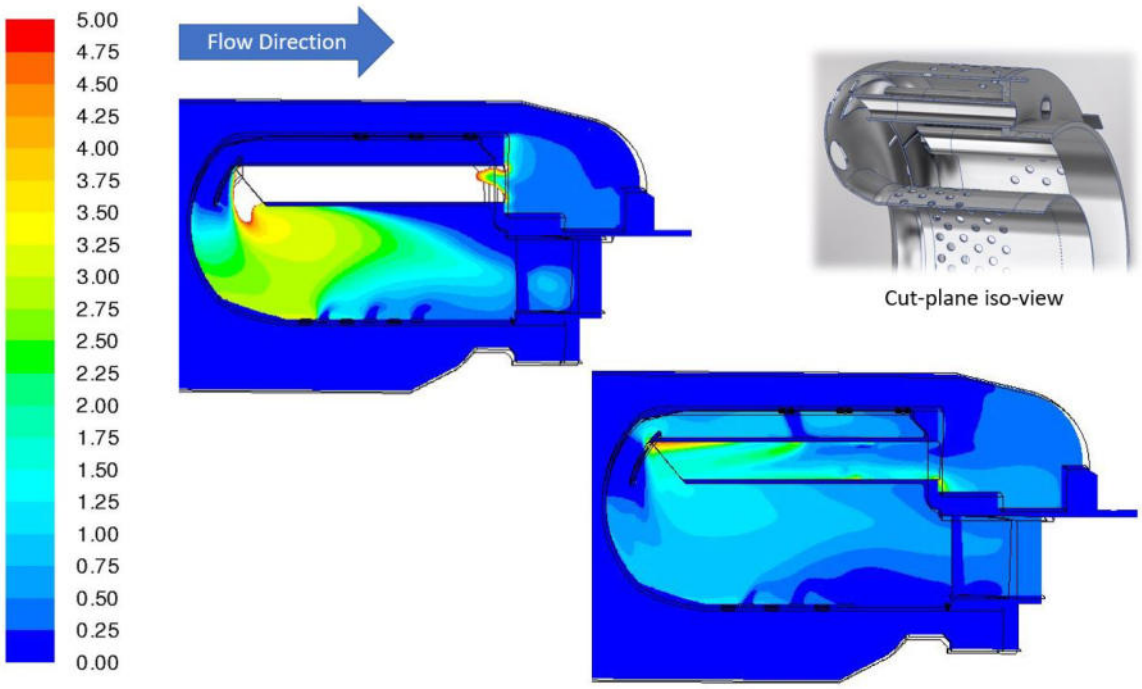

Figure 65. Equivalence ratio contours for the current study at half-idle (top-left) and idle (bottom-right) conditions

A portion of the air coming from the compressor was designed to enter the backside of the fuel-air mixing tubes to mix with the fuel and lean out the mixture. At design conditions, roughly 13% of the air coming from the compressor traveled through the backside of the tubes. The global equivalence ratio was 0.34 in the combustor [3]. At this half-idle condition, only 6% of the air coming from the compressor was entering the tubes, leading to a very rich fuel-air mixture within and exiting the fuel tubes. As the mass flow was increased to an idle condition, also shown in Figure 65, the amount of air coming from the compressor and entering the tubes increased to 8%

which leaned out the fuel-air mixture, however, the mixture was still too rich to burn directly behind the bluff-body. This effect coupled with the lack of flame-holders present in the primary zone of the combustor caused CFD to predict no burning at an idle condition.

3.6 JetCat P400 Compact Combustor Design

To resolve the issue of residence time requirements associated with smaller scale engines, it was desirable to scale the P160 compact combustor up to the P400 scale to improve its operability and provide more volumetric space to implement novel flame-stabilization techniques. Based on the computational results of the JetCat P160 equipped with the compact compact, rather than scaling the bluff-body compact combustor to the P400 scale, an entirely new flame stabilization scheme was used. The current compact combustor designed for the P400 engine was a trapped-vortex combustor which still had to meet the following constraints provided by the engine. Table 2 shows a table comparing some of the design parameters between the P160 and P400 gas turbine engines. While both engines share the same pressure ratio, the P400 engine houses a larger compressor and turbine enabling the maximum air mass flow rate and thrust to be higher. Additionally, this increase in rotational mass causes the P400 engine to have a slightly lower idle and maximum speed compared to the P160 engine.

Figure 66 outlines the critical components of the JetCat P400 engine which, similar to the P160 engine, includes a starter motor, compressor, diffuser/deswirler, combustor, NGV housing, turbine, and exhaust nozzle. Regarding the stock P400 combustor, there are subtle differences in the design compared to the stock P160 combustor. While both the stock P160 and P400 combustors make use of fuel vaporization tubes to inject a mixture of fuel and air into the primary zone, the tubes in the P400 com-

Table 2. JetCat P160 and P400 Engine Comparison Chart [4][32]

	JetCat P160 RXi-B	**JetCat P400**
Pressure ratio	3.8	3.8
Max air mass flow [kg/s]	0.38	0.67
Max fuel consumption [ml/min]	510	1300
Weight [g]	1670	3650
Engine casing diameter [mm]	112	148.4
Length [mm]	297	353
Idle speed [1/min]	32000	30000
Max speed [1/min]	122000	98000
Thrust at idle [N]	7	14
Max thrust [N]	158	397

bustor angle inwards by 6 degrees towards the centerline of the engine. Additionally, the fuel tubes grow in diameter from the starting and ending points of the tubes. The slight angle inwards causes the fuel-air mixture within the tubes to swirl and enhance the mixing process, and the expansion of the tubes as the fuel-air mixtures progress down the length of the tube enables the fuel-air mixture to diffuse and occupy as much volume within the primary zone as possible for even circumferential burning.

The design of the TVC was built off the work of Briones et al. [31] who performed a parametric study on a TVC at the P400 scale and matched the axial length of the stock burner. The goal of their study was to vary parameters such as cavity height, air driver hole locations, and air driver hole diameters to reach an optimized TVC design. The study looked at output variables such as average and maximum combustor exit temperatures, combustion efficiency, pattern factor, critical liner area factor, and total pressure loss (TPL) as figures of merit. Through this effort, they reported on three of the best designs based on the figures of merit, as seen in Figure 67, where design iteration 58 (DP58) was chosen as the "best" design. However, for the present effort, the goal was to shorten the length of the combustor. Based on this criteria, design iteration 43 (DP43) was chosen over 58 and 38 as it revealed a

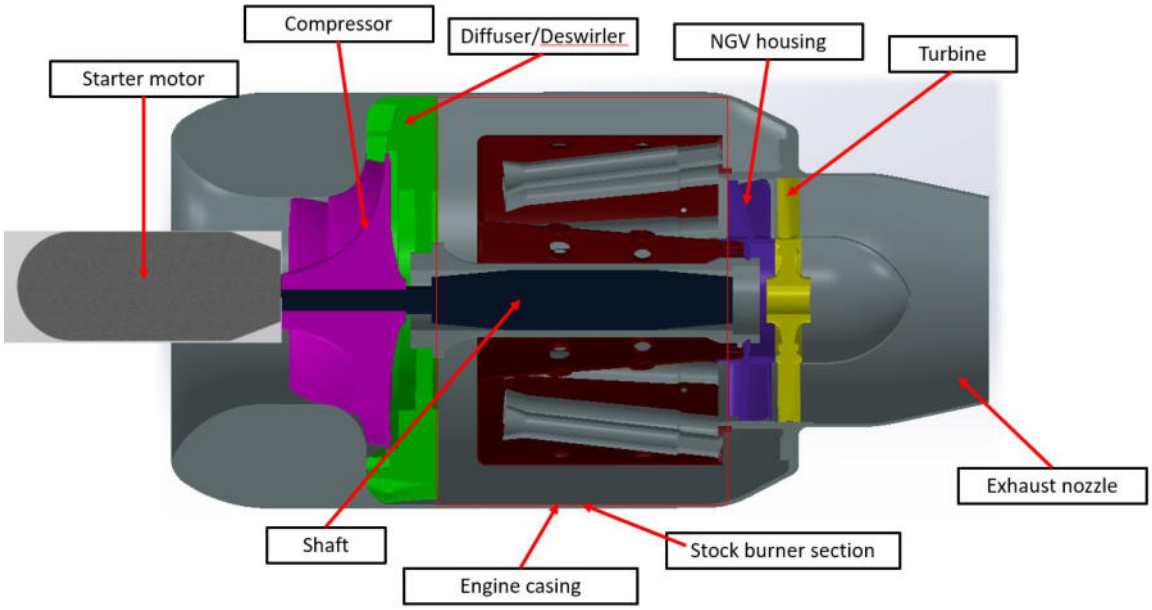

Figure 66. CAD model of JetCat P400 engine equipped with the cavity-stabilized compact combustor

condition with the most complete combustion in the TVC cavity and little variation in temperature after approximately 50% travel between the TVC cavity and the nozzle guide vane inlet. This meant that the axial length of the combustor downstream of the cavity could possibly be reduced while still retaining the cavity dimensions specific to the DP43 design. Section 3.6.1 discusses all of the design iterations that were analyzed computationally to arrive at a final manufacturable model that would mate within a stock P400 engine.

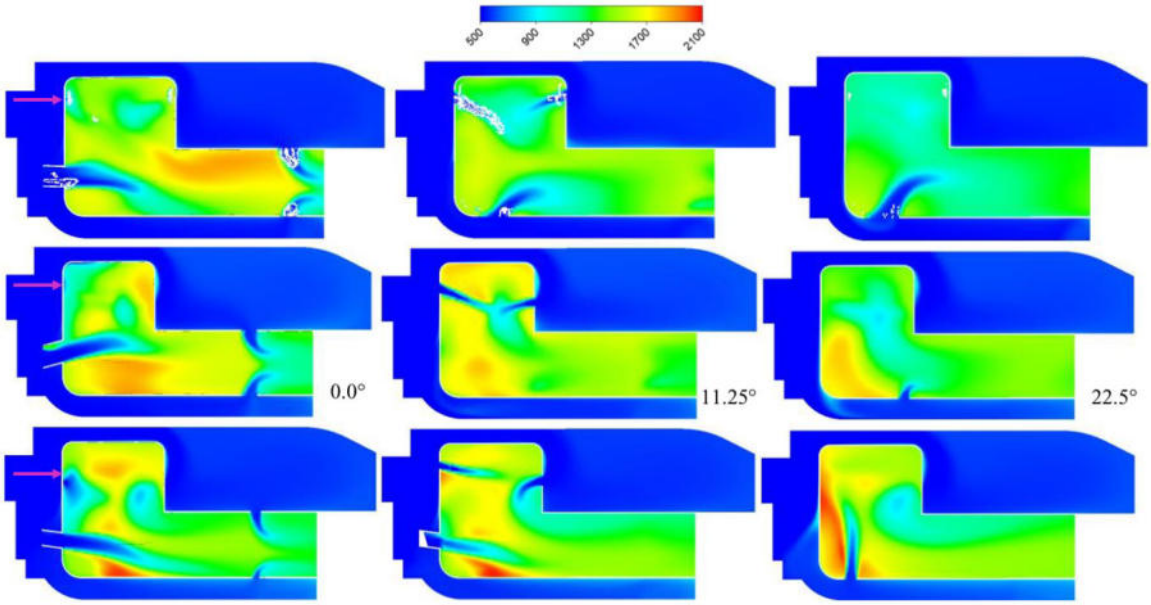

Figure 67. Temperature distributions at the centerplane (0°), staggered plane (11.25°), and periodic plane (22.5°) for the "best" design points [(top) DP58, (middle) DP38, and (bottom) DP43] Adapted from [31]

3.6.1 JetCat P400 TVC Iterative Designs.

Since the bluff-body flame stabilization technique was not able to hold a stabilized flame at the P160 scale, a new trapped-vortex stabilization scheme was designed and implemented for the P400 scale. Previous work by Briones et al. [31] looked at designing and optimizing a P400-scale outboard cavity combustor, as shown in Figure 68. This design featured forward and aft air driver holes to establish and maintain a vortex within the cavity, a radially-located liquid fuel spray, chutes which were designed to close off the cavity and trap the vortex, and dilution jets to both cool the inner and outer liners and dilute the combustion byproducts.

Since the goal of the current study was to design a compact combustor at the P400-scale which utilized all of the pre-existing engine hardware, the fuel injection system in the analyses of Briones et al. [31] needed to be addressed in the DP43 design. The DP43 computational design of Briones et al. [31] featured a liquid-fuel

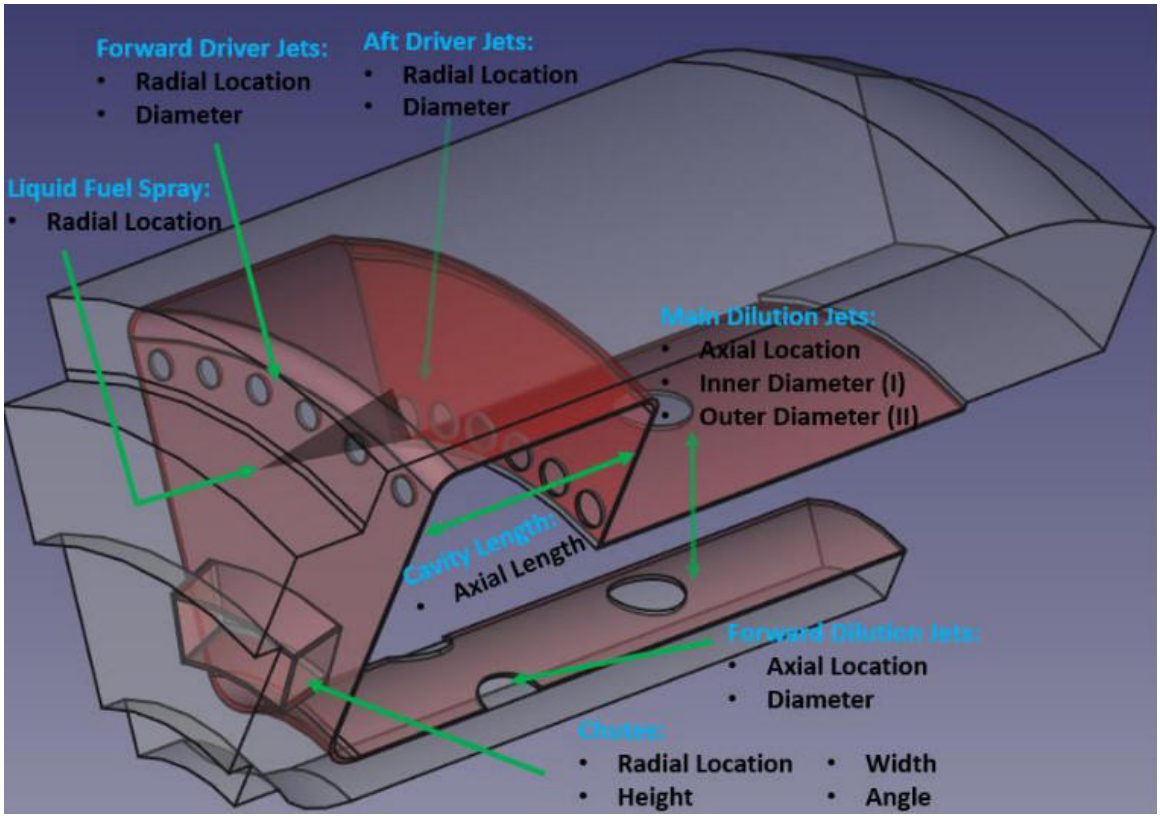

Figure 68. P400 Outboard Cavity Combustor Baseline Geometry [31]

atomized spray which was injected directly into the cavity, shown in Figure 68, off of the back face of the forebody of the combustor. To achieve this kind of injection scheme, a swirler coupled with a high-pressure fuel pump (higher pressure compared to the stock P400 fuel pump) would need to be designed and implemented. The stock P400 fuel injection system, shown in Figure 69, featured twelve 1 mm diameter tubes which rested in vaporization tubes. These fuel-injection tubes all featured a hook-like bend at one of the ends which injected fuel down each vaporization tube opposite the flow through the engine. If the new compact combustor were to mate accordingly to this type of fuel-injection scheme, the novel combustor would also need to feature vaporization tubes.

The first TVC design iteration for the P400 engine, shown in Figure 70, featured

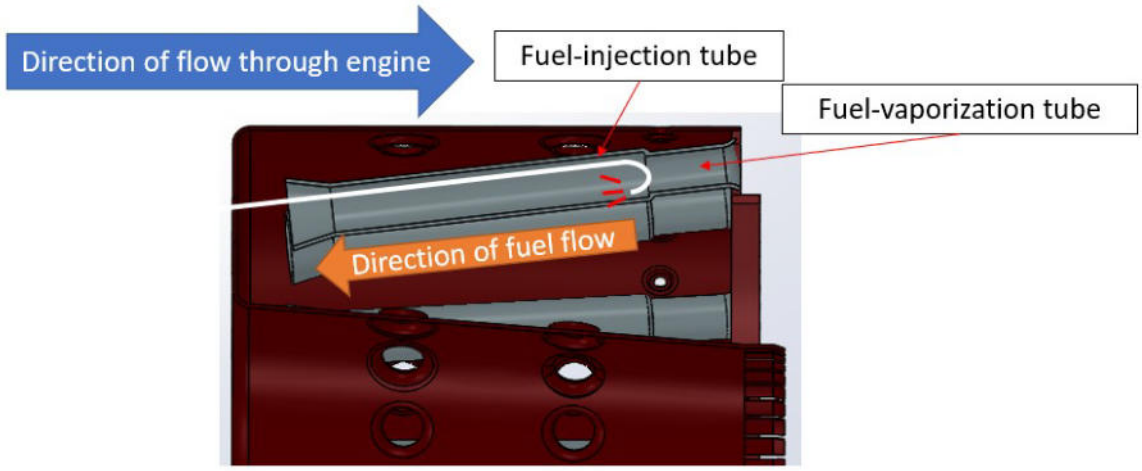

Figure 69. Fuel-injection scheme shown through the cross-section of the stock P400 combustor

fuel vaporization tubes which retained the same ID, OD, and length as the stock P400 fuel vaporization tubes. Since the flame stabilization area within the TVC was within the cavity rather than at the end of the fuel vaporization tubes, like in the stock P400 combustor, a showerhead arrangement of holes was placed on each vaporization tube such that fuel was injected directly into the cavity. Additionally, this simulation was performed utilizing the DP43 cavity dimensions and the length of the stock P400 burner with the addition of the vaporization tubes. Computational simulations were initially performed at the stock length of the P400 burner to optimize the performance of the TVC with the vaporization tubes. Additionally, the stock length of the P400 vaporization tubes were initially used in these simulations where they could later be optimized once an optimum showerhead design had been achieved. Initially, these fuel vaporization tubes featured three rows of four holes where each row was spaced 60-degrees from one another. Additionally, all of the holes were centered about the cavity. Row spacings of 30 and 45 degrees were also computationally solved for the same hole count, however, the 60 degree spacing filled the volume within the cavity with fuel the best as supported by Figure 71. Figure 71 shows static temperature

contours at axial and radial cut-planes through the TVC cavity at a design condition. These contours showed a lack of uniform combustion occurring within the cavity, and also showed combustion occurring outside of this region. To achieve comparable performance to the DP43 computational design of Briones et al. [31] and the stock P400 burner at a reduced length, all of the combustion needed to occur within the cavity to ensure the reactions had ample residence to burn completely prior to the exit plane.

With the 12 hole arrangement, this filled the cavity with a localized rich pocket of fuel causing combustion to occur along the edges of the cavity as well as below the cavity. This combustion occurring below the cavity would lead to undesirable pattern factors at the combustor exit plane, and even more when the combustor length is shortened. This lead to the investigation of other fuel vaporization tube showerhead arrangements.

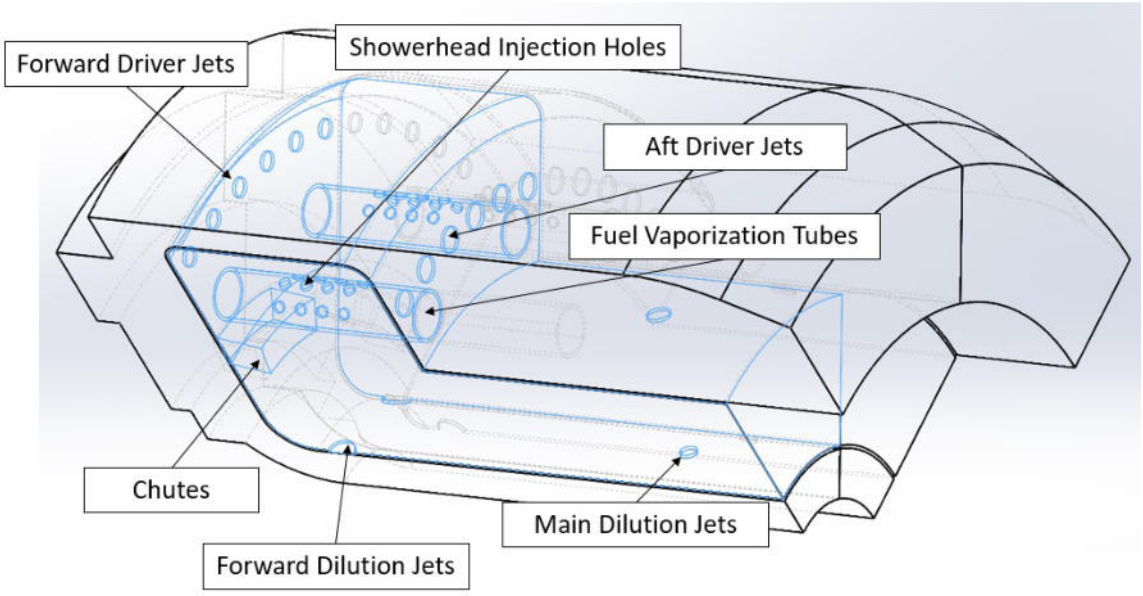

Figure 70. JetCat P400 TVC intial design iteration utilizing fuel evaporation tubes

Several iterations of the TVC design were ran where the focus was on the showerhead injection scheme implemented into the fuel vaporization tubes. These iterations

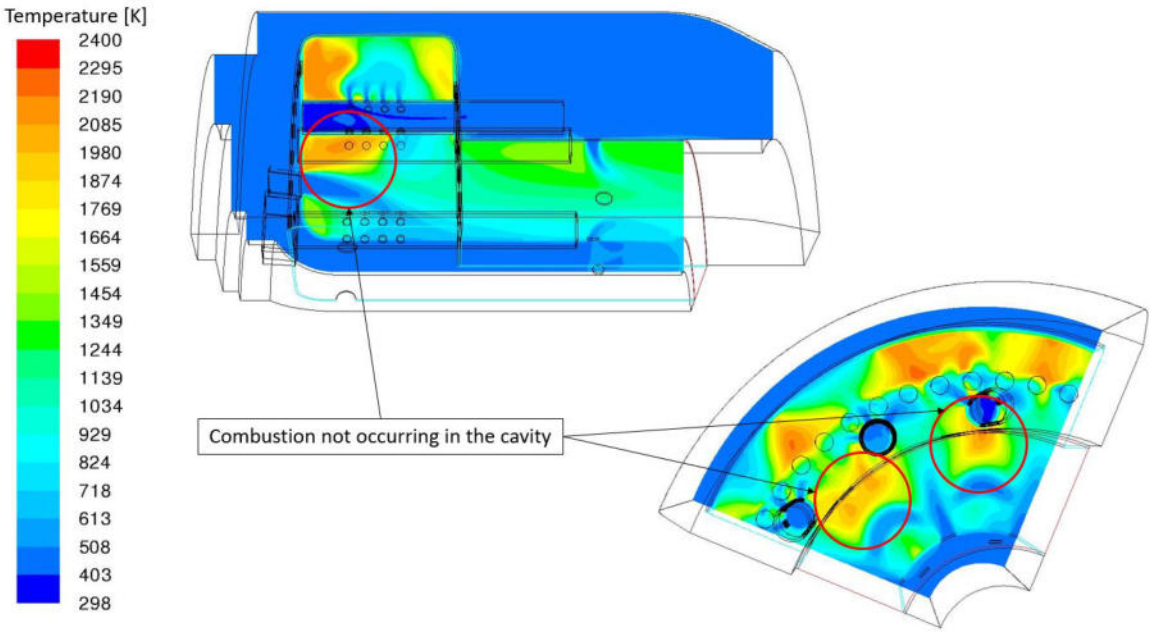

Figure 71. Contours of static temperature for the initial TVC design iteration at an axial cut-plane through one of the fuel vaporization tubes (top-left) and at a radial cut-plane halfway through the cavity (bottom-right)

included increasing the number of holes from 12, to variations of 18, 20, and 22 while maintaining a constant injection angle of 60 degrees. In the end, the 22 hole configuration with a 60-degree injection angle yielded the best results, shown in Figure 72, where a majority of the combustion was occurring in the cavity. This showerhead configuration featured a staggered arrangement of 22 holes which were divided into fives rows. Three of the rows featured four holes and the other two featured five holes, all of which were centered within the cavity. This arrangement more effectively dispersed the fuel to the TVC cavity so that all of the combustion was entrained within the cavity. This showerhead fuel vaporization tube arrangement would enable the TVC length to be reduced from the stock P400 length while still ensuring a combustion efficiency comparable to or greater than the stock P400 burner. Additionally, the length of the vaporization tubes could be reduced from their stock length to a shorter length similar to the length of the TVC cavity to reduce aerodynamic losses.

After this, the combustor would be shortened, optimized, and simulated across an operating range.

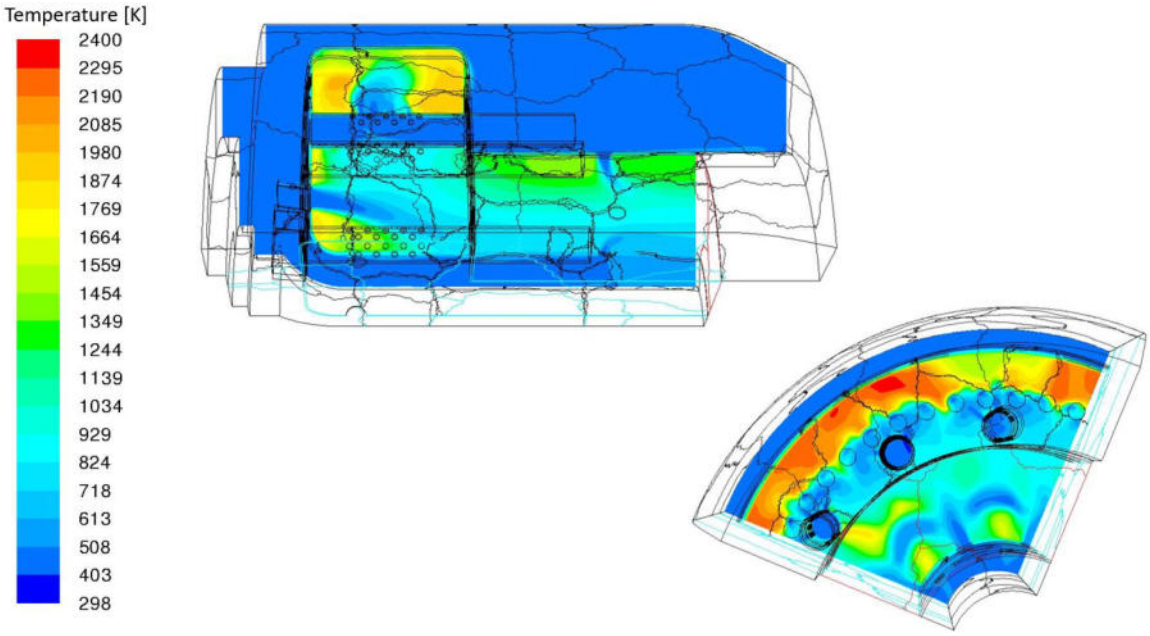

Figure 72. Contours of static temperature for the initial TVC design iteration at an axial cut-plane through one of the fuel vaporization tubes (top-left) and at a radial cut-plane halfway through the cavity (bottom-right)

With a working design utilizing the stock length of the burner section at the P400 engine scale, it was the goal of this study to reduce the length of the novel combustor. To reduce the length, material was removed from the dilution section of the combustor rather than from the cavity/primary zone. Initially, 2.5 cm was removed from the dilution zone, shown in Figure 73, of the burner since this was roughly the distance from the exit of the TVC cavity to the first series of downstream dilution holes from the DP43 computational model of Briones et al. [31]. Initially, the dilution hole area was kept the same between the stock DP43 design and the current TVC at 1.25 cm^2. This included eight dilution holes on the outer liner with a diameter of 3.6 cm and eight dilution holes on the inner liner with a diameter of 2.6 cm. However, after several computational simulations, it was found that the dilution

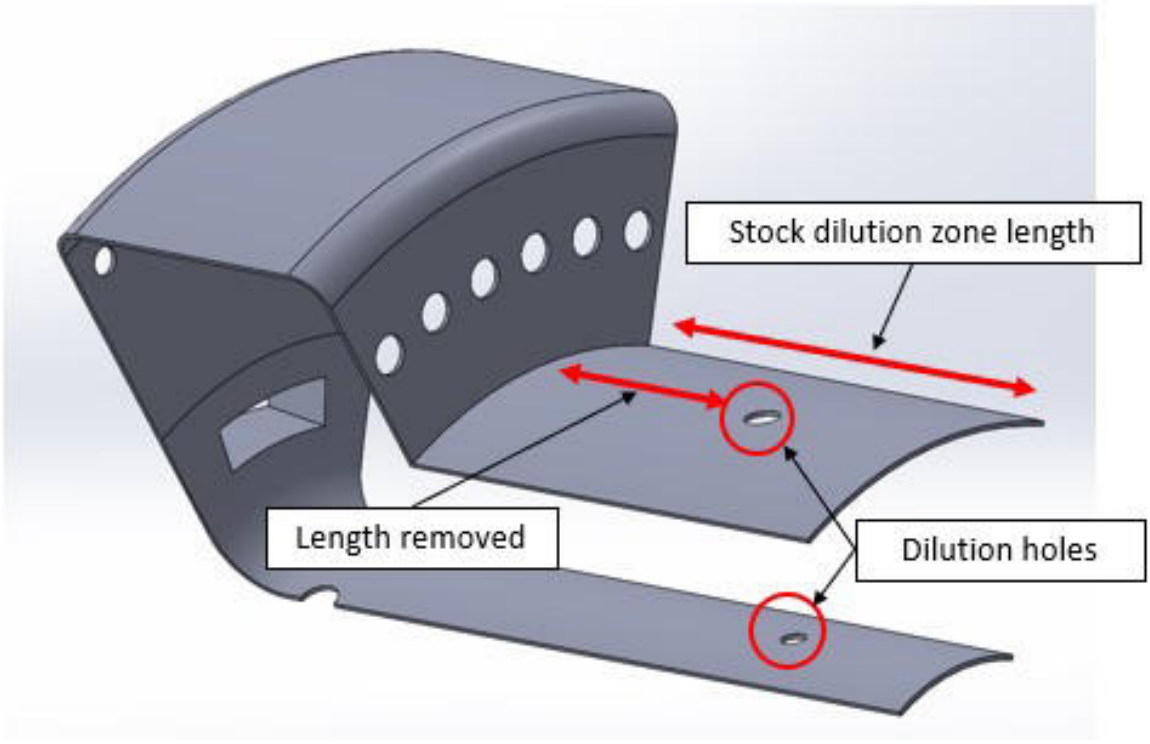

Figure 73. Initial length removed from the DP43 computational model of Briones et al. [31]

hole area needed to be increased to 4.13 cm^2 to quench reactions, shown in Figure 74, prior to the combustor exit plane due to the 2.5 cm reduction in length. Figure 74 shows contours of OH at the combustor exit plane before and after the increase in dilution hole area where the increased dilution hole area saw no concentrations of OH at the exit plane suggesting no burning. Increasing the dilution hole area was done by having four staggered rows of dilution holes on the outer liner that varied in diameter further downstream. The first row featured 24 holes with a diameter of roughly 0.36 cm. The next two rows also featured 24 holes with a smaller diameter of 0.18 cm. The final row of holes featured 100 holes at a diameter of 0.508 mm with the intention of providing a thin layer of cooling flow to the turbine stator vanes. A similar row of 0.508 mm dilution holes was placed on the inner liner for the same purpose. Overall, the current TVC was roughly 20% (2.5 cm) shorter compared to

the stock burner and provided the same length savings within the P400 engine.

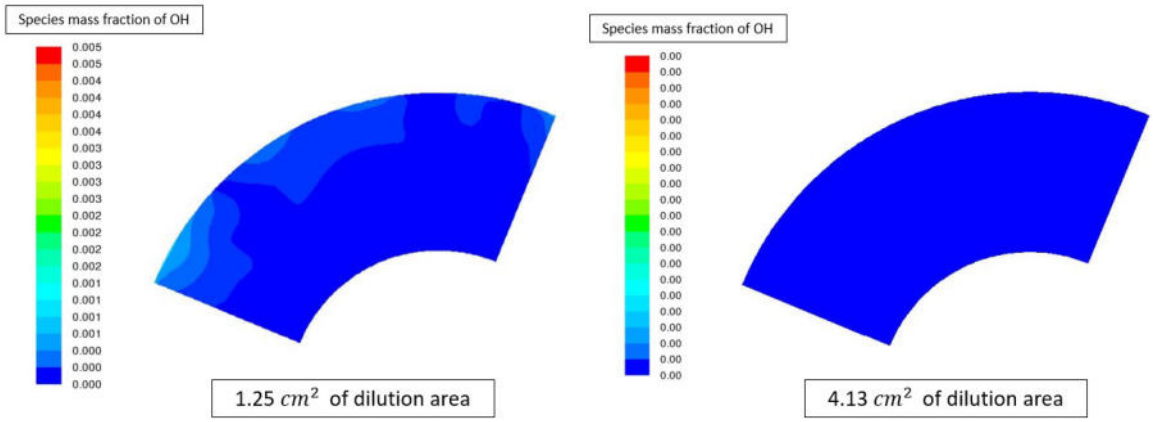

Figure 74. OH contours at the combustor exit plane for the original dilution hole area (left) and final dilution hole area (right)

The DP43 computational domain of Briones et. al. [31] was modified while maintaining the overall cavity dimensions, initial dilution hole location and size, forebody and aftbody driver jet locations and size, and air chute location, size, and injection angle. To mate accordingly within the engine, the inner and outer liners downstream of the TVC cavity needed to match the constraints provided by the nozzle guide vane housing. This led the outer liner of the dilution section of the TVC to possess a slight expansion downstream to meet the outer diameter of the NGV housing. Additionally, the inner liner OD was reduced to match the inner diameter of the NGV housing, which constrained the inner and outer liner diameters to 42.32 mm and 93.36 mm, respectively. Finally, the engine casing ID was changed from 14.8 cm to 14.6 cm to match the casing ID.

3.7 JetCat P400 Compact Combustor Computational Setup

To design and optimize an outboard cavity-stabilized compact combustor at the P400-scale intended to be later integrated into a JetCat P400 engine, computational simulations were performed in ANSYS Fluent for half-idle, idle, mid-power, and de-

sign conditions using liquid kerosene fuel. Section 3.7.1 discusses the grid generation process used for generating a usable mesh for computational calculations. Section 3.7.2 discusses the parameters, solvers, and boundary conditions, used to simulate the P400 computational model. Finally, Section 3.7.3 discuss the grid independence study performed after the initial simulations to validate the computational results.

3.7.1 JetCat P400 Compact Combustor Grid Generation.

To generate a grid of the burner section of the P400 engine equipped with the compact combustor, a negative CAD model of a 90^o sector of the burner section was designed in SolidWorks and exported as an IGES file to be read by Pointwise. A 90^o sector was considered due to the twelve vaporizer tubes and eight air chutes present in the 360^o periodic model. This negative CAD model featured an inlet condition that represented the compressor exit of the engine and an exit condition that represented the turbine inlet of the engine. Additionally, to match the inlet combustor volume between the DP43 computational domain used by Briones et al. [31], which matches the length of the stock P400 combustor, and the current efforts, the 20% length reduction was removed from the dilution zone of the combustor so that the flow splits in and around the outboard cavity remained the same. To match the combustor inlet conditions between the computational domain and experiment, and spacer would need to be designed to account for the 20% length reduction, which is discussed in Section 3.8.2.

Once imported into Pointwise, similar methodology to the P160 grid generation was used to generate a mesh, create boundary and volume conditions, and export to ANSYS Fluent. A uniform node spacing of 0.012 mm was used where a boundary layer decay of 0.80 was applied to all domains and blocks. This enabled the volume near and around the walls to be refined, resolving the boundary layer, and allowing the volume

far from the walls to be more coarse. Additionally, the same boundary conditions, as shown in Figure 75, were used in the P400 computational model as previously used in the P160 computational model. The final grid used for all computational simulations contained 50 million cells.

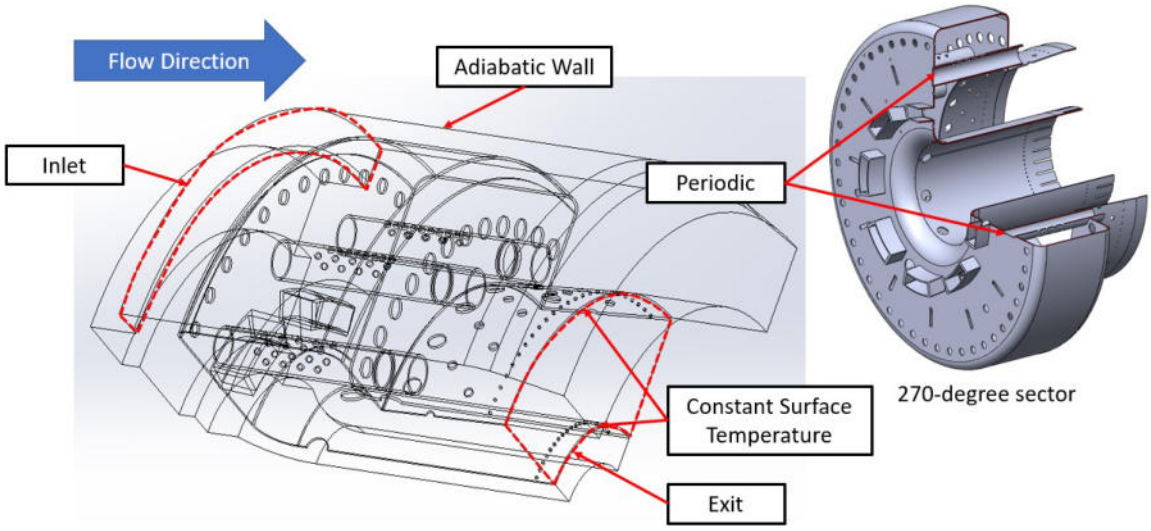

Figure 75. Boundary conditions applied to the cavity-stabilized combustor computational domain

3.7.2 JetCat P400 Compact Combustor CFD Simulation.

ANSYS Fluent was used to simulate the performance of the P400 compact combustor under the use of liquid kerosene for half-idle and idle conditions. To accurately simulate the flow-field within the combustor, several models were used within ANSYS Fluent. Simulations for all three cases utilized pressure-based, steady-state solvers equipped with a $\kappa - \epsilon$ realizable turbulence model with enhanced wall treatment. Additionally, the combustor was modeled utilizing a partially premixed kerosene-air mixture with flamelet generated manifold and diffusion flamelets. This model could predict quenching due to interactions between the flamelets and wall surfaces, which supplemented the conjugate heat transfer solver. The combustor walls were modeled

as Inconel-600 matching the compact combustor physical hardware, all matching the methodology used for the P160 compact combustor computational simulation.

3.7.3 JetCat P400 Grid Independence Study.

To validate the results from the computational simulations of the P400 compact trapped-vortex combustor, the base grid was uniformly refined and coarsened by roughly 20% and simulations were performed at the design point condition. The base grid contained roughly 50 million cells which meant the coarsened and refined grids contained roughly 40 and 60 million cells, respectively. To compare the results between each grid, circumferentially averaged velocities and temperatures were analyzed at the combustor exit plane, as shown in Figure 76.

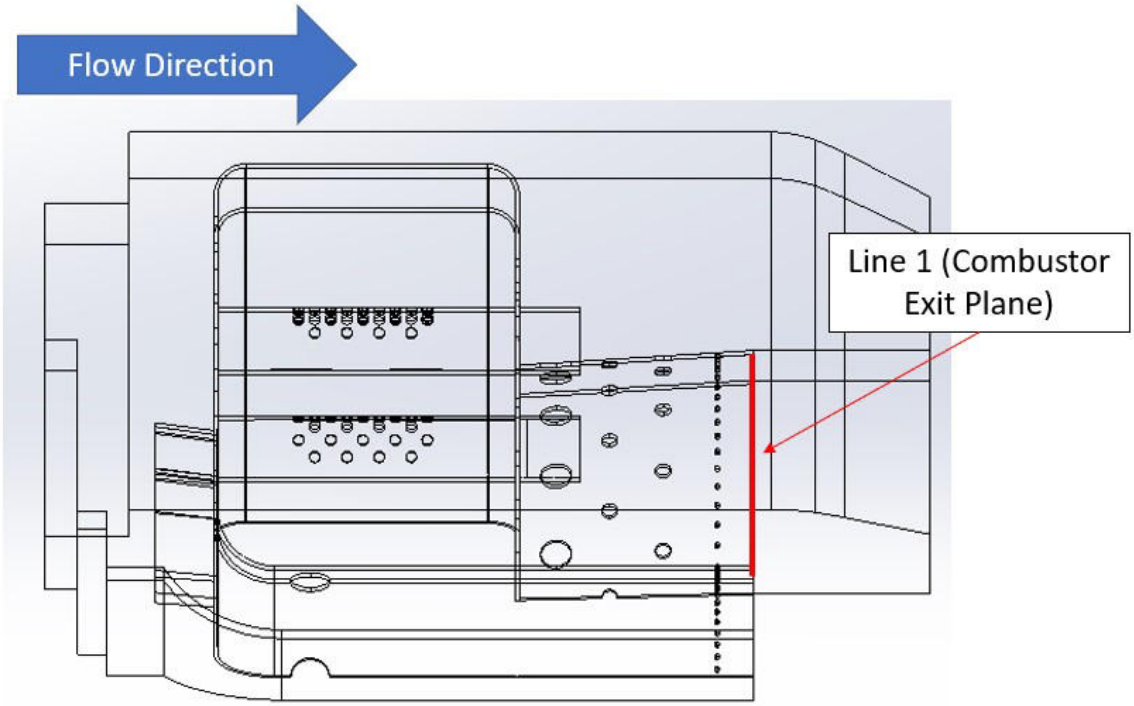

Figure 76. Location used to determine grid independence between coarsened, base, and refined grids

As a result of the grid independence study, a sensitivity to the number of patches

initiated between simulations was discovered. A "patch" enables all of the cells/grids in the simulation to have the same temperature, or boundary condition, and is commonly used to initiate a combustion reaction in a simulation. For this study, two patches were placed for each simulation where the progress variable was set equal to one. This tells the simulation that combustion is occurring in every cell and allows the software to solve backwards and converge towards a steady-state solution. However, it was found that after two patches at the design point simulation between the coarsened, base, and refined grids that not all of the combustion was occurring within the TVC cavity, which lead to large variations in exit temperature and velocity profiles between grid resolutions as supported by Figures 77 and 78. This was likely due to the discrete phase model solver within ANSYS Fluent, which was responsible for simulating the liquid kerosene injection into the computational domain, not simulating the vaporization of all of the fuel being injected into the cavity.

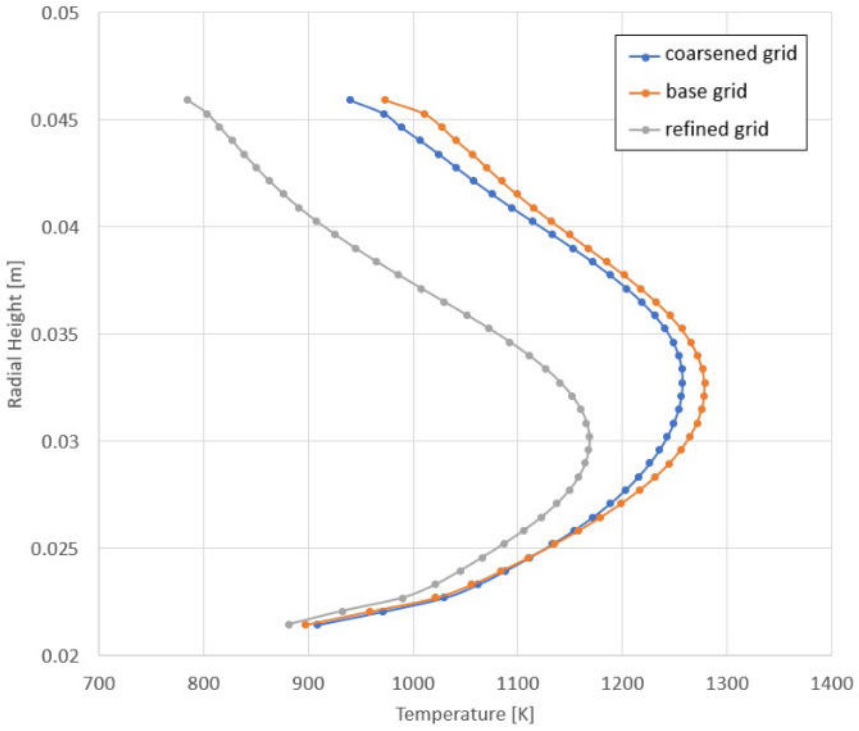

Figure 77. Temperature profile at Line 1 after two patches

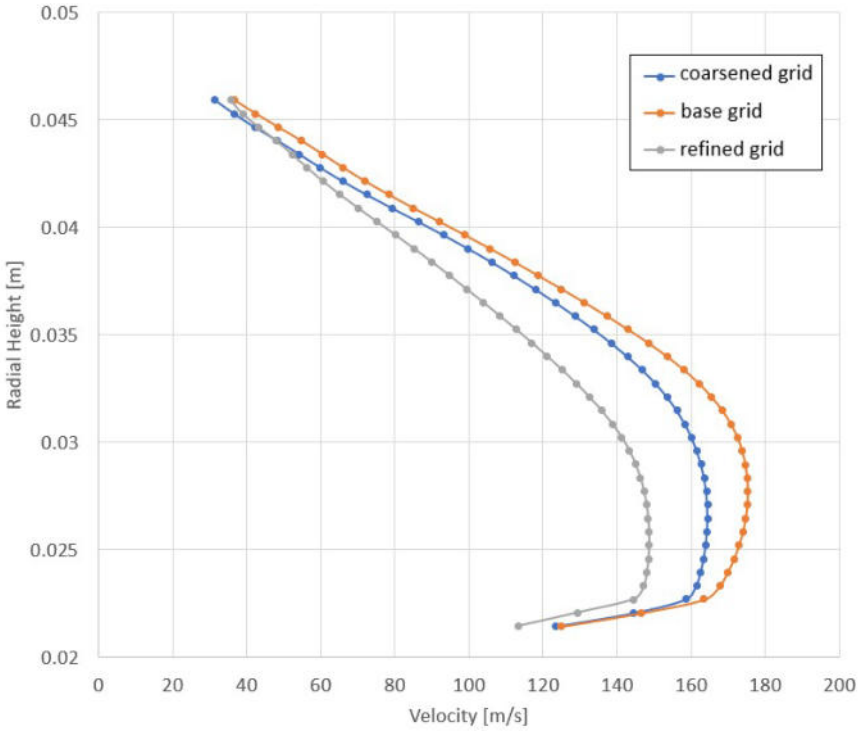

Figure 78. Velocity profile at Line 1 after two patches

As a result, a sensitivity study on the number of patches was performed to determine the number of patches necessary to arrive at comparable computational results between grid resolutions. An example can be seen in Figure 79 where exit temperature data was gathered for two, four, six patches at a mid-power condition. As a result, the 4 and 6 patch profiles closely matched resulting in each grid analyzed in this study to be patched 6 times.

Figure 80a and 80b show the circumferentially averaged exit temperature and velocity profiles at a design condition. There was a maximum deviation of 6.7% and 10.8% in velocity and temperature, respectively, across all grid resolutions. This variation in temperature and velocity between grid resolutions was likely due to the combustion fluctuations occurring with the combustor between simulations along with flucuations in dilution hole effects. Overall, this grid independence study suggested that the 50 million cell base grid was adequate for the remainder of the computational simulations of the present study.

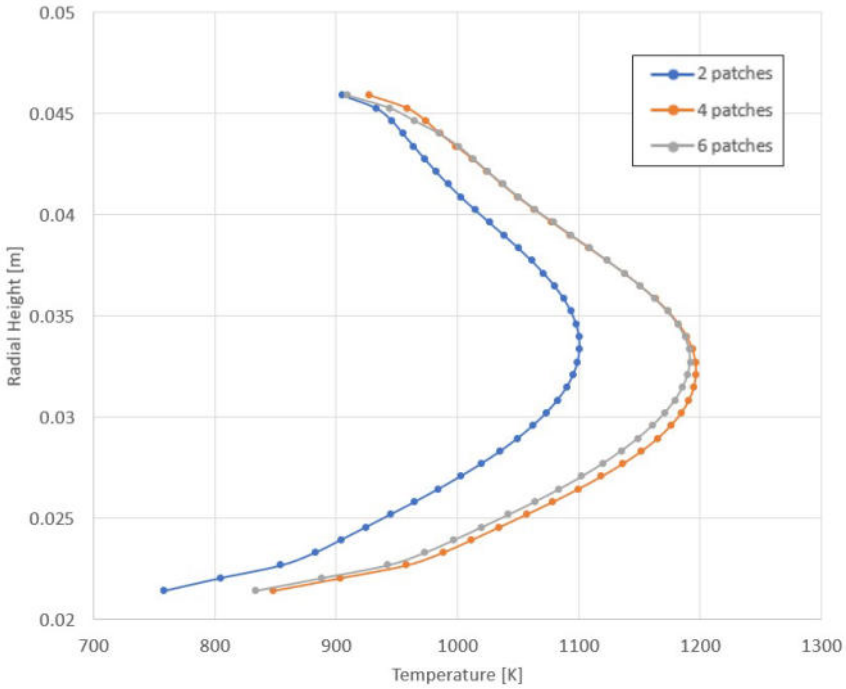

Figure 79. Temperature profile at Line 1 where the number of patches was varied for the base grid

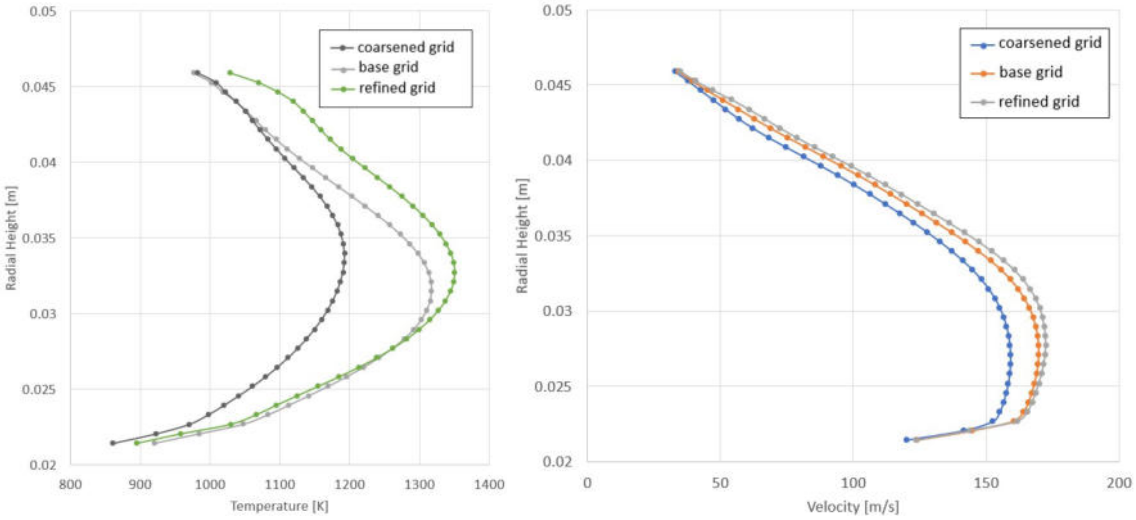

(a) (b)

Figure 80. (a) Temperature profile at Line 1 after six patches and (b) velocity profile at Line 1 after six patches

3.8 JetCat P400 Compact Combustor Hardware and Assembly

To manufacture the current TVC design, shown in Figure 81, the forebody, aftbody, cavity, and inner and outer dilution liners were water-jet cut and rolled out of Inconel-600 by the AFIT Model Shop. Additionally, the air chutes were manufactured out of the same materials, while the fuel vaporizer tubes were manufactured from 316 stainless steel. Once all of the components were manufactured, they were welded in two sections.

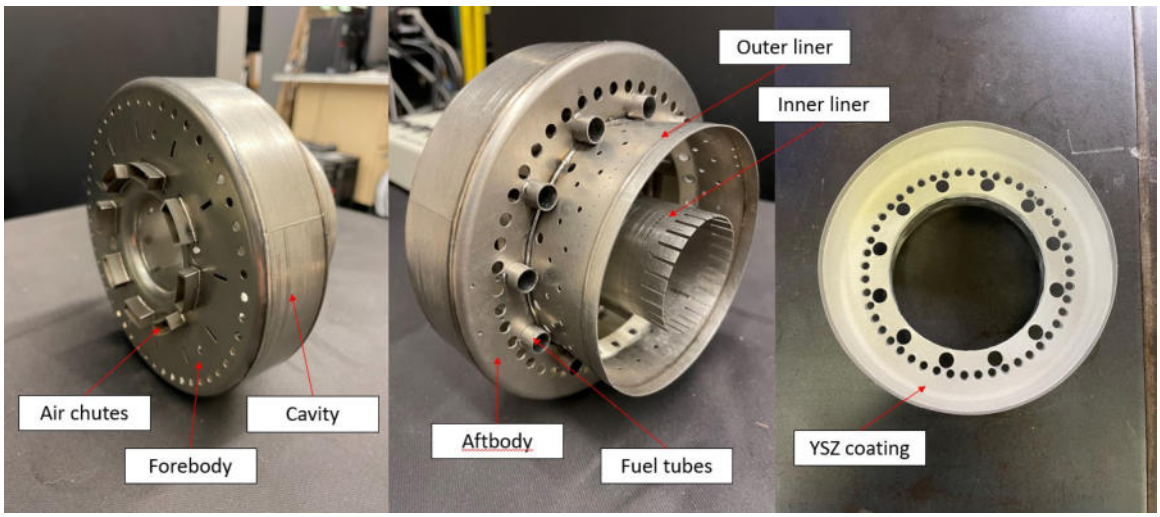

Figure 81. TVC compact combustor with YSZ coating applied to internal cavity surfaces

One of the sections included the cavity, aftbody, and outer liner. Once these three components were welded together, this portion was coated with a yttria-stabilized zirconia (YSZ) thermal barrier coating, which was 12 microns in thickness and applied by the company APS materials. This coating was applied due to the computationally predicted liner temperatures approaching Inconel melting temperatures around 1600-1700 K at the mid-power and design conditions, as shown by Figure 82. Figure 82 shows conjugate heat transfer results from the cavity-stabilized compact combustor computational simulations across off-design and design conditions. The hottest re-

gions observed along the liner surfaces were along the cavity and aftbody surfaces in bewteen the fuel vaporizer tubes at the mid-power and design conditions. Once this coating was applied, this portion was joined together with the other section of the combustor, which included the forebody, air chutes, fuel vaporizer tubes, and inner liner.

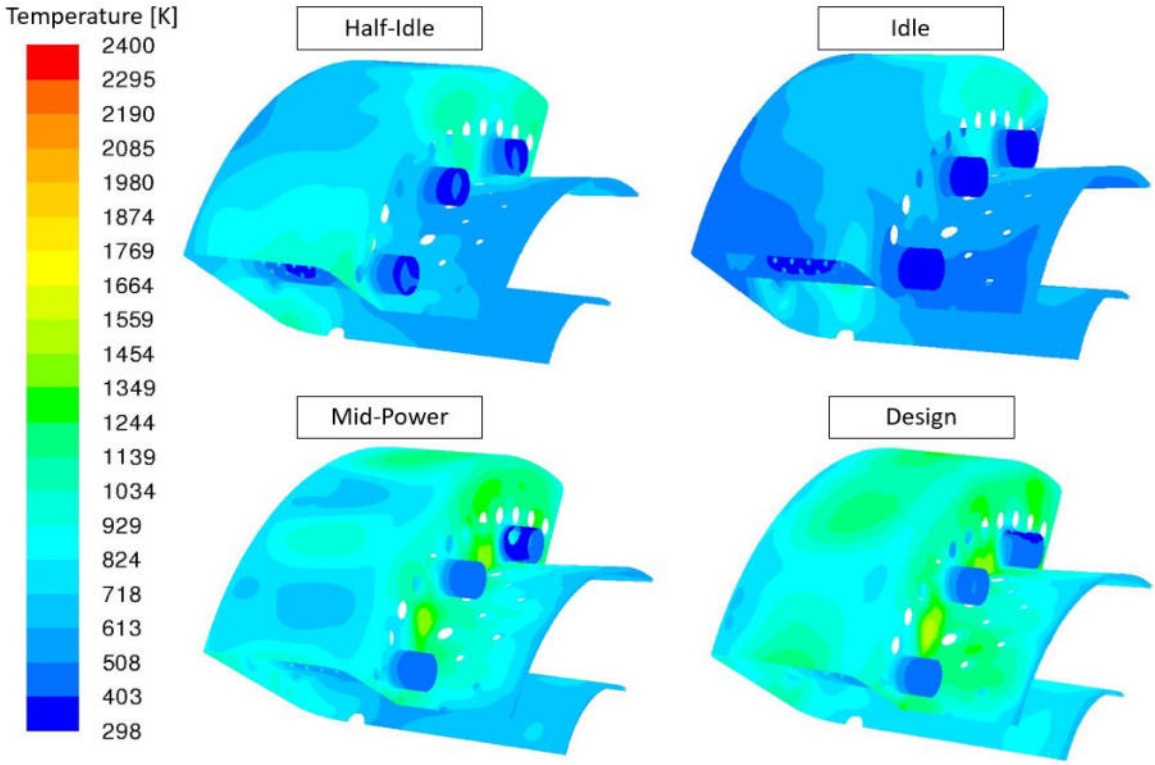

Figure 82. Conjugate heat transfer results for the computational cavity-stabilized combustor combustor model

Once the manufacturing of the combustor was completed, it needed to be instrumented prior to being installed in the new test rig. Section 3.8.1 discusses the instrumentation used to characterize the compact combustor during operation. Section 3.8.2 discusses the assembly of the supporting hardware surrounding the cavity-stabilized compact combustor along with the test rig.

3.8.1 P400 Compact Combustor Instrumentation.

To monitor temperatures and pressures at each station within the test rig, thermocouples and pressure probes were placed in the following locations according to Figure 83. To verify the inlet conditions used during testing, T_3 and P_3 measurements were needed and devices installed. Additionally, to obtain a pressure drop across the combustor, static pressure ports were placed at the upstream and downstream ends of the combustor spool, equivalent to the P_2 and P_5 locations. To record static temperatures at Stations 2 and 3, 0.1 cm diameter thermocouples (SCAIN-040U-48) with an Inconel-600 sheath were used. To measure the static pressure in Stations 2-5, similar OMEGA high performance pressure transducers used in the P160 compact combustor testing.

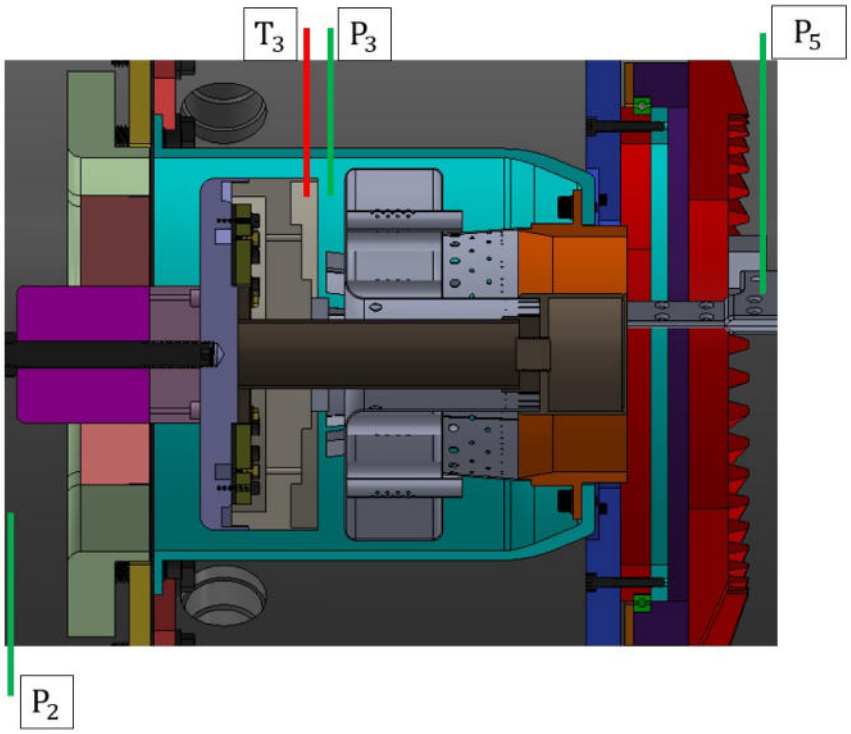

Figure 83. Inlet and outlet instrumentation used during experimental testing within the P400 test rig

To validate the computational results of the P400 compact combustor, 0.1 cm

probe diameter thermocouples (SCAIN-040U-48) were placed throughout the combustor corresponding to the locations outlined in Figure 84, which shows static temperature contours of the P400 compact combustor simulation through a bi-section of one of the fuel vaporization tubes at a design condition. These seven additional locations were chosen since computational simulations indicated regions of burning occurring within these areas.

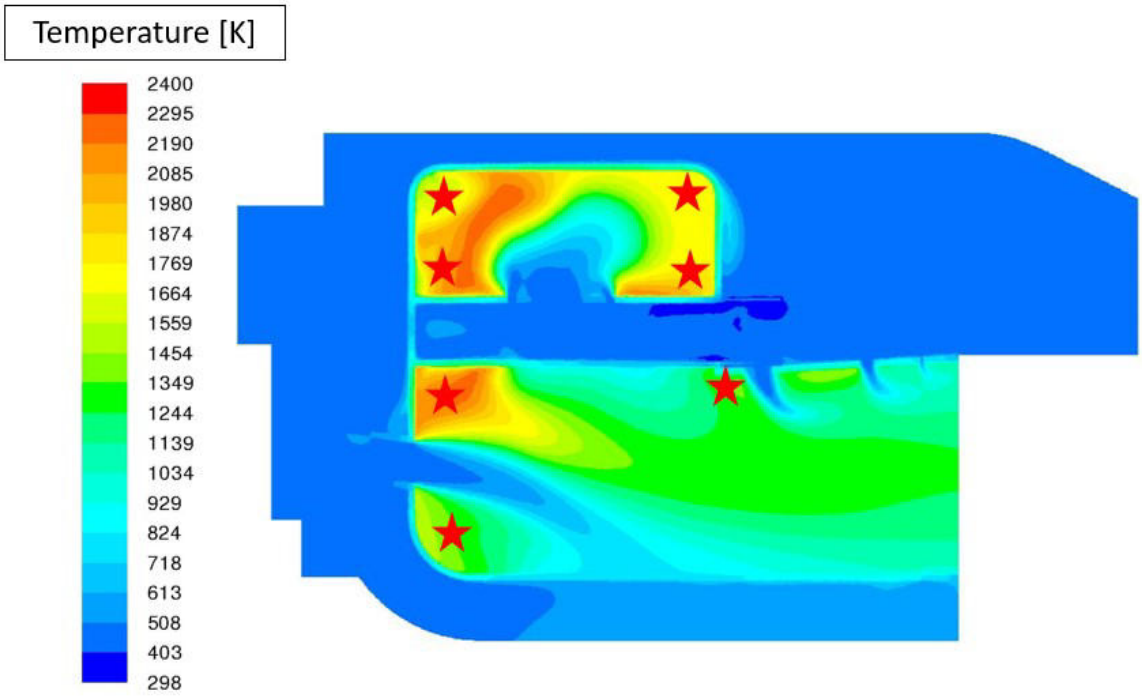

Figure 84. Additional temperature locations installed based off of static temperature contours from computational results

Figures 85 and 86 show all of the actual locations along the combustor where thermocouples were placed. In total, seven forebody thermocouples were installed where areas at two different vaporizer tube locations were investigated to check for periodic behavior. Four aftbody thermocouples were installed analyzing regions at and between fuel vaporizer tubes. Five thermocouples were installed along the dilution section of the combustor to 1) ensure combustion wasn't occurring just downstream of the cavity and 2) measure the temperature just upstream of the exit plane at radial

spans of 25%, 50%, and 75%. Finally, four thermocouples were welded to the outside of the combustor liner material in locations corresponding to the highest predicted liner temperatures, shown in Figure 86. These locations were directly between the fuel vaporizer tubes along the cavity and aftbody.

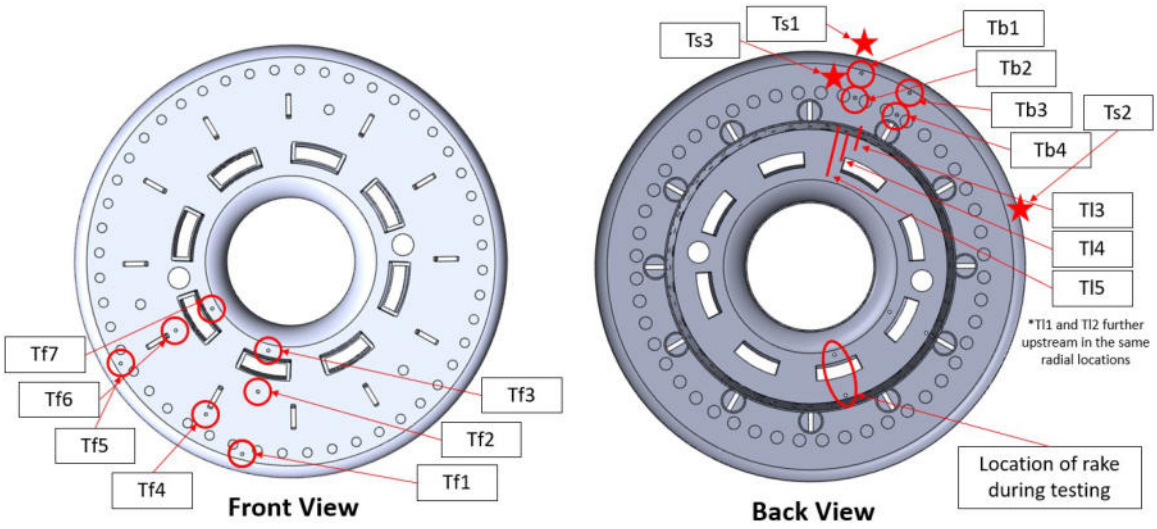

Figure 85. Fluidic temperature locations measured across the combustor

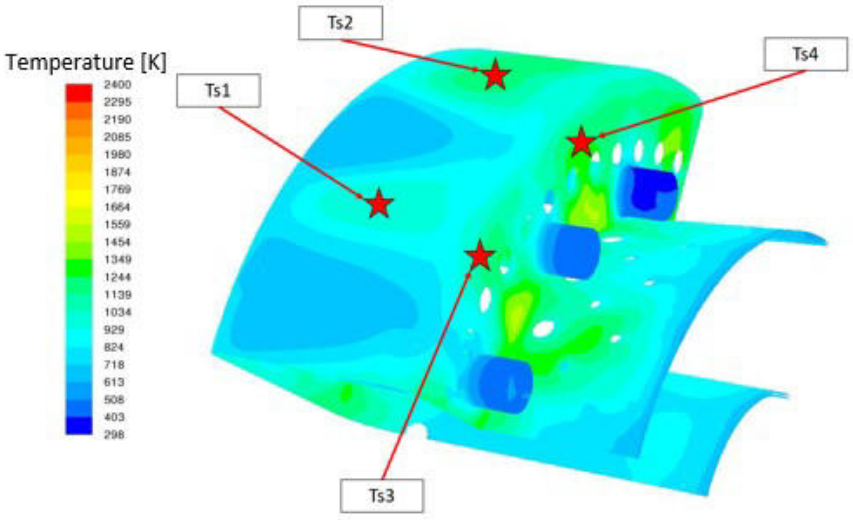

Figure 86. Temperature locations measured along the surface of the combustor liner

To further analyze the performance of the P400 compact combustor, a travers-

ing thermocouple rake assembly was designed so that total temperatures could be recorded at four radial locations at the combustor exit plane to gain profile and pattern factor data. Figure 87 shows the manufactured rake prior to installation in the test rig. This thermocouple rake was manufactured from Inconel-718, featured a Keil-head probe, and also featured four thermocouple channels for four K-type thermocouples (SCAIN-040-60). This thermocouple rake was mounted to a traverse gear which featured 45 teeth. This traverse gear mated to an 18-tooth driver gear which was coupled to a NEMA-17 stepper motor, as shown in Figure 88, which featured a 51:1 gear reduction. This reduction coupled with the gear set gave a total reduction of 127.5:1. The Keil head, when mounted, would be able to measure total temperatures perfectly in-line with the combustor exit plane, and rested between the ID of the NGV housing and the OD of the shaft housing with roughly 0.050" of clearance on either side.

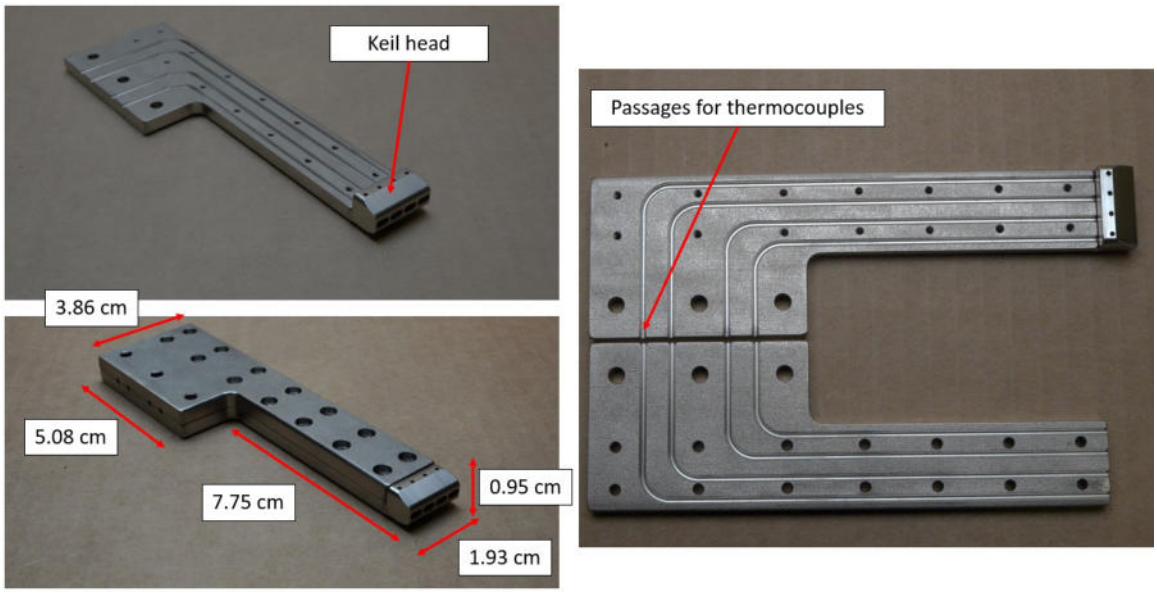

Figure 87. Thermocouple rake prior to thermocouple installation

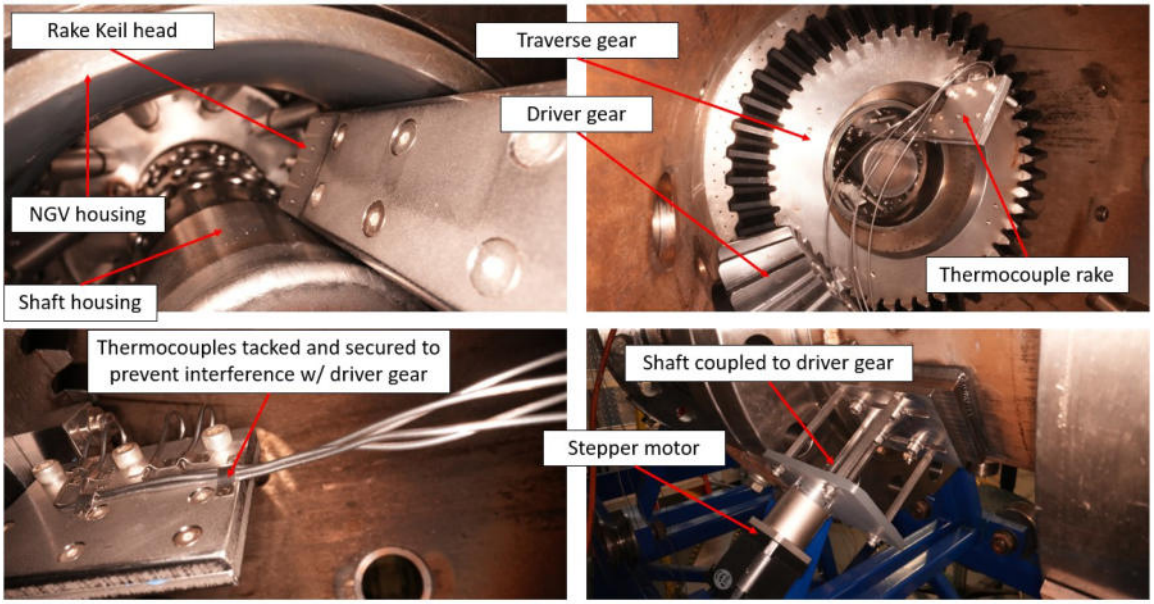

Figure 88. Thermocouple rake installed into the P400 test rig

3.8.2 JetCat P400 Test Facility.

To test the TVC on liquid kerosene fuel in a non-rotating turbomachinery setup, experiments were conducted within AFRL's Bldg. 490 Test Cell 151 [33]. Reciprocating positive displacement compressors were capable of supplying a maximum flow rate through the test section of 0.45 kg/s at a maximum pressure of 655 kPa. Measurements of air mass flow rate were recorded with Coriolis and Venturi mass flow meters with an accuracy of 0.25% of full-scale value. Measurements of fuel flow rate were recorded with Coriolis flow meters with an accuracy of 0.25% of full-scale value. The fuel supplied was pumped through a series of positive displacement pumps capable of supplying pressures up to 6.8 MPa.

The newly designed test rig supporting testing of the JetCat P400 with the integrated compact combustor is shown in Figure 89. The facility featured several "spool" sections including an inlet spool (1), an instrumentation spool (2), and an exhaust spool (3). The inlet spool section, shown in more detail in Figure 90, housed the combustor hardware and incorporated an ethylene-air torch to ignite the fuel-air

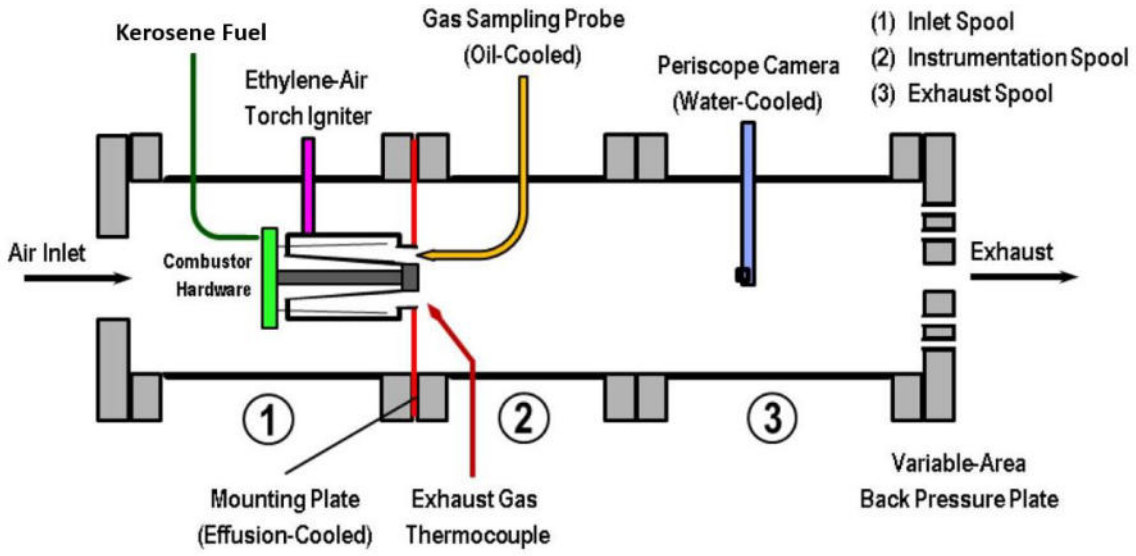

Figure 89. Bldg. 151 test rig schematic

mixture within the burner. This combustor hardware included the inlet assembly, diffuser/deswirler, fuel manifold, shaft housing, combustor, NGV housing, cold-box flange, and engine casing.

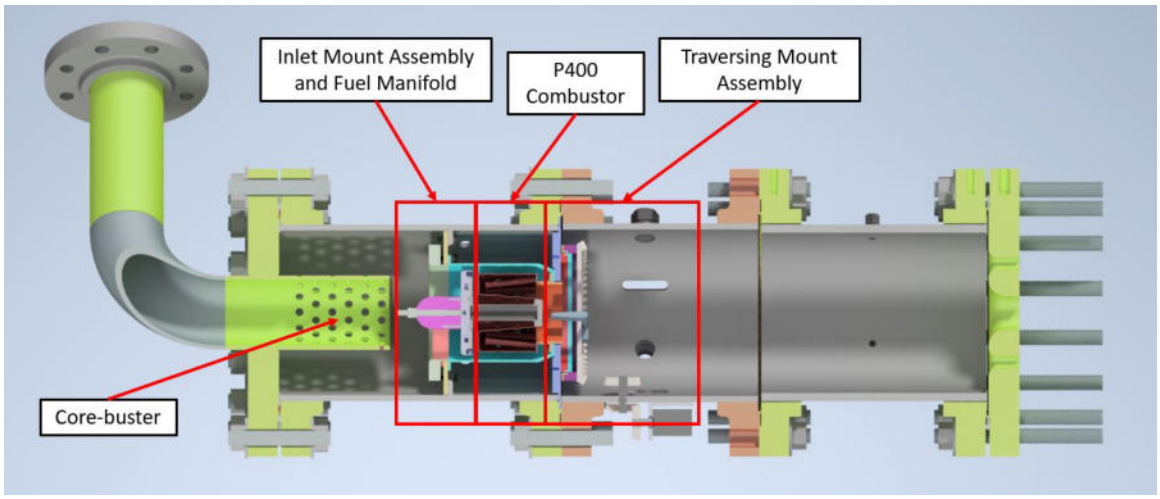

Figure 90. CAD model including new hardware changes to the P400 test rig

The diffuser/deswirler, shown in Figure 91, was machined from 316 stainless steel and featured two fuel inlet ports and two ethylene-air torch ports on the front face of

the part. The two fuel inlet ports were 1/16" Swagelock fittings, while the ethylene-air torch ports were 1/4" Swagelock fittings which were all welded to ensure a leak-proof seal. The back-side of the diffuser/deswirler featured a fuel plenum, through-holes for the ethylene-air torches, and mounting points for the fuel manifold to cover and seal the fuel plenum. This fuel plenum was filled at two equally spaced locations to ensure the plenum filled evenly with fuel.

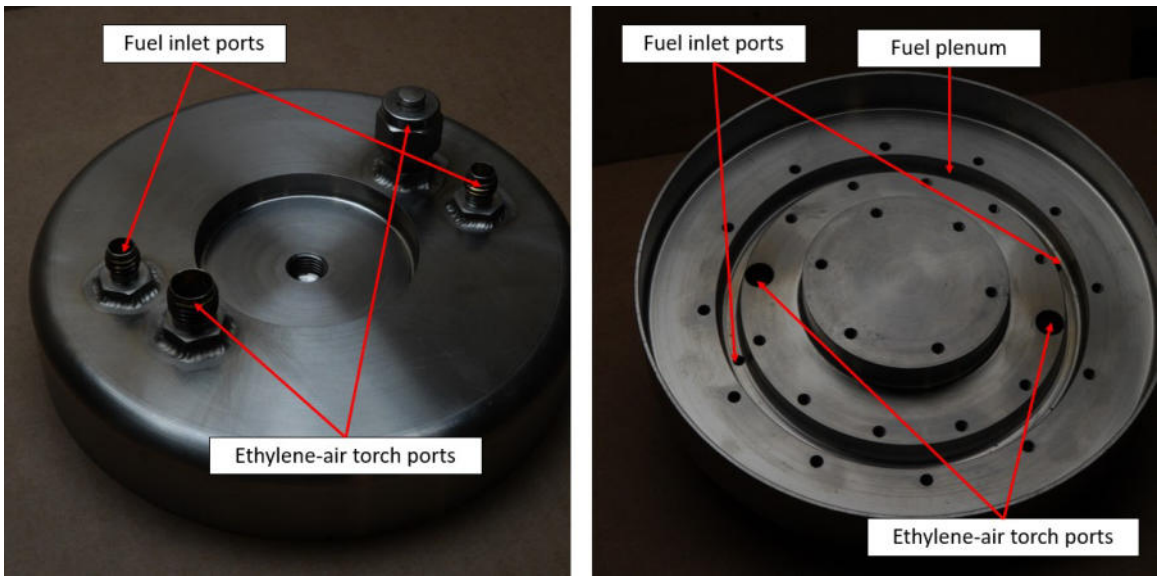

Figure 91. Machined diffuser/deswirler for the P400 test rig

The fuel manifold and shaft housing can be seen in Figure 92 with the addition of the fuel lines used to inject fuel within the vaporization tubes. This fuel manifold coupled with the diffuser/deswirler was designed to closely resemble the stock P400 fueling system components where fuel was fed into a plenum and exited out of twelve fuel lines into the vaporization tubes. The current fuel manifold featured twelve M3 threads radially centered above the fuel plenum on the backside of the diffuser/deswirler. These threads housed fuel lines which were made in-house from brass hex-head fittings brazed to 304 stainless steel 0.038" OD tubing. To create the hook-like bend at the end of the fuel lines, the end of the tube was bent around a

#31 drill bit to match the radius of the stock P400 fuel line.

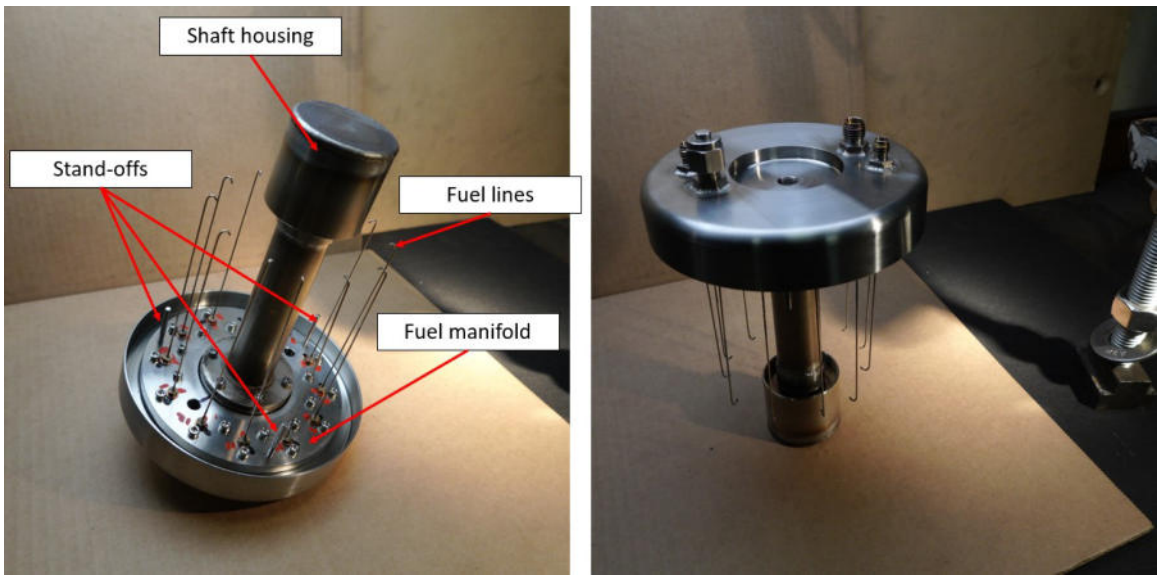

Figure 92. Fuel system assembled for the P400 test rig

For the TVC compact combustor testing, a 3-D printed Ultem spacer was attached to the diffuser/deswirler, shown in Figure 93, to match the fluidic volume present upstream of the combustor in the computational domain, outlined in Figure 94. The CFD domain spacer was printed in two halves which bolted together and hugged to the shaft housing to stay in place during testing. Ultem was originally selected due to its availability and ease of manufacturing. Figure 93b shows the addition of aluminum tape placed over the fuel line slots along the forebody of the combustor. This was done because computational simulations predicted fuel leakage coming from these slots, shown in Figure 95, which would cause fuel to enter into the air chutes where burning would occur just below this region. To monitor if burning occurred within this region, thermcouples were placed in this area as previously shown in Figure 85.

To ensure even fuel distribution across the twelve fuel lines, each fuel line that was made was tested where the pressure drop across each fuel line was measured. To arrive at twelve optimal fuel lines that could be used during testing, 48 were manufactured

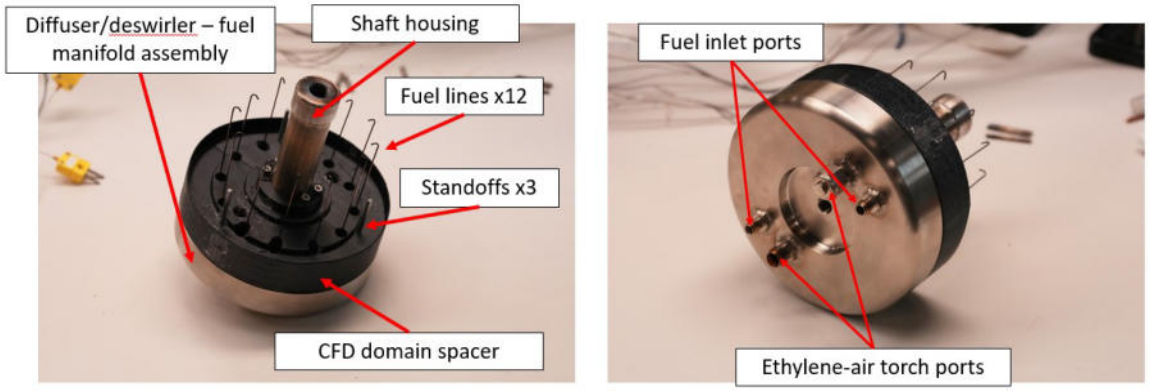

(a)

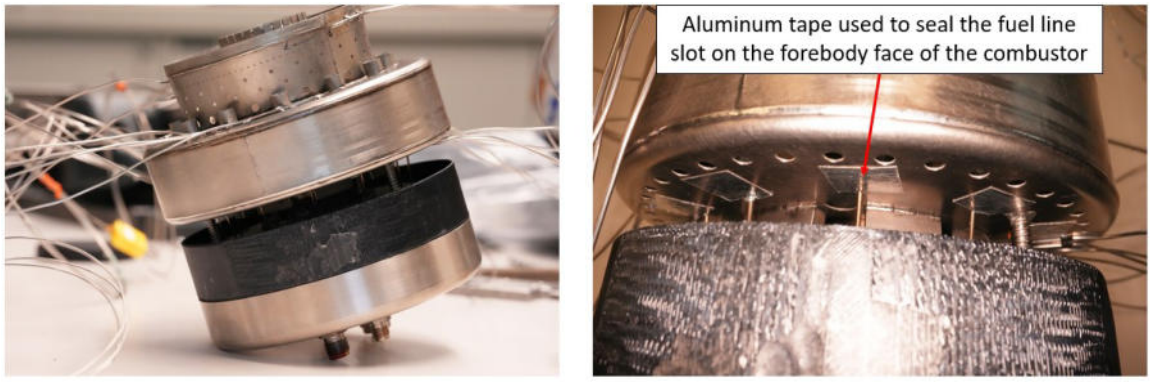

(b)

Figure 93. The outboard cavity-stabilized compact combustor assembled with the fuel manifold assembly, CFD domain spacer, and shaft housing

and tested where the lines with the lowest pressure drop were used during testing. To manufacture the fuel lines, 0.91 mm OD 304 stainless steel tubes were soldered to M3 brass fittings which had a 1 mm hole drilled through the fitting. Once the fuel lines were soldered to the fittings, each line was installed on the fuel manifold where each tip was bent such that the end of the fuel line was parallel with the centerline of the combustor. The end result produced two sets of twelve fuel lines where the best out of two at each circumferential locations was used during testing.

To measure the pressure drop across each fuel line, the following setup was used, as shown in Figure 96, where the stock JetCat P160 fuel pump coupled with its ECU and GSU was utilized to control the fuel flow rate of liquid kerosene through the fuel

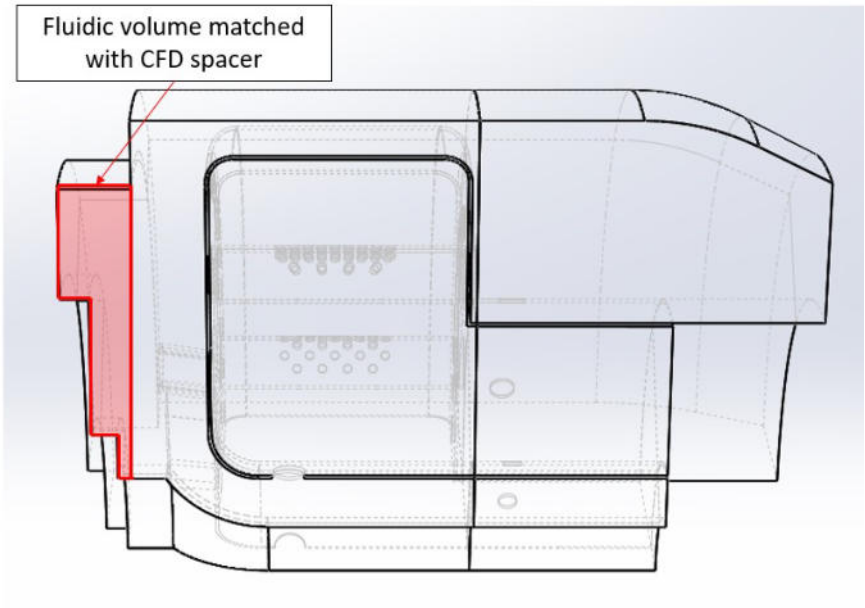

(a)

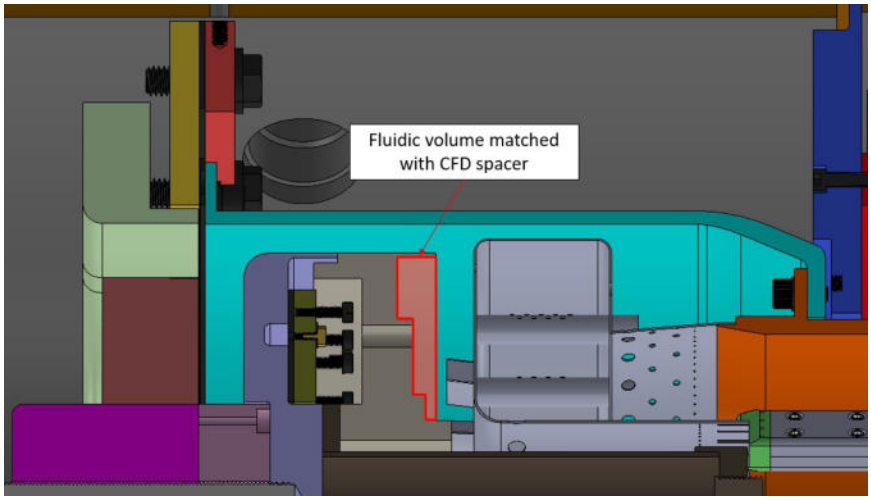

(b)

Figure 94. Combustor fluidic volume that was matched between the (a) computational and (b) experimental domains through the use of the CFD domain spacer

line. The fuel flow rate through each fuel line tested was set at 0.5 g/s. Additionally, an OMEGA high performance pressure transducer (Model No: PX429-250A5V) was installed prior to the fuel line to measure the pressure drop across the tube. This pressure transducer was calibrated using the following calibration curve collected prior to testing as shown in Figure 97. Additionally, this transducer measured the absolute

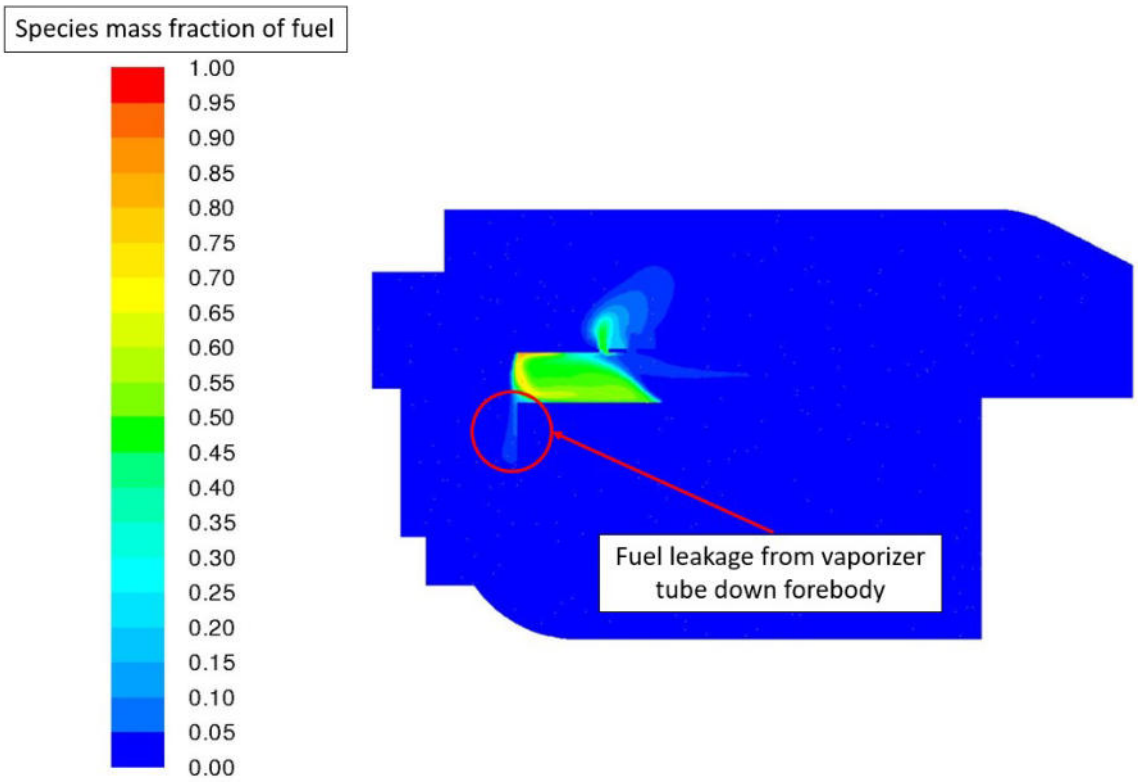

Figure 95. Fuel leak shown computationally through a cross-section bisecting one of the fuel vaporization tubes

pressure at its location within the experimental setup. Out of all 48 fuel lines tested, the maximum pressure drop measured was 337.8 kPa, the minimum was 155.8 kPa, and the average pressure drop was 195.8 kPa. Table 3 highlights the pressure drops measured for the twelve fuel lines used in the P400 test rig, where the best fuel line (out of two) was used for each injection location. There was a maximum deviation in pressure drop of roughly 25% between the twelve fuel lines used during testing, which was a result of inconsistencies in the "hook" shaped bend towards the end of each fuel line. A single "hook" shaped bend exhibiting a slightly tighter bend radius than another fuel line would likely exhibit a higher pressure drop across the fuel line as a result.

With the fuel system assembled, the current compact combustor was installed and

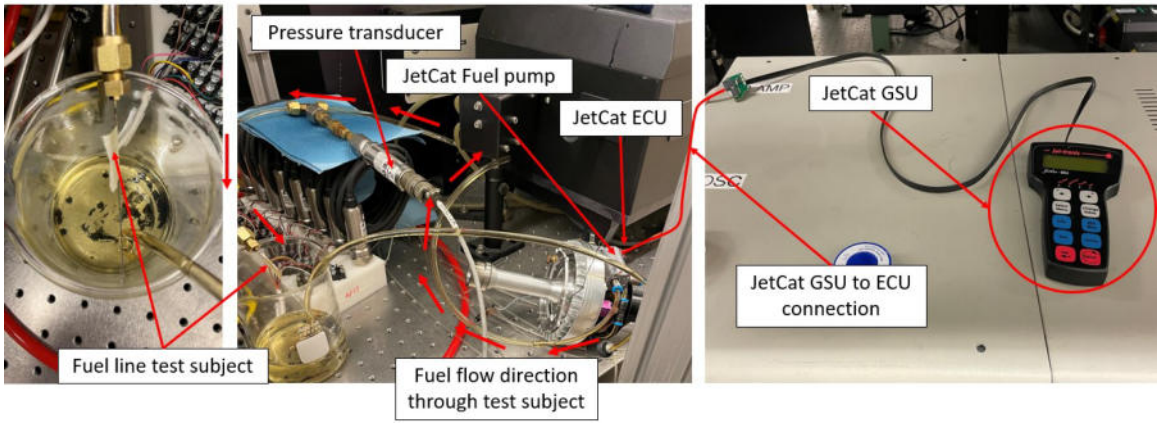

Figure 96. Fuel line pressure drop measurement setup

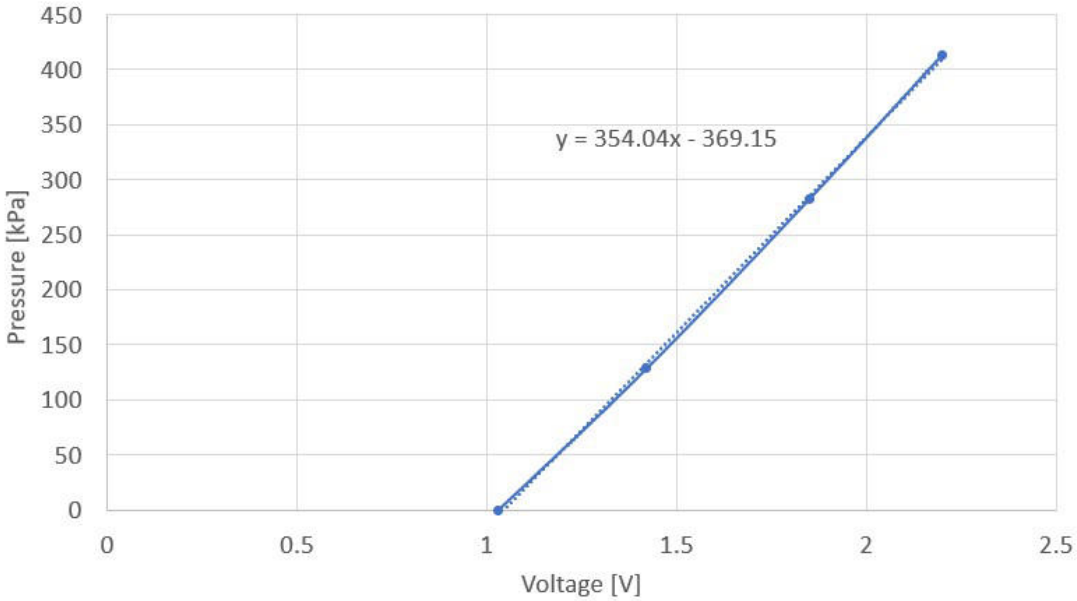

Figure 97. Pressure transducer calibration curve created prior to fuel line pressure drop test

placed over the shaft housing, as shown by Figure 93. The end of the shaft housing threads on and constrains the combustor into place. Additionally, the twelve fuel lines were fitted through slots on the upstream face of the combustor into the vaporization tubes. Also, the three stand-offs housed inside of springs were placed within the holes on the forward face of the combustor. With the combustor constrained at the

Table 3. Pressure drop readings across twelve fuel lines used

Fuel line #	Pressure reading [kPa]
Line 1	162.0
Line 2	168.9
Line 3	168.9
Line 4	195.1
Line 5	176.5
Line 6	162.7
Line 7	165.5
Line 8	170.3
Line 9	194.4
Line 10	155.8
Line 11	164.1
Line 12	166.2

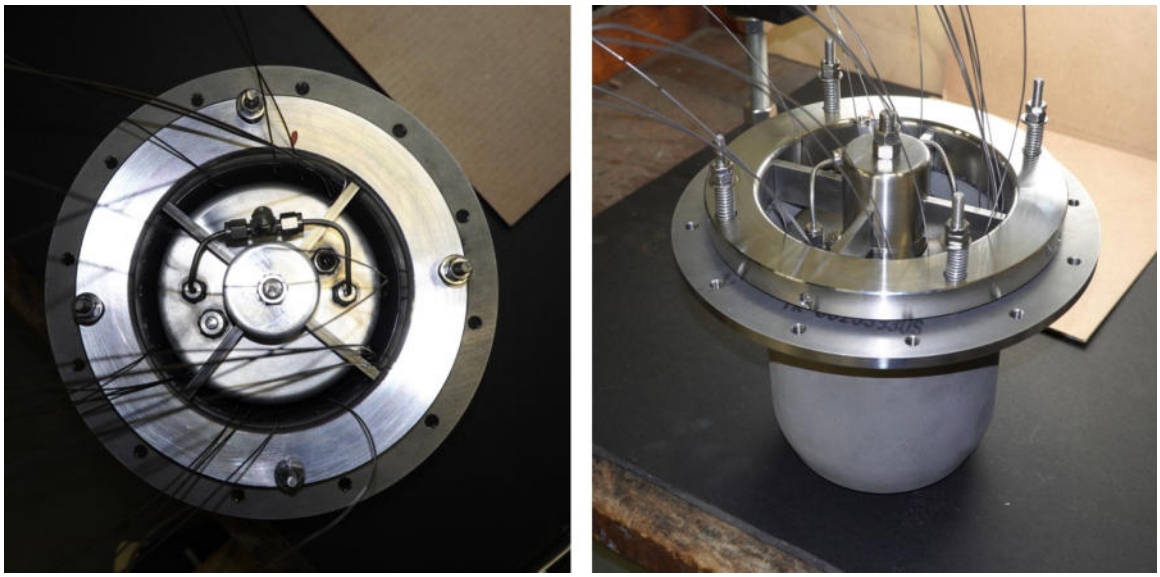

Figure 98. Entire combustor section assembled for the P400 test rig

downstream end, the springs coupled with the stand-offs ensure that the combustor will thermally expand upstream in the axial direction. With this portion of the P400 rig assembled, this sub-assembly could be placed within the new engine casing, as shown in Figure 98. This engine casing was 3D printed out of Inconel-600 and had an increased wall thickness compared to the stock P400 engine casing, while still

retaining the same ID as the stock engine casing.

The NGV housing, which didn't contain turbine stators, mated to the downstream end of the engine casing while a cold-box flange mated to the upstream end of the engine casing. This cold-box flange mates to a welded flange within the inlet spool of the P400 test rig and restricts the core flow from flowing up and around the engine casing, which can be seen in greater detail in Figure 99. The inlet assembly mated to the cold-box flange and provide support to all of the components contained within the engine casing.

With all of the components assembled in and around the engine casing, it could be installed within the inlet spool, as shown in Figure 99. With this sub-assembly installed, the ethylene-air torch and fuel lines could be installed. The ethylene-air torch featured a piece of 1/4" copper tubing with housed an insulated piece of 1/16" Inconel-600 welding rod. Towards the tip of the ethylene-air torch, the welding rod was exposed so that when a 110 V signal was passed through the rod, it would arc at the tip and ignite the ethylene-air mixture flowing around it. Regarding the fuel lines, a Swagelok T-fitting was installed to join the two fuel inlet ports where a single 316 stainless steel 1/16" line was fed through the inlet spool.

Additionally, the inlet spool housed the core buster, shown in Figure 100, which was designed to create a uniform flow profile prior to the inlet of the test section, inlet mount and fuel manifold assembly, and P400 combustor. While the inlet mount assembly was specific to the rig, the remaining components, such as the fuel manifold, were designed to resemble the stock P400 hardware.

The instrumentation spool featured gas sampling probes to collect a radial span of emissions measurements. Additionally, hardware was available to support several pressure and temperature measurements throughout the combustor rig to gather information such as pattern factor and combustion efficiency with an accuracy of $\pm 0.8\%$

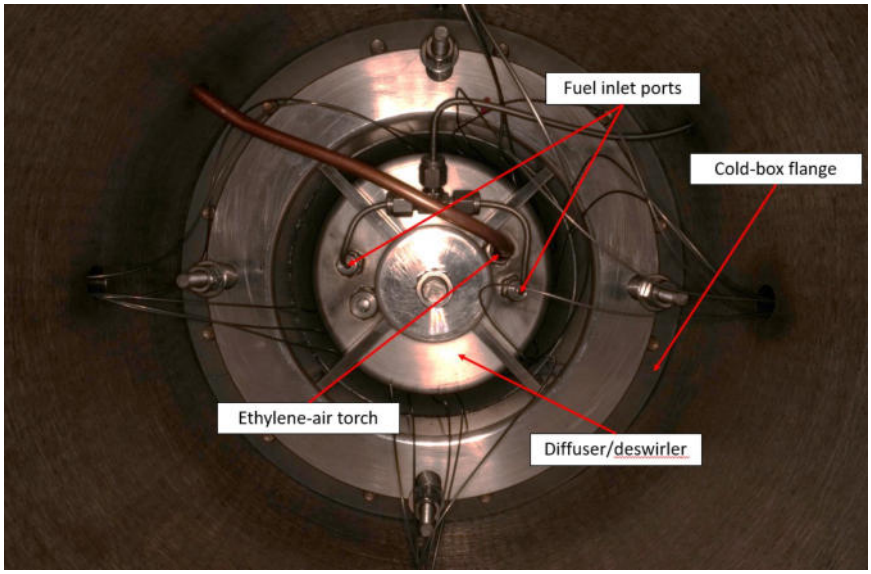

Figure 99. Inside of the inlet spool of the P400 test rig

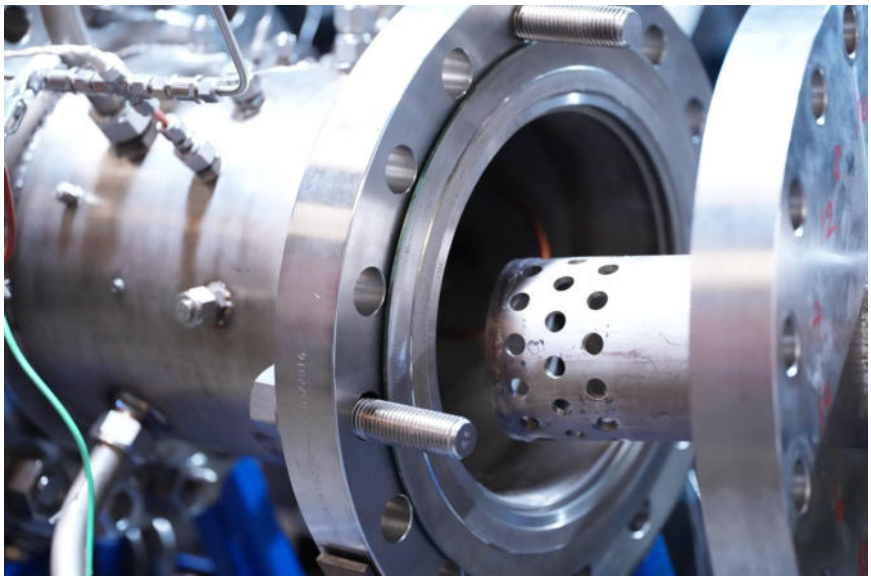

Figure 100. Core buster used in the P400 test rig

of full-scale value. The instrumentation spool also featured a traversing mount assembly designed to take circumferential temperature measurements.

The exhaust spool featured a water-cooled periscope camera, shown in Figure 101, useful for imaging the combustion regions at the upstream ends of the fuel-air mixing tubes. Additionally, the exhaust spool featured a variable geometry back-pressure

plate to ensure the rig was at design conditions without the presence of stator vanes. Finally, the exhaust spool fed into a water curtain spool and exhaust stack which featured several water curtains to de-energize the flow and reduce noise.

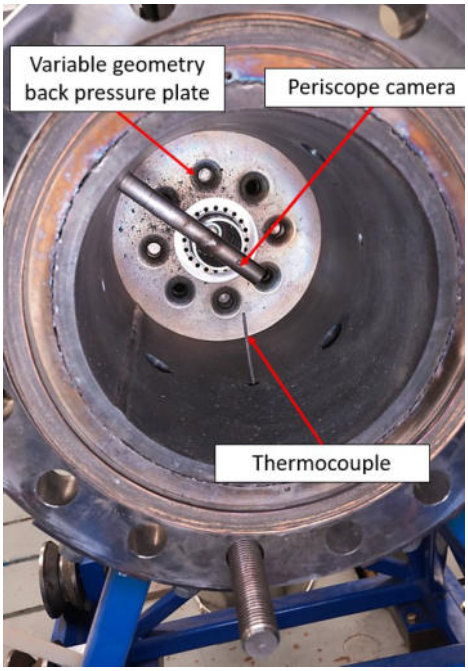

Figure 101. P400 rig exhaust spool section

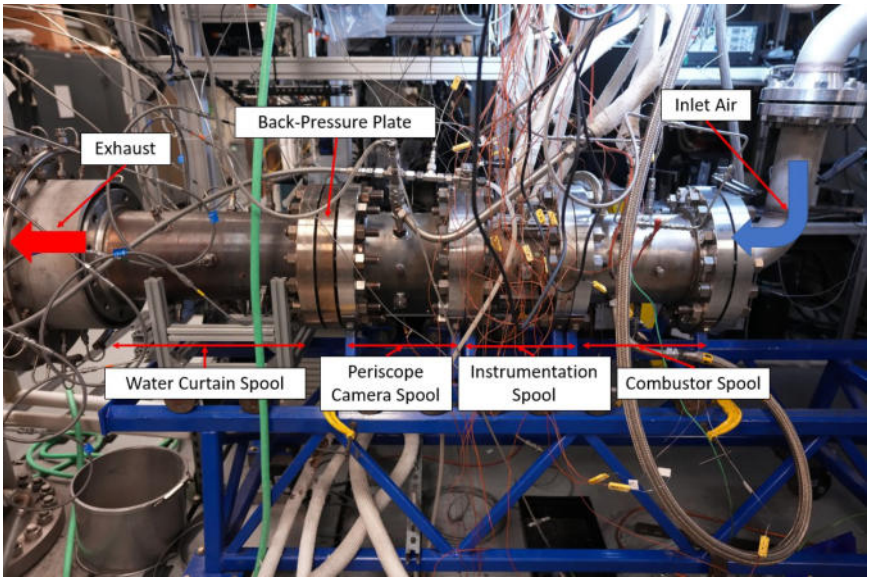

Figure 102. P400 rig fully assembled

IV. Results

This chapter presents the computational and experimental results of the outboard cavity-stabilized compact combustor designed for integration in a JetCat P400 small-scale gas turbine engine. The motivation for transitioning from the P160-scale to the P400-scale was to make use of the additional axial length and volume associated with the larger scaled engine. However, as a result of the JetCat P160 experimental testing, a new flame stabilization scheme was required, designed, and incorporated in the P400-scale compact combustor in an effort to improve its performance with liquid kerosene fuel. Section 4.1 discusses the computational results of a 90-degree sector of the compact combustor design analyzed at off-design and design conditions. Section 4.2 discusses experimental testing of the stock P400 combustor, which the current compact combustor was compared against, and the compact combustor which occurred in a test facility with no rotating turbomachinery, but featured a traversing thermocouple rake to gather circumferential temperatures at four radial spans at the combustor exit plane matching the computational domain.

4.1 JetCat P400 TVC Computational Results

Given the computational domain with prescribed boundary conditions, simulations were performed in ANSYS Fluent for half-idle, chosen to be 15,000 RPM, idle

Table 4. CFD boundary conditions used for off-design operating conditions. (To determine full engine flow rates, multiply the listed value by 4)

	Half-Idle	**Idle**	**Mid-Power**	**Design**
Air mass flow [kg/s]	0.018	0.040	0.135	0.1675
Fuel mass flow [g/s]	0.17	1.00	3.00	3.87
Global Equivalence Ratio	0.334	0.34	0.34	0.38
T_{t3} **[K]**	292	316.4	428.4	495
P_{t3} **[absolute, kPa]**	98.4	106.4	323.5	374.0

(36,000 RPM), mid-power, chosen to be 80,000 RPM, and full-power (98,000 RPM) conditions. While JetCat reports engine performance data at the design condition, the half-idle, idle, and mid-power condition parameters, such as air and fuel flow rate, were gathered from previous experimental testing of a stock JetCat P400 engine within AFRL from research engineer Nick Grannon. Table 4 outlines the parameters used for these conditions per the 90-degree sector used in this study. Regarding Table 4, the global equivalence ratios ramp up from 0.334 at a half-idle condition to 0.38 at the design point. The equivalence ratio at the design point was based on the maximum fuel consumption and maximum air flow rate through the engine at the design condition reported by JetCat. JetCat also reports a fuel consumption at idle of 200 ml/min. From here, the experimental data gathered from previous P400 engine testing, which featured a JetCat P400 engine equipped with a mass air flow (MAF) sensor for gathering air flow rate data, was used to determine the global equivalence ratio at the idle condition, and approximate the global equivalence ratios at the half-idle and mid-power conditions. These global equivalence ratios corresponded to adiabatic flame temperatures of 1184.5 K for $\phi = 0.334$, 1218.6 K for $\phi = 0.34$ (idle), 1310.6 K for $\phi = 0.34$ (mid-power), and 1453.4 K for $\phi = 0.38$.

Figure 103 shows temperature contours of the off-design and design conditions at a cross-section bisecting a fuel-vaporizer tube. These contours show that a majority of the combustion is contained within the cavity. The effect of the dilution holes can also been seen where peak temperatures are concentrated towards radial spans of 50% and both inner and outer liner walls remain well below their melting temperatures of 1650 K. Additionally, Figure 104 shows static temperature contours at a cut-plane halfway through the outboard cavity for all off-design and design conditions. These contours show a majority of the combustion occurring within the outboard cavity above the fuel vaporizer tubes across all conditions. Regarding the half-idle and

idle conditions, a majority of the combustion was skewed towards the forebody and aftbody faces, shown in Figure 103, which explains why the temperature contours through the cavity aren't showing combustion occurring at this cross-sectional view.

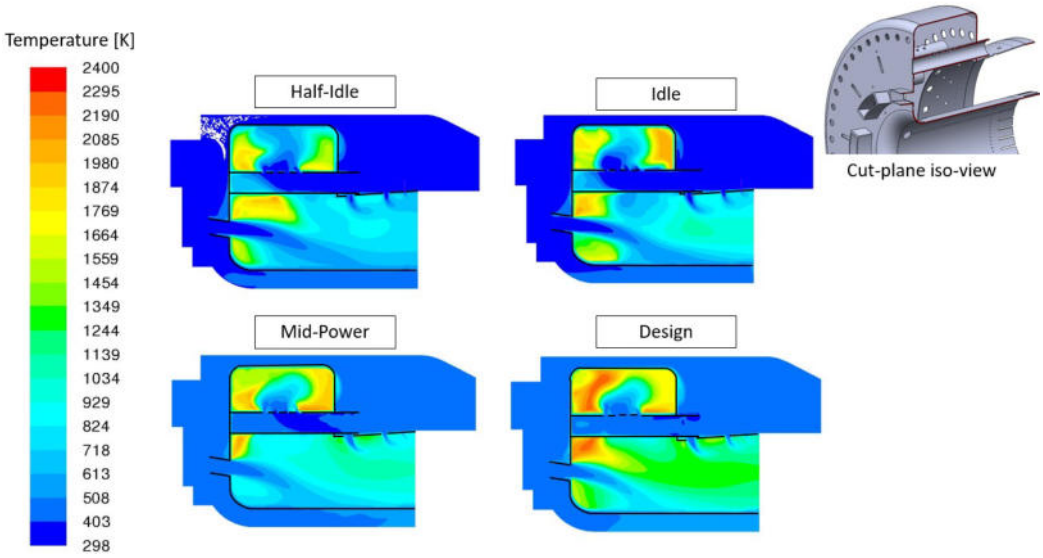

Figure 103. Temperature contour plot shown at a fuel vaporizer tube cross-section for all conditions

Figure 105 shows static temperature contours through cross-sections of the front, middle, and back of the outboard cavity for the design condition. These temperature contours show that a majority of the combustion was occurring above the vaporizer tubes across the entire length of the cavity. Additionally, the combustion was slightly skewed towards the forebody of the cavity.

Figure 106 shows contours of surface temperatures along the combustor liner for off-design and design conditions. Going from the half-idle to idle case, the contours revealed a decrease in liner temperature which was most likely a result of the increase in air flow rate over the liner, which provided additional cooling. At the half-idle condition, the flow rate was nearly stagnant which limited the amount of air flow to cool the liner surfaces. This was likely the cause of the disparity between the half-idle and idle conjugate heat transfer results. Between the idle, mid-power, and design

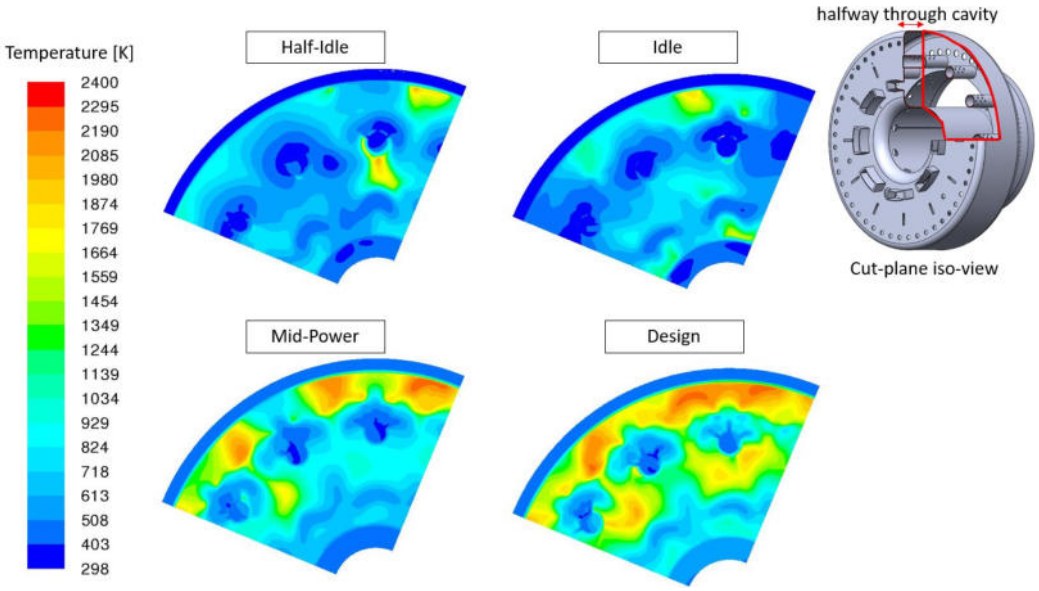

Figure 104. Temperature contour plot shown at a cross-section at a cut-plane halfway through the outboard cavity for all conditions

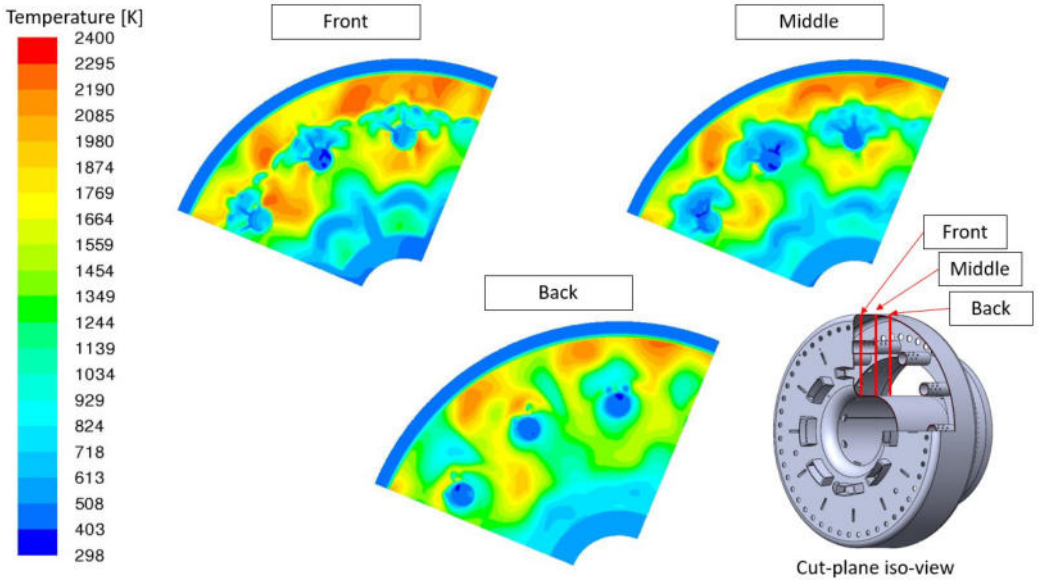

Figure 105. Temperature contour plot shown at a cross-section at a cut-plane (a) towards the front, (b) halfway, and (c) towards the back of the outboard cavity for the design condition

conditions, the combustor clearly ramped up uniformly as fuel flow rate and air flow rate increased to the design point condition. The hottest regions observed along the

combustor liner were regions along the cavity in between each fuel vaporizer tube, regions along the aftbody in between each fuel vaporizer tube where temperatures peaked above 1650 K, the melting point of the liner material, between the mid-power and design conditions.

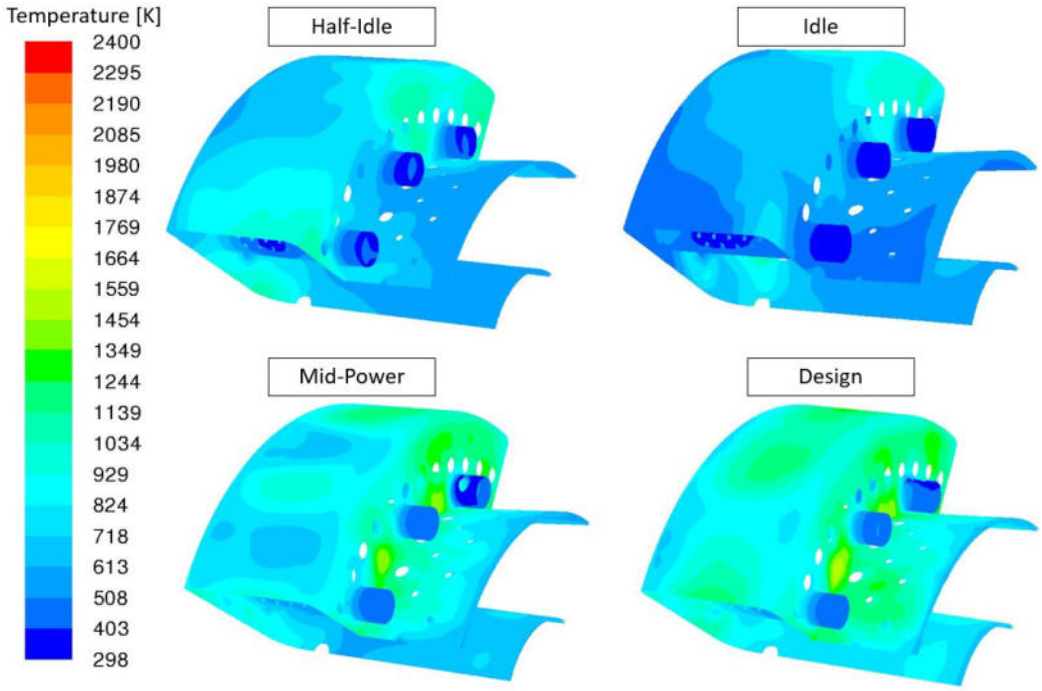

Figure 106. Combustor liner surface temperatures across all operating points simulated in CFD

Figure 107 shows pathlines colored by velocity magnitude for half-idle, idle, mid-power, and design conditions through a cross-section bisecting one of the fuel vaporizer tubes. Across all conditions, there was a presence of two vortices within the outboard cavity above the vaporizer tubes. However, directly in between each fuel vaporizer tube, only one vortex was present, as shown in Figure 108. This was also seen in the DP43 computational design of Briones et al. [31], shown in Figure 109, where the centerplane showed the presence of two vortices within the cavity, while the staggered plane showed the presence of only one vortex within the cavity. Due to the presence of fuel vaporizer tubes in the current compact outboard cavity combustor design,

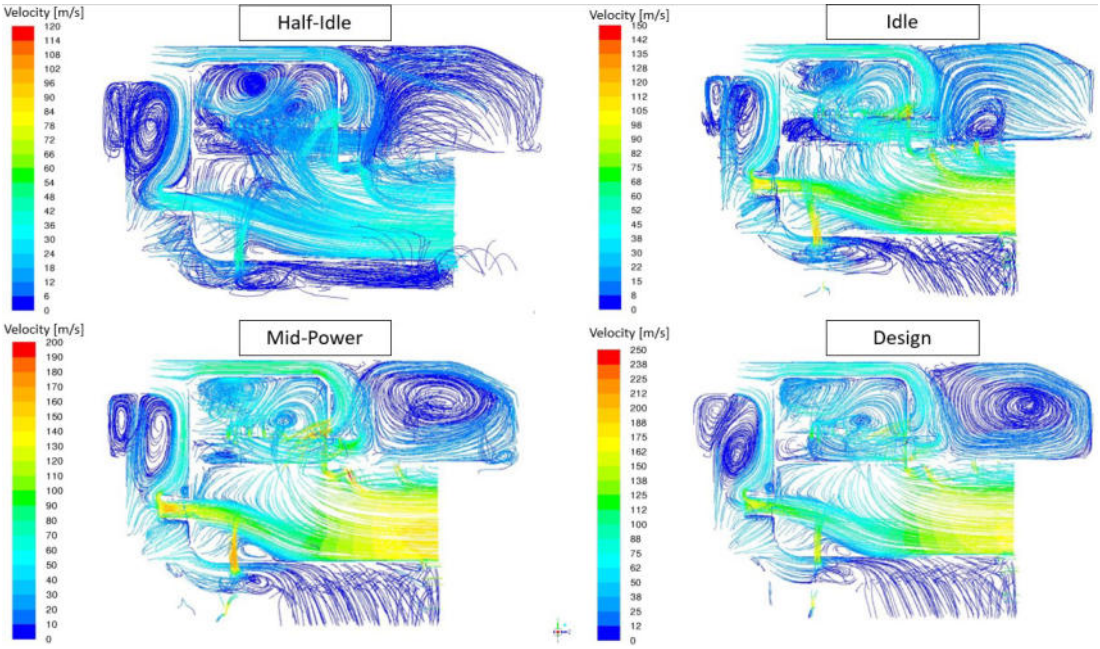

Figure 107. Pathlines colored by velocity magnitude at a cross-section bisecting the fuel vaporizer tubes across all conditions

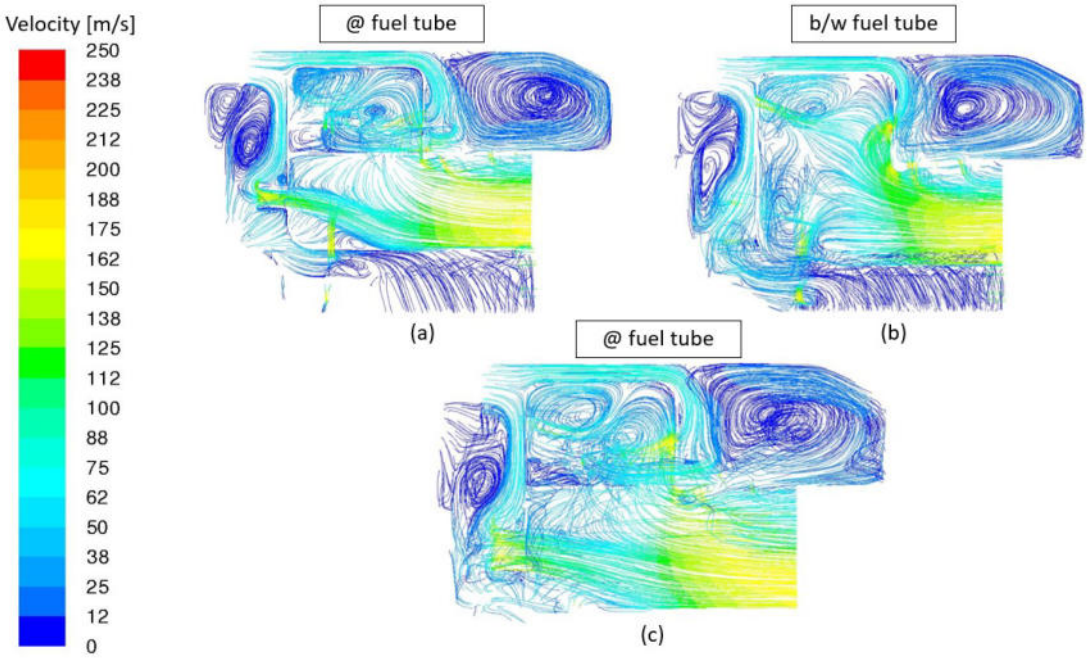

Figure 108. Pathlines colored by velocity magnitude at a cross-section bisecting (a) the fuel vaporizer tube, (b) the location between each fuel vaporizer tube, and (c) the following fuel vaporizer tube at the design condition

the two vortices present above the vaporizer tubes shifted and have centered about the cavity compared to the ones seen in the centerplane in the case of Briones et al. [31]. Additionally, the single vortex present between each vaporizer tube was radially higher within the cavity compared to the single vortex seen in the staggered plane case of Briones et al. [31]. Having the vortices present within the outboard cavity radially outboard enabled flame stabilization to exist within the cavity where a majority of the combustion occurred.

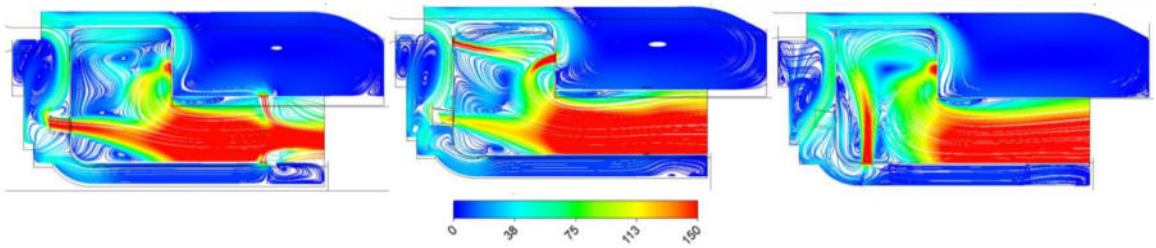

Figure 109. Streamlines colored by velocity magnitude for the DP43 computational design of Briones et al. [31] at the centerplane (left), staggered plane (center), and periodic plane (right)

Figure 110 shows static temperature contours at the combustor exit plane for half-idle, idle, mid-power, and design conditions. For all conditions, peak temperature contours were located near a radial span of 50% where the inner and outer liners remained cool, however, the idle case showed temperature contours in a localized region at the exit plane indicating uneven burning occurring within the cavity, whereas the half-idle, mid-power, and design cases were more symmetric suggesting stable and uniform burning.

To observe the exit temperature profile going into the turbine inlet plane, circumferentially average exit temperature profiles were gathered, as shown in Figure 111. The dilution zone caused the temperature profiles at the combustor exit plane to closely resemble a parabolic curve where the peak circumferentially averaged temperatures for all conditions were centered around the 50% radial span mark. Additionally,

Figure 111 showed that the average combustor exit temperatures increased from 722 K at a half-idle condition to 1152 K at the design condition as both air and fuel flow rates increased. Since the global equivalence ratio remained around 0.34 for all conditions, the increase in average combustor exit temperatures was likely due to the enhancement of the trapped vortices present within the cavity improving fuel-air mixing and promoting more complete combustion.

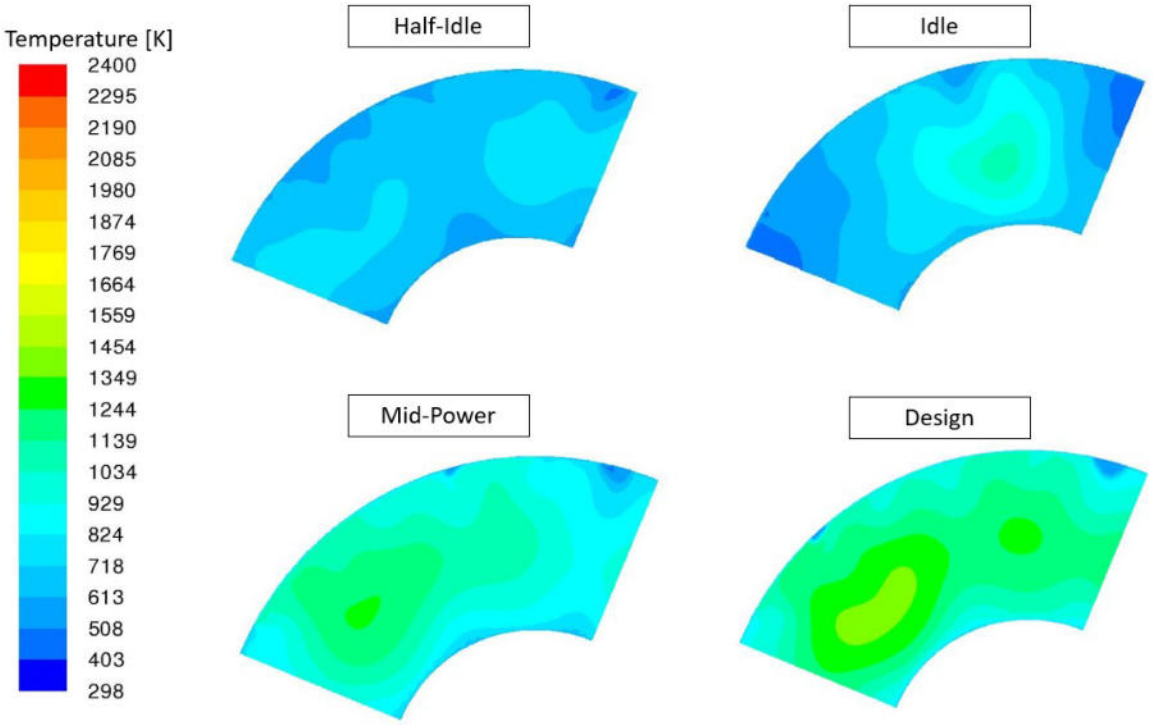

Figure 110. Computationally predicted static temperature contours at the combustor exit plane for all conditions

Figure 112 compares the circumferentially averaged exit temperature profile of the current compact combustor against the "best" computational designs of Briones et al. [31] at the design condition. Comparing the base DP43 computational design with the current effort, the DP43 computational design of Briones et al. [31] exhibited a more uniform exit temperature profile where average temperatures at radial spans of 100% and 0% were 1252 K and 1370 K, respectively. Additionally, peak temperatures

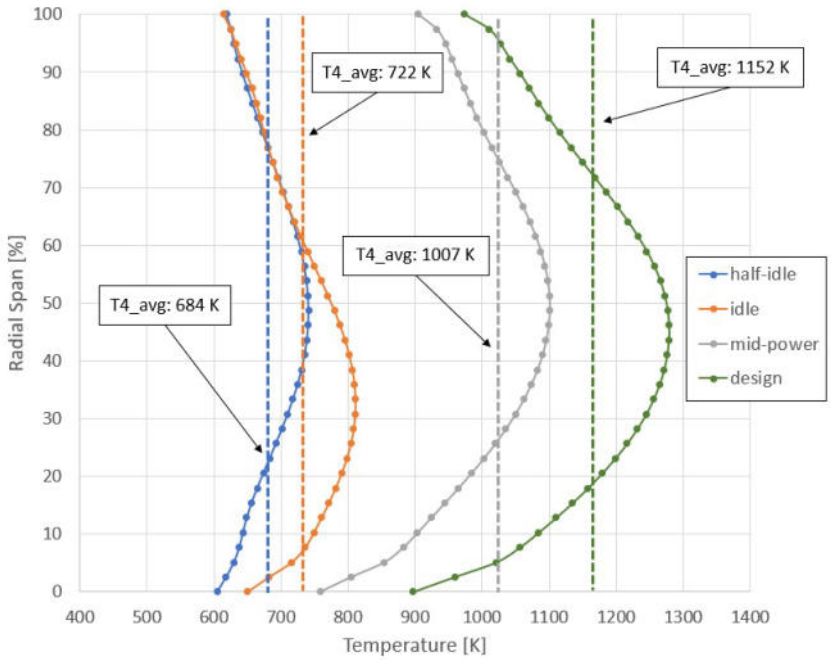

Figure 111. Circumferentially averaged temperature profiles gathered at the combustor exit plane for all computational simulations

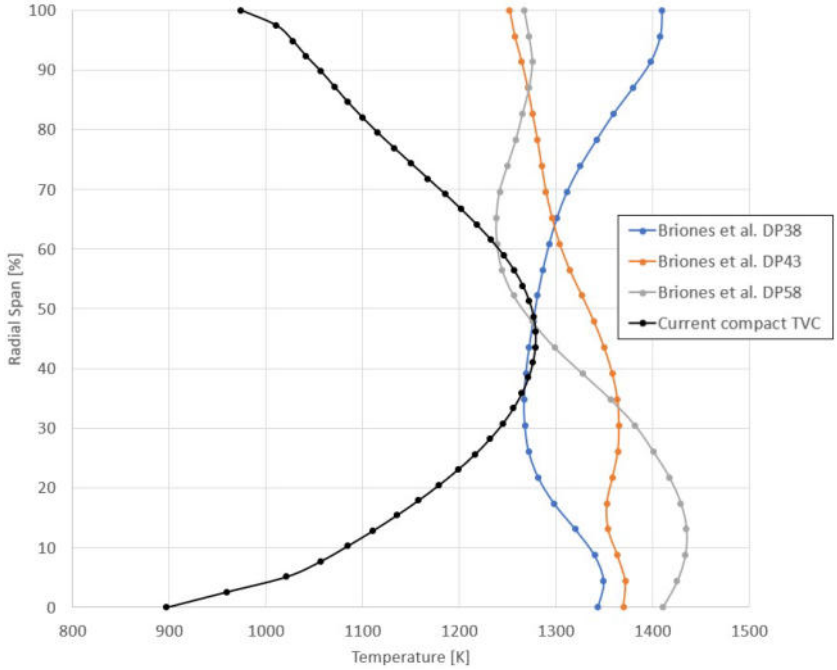

Figure 112. Circumferentially averaged temperature profile at the design condition compared to the computational designs of Briones et al. [31]

near the 30% radial span where the current combustor's peak temperatures occurred at a 50% radial span. However, the current compact combustor's exit temperature profile was significantly cooler along the OD and ID resulting in a nearly 500 K temperature difference between the current combustor and the computational designs of Briones et al. [31].

The likely cause between this discrepancy in temperature along the OD and ID walls was due to the boundary conditions used in the computational domain along the liner walls at the exit plane. The current study used a constant surface temperature boundary condition where a temperature of 600 K was forced and held constant throughout the simulation, likely resulting in liner temperatures that were cooler compared to the computational results of Briones et al. [31], therefore causing the difference between the current combustor's and the exit temperature profiles of Briones et al. [31]. Briones et al. [31] considered the same surfaces as an adiabatic wall which likely led to increased liner surface temperatures, resulting in a higher average temperature at the combustor exit plane compared to the current effort's.

Comparing these computational profiles to the stock P400 combustor's exit temperature profiles, peak temperatures were centered around the 70% radial span where exit temperatures were skewed more towards the OD compared to the computational designs. Additionally, the average and peak temperatures of 1145 K and 1434 K, respectively, were within the same regime as the current compact combustor's computational predictions for the design condition.

Table 5 compares selected parameters between each operating condition of the current compact combustor versus the DP43 computational design of Briones et al. [31] which was run at conditions equivalent to "Design". The parameters such as pattern factor (PF), total pressure loss (TPL), combustion efficiency (η), and critical

liner area factor ($A_{critical}$) used in Table 5 were calculated from Equations 11-14

$$PF = \frac{T_{4,max} - T_{4,avg}}{T_{4,avg} - T_{3.1}} \tag{11}$$

$$TPL = \frac{P_{T,4} - P_{T,3.1}}{P_{T,3.1}} \tag{12}$$

$$\eta = \frac{T_{4,avg} - T_{3.1}}{T_{4,ideal} - T_{3.1}} \tag{13}$$

$$A_{critical} = \frac{\sum_{liner} dA_{T>1300K}}{\sum_{liner} dA} \tag{14}$$

where Stations 3.1 and 4 denote the inlet and exit plane of the combustor, respectively [34]. Additionally, $T_{4,ideal}$ represents the adiabatic flame temperature, which was determined at half-idle, idle, mid-power, and design conditions corresponding to global equivalence ratios of 0.334, 0.34, 0.34, and 0.38, respectively.

Table 5. Results comparison of all evaluated conditions and the DP43 TVC results of Briones et al. [31] at design condition

	Half-Idle	**Idle**	**Mid-Power**	**Design**	**Briones et al.** [31]
T_{4avg} **[K]**	684	722	1007	1152	1325
T_{4max} **[K]**	823.5	1139	1349	1454.1	1426
PF	0.36	0.61	0.59	0.43	0.12
TPL [%]	1.5	6.8	11.9	11.0	13.3
η [%]	43.9	45.0	65.6	70.3	97.1
$A_{critical}$ [%]	0	0	2.3	2.3	13.8

While the maximum temperatures at the combustor exit plane were relatively similar, the pattern factors and critical liner area factor differed significantly. The critical liner area factor compares the surface area of the combustor where temperatures exceed 1330 K against the total surface area of the combustor. In the DP43 design, since fuel was injected along the backside of the forebody, the burning was preferentially occurring within this region rather than in the cavity where there was a constant exchange of cool reactants and hot products. This localized heating drove

the critical linear area factor up compared to the current compact TVC where a majority of the burning occurred within the TVC cavity and off the walls.

Additionally, differences in boundary conditions at the combustor exit plane between the current combustor and the computational domain of Briones et al. [31] resulted in lower average exit temperatures, which resulted in undesirable combustion efficiencies across the operating range. Modifying the boundary conditions accordingly to match those of Briones et al. [31], who considered the liner surfaces at the exit plane to be adiabatic walls, resulted in a 30 K increase in average combustor exit temperature, which shifted the parabolic exit temperature profile to the right by this amount. While there was a slight increase in the average combustor exit temperature as a result of matching the boundary conditions of Briones et al. [31], there was still roughly a 150 K temperature difference between the current design case and the DP43 design of Briones et al. [31]. To gain insight into the actual temperatures at these prescribed locations where the adiabatic wall boundary conditions were applied, thermocouples were welded to the liner in these locations to record temperatures to be used to improve the accuracy of the CFD simulations at the design point.

The DP43 design was able to utilize its stock length with minimum dilution area ($1.25 cm^2$) to ensure burning was complete prior to the exit plane. The current compact TVC needed additional dilution area ($4.13\ cm^2$) to quench reactions prior to the combustor exit plane as a result of its reduced length. While the maximum exit temperature was similar compared to the DP43 design, the additional cooling reduced the average exit temperature by quenching reactions prior to the combustor exit plane allowing unburned fuel to continue past the exit plane, as represented by the contours of CO at the exit plane shown in Figure 113. This reduction in average combustor exit temperature increased the pattern factor from 0.12 to 0.43.

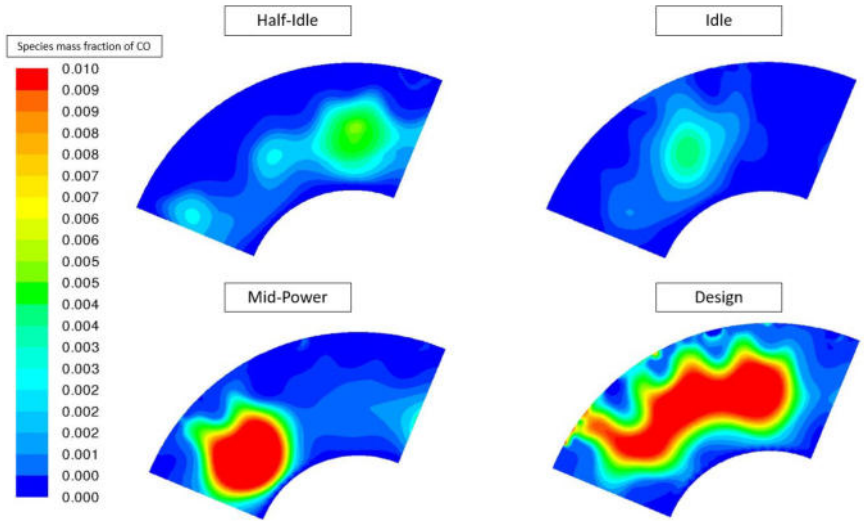

Figure 113. CO contours at the P400 compact combustor exit plane at the design condition

4.2 JetCat P400 TVC Experimental Testing

With the new P400 test rig assembled, the stock P400 combustor was used to perform baseline tests to ensure the test rig and surrounding hardware performed as intended. This allowed circumferential temperature data to be captured at the exit plane of the stock P400 combustor to be later compared against the P400 compact combustor. Section 4.2.1 discusses the test matrix used to perform the initial shake-down run of the newly designed test rig with the stock P400 burner. Section 4.2.2 discusses the test matrix used to match and compare the current compact combustor data with the previously tested stock P400 combustor. Finally, Section 4.3 discusses the results from experimental testing of the stock P400, andSections 4.4-4.6 discuss the results from testing the P400 compact combustor.

4.2.1 Stock JetCat P400 combustor experimental test matrix.

The test matrix shown in Table 6 features nine test points used to perform initial tests on the stock P400 combustor in the new P400 test rig. These nine test points

were based off of a P400 cycle that was calculated within AFRL by a team of engineers to replicate the operating conditions within the JetCat P400 engine. Test Points 1-8 are a ramp-up from an idle condition to a design condition where the equivalence ratio ramps up from 0.14 to 0.28, respectively. The equivalence ratio at Point 2 is lower compared to the equivalence ratio at Point 1 because previous P400 engine testing showed a sudden decrease in fuel-air ratio (FAR) as the engine accelerated past an idle condition. This was a result of the fuel flow not being able to keep up with the air flow coming from the compressor, which caused a momentary decrease in FAR during operation.

Additionally, there were two design conditions within the test matrix where the equivalence ratio was increased from 0.28 to 0.33. The equivalence ratio of 0.28 was based off of the P400 cycle that was calculated, while the equivalence ratio of 0.33 was an estimate based off of the reported fuel flow consumption and air flow at the design point published by JetCat.

Table 6. Baseline P400 compact combustor test matrix

Test Point	**N [%]**	$\dot{m}_{air}$ **[kg/s]**	$\dot{m}_{fuel}$ **[g/s]**	Fuel dp [kPa]	P_3 [kPa]	T_3 [K]	ϕ
1	30	0.15	1.40	2.76	137.90	339.82	0.14
2	41	0.20	1.69	4.14	152.72	352.59	0.13
3	51	0.30	2.85	11.03	184.30	377.59	0.14
4	61	0.37	3.79	19.31	209.60	393.71	0.15
5	71	0.44	4.99	33.09	241.80	413.71	0.17
6	81	0.51	6.56	57.92	283.72	436.48	0.19
7	92	0.60	9.41	118.59	347.36	469.26	0.23
8	100	0.64	12.41	206.15	396.24	497.04	0.28
9	100	0.64	14.62	286.13	396.24	497.04	0.33

4.2.2 Outboard cavity compact combustor experimental test matrix.

Since the objective of this current effort was to design a compact combustor at the P400-scale with the goal of achieving similar or improved performance compared to the stock P400 burner, the test matrix used for the P400 compact combustor

experimental testing was built based off of Table 6 to ensure the new non-rotating test rig was viable prior to the current compact combustor being installed. This test matrix featured the first nine test points, shown in Table 7, shown previously in Table 6. These test points served as a comparison between the stock P400 burner and the current P400 outboard cavity compact combustor. Test Points 10-13 are points that were used to be directly compared against computational results.

Table 7. Baseline stock P400 combustor test matrix with added points (10-13) to match computational conditions

Test Point	**N [%]**	$\dot{m}_{air}$ **[kg/s]**	$\dot{m}_{fuel}$ **[g/s]**	Fuel dp [kPa]	P_3 [kPa]	T_3 [K]	ϕ
1	30	0.15	1.40	2.76	137.90	339.82	0.14
2	41	0.20	1.69	4.14	152.72	352.59	0.13
3	51	0.30	2.85	11.03	184.30	377.59	0.14
4	61	0.37	3.79	19.31	209.60	393.71	0.15
5	71	0.44	4.99	33.09	241.80	413.71	0.17
6	81	0.51	6.56	57.92	283.72	436.48	0.19
7	92	0.60	9.41	118.59	347.36	469.26	0.23
8	100	0.64	12.41	206.15	396.24	497.04	0.28
9	100	0.64	14.62	286.13	396.24	497.04	0.33
10	15	0.07	1.65	1.38	90.25	292.04	0.34
11	30	0.16	3.99	2.76	106.39	316.48	0.34
12	80	0.54	12.74	57.92	278.55	428.15	0.34
13	100	0.67	15.46	286.13	373.97	495.00	0.38

Table 8 shows additional testing conditions that were run by Paxton et al. [33] within AFRL's Test Cell 151 for the stock P400 burner which was cycled through a range of equivalence ratio sweeps. The goal for the current compact combustor during experimental operation was to match these conditions as best as possible and build an operating map based on these test points to be compared against the stock P400 combustor operating map.

Table 8. Characterization of P400 compact combustor test matrix

Test Point	**N [%]**	$\dot{m}_{air}$ **[kg/s]**	$\dot{m}_{fuel}$ **[g/s]**	Fuel dp [kPa]	P_3 [kPa]	T_3 [K]	ϕ
14	30	0.15	0.96	1.38	137.90	339.82	0.09
15	30	0.15	1.18	2.07	137.90	339.82	0.11
16	30	0.15	1.85	4.83	137.90	339.82	0.18
17	30	0.15	2.60	8.96	137.90	339.82	0.25
18	30	0.15	1.15	2.07	137.90	339.82	0.14
19	30	0.15	1.79	4.14	137.90	339.82	0.14
20	41	0.20	1.30	2.07	152.72	352.59	0.09
21	41	0.20	2.46	8.27	152.72	352.59	0.18
22	51	0.30	LBO	LBO	184.30	377.59	LBO
23	51	0.30	1.13	2.07	184.30	377.59	0.05
24	51	0.30	1.70	4.14	184.30	377.59	0.08
25	51	0.30	2.27	6.89	184.30	377.59	0.11
26	51	0.30	3.41	15.86	184.30	377.59	0.16
27	51	0.30	4.55	27.58	184.30	377.59	0.22
28	51	0.30	5.13	35.16	184.30	377.59	0.25
29	51	0.30	5.71	43.44	184.30	377.59	0.28
30	71	0.44	3.30	14.48	241.80	413.71	0.11
31	71	0.44	6.58	57.92	241.80	413.71	0.21
32	100	0.64	LBO	LBO	396.24	413.71	LBO
33	100	0.64	4.96	33.09	396.24	413.71	0.11
34	100	0.64	7.45	74.46	396.24	413.71	0.16
35	100	0.64	9.93	132.38	396.24	413.71	0.22
36	100	0.64	16.13	348.87	396.24	413.71	0.36
37	100	0.64	18.90	478.50	396.24	413.71	0.42
38	100	0.64	20.35	555.03	396.24	413.71	0.46
39	100	0.64	9.60	123.42	396.24	413.71	0.29
40	100	0.64	14.49	281.31	396.24	413.71	0.29

4.3 Stock JetCat P400 combustor test results

Prior to the testing of the outboard cavity-stabilized compact combustor in the P400 rig, a stock P400 combustor was first tested to ensure the feasibility of the newly designed test rig. The data presented in this section outlines the post-processed thermocouple rake data ranging from 31-100% engine speed conditions.

The thermocouple rake used featured four K-type thermocouple probes placed

in-line with the combustor exit plane. Figure 114 shows the circumferential paths of each individual thermocouple probe in the rake where Rakes 1-4 are placed at radial spans of roughly 76%, 56%, 35%, and 15%, respectively, between the ID of the outer liner and the OD of the shaft housing. Figure 115 shows the circumferential clocking positions every 30 degrees which aligned with each vaporizer tube. The rake took

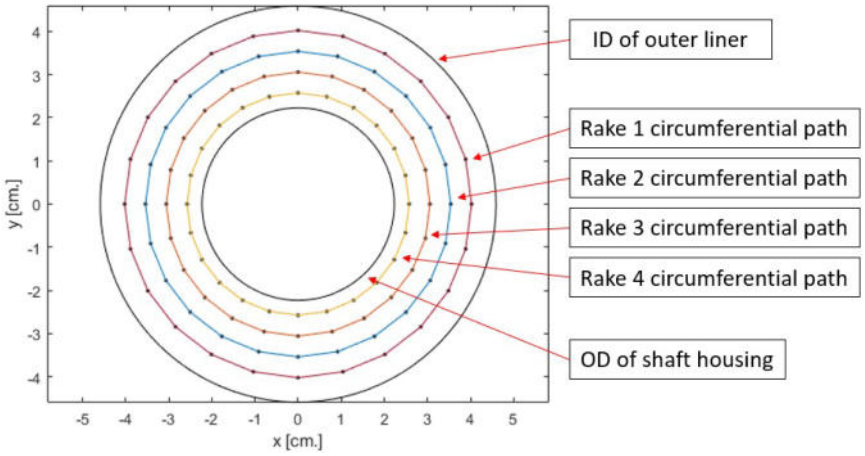

Figure 114. Thermocouple rake circumferential paths

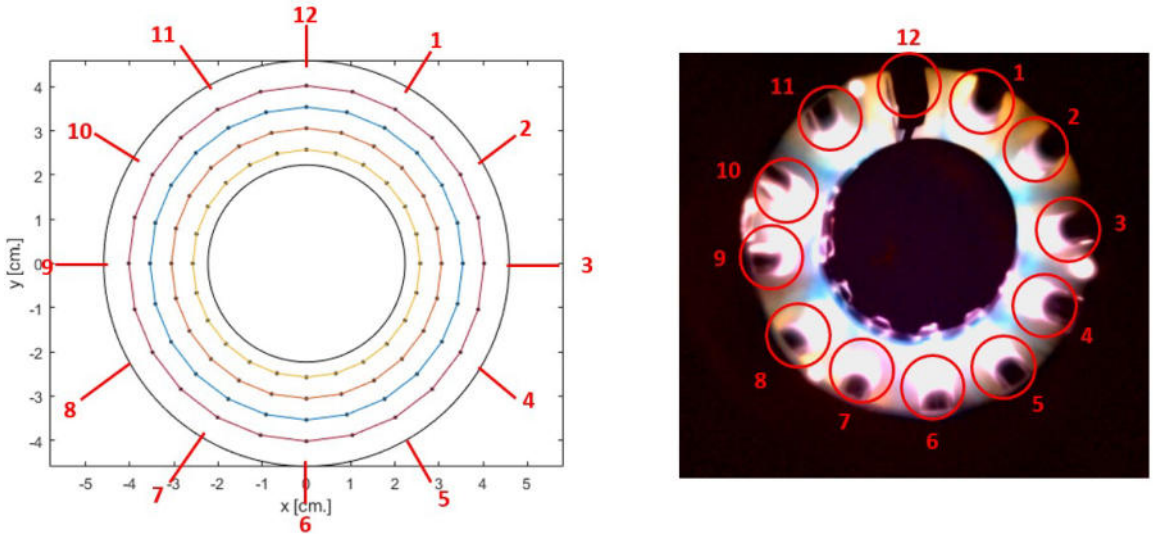

Figure 115. Thermocouple rake circumferential clocking

circumferential temperature measurements every 15 degrees totaling 24 measurements across the combustor exit plane, enabling measurements to be captured at and between each fuel vaporizer tube. The rake always started in the 12-o-clock position

and ended in its original starting position during testing.

Figure 116 shows total temperature contours at the exit plane of the stock P400 combustor for 31%, 41%, 51%, 61% of maximum engine speed conditions, and Figure 117 shows similar contours for 71%, 81%, 92%, and 100% operating conditions. Across

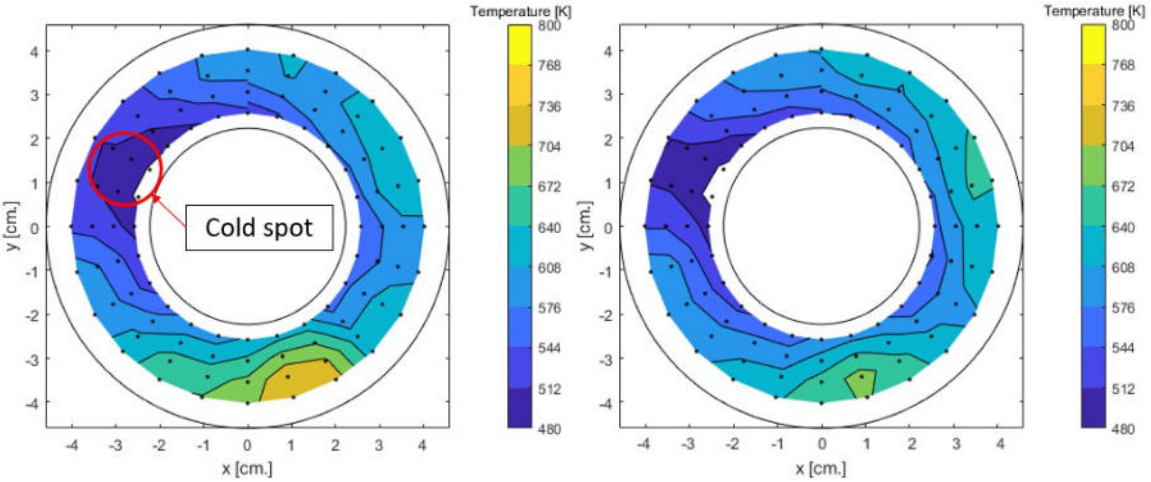

(a) 31% N (b) 41% N

(c) 51% N (d) 61% N

Figure 116. Exit temperature contours across an operating range of 31-61% N of the stock P400 combustor liner

all conditions, there was a cold region between the 9 and 10-o-clock positions caused by the ethelyne-air torch port. Figure 118 shows an air gap present between the glow plug port, which is attached to the inside of the combustor liner, and the ethylene-air

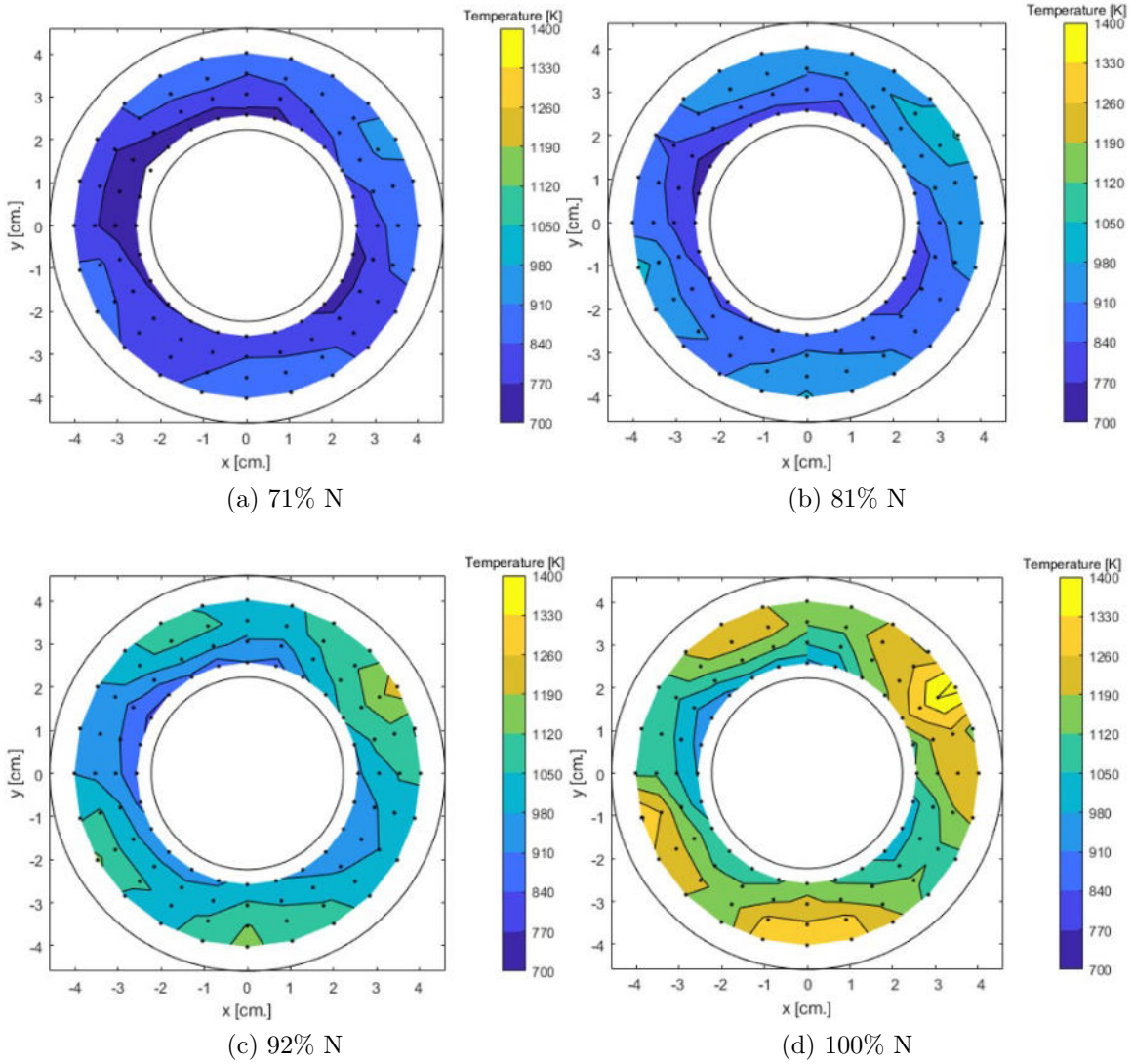

(a) 71% N (b) 81% N

(c) 92% N (d) 100% N

Figure 117. Exit temperature contours across an operating range of 71-100 % N of the stock P400 combustor liner

torch. This air gap allowed T_3 air to pass through and quench reactions occurring within this region causing this local cold-spot across all conditions.

Additionally, a localized hot-spot was observed near the 6-o-clock position for the 31% and 41% conditions, which was likely a result of insufficient pressure drop across the fuel manifold plenum to evenly distribute fuel across all twelve fuel vaporizer tubes. At low power conditions, the fuel flow rate was low such that the pressure drop across the fuel lines within the vaporizer tubes was comparable to the pressure

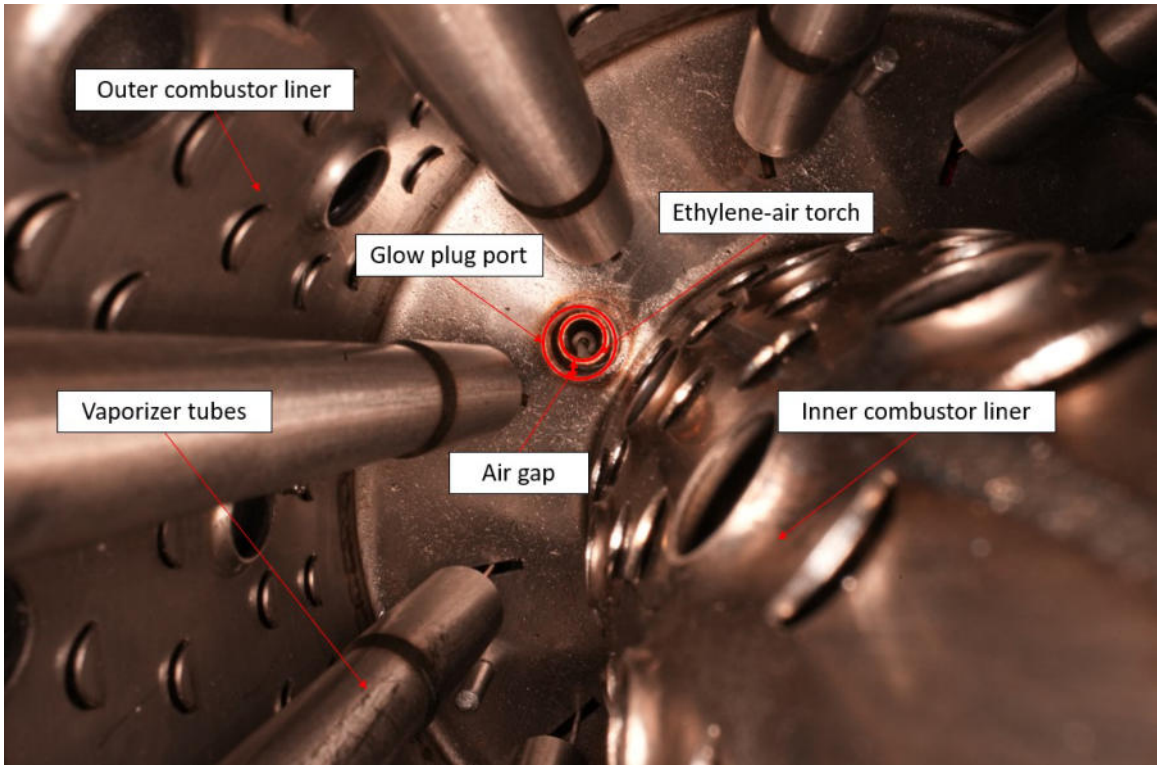

Figure 118. Air gap between glow plug port and ethylene-air torch within the stock P400 combustor liner

drop across the fuel plenum, which allowed the fuel distribution to be influenced by gravity and favor the fuel lines towards the 6-o-clock circumferential positions. Once the flow rates increased past the 41% mark, the pressure drop increased within the fuel manifold which then behaved as a plenum distributing fuel evenly across all twelve vaporizer tubes.

To visualize local hot-spots and/or cold-spots at the exit plane, the total temperature measurements were non-dimensionalized by the plane average temperature, T_{avg}, for each condition. Figure 119 shows dimensionless temperature contours at the exit plane of the stock P400 combustor for 31%, 41%, 51%, 61% of maximum engine speed conditions, and Figure 120 shows similar contours for 71%, 81%, 92%, and 100% operating conditions. Based on these contours, the cold-spot previously mentioned between the 9 and 10-o-clock circumferential positions, was more evident across all conditions. Similarly, the hot-spots at the 31% and 41% conditions as a

result of poor fuel distribution were more evident. An additional hot-spot was noticed at the 2-o-clock position for the 51%-100% conditions. Also, as the conditions were ramped up to the design case, four hot-spots emerged at roughly 11, 2, 6, and 8-o-clock positions.

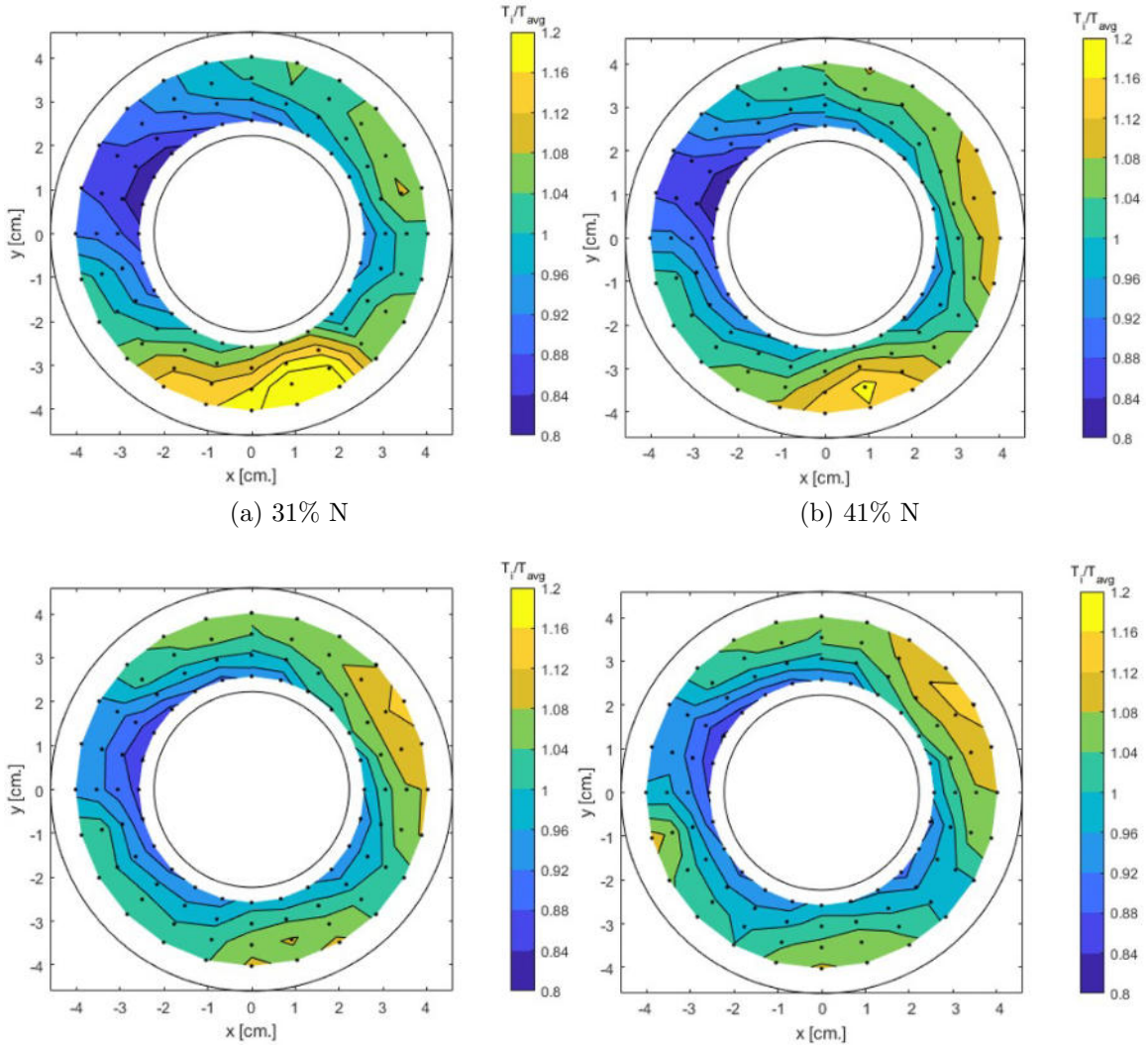

(a) 31% N (b) 41% N

(c) 51% N (d) 61% N

Figure 119. Non-dimensional exit temperature contours across an operating range of 31-61% N of the stock P400 combustor liner

Table 9 shows outputs of T_3, T_{max}, T_{avg}, and pattern factor across all conditions tested. An average combustor exit temperature and pattern factor of 1145 K and 0.45, respectively, was achieved for the design condition.

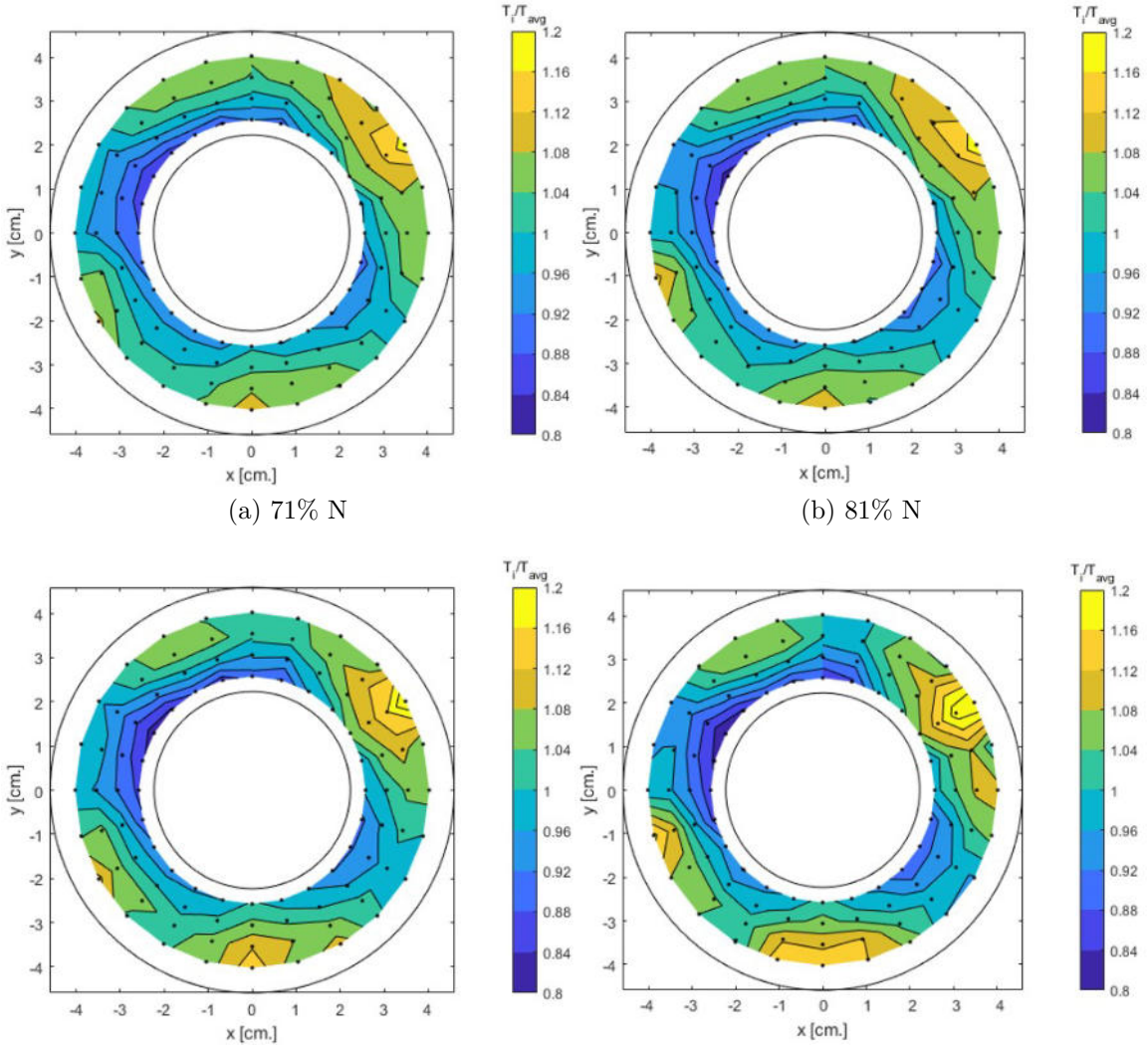

(a) 71% N

(b) 81% N

(c) 92% N

(d) 100% N

Figure 120. Non-dimensional exit temperature contours across an operating range of 71-100% N of the stock P400 combustor liner

Table 9. Tabulated results from the thermocouple rake for the stock P400 combustor liner tested in the P400 test rig

Throttle	**31%**	**41%**	**51%**	**61%**	**71%**	**81%**	**92%**	**100%**
T_3 **[K]**	341	353	378	394	414	436	469	497
T_{max} **[K]**	731	686	767	853	964	1064	1250	1434
T_{avg} **[K]**	586	582	664	733	814	889	1006	1145
PF	0.59	0.45	0.36	0.36	0.37	0.39	0.45	0.45

Table 10 compares the pressure drop measured across the fuel lines before and after testing the stock P400 burner, where the pressures recorded were absolute pressure measurements. All of the fuel lines exhibited lower pressure drops after testing with the exception of Lines 1 and 12 which exhibited pressure drops 10.7% and 50.6% higher than initial measurements, respectively. These increases in pressure drop were due to metal burs present towards the tips of the fuel lines blocking a portion of the opening in the fuel line. Having a pressure drop increase of 50.6% would have prevented fuel flow to this location compared to other locations, however, this was not observed through the exit temperature contour plots.

Table 10. Pressure drop readings across twelve fuel lines used before and after testing

Fuel line #	**Pressure reading [kPa]**	**Pressure reading [kPa]**	**% Change**
	Before Testing	**After Testing**	
Line 1	162.0	179.3	+10.7
Line 2	168.9	153.1	-9.4
Line 3	168.9	154.4	-8.6
Line 4	195.1	149.6	-23.3
Line 5	176.5	152.4	-13.7
Line 6	162.7	129.6	-20.3
Line 7	165.5	157.9	-4.6
Line 8	170.3	141.3	-17.0
Line 9	194.4	175.8	-9.6
Line 10	155.8	133.1	-14.6
Line 11	164.1	148.2	-9.7
Line 12	166.2	250.3	+50.6

4.4 P400 compact combustor test results

With the outboard cavity-stabilized compact combustor fully installed in the new P400 test rig, the freestream air was initially preheated to 350 K and set to a flow rate and pressure of 0.30 kg/s and 180 kPa, respectively, corresponding to conditions around 51% of maximum engine speed. However, the combustor struggled to ignite

at these conditions with the assistance of the ethylene-air torch, so the temperature and pressure were increased in an attempt to quickly vaporize the fuel upon injection. Additionally, the air mass flow rate was reduced to allow as much heat coming from the ethylene-air torch to radiate into the outboard cavity and ignite the premixed fuel-air mixture. With the air flow rate reduced to 0.15 kg/s, T_3 and P_3 increased to 490 K and 200 kPa, respectively, ignition was achieved and a flame was distributed around the combustor. However, burning was only occurring in certain localized areas, as shown by Figure 121.

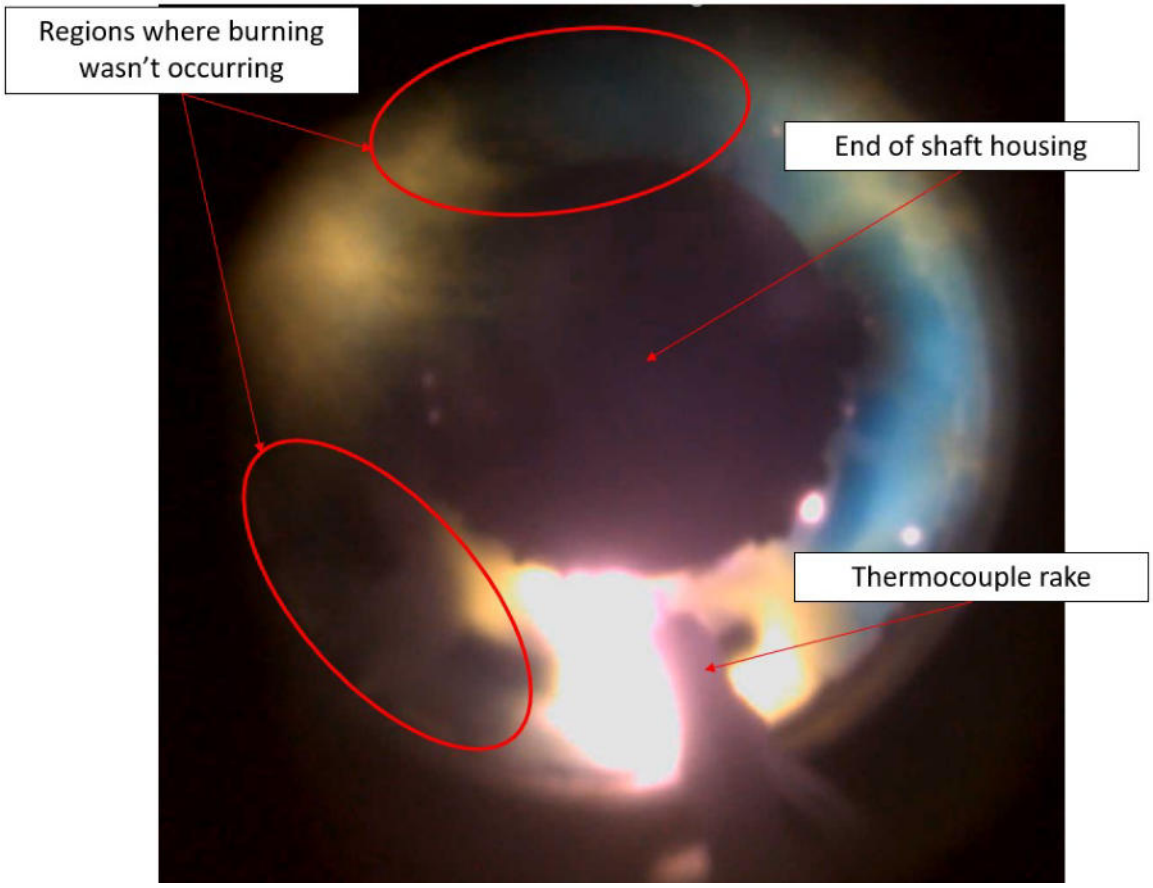

Figure 121. Burning occurring within the cavity-stabilized compact combustor during the first round of testing

As a result of having to increase the freestream temperature to 490 K to achieve ignition, the CFD domain spacer, which was made out of Ultem, quickly melted and

began breaking apart and flowed through the combustor. The entire duration of the test lasted 20 minutes where the air mass flow rate was increased from a 30% to an 80% condition, while P_3 was increased from a 61% condition to the design pressure within the same time frame. T_3 on the other hand was maintained at the design point temperature throughout the entire duration of the test. Within the first few seconds of the test after ignition was achieved, the integrity of the Ultem spacer was lost. The Ultem melted during the test as seen in Figure 122, after initial testing had been completed. The melted Ultem worked its way through and around the combustor blocking critical air driver holes on the forebody and aftbody portions of the combustor. Additionally, fuel lines became clogged, as shown by Figure 122a, which prevented fuel from traveling down the vaporizer tubes entirely. This was likely the cause of the regions where burning wasn't occurring, shown in Figure 121, during testing.

Figure 122 also shows fuel lines protruding from the vaporizer tubes which was a result from the core buster unintentionally pushing the inlet assembly further downstream due to improper assembly. Since the inlet assembly and fuel manifold assembly are coupled, fuel lines were also pushed downstream causing them to extend out past the vaporizer tubes. Some were extended farther than others preventing any fuel from entering the vaporizer tubes, however, due to the recirculation pocket located downstream of the cavity, the air flow would entrain and carry fuel down the vaporizer tubes still allowing combustion to occur between the 12-o-clock and 6-o-clock (going clockwise) positions in the combustor despite of the fuel lines protruding from the vaporizer tubes.

In addition to the melted Ultem causing some performance issues during testing, the screws holding the CFD domain spacer together against the shaft housing were freed once the part lost its integrity. This caused significant damage to the combustor,

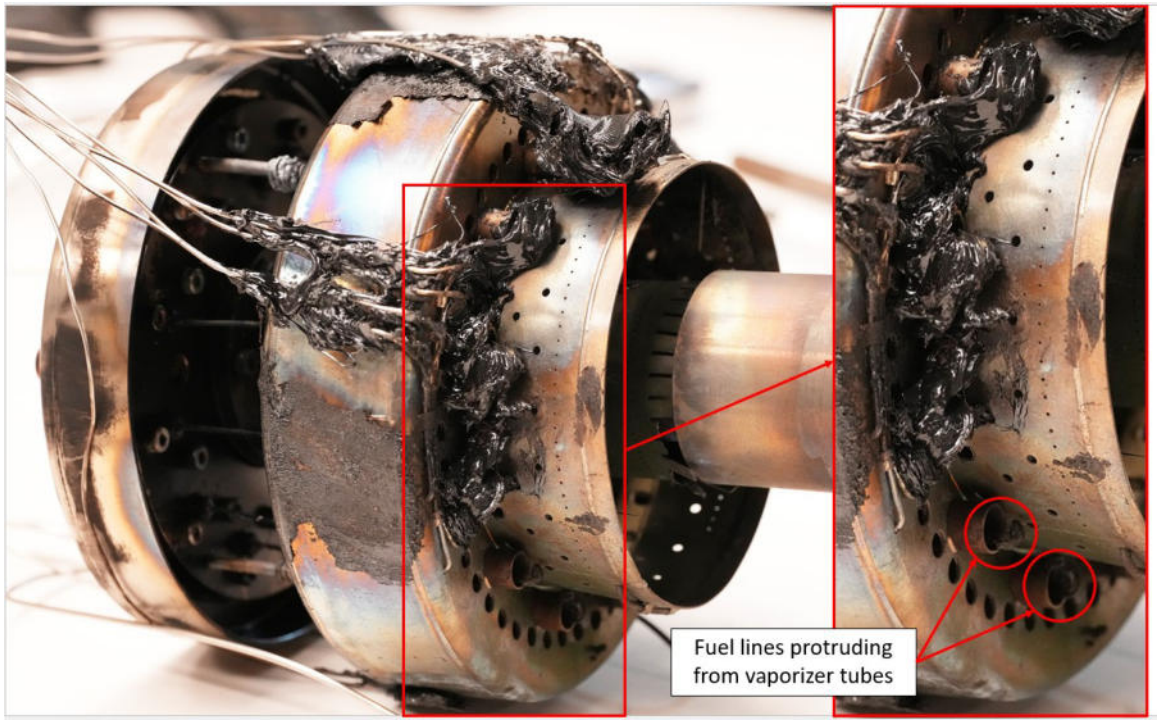

(a)

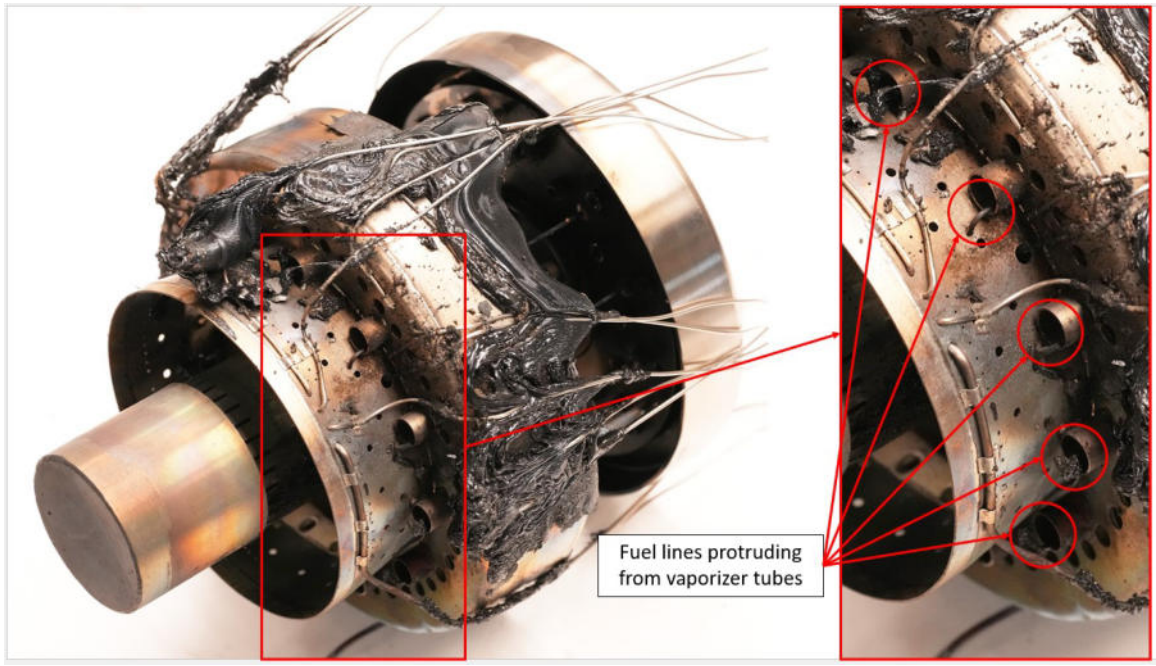

(b)

Figure 122. The outboard cavity-stabilized compact combustor after the first round of testing

as shown in Figure 123a, leading to some of the air chutes being compromised along with the end of the inner liner that mated with the shaft housing. Additionally, the lack of fuel flowing through some of the tubes prevented these tubes from being cooled from the hot combustion gases around them. This led to excessive corrosion and even failure in three of the vaporizer tubes, as shown in Figure 123b, which all had holes melted in them due to a lack of cooling. The plastic coupled with the stainless steel screws flowing through the test rig during operation also had an effect on the thermocouple rake, as shown in Figure 123c, where the Kiel head experienced significant damage.

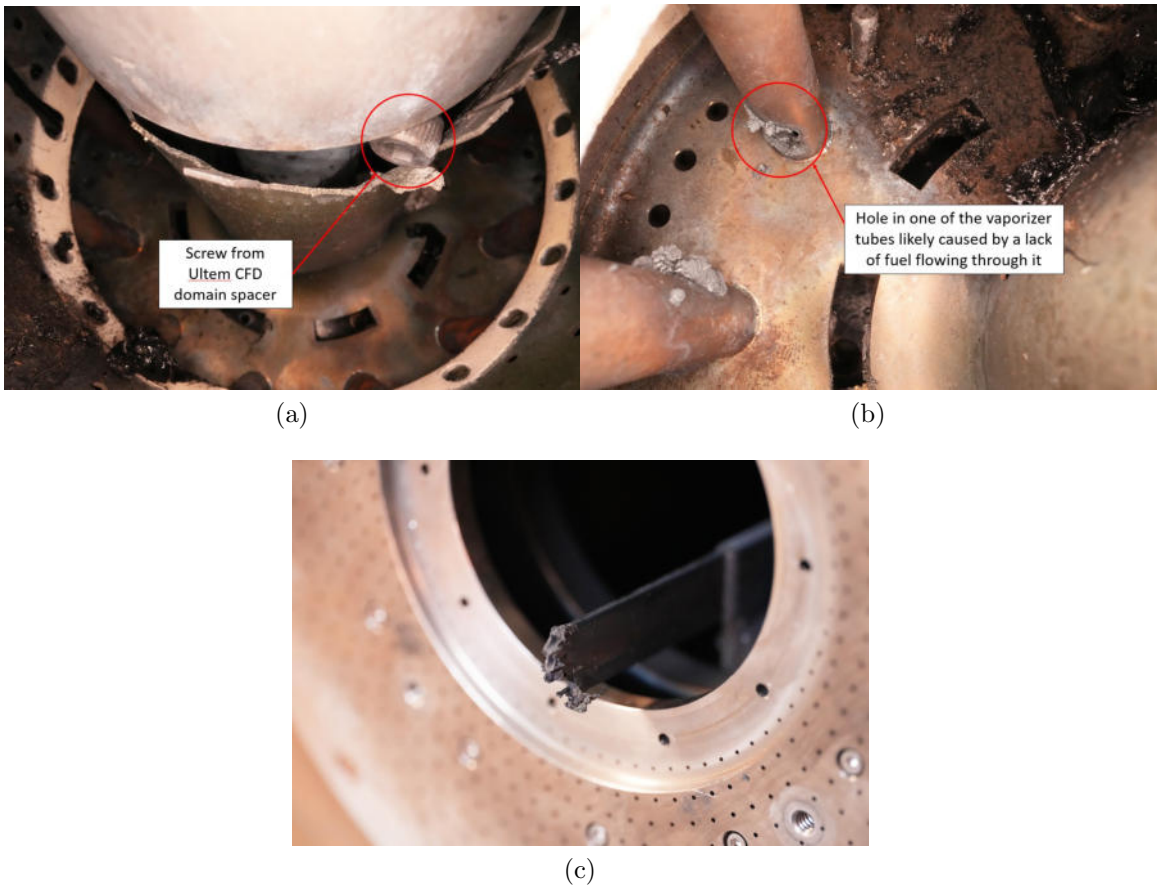

(a) (b)

(c)

Figure 123. The result of the (a) vaporizer tubes, (b) inner liner, and (c) thermocouple rake after initial testing with the current combustor

Despite the test conditions for the compact combustor being less than optimal

during testing, data was recorded throughout the entirety of the test and was analyzed. The test from point of ignition to blow out lasted roughly 20 minutes, where blow out occurred due to the equivalence ratio spiking above stiochiometric due to a facility malfunction. Figures 124-126 show T_3, P_3, and air mass flow (AMF) rate throughout the entirety of the test where ignition conditions based on T_3 were initially at and continued above design point temperatures (490 K), P_3 was at roughly 61% of design point and ramped up above the design pressure of 374 kPa before blowout occurred, and AMF was at roughly 30% of the design point and ramped up to roughly 80% of the design point before blowout occurred. Throughout the duration of this test only the air and fuel mass flow rates were adjusted. Fuel flow was increased to maintain an equivalence ratio of 0.38 during the ramp up towards the design point. P_3 increased during to the increase of back pressure within the test section as a result of sending more air mass flow through the rig.

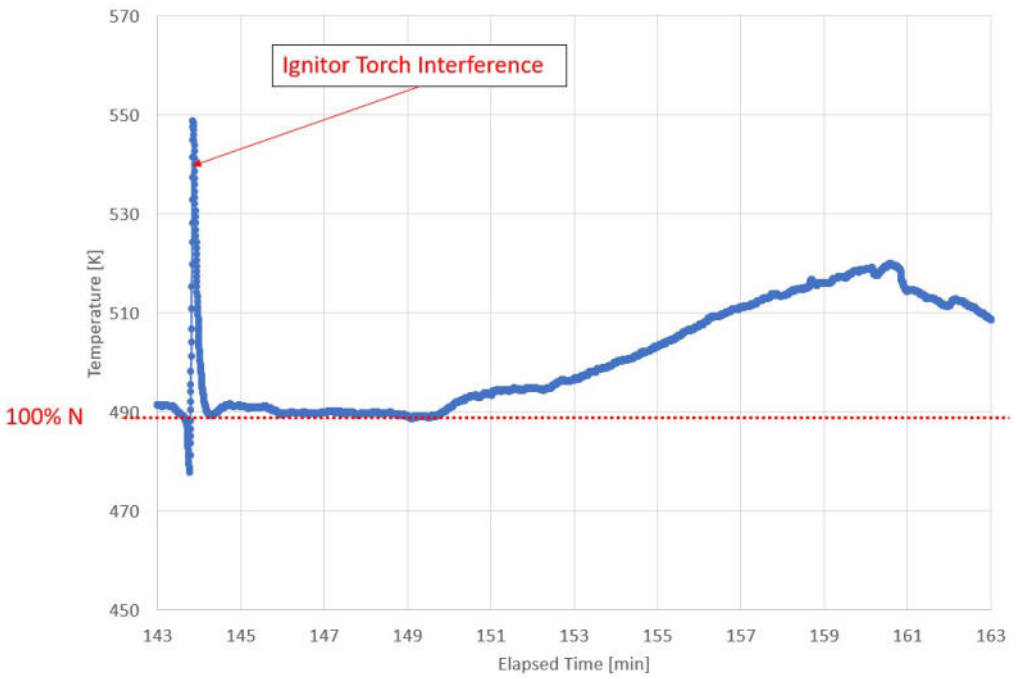

Figure 124. T_3 throughout the initial compact combustor testing (N represents equivalent engine speed)

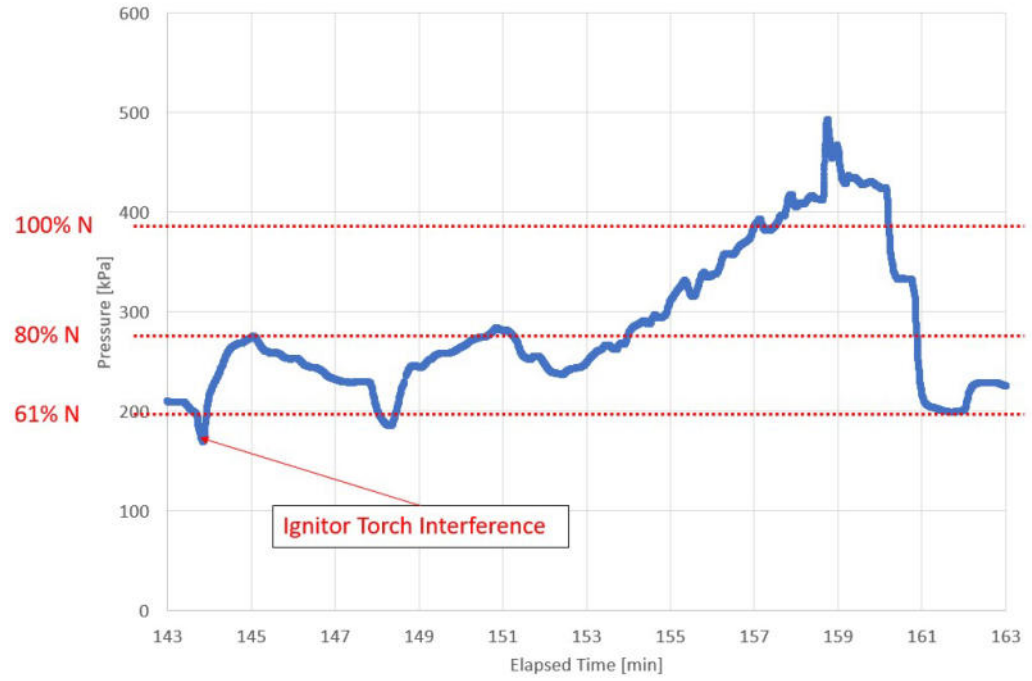

Figure 125. P_3 **throughout the initial compact combustor testing**

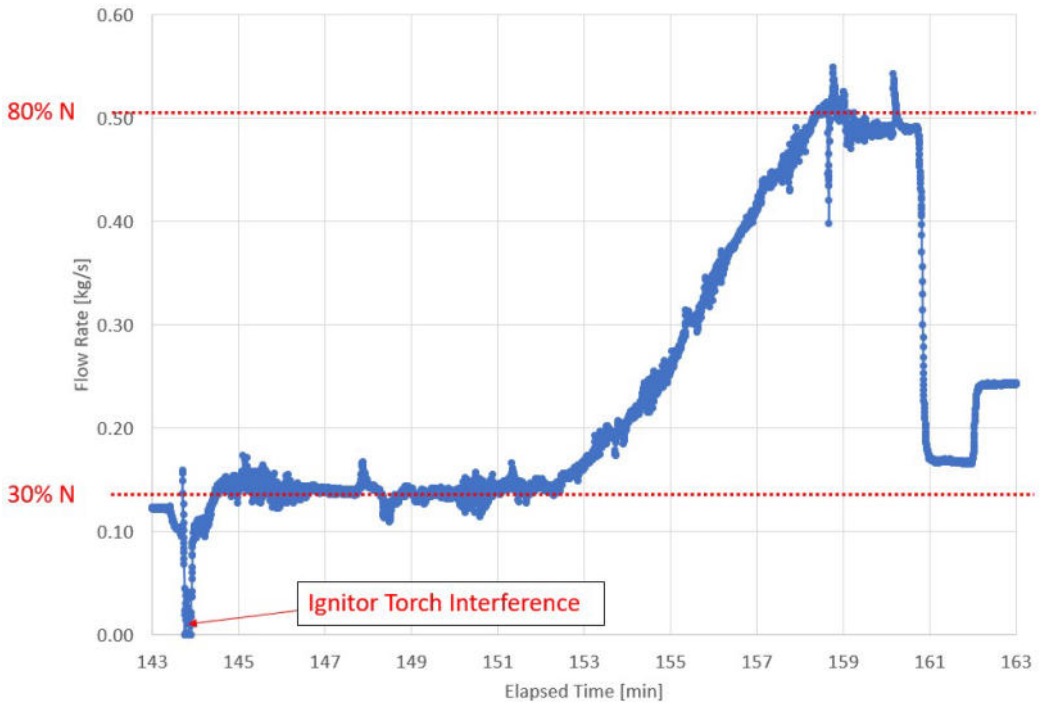

Figure 126. Air mass flow rate throughout the initial compact combustor testing

Despite an actual test point on the test matrix not being hit, temperature and pressure data surrounding the combustor was recorded throughout the entirety of the test. Figure 127 shows the orientation of the compact combustor during testing with regards to locations of instrumentation. Based on this orientation and the burning patterns shown from the back-end of the combustor from the periscope camera in Figure 121, all of this instrumentation was located in regions where burning was occurring.

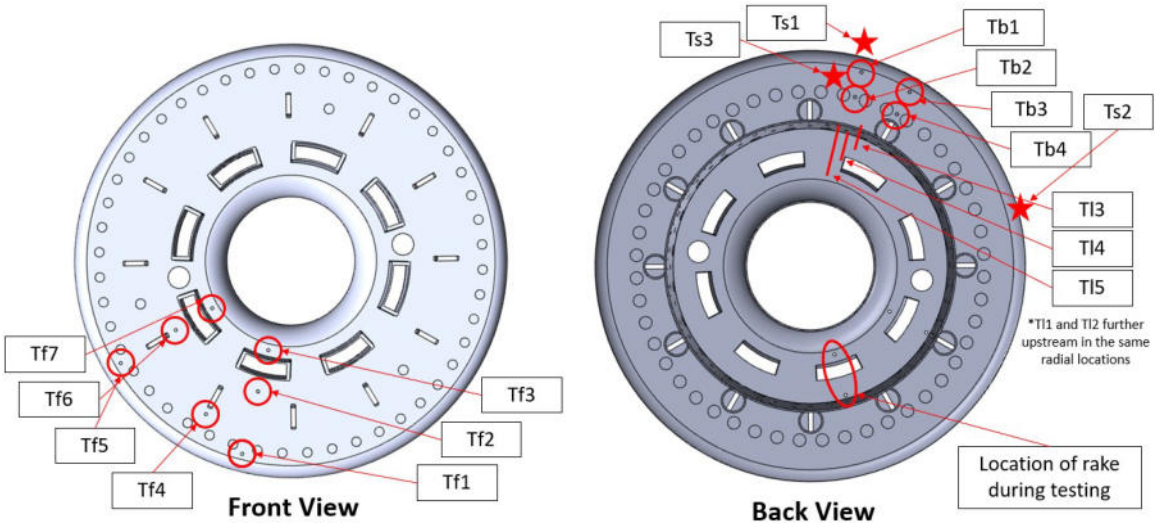

Figure 127. Orientation of the compact combustor during testing with instrumentation callouts

Figure 128 shows a plot of the total pressure drop across the combustor throughout the entirety of the testing duration, where a peak drop of roughly 14% was measured before blowout occurred. Additionally, before the ramp-up towards the design point condition, the pressure drop was measured at roughly 4% for an air flow rate and P_3 equivalent to 30% and 70% of the design point, respectively. The computational results predicted a TPL of 1.5% at the half-idle condition (15% of design point) and 6.8% at the idle condition (30% of design point), which was within the regime that was expected considering the melted Ultem managed to block portions of air driver

holes along the combustor during operation likely leading to an increase in TPL.

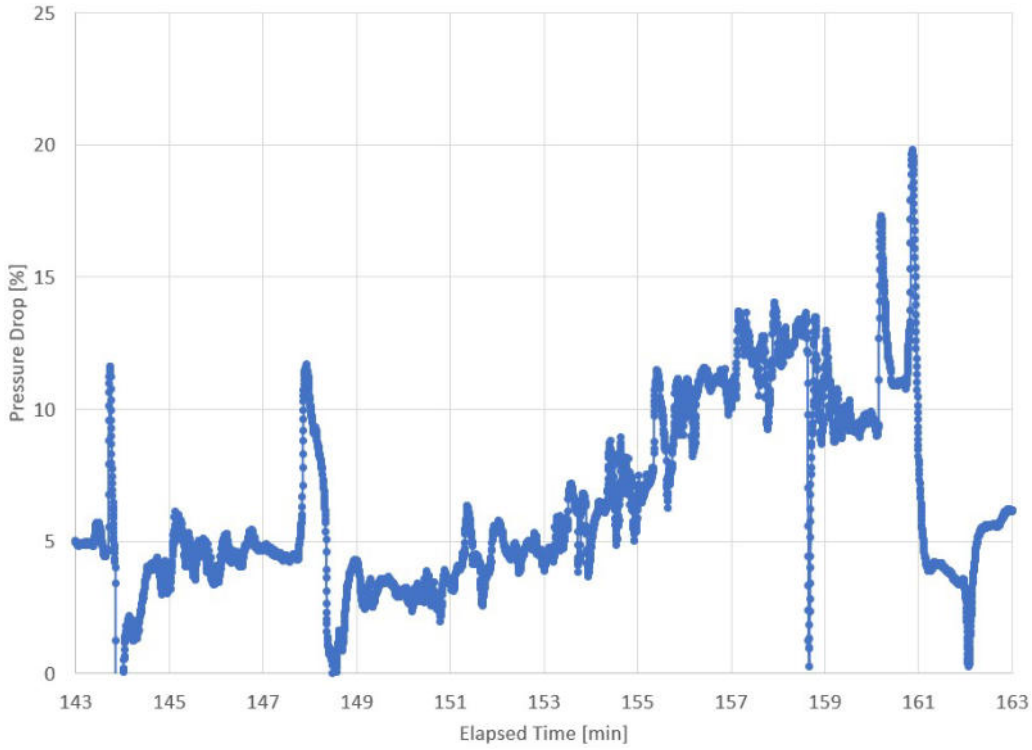

Figure 128. Total pressure drop measured throughout the initial compact combustor testing

Figures 129-131 show the temperatures measured along the forebody, aftbody, and liner surfaces, respectively. Starting with the forebody temperatures recorded throughout the test duration, Tf3, which was located below one of the air chutes shown in Figure 127, remained relatively cool while Tf7, which was located below one of the other air chutes, measured temperatures indicative of combustion occurring within the area. This was likely a result of fuel leaking from the slots along the forebody allowing access for the fuel lines for the vaporizer tubes. Fuel could leak from these slots, travel down the forebody face, and then travel into the air chute and burn in the recirculation region just below. Prior to the combustor being installed in the non-rotating test rig, all of these slots along the forebody were blocked with aluminum tape once the fuel lines were installed to prevent this from happening

since this behavior was computationally predicted. However, the CFD domain spacer melting and flowing through the combustor during operation likely freed the tape from their locations and allowed some fuel to leak in certain localized areas.

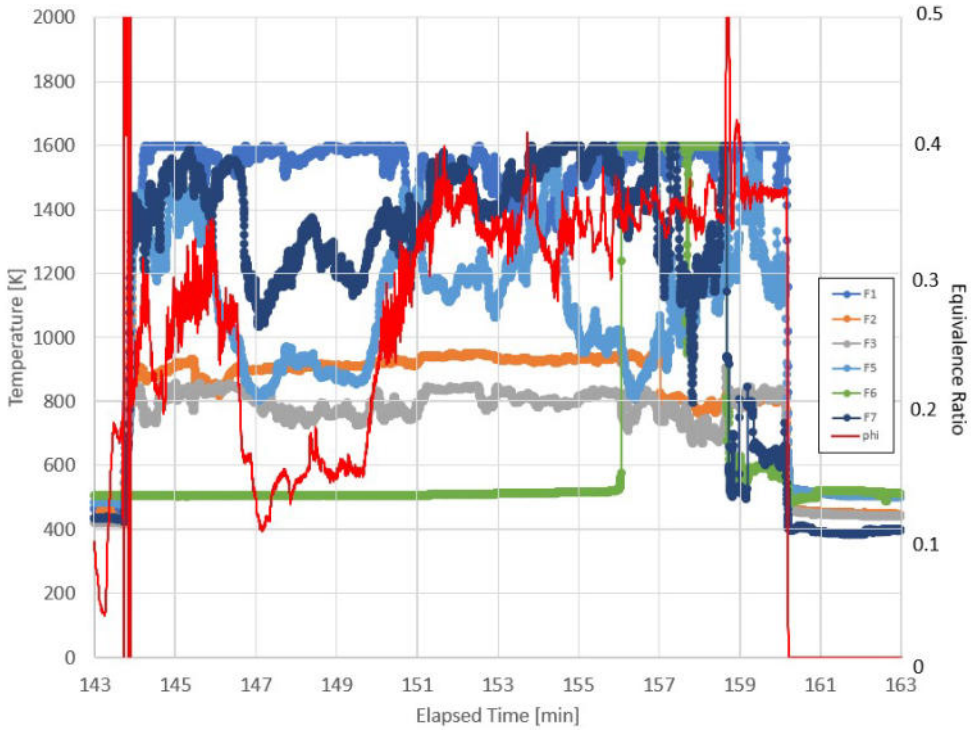

Figure 129. Forebody temperatures plotted against equivalence ratio for the duration of the initial P400 compact combustor testing

Looking at temperatures measured along the aftbody, shown in Figure 130, into the outboard cavity, Tb1 and Tb3, whose locations are shown in Figure 127, showed hotter temperatures compared to Tb2 and Tb4 as expected since computational results predicted hotter temperatures towards the ceiling of the cavity compared to slightly above the vaporizer tubes. Additionally, based on the magnitudes of these temperatures, its likely that a majority of the combustion was occurring towards the forebody than the aftbody, which was a trend seen in the computational simulations.

Finally, temperatures measured along the surface of the liner are shown in Figure 131 where thermocouples were welded along the surfaces of the cavity and aftbody

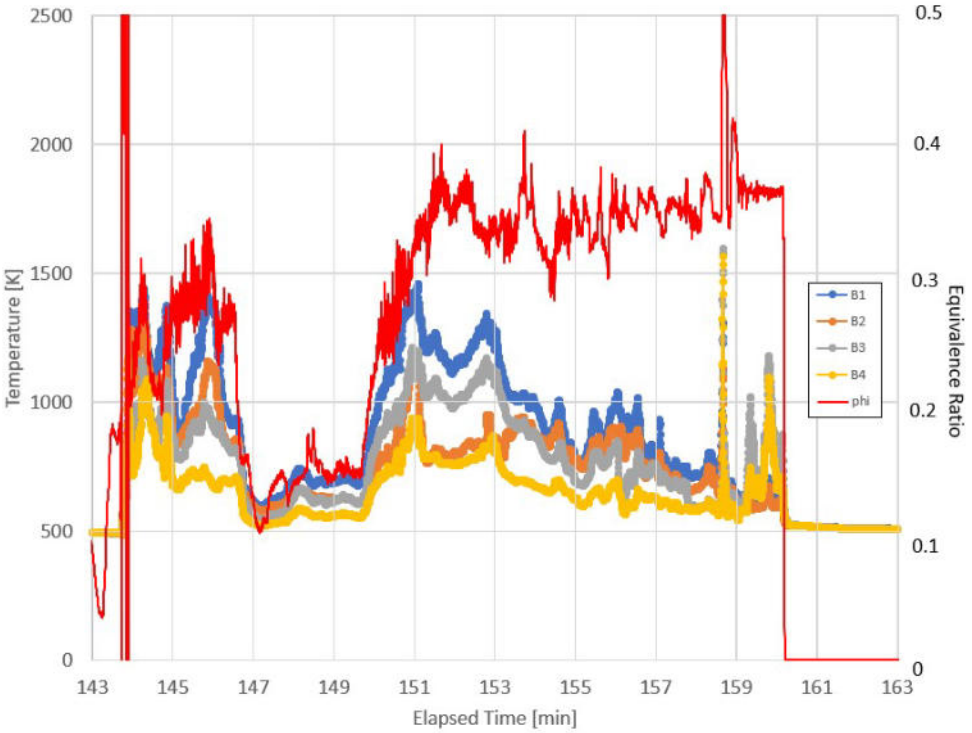

Figure 130. Aftbody temperatures plotted against equivalence ratio for the duration of the initial P400 compact combustor testing

such that they corresponded to the hottest regions observed from the computational results. These hottest regions were observed directly in between the fuel vaporizer tubes along the cavity, and directly in between the vaporizer tubes below the driver jets on the aftbody. Computational results, shown previously in Figure 106, showed Ts2 being a hotter location compared to locations Ts1 and Ts3, which was also seen experimentally. Additionally, CFD also predicted Ts1 and Ts2 having similar temperatures which was seen experimentally.

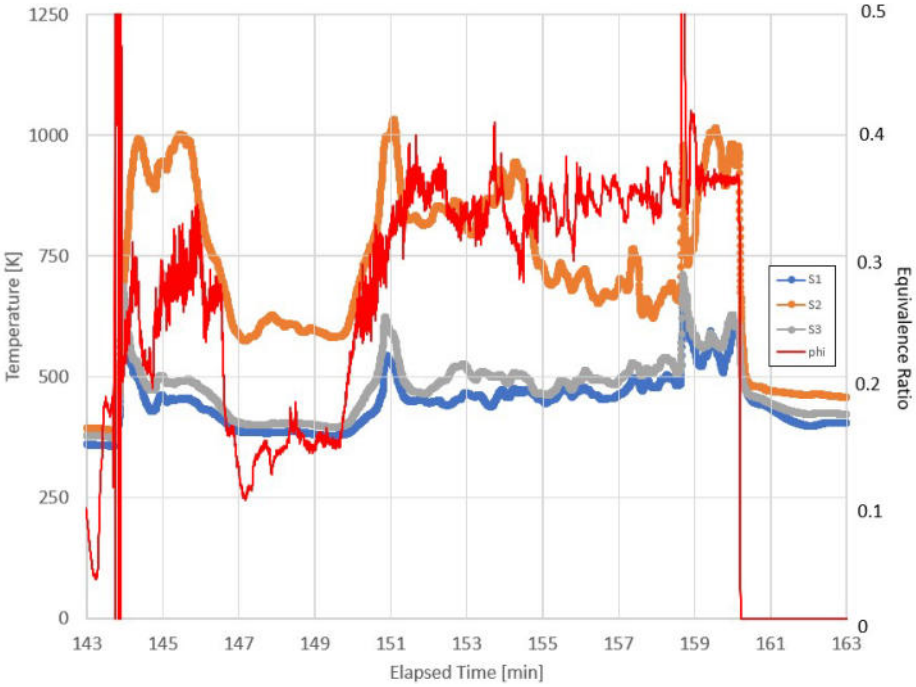

Figure 131. Surface temperatures plotted against equivalence ratio for the duration of the initial P400 compact combustor testing

4.5 Second iteration of P400 compact combustor testing

Given the outcome of previous testing with the P400 compact combustor, a new combustor was machined, coated, and welded together following the same methodology used to manufacture the previous P400 compact combustor. Prior to installing this new combustor in the P400 test rig, a couple of changes were made to improve the combustor's operability and prevent similar failures that occurred in previous testing.

Firstly, the CFD domain spacer was remade from 316 stainless steel, shown in Figure 132, rather than Ultem to prevent the outcome which occurred in previous testing. This newly manufactured spacer featured the same design as the Ultem spacer and coupled to the shaft housing to remain secured during testing.

Lastly, the ethylene-air torch location was revised since achieving ignition was difficult during prior testing. Figure 133 shows the revised ethylene-air torch design,

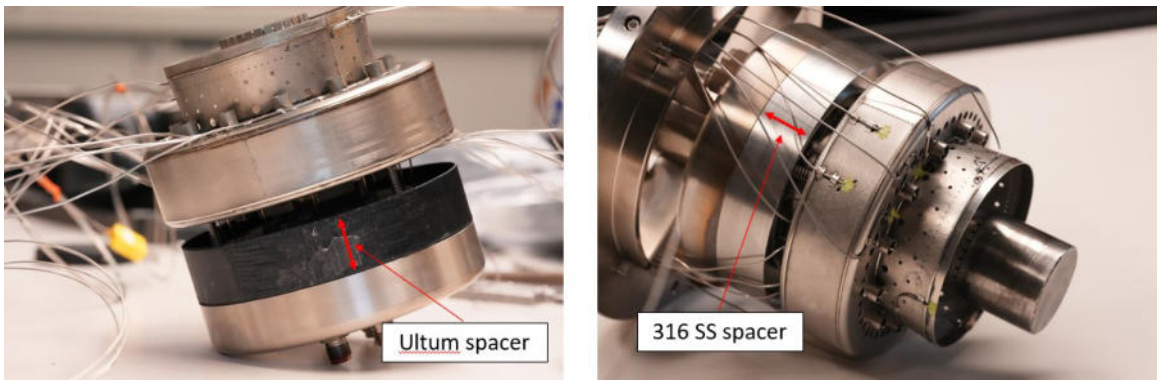

Figure 132. New CFD domain spacer manufactured from 316 stainless steel compared to the original spacer

which featured a 0.635 cm stainless steel tube welded directly at the interface between the forebody and TVC cavity. This allowed the torch to be located directly within the cavity to ignite the fuel-air mixture present, rather than originally being located radially aligned with the air chutes matching the stock P400 location. At the previous location, no fuel-air mixture was present which caused the difficulties with ignition. These previous holes on the forebody intended for the ethylene-air torch to rest were covered with Nichrome strips which were tack-welded into place.

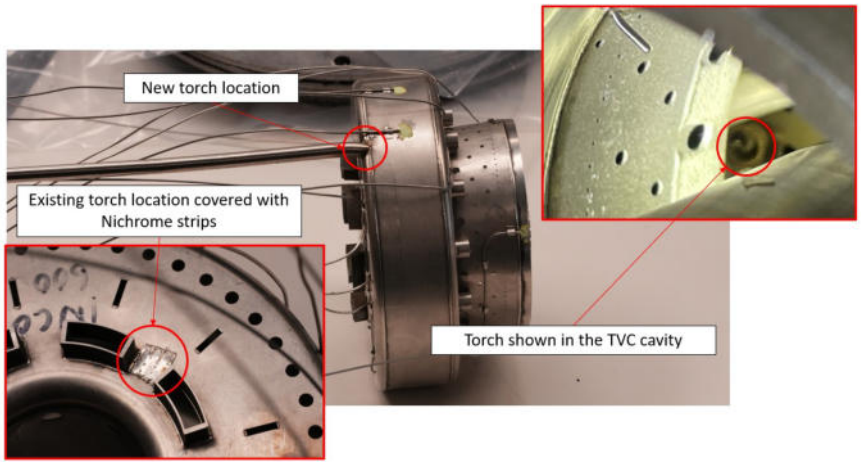

Figure 133. Revised ethylene-air torch design with the P400 compact combustor cavity

Figure 134 shows the new ethylene-air torch pass-through location compared to

the previous torch location used in the stock P400 combustor and initial compact combustor tests. Rather than originally passing through the diffuser/deswirler and fuel manifold assembly, the new torch lay between the diffuser/deswirler and engine casing and rested axially just upstream of the inlet assembly. From there, a copper tube joined to the welded stainless steel tube so that it could be bent accordingly and worked outside of the combustor spool section.

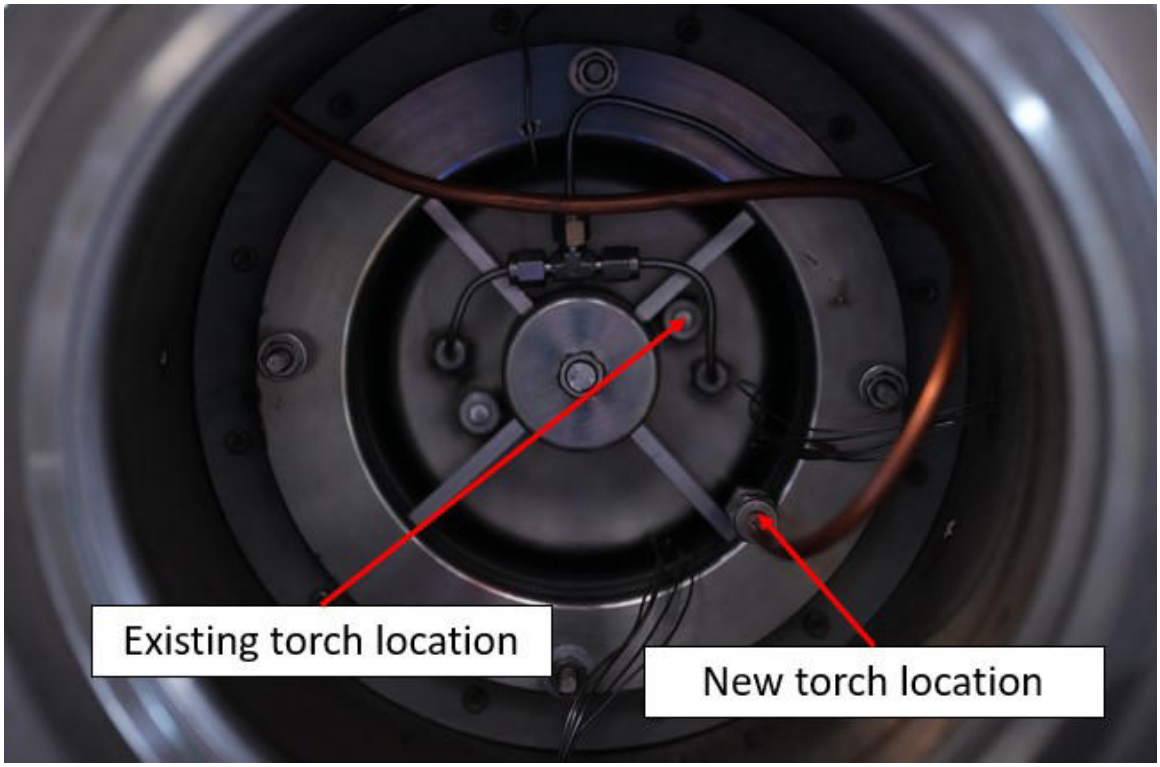

Figure 134. Revised ethylene-air torch location compared to its existing location used previously in testing

With these modifications made, the goal of this second round of testing was to determine the operability of the combustor by determining the LBO limits across an operating range. This pertained to Test Points 1-8 in Table 6 ranging from 30-100% conditions where the equivalence ratio was varied to achieve stable operation and eventually lowered to determine the LBO at each condition.

As a result of testing, it was found that the current compact combustor achieved

stable operations at Test Points 1-6 at equivalence ratios considerably higher compared to what was simulated computationally. Ignition was achieved similarly to before where the air flow rate was set at a 10% condition, the temperature was set to the design condition, the pressure was set to an 80% condition, and the equivalence ratio was set at 0.80. As the fuel and air flow rates were slowly ramped up to each test condition, the equivalence ratio was held constant at 0.75 and then fuel flow was slowly lowered once the combustor was on condition to determine the LBO limit. For the 30%, 41%, 51%, 61%, 71% and 81% conditions tested, the LBO limits were roughly 0.75, 0.738, 0.625, 0.625, 0.61, and 0.53, respectively. Extrapolating this trend out towards the design condition, an equivalence ratio LBO limit below 0.46 would be expected.

While the combustor's performance improved as the conditions ramped up towards the design condition, the global equivalence ratios at which LBO occurred were higher than expected given computational simulations predicted stable operation at a mid-power condition (equivalent to an 81% condition) at an equivalence ratio of 0.34. The cause for the LBO limits being significantly higher than expected had to do with the twelve fuel slots outlined in Figure 135. These twelve slots allow the fuel lines coupled to the fuel manifold to pass through the forebody and rest within the vaporization tubes. Since computational simulations predicted fuel leakage from these locations at a design condition, these slots were blocked prior to testing with aluminum sealing tape. However, after testing it was revealed that this tape was no longer adhered to the surface and these slots were likely exposed throughout the entire duration of testing.

These exposed slots posed several issues: 1) at the low flow rate off-design conditions, which were first tested during the LBO test sequence, there was not enough air flow passing over the forebody plate to seal off the slots and prevent fuel from leaking

out. 2) This fuel was able to travel down the forebody face and pass through the air chutes where burning would continue to occur downstream of the cavity towards the combustor exit plane.

As the air flow rate increased during testing, there was more air flow passing over the forebody face sealing the fuel slots enabling the majority of the fuel to flow through the showerhead holes in the vaporization tubes as intended. Since a majority of the fuel was being injected into the cavity as designed, the LBO limits decreased suggesting that the flame stabilization technique was sufficient at holding a flame within the cavity and its performance improved as conditions approached the design point. If testing were to continue, blocking off the fuel slots entirely would not only match the conditions used in the computational simulations but it would ensure that all of the fuel being injected would travel through the showerhead holes in the vaporization tubes, hopefully matching the operability computationally predicted.

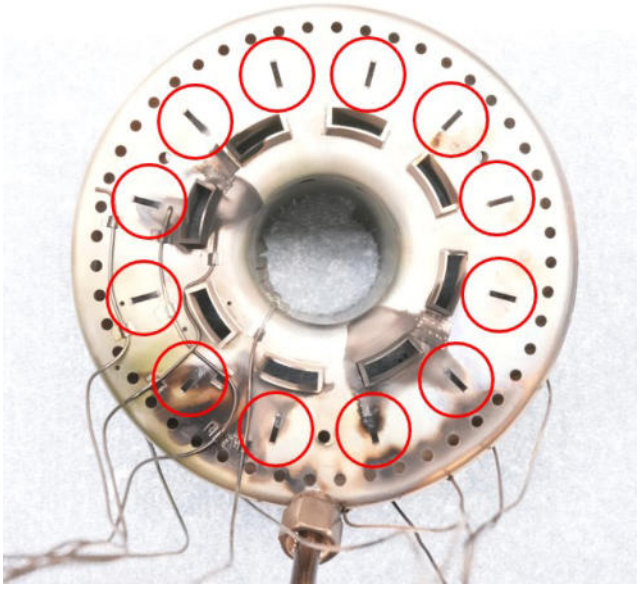

Figure 135. Location of the fuel slots along the upstream face of the forebody on the P400 compact combustor

4.6 Third iteration of P400 compact combustor testing

Based on the outcome of the second iteration of testing, the twelve fuel slots located on the forebody of the P400 compact combustor were sealed to prevent fuel leakage during future testings, as shown in Figure 136. These fuel slots were sealed by Matt Darby, a certified welder within AFRL, who laser-welded Nichrome strips over each fuel slot opening.

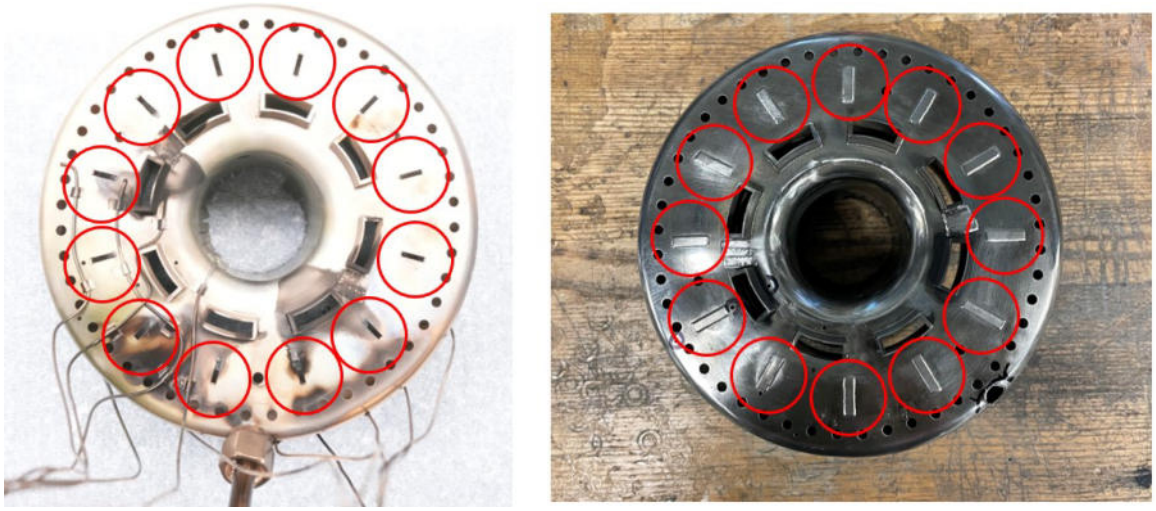

Figure 136. (Location of the fuel slots along the upstream face of the forebody on the P400 compact combustor (left) and these same fuel slots closed off with laser-welded Nichrome strips (right)

Since the fuel slot openings were sealed, the fuel lines needed to be routed differently to inject fuel within the vaporization tubes. Figure 137 outlines the previous fuel line schematic along with the new routing method. Rather than passing through the fuel slot on the forebody, the fuel line would wrap around the cavity and hook into the back-end of the vaporization tubes. The final result can be seen in Figure 138, which shows the fuel lines wrapped around the cavity and tack-welded into place with a Nichrome strip, and bent into the back-end of each vaporization tube.

As a result of wrapping the fuel lines around the entire length of the P400 compact combustor cavity, additional fuel line length was required. These twelve new fuel lines

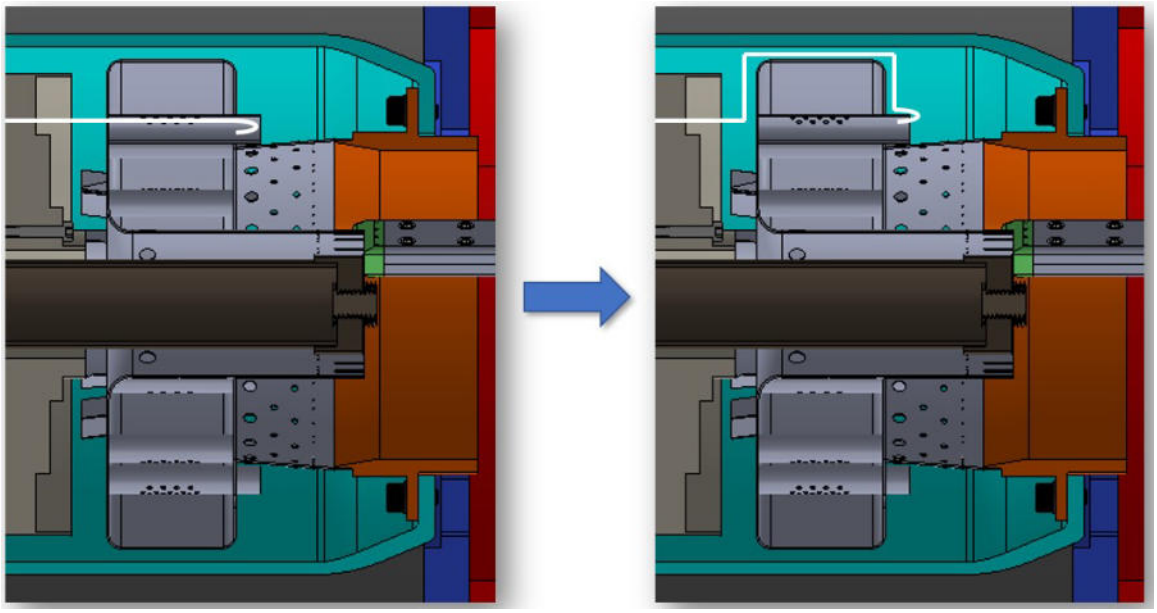

Figure 137. Previous fuel line routing (left) versus new routing layout (right)

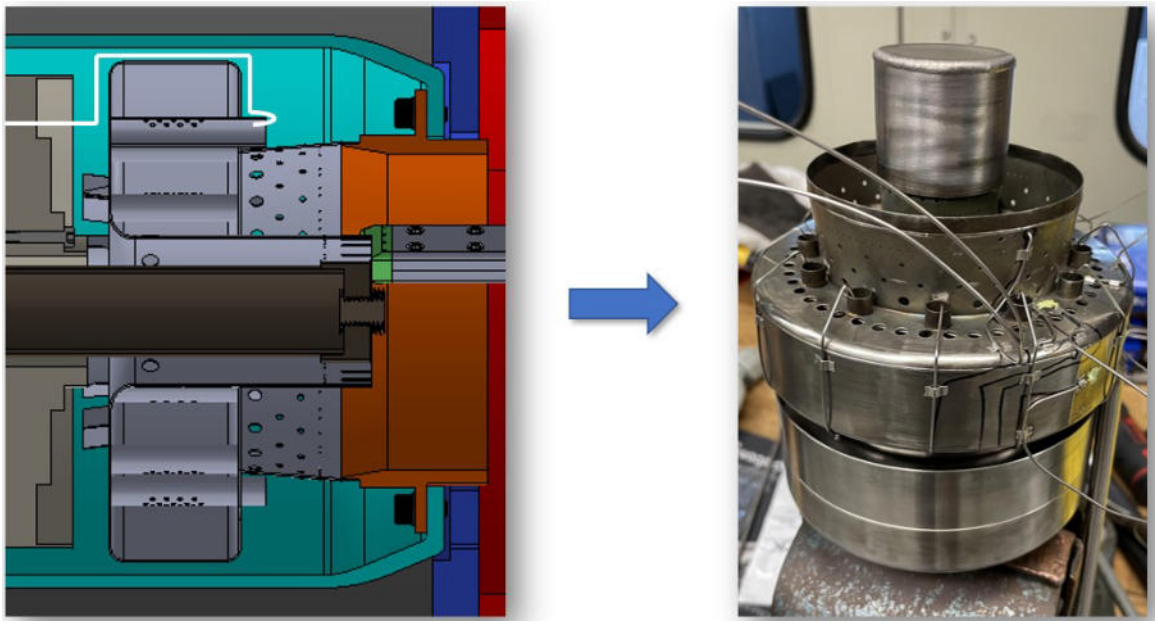

Figure 138. Fuel line routing modification idea (left) versus reality (right)

were 13.34 cm in length and were bent on-the-fly as the combustor was installed due to the large bend radii interfering with the CFD domain spacer, rather than being pre-bent in prior tests. This meant the pressure drop could not be measured across

each of the twelve new fuel lines prior to testing, however, a fuel line was bent to match the bend radii of the twelve used during this iteration of testing and flow checked where a pressure drop of 186 kPa was measured. The average pressure drop for the stock P400 fuel lines was roughly 172 kPa so the additional length and bends in the new fuel lines only contributed to an increase in pressure drop of roughly 8%.

With these modifications made, the P400 compact combustor was installed back within the P400 test rig where a repeat of the LBO study performed for the second iteration of testing was performed to observe an improvement in the combustor's operability as a result of sealing the fuel slots and re-routing the fuel lines. While operability during testing based off of the video feed from the periscope camera initially looked improved compared to previous testing, it was apparent that the combustor's operability worsened throughout the extent of testing. Figure 139 shows a plot of temperatures measured at the cavity exit, Tl1, and just upstream of the exit plane, Tl2, throughout the duration of testing. From Figure 139, it can be seen that the combustor's performance between the 2:00-2:30 and 3:30-4:00 timestamps was different. The sudden rises and dips in temperature between the 3:30-4:00 timestamp suggested a lack of burning occurring within this region of the combustor during operation. Additionally, looking at the 2:00-2:30 timestamp, there was little discrepancy between the Tl1 and Tl2 temperatures which suggested that not all of the fuel being injected was vaporized, therefore causing burning to occur further downstream of the cavity and within the dilution section of the combustor.

Figure 140 shows a plot of the cavity temperatures plotted throughout the duration of testing. Figure 140 shows that Tf3 exhibited the highest temperatures throughout testing, rather than Tf1 and Tf2 which rest within and below the cavity, respectively. For Tf3 to exhibit the highest temperatures throughout the duration of testing suggested that burning was occurring below the air chutes, which was only

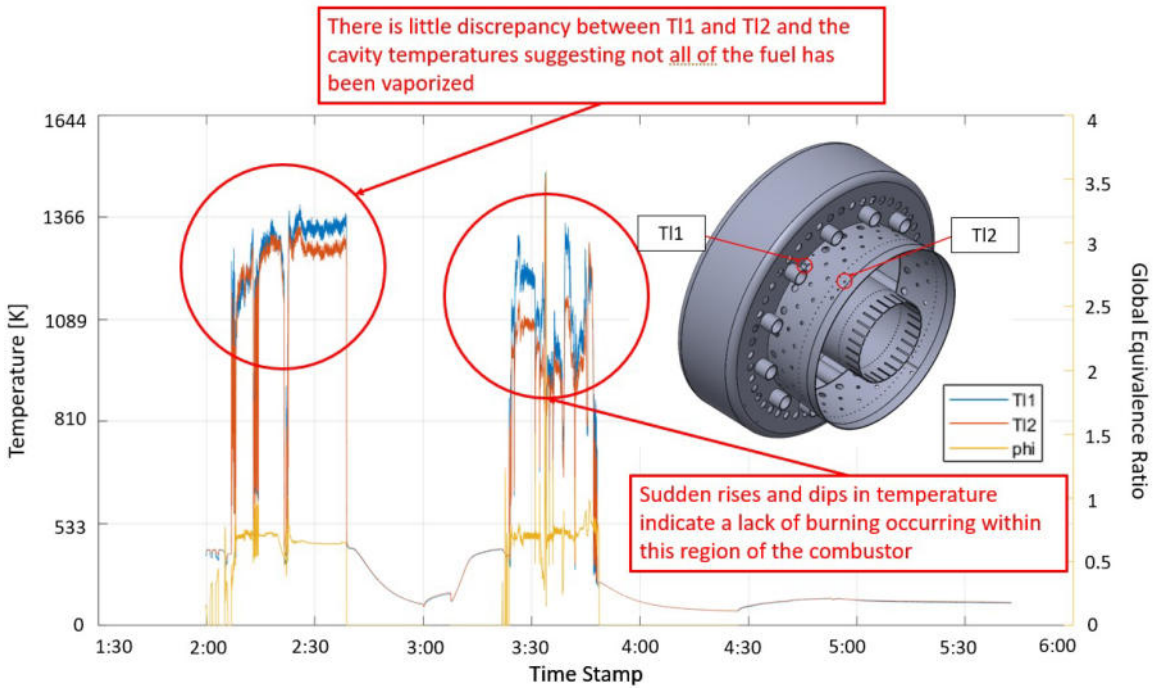

Figure 139. Liner temperatures and global equivalence ratio plotted throughout the third test iteration

possible if fuel was leaking from some location and passing through the air chutes. Since the fuel slots were blocked, this fuel leakage had to be coming from somewhere upstream of the combustor. Figure 141 shows, after disassembly, the fuel manifold gasket after the third iteration of testing, which showed several potential sources of leaks due to the integrity of the gasket being compromised during testing. Fuel leaking from these areas would explain why combustion was occurring below the air chutes as well as why combustion was continuing to occur further downstream from the cavity. This fuel leak caused a fuel distribution issue, allowing more fuel to be injected in one half of the combustor and not enough in the other half. This explained why a portion of the combustor was not burning during operation (the 3:30-4:00 timestamp) as well as a fuel vaporization issue causing burning to continue within the dilution zone and further downstream.

The potential cause for the loss of integrity of the fuel manifold gasket could be

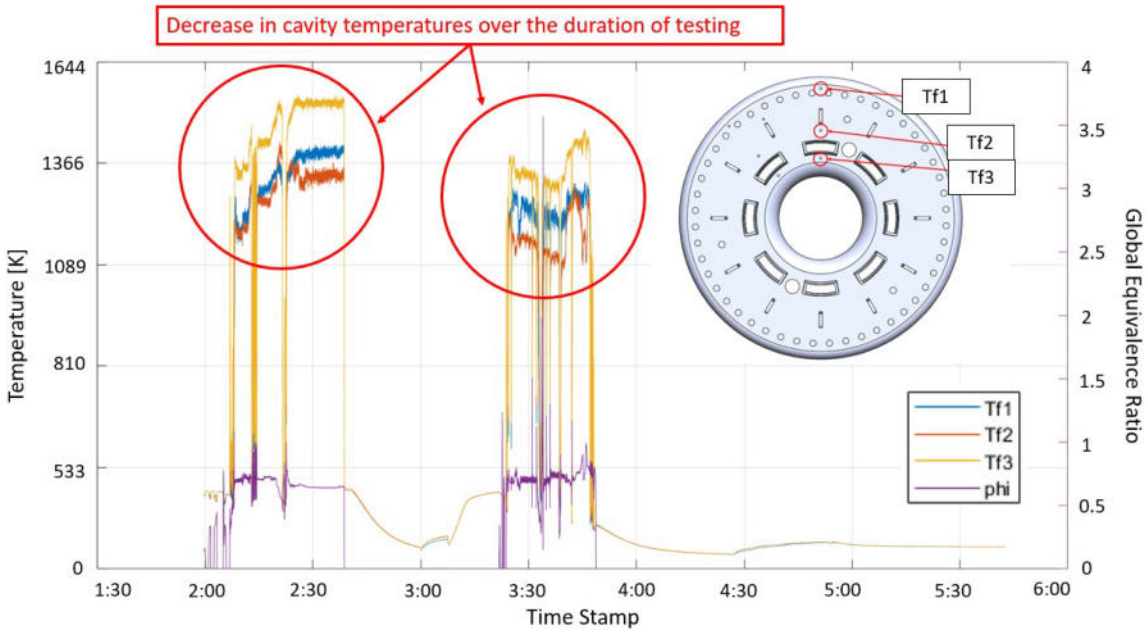

Figure 140. Cavity temperatures and global equivalence ratio plotted throughout the third test iteration

Figure 141. Fuel manifold gasket after the third iteration of testing

attributed to the increase in the fuel manifold pressure during testing. Just after ignition, the gauge pressure within the fuel manifold was set at 345 kPa, which was roughly 5-6 times the gauge pressure previously used in the stock P400 combustor testing at the same ignition conditions. This gauge pressure was set within the fuel manifold since the previous LBO testing showed the outboard cavity compact combustor preferred global equivalence ratios around 0.70, so this equivalence ratio was chosen for ignition at the start of testing. To flow the additional fuel required to reach this global equivalence ratio, more power must be demanded from the fuel pump which, in turn, increases the pressure within the manifold. As a result of this increased pressure within the fuel manifold, the integrity of the gasket was lost during testing, which lead to fuel distribution issues throughout the remaining duration.

V. Conclusion

The present research featured two primary goals: 1) modify the UCC of Holobeny et al. [2], which was designed to operate in a JetCat P90 engine on gaseous propane, to be integrated into a JetCat P160 engine using liquid kerosene as a fuel source and 2) design and test a compact combustor at the larger P400-scale to make use of the larger volume present to improve residence time requirements. These goals were supported by five objectives which involved modifying and integrating the compact combustor of Holobeny et al. [2] into the P160 engine, testing the previous compact combustor integrated into the P160 engine using liquid kerosene fuel, designing a compact combustor for the larger P400-scale gas turbine engine, and testing the P400-scale compact combustor in a non-rotating configuration to determine its viability in an engine configuration.

5.1 P160 Compact Combustor Integration

The JetCat P160 small-scale gas turbine engine was selected as the vessel to house the compact combustor of Holobeny et al. [2] due to its dimensional similarity with the JetCat P90 engine, which was used in previous studies [1][2][3][4]. As a result, the compact combustor of Holobeny et al. [2] was integrated into the JetCat P160 engine with only minor modifications. These minor modifications included removing the previous propane fuel delivery system so the combustor operated on liquid kerosene fuel, manufacturing a new combustor back plate that mated to the engine's NGV housing, machining a hole on the forward dome of the combustor to allow access for the P160 engine's glow plug for ignition, and incorporating spacers for the glow plug so that it extended further from the diffuser/deswirler as a result of the 33% axial length reduction from the compact combustor.

Starting with the fuel delivery system, the external propane fuel delivery hardware was removed. Additionally, new fuel vaporizer tubes were manufactured since the existing ones had a hole within them for propane fuel injection. These new tubes resembled the same dimensions as the design of Holobeny et al. [2] without the addition of the propane fuel delivery hole.

Coupled to the vaporizer tubes was the combustor backplate, which mated to the NGV housing. Due to the P160 engine having a larger turbine compared to the P90 engine, a new backplate was manufactured that possessed a slightly larger ID and OD to compensate for the larger turbine.

Finally, to ensure ignition occurred within the newly integrated compact combustor, a hole was drilled on the forward dome to allow the stock ignitor torch in the P160 engine to rest inside this location. Additionally, the glow plug's axial location was shifted upstream through the use of spacers to account for the 33% axial length reduction caused by the compact combustor.

5.2 P160 Compact Combustor Testing

The JetCat P160 engine equipped with the modified bluff-body compact combustor of Holobeny et al. [2] was tested within AFRL's Small Engine Research Lab Test Stand 5. Initial testing showed that the engine struggled to accelerate up to and stabilize at an idle condition. During this start-up sequence, a large flame was present downstream of the exhaust nozzle where burning was preferentially occurring near the glow plug location within the combustor. To promote a flame to propagate around the entire circumference of the combustor, a traversing blockage plate was designed so that during the start-up sequence of the engine, air inlet holes along the forward dome of the combustor were closed. This enabled a flame to quickly distribute around the primary zone, and once this occurred the blockage plate would

rotate allowing air to pass through the inlet holes making use of the bluff-body flame stabilization scheme to meet the residence time requirements for the shortened combustor. While the traversing blockage assembly worked in allowing a flame to quickly distribute around the entirety of the combustor during the start-up sequence, a large flame was still present downstream of the exhaust nozzle throughout the entire test operation suggesting burning was still occurring past the combustor exit plane and the bluff-body flame holding mechanism was not working as intended.

To help explain what occurred experimentally during the P160 compact combustor operation, computational simulations were performed in ANSYS Fluent for half-idle, idle, and design conditions. As a result, the simulations for the half-idle case revealed that there were no recirculation regions present directly behind the impingement plate within the combustor as previously shown in the computational results performed by Holobeny et al. [2] for the P90 compact combustor. The lack of a recirculation region present directly behind the impingment plate meant there was no constant exchange of products and reactants to enable complete combustion at a reduced axial length. Instead, combustion was occurring near the combustor exit plane, which was observed experimentally. For the idle case, due to the lack of flameholders present, simulations predicted no burning occurring, which was also observed experimentally. The lack of flameholders meant that as the mass flow rate increased through the engine, the reactions present within the combustor were blown out and exhausted.

5.3 P400 Compact Combustor Design

As a result of the P160 compact combustor testing, rather than scaling up the bluff-body flame stabilization scheme to the P400-scale, an entirely different flame stabilization method was used; trapped vortex combustion. Due to the increase in fluidic volume present within the burner section of a stock P400 engine and the slightly

longer axial length, a trapped vortex compact combustor could be designed that meets residence time requirements where the recessed cavity promotes an environment for stable combustion across the operation regime of the engine.

A previous novel combustor design was chosen from Briones et al. [31] which featured an outboard cavity design that matched the length of the stock P400 burner and was optimized based on figures of merit including combustion efficiency, total pressure loss, maximum and average combustor exit temperatures, pattern factor, and critical liner area factor. With the goal of designing a compact combustor at the P400-scale, the DP43 outboard cavity-stabilized combustor design of Briones et al. [31] was used with the goal of achieving a manufacturable design that could easily be integrated into a stock P400 engine at a reduced axial length.

To reach a design that could be integrated into a stock P400 engine and run using the stock surrounding hardware, several changes were made to the original DP43 design of Briones et al. [31]. Their computational design featured a liquid spray atomizer located within the outboard cavity which was not a feasible injection scheme since the current effort wanted to use the stock P400 fueling system. Instead, vaporizer tubes, similar to the ones used in the stock P400 burner, were designed and implemented which featured a showerhead injection scheme that evenly distributed fuel into the outboard cavity. Additionally, the goal of this effort was to arrive at a shortened combustor at the P400-scale which closely resembled the performance of the stock burner. Given this, the axial length of the combustor was reduced by 20% and the dilution area was increased by a factor of three to quench reactions prior to the combustor exit plane. As a result of this, a compact combustor was designed at the P400-scale which featured vaporization tubes that could be coupled to the stock P400 fueling system and was 20% shorter in axial length compared to the stock burner.

5.4 P400 Compact Combustor Testing

A non-rotating test rig was designed and built in AFRL's Test Cell 151 which featured a traversing thermocouple assembly to take circumferential temperature measurements at four radial locations at the combustor exit plane. Prior to testing the P400 compact combustor, testing was performed on the stock P400 combustor where circumferential temperatures were measured at conditions ranging from idle to design speeds. As a result, a maximum and average combustor exit temperature of 1434 K and 1145 K, respectively, and a pattern factor of 0.45 was recorded at the design condition. Additionally, circumferential temperature profiles were gathered at the combustor exit plane which showed the maximum plane average combustor exit temperature was seen at a annulus height of roughly 68%. This meant combustion products were skewed towards the OD of the exit plane.

With the stock P400 combustor testing completed, the P400 compact combustor was installed into the new test rig. The compact combustor struggled to ignite at the same 51% setpoint that the stock P400 burner ignited at. Instead, the inlet temperatures and pressures were increased to near design condtions where the air flow rate was reduced to an equivalent idle speed. This allowed the fuel to quickly vaporize and allow heat from the ethylene-air torch to radiate into the outboard cavity to achieve ignition. Once ignition occurred, however, as a result of igniting the combustor at near design temperatures and pressures, the CFD domain spacer, which was 3-D printed from Ultem, had lost its integrity, sending plastic through the combustor during testing. This blocked crucial air driver holes, fuel lines, and vaporizer tubes critical to the operation of the combustor. Despite this, burning occurred in a majority of the combustor where the air and fuel flow rates were able to be accelerated to an 80% condition before blow out occurred due to external error (not pertaining to the combustor). This was a significant improvement over previous

studies and showed promise for the combustor's design.

An additional compact combustor was manufactured along with a new CFD domain spacer from 316 stainless steel rather than Ultum. A LBO study was investigated on the newly manufactured compact combustor at conditions ranging from 30-81% of the design point. As a result from this testing, LBO limits of 0.75, 0.738, 0.625, 0.625, 0.61, and 0.53 were recorded for conditions pertaining to 30%, 41%, 51%, 61%, 71%, and 81% conditions, respectively. While the LBO limits were higher than expected due to fuel leakage occurring at the upstream end of the vaporization tubes, the decreasing trend of the LBO limits as conditions approached the design point suggested that the TVC cavity was performing as intended and if the fuel slots would have been blocked, matching the computational domain, all of the fuel would have traveled through the showerhead holes in the vaporization tubes and the combustor would likely have performed as intended based on the computational predictions.

Overall, the objectives outlined throughout the scope of this project were met. 1.) The compact combustor of Holobeny et al. [2] was modified and integrated into a JetCat P160 engine to be operated on liquid kerosene fuel. 2.) The compact combustor of Holobeny et al. was modified and tested in a JetCat P160 engine using a liquid kerosene fuel source where a brief sustained operation was achieved at an idle condition of 33,200 RPM. There was a caveat in that this condition was achieved while not using the novel bluff-body flame holding mechanism crucial to the compact combustor's design. 3.) As a result of the testing which occurred at the P160 scale, rather than scale the bluff-body compact combustor up to the P400-scale to make use of the larger volume present, an outboard cavity-stabilized compact combustor was designed at the P400 scale where the cavity design was previously optimized by Briones et al. [31]. 4.) CFD was used to analyze the P400 compact combustor at half-idle, idle, mid-power, and design conditions where the combustor showed stable

burning occurring withing the outboard cavity across the combustor's operating range at a reduced axial length of 20%. Finally, 5.) the P400 compact combustor was manufactured out of Inconel-600 sheet metal and tested within a newly designed test rig within AFRL's Test Cell 151 in a non-rotating configuration. A LBO operability study was performed showing the combustor operated at global equivalence ratios higher than computationally simulated due to the combustor's inability to vaporize all of the fuel within the vaporization tubes prior to being injected into the cavity.

5.5 Recommendations

While the objectives outlined throughout the scope of this project were met, there were some recommendations if this research effort were to continue.

1. Welding the fuel manifold to the diffuser/deswirler would ensure a perfect seal between both components and prevent any potential leak paths during operation, regardless of an increase in the fuel manifold pressure. This would be the best path moving forward if testing were to continue on the P400 compact combustor.

2. If future CFD simulations were to be ran simulating liquid kerosene injection within a combustor, it is important that rather than simulating a droplet injection scheme, which was used for this present effort, that the entire fuel line within the vaporization tube be simulated. Fuel leaves the fuel lines within the vaporization tubes as a laminar jet which needs sufficient time to mix with the air and breakdown into drops and eventually atomize. The CFD simulations which were ran, on the other hand, modeled the injection scheme in which the liquid kerosene fuel being injected was already broken down into droplets, allowing them to mix with the air and atomize much more quickly.

Bibliography

1. Bohan, B. T. and Polanka, M. D., "Experimental Analysis of an Ultra-Compact Combustor Powered Turbine Engine," *Journal of Engineering for Gas Turbines and Power*, Vol. 142, May 2020, pp. 051014–1–10, https://doi.org/10.1115/1.4046759.

2. Holobeny, D., Bohan, B. T., and Polanka, M. D., "Computational and Experimental Analysis of a Compact Combustor Integrated into a JetCat P90 RXi," *Journal of Engineering for Gas Turbines and Power*, Vol. 143, September, 2021, pp. 091023:1–8, https://doi.org/10.1115/1.4051348.

3. Holobeny, D., *Design and Analysis of a Compact Combustor for Integration with a JetCat P90 RXi*, Master's thesis, Air Force Institute of Technology, March 2020.

4. Bohan, B. T., *Combustion Dynamics and Heat Transfer in an Ultra Compact Combustor*, Ph.D. thesis, Air Force Institute of Technology, 2018.

5. Mattingly, J. D., Heisser, W. H., Boyer, K. M., Haven, B. A., and Pratt, D. T., *Aircraft Engine Design*, AIAA, third edition ed., 2018.

6. Hsu, K. Y., Goss, L. P., and Roquemore, W. M., "Characteristics of a Trapped-Vortex Combustor," *Journal of Propulsion and Power*, Vol. 14, 1998, pp. 57–65, https://doi.org/10.2514/2.5266.

7. Zelina, J., Ehret, J., Hancock, R. D., Shouse, D. T., Roquemore, W. M., and Sturgess, G. J., "Ultra-Compact Combustion Technology Using High Swirl for Enhanced Burning Rate," *38th AIAA/ASME/SAE/ASEE Joint Propulsion Conference and Exhibit*, July 2002, https:/doi.org/10.2514/6.2002-3725.

8. Briones, A. M., Sekar, B., and Erdmann, T., "Effect of Centrifugal Force on Turbulent Premixed Flames," *Journal of Engineering for Gas Turbines and Power*, Vol. 137, No. 1, 2015, pp. 1–10, https://doi.org/10.1115/1.4028057.

9. Damele, C. J., Polanka, M. D., Wilson, J. D., and Rutledge, J. L., "Characterizing Thermal Exit Conditions for an Ultra Compact Combustor," *American Institute of Aeronautics and Astronautics*, 2014, https://doi.org/10.2514/6.2014-0456.

10. Cottle, A. E., Gilbert, N. A., and Polanka, M. D., "Mechanisms for Advanced Flow Migration from an Annular, High-g Ultra Compact Combustor," *American Institute of Aeronautics and Astronautics*, 2016, https://doi.org/10.2514/6.2016-1392.

11. DeMarco, K. J., Bohan, B. T., Rodriguez, E. A. H., Polanka, M. D., and Goss, L. P., "Design Strategy for Fuel Introduction to a Circumferential Combustion Cavity," *American Institute of Aeronautics and Astronautics*, 2018, https://doi.org/10.2514/6.2018-1876.

12. DeMarco, K. J., Bohan, B. T., Polanka, M. D., and Goss, L. P., "Performance Characterization of a Circumferential Combustion Cavity," *American Institute of Aeronautics and Astronautics*, 2018, https://doi.org/10.2514/6.2018-4922.

13. Bohan, B. T. and Polanka, M. D., "Analysis of Flow Migration in an Ultra-Compact Combustor," *Journal of Engineering for Gas Turbines and Power*, Vol. 135, No. 5, 2013, https://doi.org/10.1115/1.4007866.

14. Hsu, K. Y., Goss, L. P., and Roquemore, W. M., "Characteristics of a Trapped-Vortex Combustor," *Journal of Propulsion and Power*, Vol. 14, 1998, pp. 57–65, https://doi.org/10.2514/2.5266.

15. Mair, W. A., "The Effect of a Rear-Mounted Disc on the Drag of a Blunt-Based Body of Revolution," *The Aeronautical Quarterly*, 1965.

16. Little, B. H. and Whipkey, R. R., "Locked Vortex Afterbodies," *Journal of Aircraft*, Vol. 16, No. 5, 1979, pp. 289–295, https://doi.org/10.2514/3.58522.

17. Colcord, B. Sirignano, W. A. and Liu, F., "Turbine-Burner Model: Cavity Flameholding in a Converging, Turning Channel Flow," *Proceedings of the Joint Propulsion Conference, Atlanta, Georgia*, 2012, AIAA-2012-3778.

18. Roquemore, W. M., Shouse, D. T., Burrus, D., Johnson, A., Cooper, C., Duncan, B., Hsu, K. Y., Katta, V. R., Sturgess, G. J., and Wihinen, I., "Trapped Vortex Combustor Concept for Gas Turbine Engines," *Proceedings of the 38th AIAA Aerospace Sciences Meeting, Reno, NV*, 2001, 10.1115/96TA019.

19. Turns, S. R., *An Introduction to Combustion: Concepts and Applications*, McGraw-Hill, New York, third edition ed., 2012.

20. Fugger, C. A., Yi, T., Sykes, J. P., Caswell, A. W., Rankin, B. A., Miller, J. D., and Gord, J. R., "The Structure and Dynamics of a Bluff-Body Stabilized Premixed Reacting Flow," *AIAA Aerospace Sciences Meeting, 2018*, 2018, https://doi.org/10.2514/6.2018-1190.

21. Monfort, J. R., Huelskamp, B. C., Caswell, A. W., and Belovich, V., "Experimental Characterization of Decay Rates in Bluff-Body Stabilized Flames Using Sodium Injection," *53rd AIAA Aerospace Sciences Meeting*, 2015, https://doi.org/10.2514/6.2015-1022.

22. Allison, P. M., Sidey, J. A., and Mastorakos, E., "Lean Blowoff Scaling of Swirling, Bluff-Body Stabilized Spray Flames," *AIAA Aerospace Sciences Meeting, 2018*, 2018, https://doi.org/10.2514/6.2018-1421.

23. Mattingly, J. D. and Boyer, K. M., *Elements of Propulsion: Gas Turbines and Rockets*, American Institute of Aeronautics and Astronautics (AIAA), VA, 2nd ed., 2016.

24. Fuchs, F., Meidinger, V., Neuburger, N., Reiter, T., and Zündel, M., "Challenges in Designing Very Small Jet Engines - Fuel Distribution and Atomization," *16th Internation Symposium on Transport Phenomena and Dynamics of Rotating Machinery, Honolulu, United States*, Apr 2016, ffhal-01891309.

25. DePaola, R., *Microturbine Turbojets: Experimental Evaluation of Commercially Available Engines*, Master's thesis, Air Force Institute of Technology, March 2020.

26. Cican, G., Toma, A., and Puşcaşu, C., "Jet CAT P80 Thermal Analyses and Performance Assessment Using Different Fuels Types," *J. Therm. Sci. 27*, 2018, pp. 389–393, https://doi.org/10.1007/s11630-018-1026-z.

27. Mattingly, J. D. and Boyer, K. M., *Elements of Propulsion: Gas Turbines and Rockets*, AIAA, second edition ed., 2016.

28. ANSYS, I., *FLUENT 17.2 User's Guide*, Canonsburg, PA, 2018.

29. Bohan, B. T. and Polanka, M. D., "A New Spin on Small-Scale Combustor Geometry," *Journal of Engineering for Gas Turbines and Power*, Vol. 141, 2019, pp. 011504–1–10, https://doi.org/10.1115/1.4040658.

30. Al-Rifai, S. H., Lin, C.-X., Bohan, B. T., and Polanka, M. D., "A Numerical Sensitivity Study of Modeling Parameters in the Combustion of a Swirler," *Proceedings of the 2021 ASME Turbo Expo*, 2021, GT2021-59392.

31. Briones, A. M., Erdmann, T. J., and Rankin, B. A., "On-Design Component-Level Multiple-Objective Optimization of a Small-Scale Cavity-Stabilized Combustor," *Proceedings of the 2021 ASME Turbo Expo*, 2021, GT2021-60102.

32. JetCat, "P160-RXi-B," `www.jetcat.de/en/productdetails/produkte/jetcat/produkte/hobby/Engines/P160_rxi_b`, 2020, Accessed: 2021-01-10.

33. Paxton, B., Fugger, C., Tomlin, A., and Caswell, A., "Experimental Investigation of Fuel Chemistry on Combustion Instabilities in a Premixed Bluff-Body Combustor," 2020, https://doi.org/10.2514/6.2020-0174.

34. S-15 Gas Turbine Perf Simulation Nomenclature and Interfaces, "Aircraft Propulsion System Performance Station Designation and Nomenclature," 1991-10-09, ARP755.

REPORT DOCUMENTATION PAGE

Form Approved
OMB No. 0704-0188

1. REPORT DATE *(DD-MM-YYYY)*	**2. REPORT TYPE**	**3. DATES COVERED** *(From - To)*
03/24/2022	Master's Thesis	Sept 2019 - Mar 2022

4. TITLE AND SUBTITLE
Design and Application of Compact Combustors in Small-Scale JetCat Engines

5a. CONTRACT NUMBER

5b. GRANT NUMBER

5c. PROGRAM ELEMENT NUMBER

6. AUTHOR(S)
Nathan A. Clark

5d. PROJECT NUMBER

5e. TASK NUMBER

5f. WORK UNIT NUMBER

7. PERFORMING ORGANIZATION NAME(S) AND ADDRESS(ES)
Air Force Institute of Technology
Graduate School of Engineering and Management (AFIT/EN)
2950 Hobson Way
Wright-Patterson AFB OH 45433-7765

8. PERFORMING ORGANIZATION REPORT NUMBER
AFIT-ENY-MS-22-M-284

9. SPONSORING/MONITORING AGENCY NAME(S) AND ADDRESS(ES)
Dr. Drew Caswell, AFRL/RQTC
2130 Eighth Street
WPAFB OH 45433-7542

10. SPONSOR/MONITOR'S ACRONYM(S)

11. SPONSOR/MONITOR'S REPORT NUMBER(S)

12. DISTRIBUTION/AVAILABILITY STATEMENT
DISTRIBUTION STATEMENT A:
APPROVED FOR PUBLIC RELEASE; DISTRIBUTION UNLIMITED.

13. SUPPLEMENTARY NOTES

14. ABSTRACT

Ultra-compact combustors (UCC) are an innovative approach to improving overall engine efficiency and thrust-to-weight ratio by reducing the axial length and weight of the engine. Previous efforts looked at integrating a UCC into a small-scale JetCat P90 engine utilizing gaseous propane fuel. The current investigation aimed to utilize the previous compact combustor design and switch fuels to liquid kerosene. Based on the results from testing, a new combustor was designed equipped with a different flame holding mechanism at the larger P400-scale while maintaining a length savings of 20%. Testing of the P400 compact combustors was performed within a newly designed non-rotating test rig.

15. SUBJECT TERMS
UCC, Small Gas Turbine Engine, Combustion

16. SECURITY CLASSIFICATION OF:			**17. LIMITATION OF ABSTRACT**	**18. NUMBER OF PAGES**	**19a. NAME OF RESPONSIBLE PERSON**
a. REPORT	**b. ABSTRACT**	**c. THIS PAGE**			Dr. Marc D. Polanka, AFIT/ENY
					19b. TELEPHONE NUMBER *(Include area code)*
U	U	U	U	192	(937) 255-3636, x4714; marc.polanka@afit.edu